UNIVERSITÄT DER BUNDESWEHR MÜNCHEN

FAKULTÄT FÜR LUFT- UND RAUMFAHRTTECHNIK

Thema der Dissertation:

Pedestrian navigation in the indoor and outdoor environment

Verfasser:

Dipl.-Ing. Herbert Niedermeier

Promotionsausschuss:

Vorsitzende:	Univ.-Prof. Dr.-Ing. Kristin Paetzold
1. Berichterstatter:	Univ.-Prof. Dr.-Ing. B. Eissfeller
2. Berichterstatter:	Prof. Dr. Terry Moore (The University of Nottingham)

Mit der Promotion erlangter akademischer Grad: Doktor der Ingenieurwissenschaften (Dr.-Ing.)

Die Dissertation wurde am 21. Januar 2015 bei der Universität der Bundeswehr München, Werner-Heisenberg-Weg 39, D-85577 Neubiberg eingereicht.

Tag der mündlichen Prüfung: 27.11.2015

Neubiberg, den 23.11.2016

Acknowledgments

I want to express my deepest gratitude to all people who supported me during my work at the Institute of Space Technology and Space Applications (ISTA), professorship of navigation, at the Universität der Bundeswehr München and who made this thesis possible.

First of all I want to thank Prof. Dr.-Ing. Bernd Eissfeller for giving me the opportunity to write this thesis and for supervising the work. Thank you for your continuous support and encouragement over this long period of time!

My respect and thanks go to my colleagues at ISTA for their excellent cooperation, fellowship and inspiration. I want to thank all persons who gave me the chance to learn from their experience. I especially want to thank Gerald Ameres, Hanno Beckmann, Thomas Pany, and Andreas Teuber, with whom I was cooperating for a long time. Your support was priceless to me.

I want to thank my family for their continuous support, encouragement and love. Nothing would have been possible without you. Finally I want to thank my wife and my son for their love, patience and support. Thank you for everything!

Abstract

Global Navigation Satellite Systems (GNSS) like the US Global Positioning System (GPS) und the European Union Galileo System are the most widely used navigation systems today. GNSS receivers are present in nearly every smart phone, in sport watches, car navigation systems, road tolling systems and many other devices of daily use. While vehicle navigation systems have entered the market already to a large extent, pedestrian navigation gains importance continuously for many applications.

GNSS are radio navigation systems which use satellite signals for positioning and depend on direct Line-of-Sight (LOS) to the satellites as well as sufficient signal strength. These signals are already very weak even without additional attenuation and under open sky conditions. Inside buildings, problems are encountered if:

- the direct LOS of the satellite signals is blocked by obstacles (Signal blockage)
- the signals are attenuated strongly, e.g. by construction elements like windows, walls and roof (Signal attenuation)
- interference between the direct LOS signal and reflected signals is present (Multipath)
- the individual satellite signals are attenuated at different levels, e.g. one direct signal through the open window and one strongly attenuated signal through the roof (Near-Far Problem)

In summary the availability, but also the accuracy of the GNSS receiver's position solution can be reduced strongly inside buildings. Therefore additional positioning sensors and systems are required to provide seamless, continuous and precise positioning capabilities to the user. They shall:

- bridge phases when GNSS is not available (Bridging)
- aid the GNSS receiver to enable the tracking of even very weak signals (Receiver aiding)

In this PhD thesis several alternative positioning systems for pedestrians have been evaluated, developed and implemented. These systems are:

- Pedestrian Navigation System (PNS), a dead reckoning system based on the detection of steps, estimation of the step length and determination of the user heading
- Attitude and Heading Reference System (AHRS), using a MEMS (Micro Electro-Mechanical System) type inertial measurement unit (IMU)
- Magnetometer based heading determination for aiding of the dead reckoning system
- WLAN received signal strength based proximity positioning system
- Linearized Kalman filter for integration of all navigation systems and observations
- Determination of the micro-trajectory, the motion of the user GNSS antenna during a two seconds integration interval. The algorithm uses a modified strap-down algorithm, the IMU inertial measurements and the a priori knowledge by the calibrated PNS system (position and velocity information).

The high resolution micro-trajectory has been integrated into a flexible software GNSS receiver. The receiver uses the user trajectory to form an exceptionally long and precise signal replica of the expected GPS and Galileo signals. While conventional high sensitivity receivers often use a replica length of up to 20 ms, this system uses a replica length of 2000 ms. The correlation gain of the receiver could be increased strongly by this method in comparison to stand alone or commercial receivers, and it was possible to track extremely weak GNSS signals in the indoor environment. Hence, the integration of alternative navigation sensors and systems provides not only a backup

solution for bridging GNSS outages, but also improves the availability and the performance of the GNSS receiver under (extreme) indoor conditions.

The capabilities and the performance of the integrated navigation system have been demonstrated and evaluated in several test campaigns. Even under harsh indoor conditions the integrated system provided continuous and sufficiently precise positioning information to the user. The dead reckoning PNS system proved to be especially powerful under indoor conditions because of its highest availability and highest relative accuracy. The micro-trajectory reduces the dynamical tracking error strongly so that two seconds coherent integration time could be realized. Finally, even very weak GNSS signals could be tracked in the indoor environment.

1. Table of content

2. Motivation

It is the natural ability, but also the desire of animals and humans, to move from one location to the next. The knowledge about the current location, also known as position, as well as the desired destination and the directions to that destination determined the fate and the way of life of animals and humans for millenniums. Migrant birds have been flying around the globe, salmons have returned to their place of birth to spawn, and animals crossed the deserts searching for water and nutrition a long time before the human started to journey the world. Their inherited knowledge of orientation has been a great inspiration for generations of navigators.

Since ancient times the number of users of navigation has increased enormously. Navigators used to operate with expensive, rare, large and heavy equipment; navigation required highly qualified and experienced operators, large data sources, and was therefore limited to a small number of specialists and a limited number of applications, like tall sailing ships, later also modern ships and aircrafts. It took a very long time to access the so called commercial market, e.g. with car navigation systems and hand-held navigation devices for pedestrians. The main driving force for navigation conquering the world of almost every individual person was the development of satellite navigation, especially the US Global Positioning System (GPS). There are various reasons for the continuous success of Global Navigation Satellite Systems (GNSS):

- The practical need of precise positioning and guidance has never been higher in history. The individual mobility, the transportation business stimulated e.g. by the globalization and e-commerce, recreational outdoor activities, automation, cell phones, and all kinds of location based services have raised the practical need for precise positioning, guidance and timing to an enormous extent never seen before.
  (GNSS-)Navigation has become widely needed.
- Today, navigation equipment can be provided to the user, which is exceptionally convenient to use. It is not necessary to be an experienced and well educated navigator to use commercial navigation equipment. Virtually everybody can use a commercial GPS receiver, e.g. in a smart phone or in a handheld GNSS receiver, even without any knowledge about how exactly it is working. The equipment is available at a very low price without serious market restrictions.
  GNSS Navigation has become convenient, reasonably priced, and available.
- The accuracy of navigation systems has increased from several nautical miles to the range of several meters. Therefore the number of applications has increased dramatically and is still enlarged by new applications every day.
  GNSS Navigation has become very accurate.

Satellite navigation has been used for many years now and a lot of the initial problems could be solved. The scientific, but also the industrial focus has concentrated on only a few unresolved problems, based on the nature of satellite navigation. One of those unresolved problems is indoor navigation, as well as seamless indoor/outdoor navigation.

This has several reasons:

- **Attenuation:** Since satellite navigation is a radio navigation system, the receiver requires to receive a certain signal power level. This signal power level is attenuated strongly by the walls, ceilings and windows of buildings. Therefore the receiver may not be sensitive enough to receive and process the satellite signals. Details can be found in chapter 18.1, 18.2 and chapter 4.
  Attenuation is limiting the indoor use of GNSS.

- **Signal blockage:** Since the satellites transmit on L-band with frequencies beyond 1 GHz, the signals are travelling virtually like optical waves. The reception of the primary wave requires direct line-of-sight (LOS) to the individual satellites. If a building blocks the signal, the receiver cannot receive the direct path signal.
  GNSS is a Line-of-Sight system and buildings can block this LOS.

- **Reflections and multipath:** If the direct line-of-sight (LOS) signal is reflected from solid or liquid surfaces, the receiver will likely produce an erroneous pseudorange. This is even more the case when the reflected wave interferes with the original LOS signal (multipath). Since the receiver is determining the current position from the measured pseudoranges, the determined position and its accuracy is likely to be deteriorated.
  Multipath deteriorates GNSS positioning accuracy.

- **Near-far problem and receiver dynamics:** GPS and Galileo, as well as the next generation of GLONASS and the Chinese Compass/Beidou system use code-division-multiple-access (CDMA) as multiplex algorithm. The codes used by the different satellites provide a certain degree of cross-correlation separation, which is sufficient for open sky operations. However, inside buildings, different LOS paths can result in very different attenuations of the individual signals. In [18] it is shown that these attenuations can reach values of 30dB and more. If one signal travels through a highly attenuating wall while a second one can enter through a window with practically no attenuation, the receiver dynamical range may be overstressed. In addition to that, cross-correlation becomes a serious threat since the cross-correlation with other satellite signals may reach the same amplitude as the auto-correlation of such weak signals. Separation of the individual signals as well as keeping track of them in the tracking loops becomes difficult.
  Individual signal attenuation may stress the GNSS receiver's dynamic.

- **Seamless navigation capabilities:** As mentioned before, indoor and outdoor scenarios are very different in their properties. In contrast to other navigation tasks like ship or aircraft navigation, pedestrian users will frequently enter and leave buildings with various degrees of indoor environments. Single source navigation systems might become unstable or will not provide positioning information under these circumstances. If GNSS cannot be used, other positioning techniques like e.g. WLAN or dead reckoning positioning might be by integrated devices like cell phones. An integrated pedestrian navigation system is supposed to work seamlessly indoors and outdoors.
  Seamless indoor/outdoor navigation requires a robust navigation system suite which provides continuous and stable positioning to the user.

A perfect navigation platform for pedestrian users should be able to provide position information to the user in all kinds of environments and at any location in the world. For the case of GNSS this means that a receiver should be able to acquire and track GNSS signals also under adverse indoor signal conditions. But there is also the possibility to use other sensors or a suite of navigation sensors to provide ubiquitous positioning, bridging gaps of GNSS, GNSS receiver aiding or similar assistance to the user and the navigation system.

It is the goal of this thesis to provide contributions to the task of seamless indoor/outdoor positioning for pedestrians, evaluating and using various different navigation sensors and technologies, as well as describing innovative algorithms for sensor fusion while using a sensor suite of several state of the art indoor positioning sensors.

3. Introduction

Pedestrian users have special requirements regarding navigation and navigation systems. They require consistent, precise and ubiquitous positioning, no matter if positioning is performed outdoors or indoors, or even in mixed scenarios. Pedestrian navigation has been performed for ages, using the stars, the sun, the compass and most probably many other navigation aids. The user was required to have at least some experience in navigation and was limited by many influences, e.g. bad weather conditions or the availability of maps. GNSS was a quantum step in pedestrian navigation, since GNSS receivers allowed worldwide, precise and reliable navigation at low cost, even for users without experience in navigation. GNSS offers relatively high accuracy, precise positioning and timing, worldwide coverage and weather independent operation using an inexpensive, small size device. However, several aspects limit the use of GNSS, especially for pedestrians. Major limitations are the dependence on line-of-sight (LOS) to the satellites, and the weak signal power in combination with attenuations, reflections, interference, near-far problems, jamming and many more. As a result, a powerful pedestrian navigation system cannot rely only on GNSS. It must be noted that practically all other navigations systems have limitations, too. Hence, a combination of various navigation instruments and systems, with GNSS being the major element of it, seems most promising.

3.1 Overview

Pedestrian navigation is not an entirely new subject, since for centuries human beings have travelled and navigated “manually”. Like in other navigation applications they used dead reckoning as well as position fix systems to find their position relative to their target. For dead reckoning, e.g. a compass to derive heading, a watch to measure time and an estimated average walking speed could be used. For position fixing, a map comparison between an available map and the travelled trajectory, landmarks and geometric road comparison could be used. And, finally, local persons with knowledge of the area could be asked. As with every navigation application, the accuracy and the reliability of the navigation solution could vary strongly. Nevertheless, automatic positioning for pedestrian became possible only after the development and miniaturization of the US Navstar GPS system. GPS truly revolutionized the personal navigation and applications can be found in nearly every cell phone, especially the smart phones, today.

If navigational aspects of the pedestrian user are analyzed, many aspects appear unusual in comparison to other navigation applications, like the low velocity, the strict ground based motion constraint and often unpredictable operation times. In contrast to applications like ship or aircraft navigation, the pedestrian user faces many situations where open sky conditions can be, but are not necessarily met. In contrast to applications like tunnel construction or submarine navigation, the user navigates in very different environments, which can change very fast and arbitrarily, the use case cannot be predicted in this respect. The pedestrian user can face pure open sky conditions, limited sky view with high walls or trees limiting the view, and indoor scenarios with totally blocked sky view within only seconds. This has a major impact on the usability of several navigation devices, especially when satellite navigation is used.

At first it must be noted that the major parameters for pedestrian navigation systems are not different from other applications, and the individual performance of a pedestrian navigation system

varies with the environment and the situation of use. A pedestrian navigation system has generally the same categories of parameters to judge the quality of operation, e.g.:

- Availability
- Continuity
- Accuracy
- Integrity

Precise definitions for the parameters above can be found in [103] and [104] for the Navstar GPS system. A simpler approach can be found in [81].

The goal for an indoor navigation system must be accurate, ubiquitous positioning with high reliability.

3.2 Satellite Navigation for Pedestrians

Global navigation satellite systems (GNSS) started with the Doppler satellite navigation systems TRANSIT and TSIKADA. Both systems are obsolete today. Satellite navigation using one-way-ranging became possible with the initial operation capability of the US Navstar GPS system being declared in 1993, and the final operation capability being declared in 1995 ([103]). Today, additional GNSS systems have appeared or are announced to be operational in the near future. The globally available systems are the Russian GLONASS, the European Galileo, the Chinese Compass/BEIDOU system and several regional systems like the Japanese QZSS and the Indian IRNSS system. Therefore, the number of GNSS satellites in space has already increased strongly and will grow even stronger in the near future. GNSS is globally available on a continuous basis, every system offers an open service free of charge and by using similar center frequencies it is possible to construct simple RF-frontends for the GNSS receiver and still use nearly all available satellites for a combined navigation solution.

Besides the undisputed great capabilities of GNSS, there are also weak sides of GNSS that limit the usability or performance of GNSS for pedestrian navigation, such as the fact that GNSS is in principle a line of sight (LOS) system. Since the satellite signals are sent on frequencies in the Giga-Hertz domain, they travel virtually like light in straight lines.

As discussed in the previous chapter, GNSS is currently extensively used for personal positioning, but suffers strongly from the challenges of indoor or combined indoor/outdoor environments. Therefore, various alternative navigation techniques for indoor positioning are discussed in scientific publications. Indoor GNSS scenarios are characterized by strong satellite signal attenuation resulting in very low Signal to Noise Ratios (SNR), which makes the acquisition and tracking of those signals very difficult. A mathematical analysis of the tracking loop stability will be given in chapter 18.2. Since the satellite signal rays are not propagating along the same path for all satellites, the attenuation of the individual signal varies strongly, e.g. when penetrating windows and solid walls. Therefore, the risk of false locks due to signal cross-correlation is evident. Signal multipath is omnipresent in indoor scenarios and has a strong negative influence on the tracking performance of the signal tracking loops.

With some exceptions like e.g. in GLONASS, most GNSS systems use code multiplex techniques (CDMA) and phase modulation (e.g. BPSK), where all satellites are transmitting their signals using the same center frequency with individual codes. By correlation of a replica signal with the received

signal, the weak satellite signals can be individually separated, acquired and tracked and the pseudoranges can be determined. From the pseudoranges, the user position can be calculated. The correlation is the major component of the GNSS receiver that enables the evaluation of the weak satellite signal while being hidden under the noise floor. It is reasonable to search for a technique to increase the correlation gain even further, so that even weaker signal, like the attenuated indoor signals, can be tracked. This increase in correlation gain can only be achieved by extending the correlation interval of the GNSS receiver. The correlation time is a multiple of the code length in CDMA systems; hence the minimum correlation time is one code length, while the maximum is limited by aspects like the length of the navigation data bits, as well as clock errors and dynamic motion of the user during the integration interval. This integration could be performed in a coherent and a non-coherent way. Coherent integration means that the replica is “one piece”, i.e. the replica carrier phase is continuously predicted for the entire integration interval without breaks in the carrier phase. Non-coherent integration would mean to sum up the correlation results for several shorter choherent integration periods until the total integration time matches again the designed integration time. A goal of the work described in this thesis is to provide contributions to the increase of the coherent signal integration time to two seconds.

Increasing the coherent signal integration time seems to be a perfect way of dealing with the problems described above. Generally, the SNR of weak signals is improved proportionately to the coherent integration time which compensates together with further non-coherent integrations for the attenuation caused by walls. Additionally, a coherent integration time of several seconds would mitigate three important indoor positioning problems: multipath, cross-correlation false locks, and the squaring loss. This fact is discussed in detail in [77]. Common Commercial-Of-The-Shelf (COTS) receivers usually limit the coherent integration time to one GPS C/A-code length, corresponding to 1 ms of coherent integration time. High sensitivity receivers usually extend this up to the length of one GPS navigation data bit, corresponding to a time of 20 ms. Therefore, a significant gain could be expected by applying a very long coherent integration.

Nevertheless, several facts also prevent the use of very long coherent integration. Since data bit transitions can occur every 20ms, assistance data must be provided to the system and a reference station with open sky conditions must be available. In addition to that the internal clock is often not stable enough to provide sufficient accuracy for the replica construction due to oscillator jitter, if long replicas are formed. Therefore, a stable oscillator, e.g. an Oven Controlled Crystal Oscillator (OCXO), is necessary to reduce oscillator jitter to acceptable values. The most challenging part, however, is the **reproduction of the user antenna motion** with high accuracy to compensate the nonlinear dynamics on the pseudorange and the signal Doppler frequency. Since the antenna is moving with significant speed and accelerations with respect to the satellites, the user motion influences the pseudorange, pseudorange dynamics and the Doppler considerably, if a replica length in the range of several seconds is used. A common approach would be to use an inertial navigation system (INS) to reproduce the user motion during the integration interval. During the work described in this thesis it turned that current COTS Micro Electro-Mechanical System (MEMS) type inertial sensors do not provide the stability to fulfill this task sufficiently, especially if they are aided only by non-precise indoor position updates. Obviously, a difference in signal replica and received signal causes a significant correlation loss, which can also destroy the gain of long coherent integration if the difference reaches half of the signal wavelength. An integrated replica error corresponding to 1.4

cm length, corresponding to a loss of 1 dB, has been defined as target. Hence, an innovative algorithm has been developed to reproduce the user motion using a sensor suite of various different sensors and especially the coupling of a Pedestrian Navigation System (PNS) with a modified inertial navigation system, called "µ-trajectory generator". The combination of the robust, but low frequent PNS with the high frequent, but only short term stable µ-trajectory generator produced promising results.

3.3 Problem Statement

The work performed in this thesis is a contribution to a complex navigation system, which has been developed by several scientists. Hence, the focus of the overall development will be described generally at first, while the focus of this thesis will be discussed in detail secondly.

Overall system

Pedestrians shall be navigated in mixed indoor/outdoor situations. One system is not able to perform under all conditions with acceptable performance. For that purpose a combined navigation system has been developed with a GNSS software receiver as main and integrating element. Due to its global coverage, position and time fixing capabilities and the generally good accuracy, GNSS is the main sensor of the system. The operation of the receiver shall be improved by the implementation of custom tracking algorithms and the use of aiding sensors.

The work has been focused on the development of a GNSS software receiver using very long coherent integration. The main idea of the concept is the extension of the coherent signal integration time of the GNSS receiver to the length of several seconds which increases the correlation gain significantly. Since conventional high sensitivity receiver use up to 20 ms coherent integration time, an increase of that time by a factor of 100, i.e. 2000 ms coherent integration gain was set as a goal. To facilitate this goal, a very long and very precise signal replica is needed. Therefore, the system must reproduce the user antenna motion, the navigation message data bits and the satellite constellation precisely. A precise prediction of the user motion, especially the antenna phase center, must be provided to care for Doppler and pseudorange dynamics over such a long integration period. The integrating element of the system is a software receiver using Ultra-Tightly Coupling (UTC) implemented by vector tracking.

Focus of the thesis

This thesis is focused on major contributions to the integrated navigation system described above. The main contributions include the replication of the user antenna motion with high frequency and accuracy. Precise knowledge of the user antenna motion is one of the major challenges in very long coherent signal integration. The individual contributions are:

- Prediction of the antenna trajectory over the integration interval of 2000 ms.
- Provide a dead reckoning trajectory as backup and as reference for the micro-trajectory generation.
- A sensor suite shall be used to exploit the best properties of all systems.
- Position Kalman filtering for the dead reckoning system using available position updates.

- Implement a WLAN based position fix system based on pass by proximity warning system.
- For project relevant reasons, AHRS was not the focus of the initial project. At first, the internal attitude reference of the used sensor system has been used. Since this gap in the implementation would affect the completeness of the thesis, the AHRS algorithms have been implemented outside the baseline of the project. The implementation and the results will be described in the thesis to give a complete picture of the subject. It will be shown that the custom implementation of the AHRS algorithms produces results which are fully comparable to the internal attitude reference system.
- Since the navigation system was a team project, not all elements of this system have been researched by the author of this thesis. The research performed by the author focuses on the prediction of the micro-trajectory of the antenna, the PNS system, the WLAN proximity positioning system and the navigation Kalman filter. The integration of the micro-trajectory in the tracking loops of the receiver have been performed by other collegues.

The work described in this thesis has been influenced by the results of the project INDOOR, funded by the German Aeronautics and Space Agency DLR (Deutsches Zentrum für Luft- und Raumfahrt), and of the project DINGPOS, funded by the European Space Agency ESA under supervision of ESA/ESTEC, and further developments of the PhD candidate.

3.4 Document Overview

Many intermediate steps are necessary to implement the ability of very long coherent integration to a software receiver. Several sensors and algorithms are necessary to reconstruct the user antenna motion precisely and to enable the forming of a precise signal replica. This thesis will describe the fundamentals, challenges and problems of indoor navigation, and the individual steps for the replication of the user motion. Various sensors and algorithms for indoor navigation will be compiled, evaluated and selected for the purpose of user motion replication. The individual sensors demand special processing and algorithms, too. They will be developed or described in the following chapters. Finally, the individual results must be fused to determine the user antenna motion precisely. In the software receiver, this user antenna motion will be used to form a precise replica. Finally the integrated system will be tested and evaluated in a realistic environment. The thesis is closed by a summary and a way ahead for future research.

In **chapter 4**, the fundamentals and problems of indoor navigation will be discussed. It will be highlighted why the indoor environment is so challenging for many navigation systems and especially for GNSS receivers. An overview and some definitions complete this chapter.

Chapter 5 presents a roundup of several navigation sensors and systems with special focus on indoor navigation. Sensors and sensor combinations are evaluated regarding the special indoor conditions, and finally the focus for this thesis is narrowed to a limited suite of sensors.

The Inertial Navigation Systems (INS) is one of the key technologies in this thesis and will be discussed in **chapter 6**. The precise replication of motion of the user antenna is mainly based on inertial navigation. Hence, in this chapter the basics of inertial navigation are described, as well as the special adjustments for the pedestrian user navigation in this thesis. The implementation and testing of the algorithms with the MEMS sensors used in this thesis will connect the theory behind the system with the practical implementation.

Chapter 7 will introduce and describe the Pedestrian Navigation System (PNS). The PNS is a major component of the combined navigation system described in this thesis. The basic idea of this system is to perform dead reckoning by detecting steps and to propagate the user position by an estimated stride in the estimated direction. Since the accelerations are not integrated, the system has a much lower tendency to drift than standard INS processing would have. PNS is an important technique to limit the position error drift of the system.

All dead reckoning navigation systems have in common a tendency for drifting position errors. The PNS as dead reckoning system is limiting this position error drift, but still accumulates error during navigation. Additionally, erroneous starting positions are maintained during normal operation. The PNS can be corrected by using observations of GNSS pseudoranges, WLAN or other available position updates. A PNS Kalman filter, integrating the PNS with GNSS and other available positioning systems will be developed and demonstrated in **chapter 8**.

An efficient approach to WLAN positioning is described in **chapter 9**. WLAN is an infrastructure which is present in many buildings today. It has been shown in many publications that WLAN received signal strength of several access points can be used for user positioning. The most common technique is called “fingerprinting”. To reduce the efforts for calibration and to give the dead

reckoning system in this thesis appropriate positions updates, an alternative proximity warning positioning system has been developed. This system indicates if a WLAN access point is passed by in close distance. In this chapter the fundamentals and the algorithm of this proximity positioning system will be described.

The determination of altitude using pressure sensors is a common technique, e.g. in aircrafts or in mountain hiking. Modern MEMS type barometers are inexpensive, very compact and lightweight sensors which allow the user to measure pressure and pressure changes quite precisely. In **chapter 10**, the determination of height from pressure measurements, calibration of the sensor and the use for the user trajectory determination will be described.

In **chapter 11**, receiver aiding for very long coherent integration is described. All navigation techniques and system studied in the course of this thesis are integrated in the GNSS software receiver. The main goal is to reproduce the antenna motion during the integration interval of the receiver. By this, the replica will match the received signal precisely and the desired integration gain is achieved. The construction of the antenna motion, called micro-trajectory, will be described in this chapter. After this, the combined system will be tested in real indoor, outdoor and mixed scenarios. The results will be evaluated and the performance of the system will be demonstrated.

The thesis is summarized in **chapter 12**.

Chapter 13 describes a possible way ahead for future research. The described system solves many problems of indoor and mixed indoor/outdoor scenarios and is therefore a very successful technical approach. Several aspects of the system can, nevertheless, be improved or simplified to make the system more user-friendly. These aspects will be described as a starting point for further research. A main topic is the reduction of the calibration effort for every user, especially for the PNS system. Modern user platforms like smart phones or tablet PCs are introduced as possible research platforms for future system evolution.

In the **appendix** in **chapter 18**, additional mathematical analysis and background for individual parts of the thesis is given.

4. Navigation in the indoor environment

Indoor navigation is a special application of general navigation. Hence, in this chapter some basics of navigation shall be discussed, while it is not possible to explain them in every detail in this thesis. The differences between indoor and general navigation applications are nevertheless important for the design of indoor navigation systems, which show many navigation restrictions and requirements. Therefore these differences and the specific problems and difficulties in indoor navigation shall be explained in more detail.

4.1 Overview and definitions

Navigation is commonly defined as the two tasks of **positioning** and **guidance**. Positioning is the task of determination of the current user position, often also the attitude, the velocity and the attitude rates. Guidance is the task of providing the directions from the current location to the desired destination.

Guidance in its simplest form can be based on a purely geometric basis. It provides directions and distance for several navigational lines, like orthodrome, rhumb line or constant bearing angle. In urban applications, restrictions like one-way streets, heading and availability of streets, obstacles, etc. limit the application of standard geometric guidance. Map-based guidance has therefore gained enormous importance in mobile navigation systems and is based mainly on database systems. All possible combinations of path segments are evaluated and the best solution is chosen based on constraints and cost functions. Since guidance is not the focus of this thesis, the subject will not be discussed any further. It must be noted that several publications exist in which map attributes are used to stabilize the guidance as well as the tracking and positioning functions of indoor navigation systems. Nevertheless, if highly precise motion replication is desired, the constraints often limit the dynamic models of motion in an undesired way. The user is not supposed to walk in straight lines since the user can move freely, especially in large rooms, and a change of direction can happen at any time. Therefore, this approach has not been chosen in this thesis.

Position is mostly expressed relative to a given reference, often by distance and angles (polar form) of the given object to the given reference. A set of (mostly perpendicular) axes with a common origin are called **coordinate system**. A **frame** is the realization of a (theoretical) coordinate system. "Degrees of freedom" is the number of parameters or coordinates that are required to uniquely define the state of an object. For a rigid body, the actual state can be described by three longitudinal and three rotational degrees of freedom. If an object is allowed to move, the derivatives of the position and orientation are also necessary, hence for describing a rigid and freely moving object in the three-dimensional space we need:

- Three positions (x, y, z)
- Three velocities (v_x, v_y, v_z)
- Three orientation angles (Φ, Θ,Ψ)
- Three rotation rates (p, q, r, or ω_x, ω_y, ω_z)

Consequently, twelve states are required to determine the full navigational state of a rigid body in three-dimensional space.

If the object is considered to be a point mass, the attitude of the object is of no concern. In that case the state vector only contains six parameters:

- Three positions (x, y, z)
- Three velocities (v_x, v_y, v_z)

If navigation on the Earth is regarded, the problem of **height reference** must be considered. The two most important height references are the simplified geometric form of the Earth, as well as the geometric surface defined by an equal gravity potential. They are called ellipsoid and geoid.

The reference **ellipsoid** is a geometric approximation of the geometric surface of the Earth as an ellipsoid, which is an ellipse rotated around its minor half axis. The coordinates are expressed as latitude, longitude, and the elevation or altitude over the ellipsoid. Therefore, elevation is also a relative representation of the vertical position relative to the surface of the reference ellipsoid, but can easily be converted to absolute coordinates when the parameters of the reference ellipsoid are known. The WGS 84 coordinate frame is the most prominent and most widely used Earth fixed reference frame. It includes a reference ellipsoid. Its importance is also accentuated by the fact that GPS uses WGS 84 as reference frame. The representation of coordinates in a Cartesian frame (x, y, z) refer to the defined Earth center, the defined reference Earth rotation axis and the zero meridian, all defined by the WGS 84 system. Further information on this subject can be found in [69] and [20].

The **geoid** is based on the model of an equipotential surface, which is defined by a theoretical mean ocean surface level for a resting Earth without tides. On all equipotential surfaces of the gravity potential, the partial derivatives in the local level x- and y-directions are zero. In other words, if a spirit level would be placed exactly on the geoid, it would indicate a zero inclination and spilled water would flow in each direction equally. Since the density of the Earth crust is neither constant nor equally distributed, the geoid is not a regular form like the ellipsoid. The geoid is the reference surface for most map heights, which are often indicated as above mean sea level. As global implementation, the Earth Gravity Model 1996 (EGM 96) is most often used. It should be noted that the model is an implementation of spherical harmonic functions and coefficients. By applying the local coefficients for the model, the local gravity undulation can be calculated. The geoid undulation is the height difference between the standardized ellipsoid and the geoid at the current location.

In chapter 6.3, several navigation frames described and their relevance for indoor navigation will be discussed.

4.2 Physical aspects of Indoor Navigation

Indoor navigation denotes especially the navigation inside of buildings. Buildings are constructed of walls, ceilings and roof and there might be basements where the rooms are below the Earth surface. Due to these constructional elements the direct line-of-sight (LOS) of signal from the outside of the building to the inside of the building is limited in all spectral bands, i.e. visible light, IR, UV and radio frequency (RF). The signals might be attenuated, reflected or totally blocked. For indoor navigation, the RF frequencies are of major importance, since radio navigation systems like GPS, which are strongly depending on the received signal power, have widely entered the market for personal navigation devices.

Attenuation describes the loss of energy of a signal while passing through a specific medium. It is expressed as ratio between the signal power after the passing and the power before the passing. The attenuation is dependent on the type of material, but also on the thickness of the material in the LOS. In Table 4-1, the attenuation of several classic construction elements and materials is summarized for the frequency of 1.5 GHz, a frequency similar to the GPS L1 center frequency.

Material	Attenuation at 1500 MHz (approx. GPS L1, Galileo E1)	
	[dB]	scalar factor
dry masonry wall	1	0.8
ply wood	1..3	0.8 .. 0.5
glass	1..4	0.8 .. 0.4
tinted glass	10	0.1
construction timber	2..9	0.6 .. 0.1
steel wire fabric	2..11	0.6 .. 0.08
roof tile, brick	5..31	0.3 .. 0.001
concrete	12..43	0.06 .. 0.00005
reinforced concrete	29..33	0.001 .. 0.0005

Table 4-1: Attenuation for typical materials and construction elements made of various materials [18]

In [19], the overall RF attenuations have been estimated for several types of buildings:

Building type	Overall attenuation at 1500 MHz (approx. GPS L1, Galileo E1)
	[dB]
residential building	5 .. 15
historical building	25 .. 35
office building	30
underground parking	>30

Table 4-2: Estimated overall RF attenuation for several types of buildings [18]

Obviously, the attenuation is strongly depending on the material and the strength of the construction. The attenuation of massive and underground buildings is much higher than the light constructions of dry walls and woods. It is clearly discernible that the attenuation can easily reach values of more than 30 dB, which makes radio navigation inside buildings very difficult. In chapter 18.1, the effect of reduced signal strength on the stability of the tracking loops of a GNSS receiver is analyzed.

At high frequencies above 1 GHz, it is assumed that the waves behave “quasi-optical”. Therefore direct line-of-sight becomes critical for the reception of the waves. If signals are reflected from

elements like walls or ceilings, the signal might travel around obstacles. The available signal is then not the LOS signal and the calculated pseudorange consequently is not correct. Even worse effects can be monitored when the reflected signal interferes with the original LOS signal. The effect is called multipath and is a severe error source for pseudorange determination.

Since not all satellites share the same transmission geometry, i.e. one low elevation satellite might transmit through an open window, while another high elevation satellite might transmit through a strongly shielding roof, the **power** of the individual signals might be very different. This effect is sometimes referenced as **near-far-problem**. In this case, the cross-correlation of a strong signal might be stronger than the autocorrelation of a very weak signal. The tracking of the weak signal would be much more difficult under those circumstances.

For **dead reckoning sensors**, the indoor environment can be very hostile, too. Especially magnetic field sensors are highly susceptible to disturbing magnetic fields. These can be produced, e.g., by metal reinforcements of concrete, metallic infrastructures like radiators, pipes, cables, wires and banisters. Hence, the determination of heading inside of buildings can be very troublesome when using magnetic sensors indoors. This has been monitored in several test campaigns. Calibration and continuous disturbance control is therefore mandatory.

Geodetic coordinates like latitude and longitude are helpful magnitudes if long distances are covered, like for ships and aircrafts. For the pedestrian user, these magnitudes often have limited usability. More often, local frames and local coordinates are much more helpful for pedestrians, like local level frame on several floors of a building, or coordinates matched to a floor plan of the building. The floor number might be more interesting as the geodetic height. A floor plan with significant landmarks like staircases, rooms, etc. can be more useful as navigation aid for indoor navigation than a street map. Digital maps of the required buildings are therefore most often necessary for practical use of indoor navigation. These maps should cover meta-information like the position of walls, staircases and constraints, like doors that open only to one side. Constraints can be effectively used to limit navigation errors, and map matching of the user trajectory with the floor plan can be useful as positioning technique itself. If navigation systems like GNSS and dead reckoning systems or WLAN positioning are combined, a frame transformation between local level frames and Earth fixed frames is often necessary.

4.3 Summary

In the last chapter, indoor navigation has been demonstrated as a special case of general navigation. The basic tasks of navigation, positioning and guidance, have been explained and the focus of the thesis has been narrowed to the positioning task. The special physical problems and challenges of indoor navigation have been highlighted. The most important points covered the construction of the building, resulting in limited line-of-sight to the outside world. This limited LOS constrains the use of modern positioning techniques, especially of satellite navigation. Finally the need of local coordinate frames and digital maps to make indoor positioning convenient to use has been expressed.

5. Sensors for Indoor Navigation

Positioning can be performed by using a broad variety of special instruments and sensors. GNSS has a special relevance within all these sensors. Due to its global coverage and high accuracy and availability, GNSS has been used extensively for positioning since its initial operational capability in 1993 ([103]). However, the indoor environment is often very challenging for GNSS applications as has been demonstrated in chapter 4. Therefore, additional sensors and positioning systems have been evaluated and are used for indoor positioning in this thesis. In the following chapter an overview of alternative sensors for indoor navigation, with special focus on the sensors used for this special application is given. These sensors cover inertial sensors, magnetic sensors, barometer, and Wireless LAN network adapters. The selection of sensors is explained, while some other sensors not used in this thesis will be commented.

5.1 Introduction

Navigation has been used for centuries by a wide range of users in very different environments. The Global Navigation Satellite Systems (GNSS), especially the US Navstar/GPS system, has become one of the most important and most widely used navigation systems of the 21st century. The popularity of GNSS can be explained by several of its outstanding features. Under open-sky conditions, it provides worldwide positioning with accuracies of several meters down to centimeter level depending on the used receiver technology and processing techniques like differential GPS. The mass market equipment has become very low-cost in recent years, and it can be used without dedicated training in classical navigation abilities. GNSS is sufficiently precise for many civil applications, even with low-cost receivers. Nevertheless, all these features only apply to open sky scenarios.

Deep indoor scenarios are one of the most challenging areas of application for Global Navigation Satellite Systems (GNSS) in personal navigation devices. Especially severe signal attenuation and heavy multipath constrain the use of GNSS in this environment.

Therefore, for unrestricted indoor-outdoor application, GNSS alone is not sufficient for providing ubiquitous, continuous and precise positioning. Additional alternative sensors and integration techniques are necessary to fulfil these requirements. Principally, the additional sensors can be grouped into position fix and dead reckoning sensors. They have in common that they are independent of the weak RF signals from the outside of the building, and many of them use basic physical properties for producing navigational information. Others, like WLAN network adapters, use signals produced inside the building which are much stronger than GNSS signals and widely available. The scope of used sensors is limited mainly to avoid the need for custom infrastructure, to reduce calibration efforts, power consumptions and prices. Many excellent sensors require expensive infrastructure in every building and had to be abandoned therefore.

5.2 Inertial Sensors

Inertial sensors are major components of the work described in this thesis. Therefore, it is important to describe and to analyze these sensors in the following chapter. In a short introduction, the historical, technical and physical backgrounds are briefly discussed. In the following subchapters, the different sensors will be characterized. Finally, the applicability for pedestrian navigation will be discussed.

5.2.1 Principles of inertial sensors

Inertial sensors are determining accelerations, gravity and rotation rates, most often by exploiting simple laws of mechanics, like Newton's second law of motion, the impulse laws or the laws of inertia. The sensors measuring accelerations are called accelerometers; the sensors measuring rotation rates are called gyroscopes. If three perpendicular accelerometers and three perpendicular gyroscopes are combined in one unit, an "Inertial Measurement Unit" (IMU) is formed.

Various sensor types based on different physical properties have been developed, while development and improvement are still ongoing. The development has been driven by the state of the art in mechanical precision fabrication, electronics and available computational power. The first sensors were purely mechanical sensors, like spring-mass accelerometer and mechanical gyroscopes, followed by electronically stabilized sensors like the Dynamically Tuned Gyroscope (DTG), the Electronically Suspended Gyroscope (ESG), or the electronically caged/stabilized accelerometer ("servo" accelerometer), which uses control systems to keep the sensor proof mass centered in the casing. Modern development concentrates on inexpensive manufacturing (e.g. on silicon wafers), mass production capabilities, miniaturization and optical or even quantum effect sensor principles.

While the major factor and primary goal in the past has been to increase the sensor accuracy, the reduction of cost of procurement and ownership is prime paramount today. Accordingly, even cell phones, toys and gaming computers can be equipped with inertial sensors today. A good example for that is the Nintendo Wii, a game console which is designed to use inertial sensors as input device for gaming.

5.2.2 Accelerometers

Accelerometers are sensors measuring the acceleration of the sensing element, most often by the displacement of a proof mass. Since the sensor is not able to distinguish between the kinematical and the gravity acceleration, the vector sum of both is measured. This phenomenon is called "Einstein's principle of equivalence" and is discussed in chapter 6 in detail. Most accelerometers are based on Newton's second law of motion which relates force and acceleration in a linear relationship with the proof mass as scalar factor (chapter 6, eq. (1) and(2)). The sensors themselves differ in their design.

The spring-mass system is a simple implementation of an accelerometer exploiting Newton's second law of motion and Hooke's law. In this implementation, the proof mass is suspended by two springs in a crank. The schematic design is shown in Figure 5-1. The sensor has one sensing axis along the crank; all other forces are directed into the crank. If accelerations along the sensing axis occur, the proof mass is shifted along the springs and this displacement can be measured by inductive or

capacitive pickups. The displacement is proportional to the applied acceleration according to Newton's second law of motion and Hooke's law.

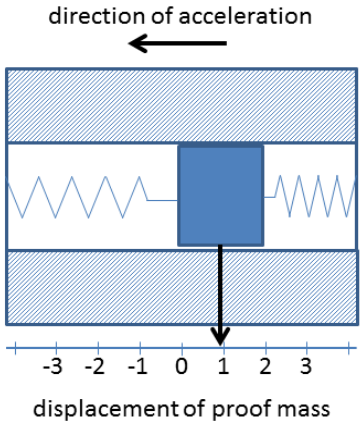

Figure 5-1: Schematic view of classical spring-mass accelerometer

While simple in design, the sensor has several drawbacks. Spring mass systems tend to oscillate after excitation. Therefore, the Eigen-dynamics of the sensor affect the output of the sensor and internal attenuation, e.g. by filling the sensor with viscous fluids, is necessary. Secondly, the proof mass must be suspended as free of friction as possible to avoid cross-axis attenuation. Thirdly, the manufacturing and calibration of the sensor must be precise to achieve good performance.

Other implementations of classical accelerometers are flex-beam accelerometers and servo-type accelerometers, and often combinations of both. For the flex-beam accelerometer several drawbacks of the classical spring-mass accelerometer are cancelled. The flex-beam accelerometer replaces the springs, the proof mass and the crank by a longitudinal, flexible beam of solid material. The beam is attached to a rigid case and has a flex point with lower stiffness at its bottom.

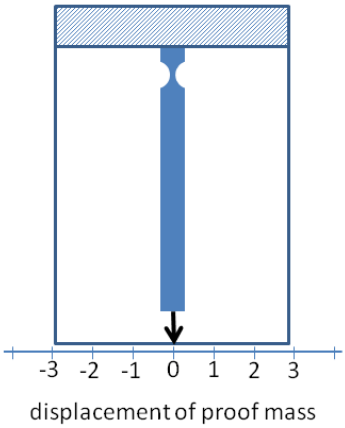

Figure 5-2: Schematic view of flex-beam accelerometer

If accelerations perpendicular to its flexible direction act on the sensor, the beam flexes in the opposite direction. The flexible hinge counteracts this deflection by its elastic force. In Figure 5-2, a schematic view of the flex-beam accelerometer is given.

Servo-type sensors are additionally equipped with an electro-magnetic caging system. The case is equipped with permanent magnets, while the proof mass carries an electrical magnet consisting of a coil and a soft-iron core. If deflections are detected, the coil is supplied with voltage and produces a

momentum that counteracts the inertial forces which are deflecting the proof mass. The voltage and the current that are necessary to keep the proof mass in the center of the sensor are used as measured magnitude.

In this thesis the 'Micro Electro-Mechanical Sensor' (MEMS) type of accelerometers will be used. MEMS sensors are miniaturized sensors based on silicon wafer design. The manufacturing process is similar to the production process of integrated circuits, i.e. the structures of the sensors are etched from silicon raw material called wafers. They are principally flex-beam accelerometers, but with sophisticated geometries and are largely reduced in size. In Figure 5-3, a schematic view of a MEMS accelerometer is given.

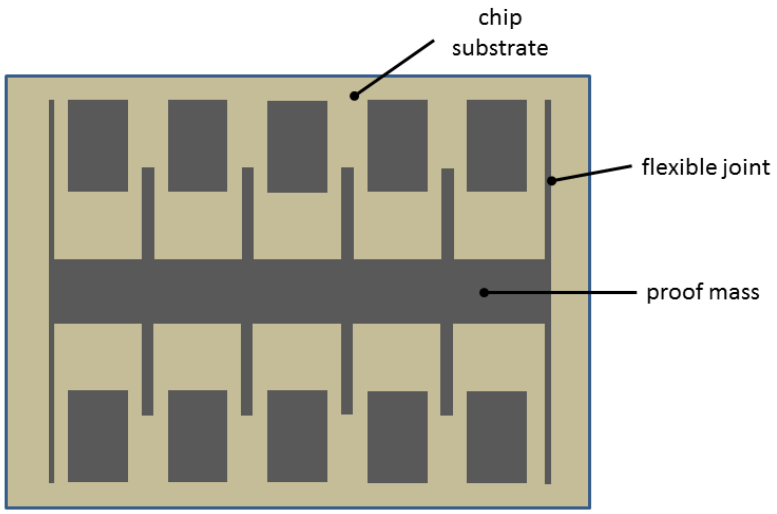

Figure 5-3: Schematic view of a MEMS accelerometer

The benefits of MEMS sensors are the small form factor, the low power consumption and the low price of the sensor due to the efficient manufacturing process and the high number of produced sensors. In sensors like the Memsense Nano IMU, three accelerometers and three gyroscopes are placed in a sensor block of less than 1 cm^3 ([62]). On the other hand, the sensor performance is often not fully up to the standard of the mechanical sensor types described above. A short evaluation of the used sensors will be given in the following chapters. More information on accelerometers can be found e.g. in [102], [8] and [88].

5.2.3 Gyroscopes

Gyroscopes are sensors measuring applied rotation rates. In general, gyroscopes can be grouped into mechanical gyroscopes, optical gyroscopes, Coriolis force gyroscopes (CVG) and cold atom interferometer gyroscopes, while the last ones are still under research and development at this time.

Mechanical gyroscopes use the law of conservation of angular momentum and the effects of precession and nutation. They consist of a spinning mass which is rotationally suspended by bearings (mechanical, electrostatical, fluid bearings) and rotated by electro-magnetical fields or pressurized air. They are not sensitive around their spinning axis, but can measure rotation rates perpendicular to it. Servo gyroscopes exist which use caging loops analogue to the ones described for servo-accelerometers.

Optical gyroscopes (ring laser gyroscopes RLG, fiber-optic gyroscopes FOG) use the Sagnac effect, which creates a phase shift between signals travelling in and against the direction of rotation. Optical gyroscopes are commonly used high accuracy devices and have replaced mechanical gyroscopes in various applications like missiles, aircrafts and ships. As will be shown in the following chapters, optical gyroscopes show excellent performance, but most often have a much larger form factor, heavier weight and higher price than MEMS gyroscopes.

MEMS type CVG gyroscopes use the small Coriolis forces which can be measured when oscillating masses are rotated perpendicular to their oscillation axis. The principle is shown in Figure 5-4 and Figure 5-5. The sensor consists of two or more proof masses, which are oscillated inwards and outwards in counter phase, e.g. by electro-magnetical or by piezo effects. Since they resemble a tuning fork, they are often referred to as tuning fork gyros. This design is demonstrated here. It must be mentioned that the geometric form is not necessarily a tuning fork. Flat or complex formed 3D objects are manufactured, too. Important examples under research are the “wine-glass gyroscopes” using a domed shape.

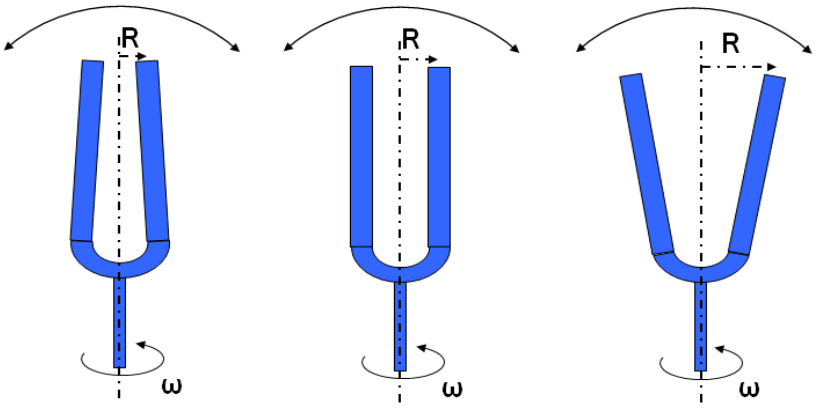

Figure 5-4: Oscillation of the Coriolis vibrating gyroscope (CVG)

If a constant rotation rate is considered, the oscillating proof masses have the correct tangential or angular velocity only in the base position. When they move outside that position, their tangential velocity is too slow for the current radius to the rotation axis. If they move inside that position their

tangential velocity is too high for the current radius. The results of these velocity mismatches are acceleration forces, which deflect the proof masses perpendicular to the oscillation direction and the rotation axis. This is depicted in Figure 5-5.

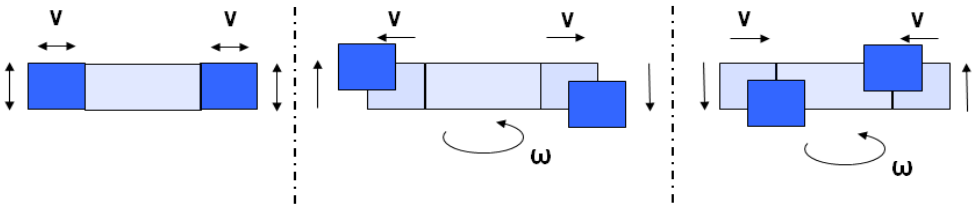

Figure 5-5: Basic function of the Coriolis vibrating gyroscope (CVG)

MEMS sensors are manufactured from silicon raw material called dies. They are manufactured in an etching process, therefore manufacturing costs are low and the manufacturing accuracy is high. Due to the properties of silicon, the main error source of MEMS sensors are temperature induced errors. The sensor noise is considered higher than for classical or optical sensors. Also the bias variation, especially the turn-on-turn-on bias variation, tested in the so called “tombstone test” ([102]), is considered a major error source that is very hard to calibrate for. Apart from the performance, the form factor of the sensors, the price and, lastly, the power consumption are strong points of this sensor class.

5.2.4 Selection of inertial sensors

When inertial sensors shall be used for pedestrian navigation, several properties become limiting factors beside the pure performance related properties. Some of these properties are:

- Size of the sensor
- Weight of the sensor
- Power consumption
- Interfaces
- Availability

Since there is a large variety of sensors and manufacturers available on the market, a survey of the instruments accessible at the Institute of Space Technology and Space Applications (ISTA) at the University of the Federal Armed Forces Munich has been performed. Most of the analyzed sensors can be seen in Figure 5-6. The sensors cover the most important sensor types and give a good overview of the sensors available on the market.

Figure 5-6: Evolution of inertial navigation measurement units over more than five decades. Sample of units from around 1960 to 2010

The following IMUs have been available for analysis:

- The **Litton/LITEF LN-3** represents the platform type class: two mechanical gyroscopes (2 DoF) and three accelerometers are suspended in a structure of four gimbals, which allow full 3d rotation of the sensors with respect to the carrier vehicle. The fourth gimbal is used to avoid the “gimbal lock” effect. The LN-3 uses two mechanical gyroscopes of DTG type. The unit was introduced in the German air force with the F-104G aircraft in 1960.
- The **Sagem Sigma 30** is a modern high performance strapdown IMU using three ring-laser gyroscopes (RLG) of high accuracy, often referred to as “navigation grade IMU”. The RLGs are optical gyroscopes. RLGs are considered as more accurate than fiber-optic gyroscopes, but

larger and mechanically more complex. The price range for a single unit of the RLG class must be considered above 100.000 €.

- The **Litton LN-200** (today Northrop Grumman LN-200) is a medium accuracy IMU using fiber-optic gyroscopes (FOG) and silicon accelerometers. The LN-200 is part of a family of IMUs which has been successfully integrated, e.g. into several military missile systems ([118], [57]). The LN-200 has a superior form factor in its class and has a very compact, rugged design. The price range for a single unit of the FOG class must be considered above 25.000 €.
- Five additionally evaluated IMUs are of MEMS type. The **BEI Systron Donner MotionPak** and the **Boeing DQI** (Digital Quartz IMU) are early MEMS IMUs. Characteristic is the quite large volume compared to modern MEMS IMUs. The **Xsense MTi** and **MTi-G**, as well as the **Memsense NANO IMU** can be considered as current units at the time of writing. The price range for single IMUs of the MEMS class, including development kit if available, is in the magnitude of less than 3000 €. OEM versions have a lower price of at least one order of magnitude.

The physical properties of the units can be found in Table 5-1.

Manufacturer	Instrument	Type	Weight [kg]	Length [mm]	Width [mm]	Height [mm]
Litton/LITEF	LN-3/P200	DTG IMU	13.62 (30 lbs)	363	248	~ 240
Sagem	Sigma 30	RLG IMU	19.4	410	260	255
Litton	LN-200	FOG IMU	0.7	ø 85	ø 85	85
Boeing	Boeing DQI	MEMS IMU	0.96	90	82	97
BEI Systron Donner	Motion Pak	MEMS IMU	0.89	75	75	90
Xsense	MTi-G	MEMS IMU	0.068	58.7	57.9	33
Xsense	MTi	MEMS IMU	0.05	58.7	57.9	23
MEMSense	NANO IMU	MEMS IMU	0.015	46.5	22.9	13.9

Table 5-1: Overview of the physical properties of current inertial measurement units (IMUs) of various technologies

The properties summarized in Table 5-1 show that the sensor technology has a large influence on the size and weight of the sensor units. Gimbaled/platform systems are very large and heavy and therefore not suitable for pedestrian users. The RLG based Sagem Sigma 30 is even heavier, while integrating computer systems, too. Due to the high system price RLG based systems cannot be considered suitable for mass market applications like pedestrian navigation.

FOG based IMUs can achieve form factors which make them suitable for pedestrian navigation. Nevertheless, the size and weight would still be inconvenient for the average user, while the high power consumption of more than 15W would require heavy battery systems to achieve reasonable operation times. The price of FOG units, although lower than the previous high accuracy sensor systems, is still not adequate for pedestrian users in general use cases. Furthermore it must be noted that high accuracy IMUs are usually ITAR regulated goods and procurement can therefore be difficult and time consuming, which limits the availability of the sensor.

The MEMS type sensors combine a very compact form factor with low sensor weight and low power consumption. The prices for the sensors are comparatively low and can be expected to decrease

even further due to high production numbers and applications in the future. OEM versions without casing and with custom data connections are available and the sensor can be tailored to the specific needs. Many MEMS sensors are available on the market and most of them are not ITAR regulated which increases availability. Hence, MEMS type sensors are most suitable for pedestrian navigation.

5.2.5 Demonstration of MEMS sensor performance

In this chapter the performance of MEMS IMUs shall be demonstrated by two simple bench tests. It is not the goal to perform a full sensor calibration, but to show the basic sensor behaviour and the range of sensor errors. Beside the positive factors like size, weight and costs, the major drawback of MEMS sensors is the sensor accuracy. MEMS sensors are known to have significant error budgets and a lack of stability. Their parameters also change significantly with the sensor temperature. For those reasons, quite large errors are to be expected while levelling. Gyro compassing is not applicable to MEMS gyroscopes due to their lack of resolution. The earth rate is approximately $7.29*10^{-5}$ rad/s and therefore far below the sensor resolution, the sensor biases and the sensor noise levels. A Xsens MTi IMU has been used for the test.

The first test has been executed to demonstrate the temperature sensitivity and the performance of the internal calibration of the IMU. The unit was stored at room temperature for several hours and kept static during the test. Immediately after powering of the unit, the raw inertial measurements of the gyroscopes as well as the internally calibrated measurements were recorded and analyzed. On the left hand side of Figure 5-7, the uncalibrated measured rotation rates are presented. Obviously all three channels show a bias of up to 0.2°/s, as well as significant sensor noise. The bias is decreasing after several minutes of runtime. This effect is characteristic for MEMS type sensors and can be demonstrated with other models of MEMS sensors as well. The reason for the bias drift is the increasing sensor temperature after powering the unit. When the sensor temperature reaches a static level after several minutes of operation, the sensor bias also stabilizes.

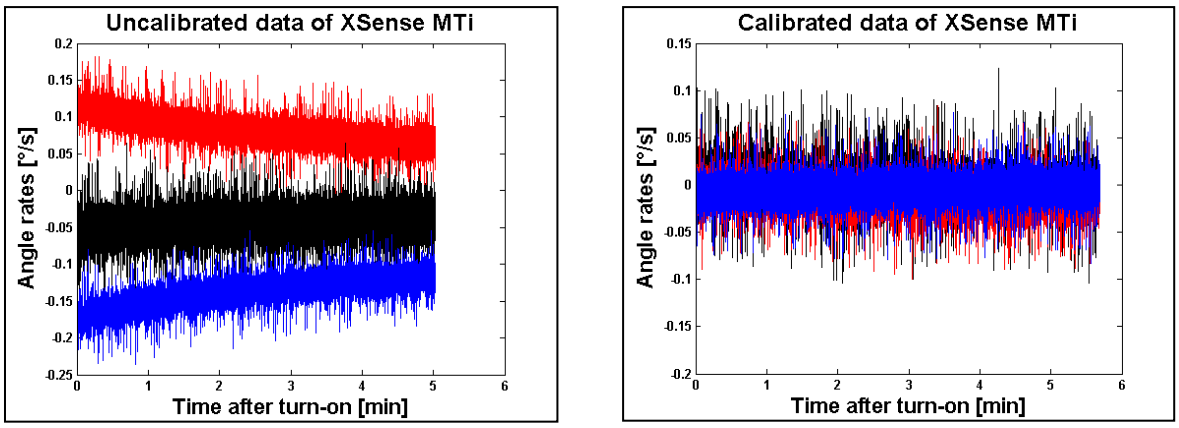

Figure 5-7: Comparison between calibrated and uncalibrated sensor data from MEMS IMU. The effect of temperature compensation is obvious.

On the right hand side of Figure 5-7, the internally calibrated measurements are presented. The temperature influence is cancelled in this dataset. It is clearly discernable that the factory calibration of the sensor with respect to temperature improves the sensor accuracy strongly. The noise cannot be reduced without filtering, which would limit the sensor dynamic range. The fact that the sensor bias could be reduced so strongly in this test can nevertheless not be expected in general, as the bias

is subject to certain turn-on-turn-on variations. This phenomenon is referred to as the “tombstone test” in [102].

In the second test, the unit has been mounted on a three-axis rate table. The unit was rotated for each individual axis and for various angular speeds from -135°/s to +135°/s in steps of 45°/s.

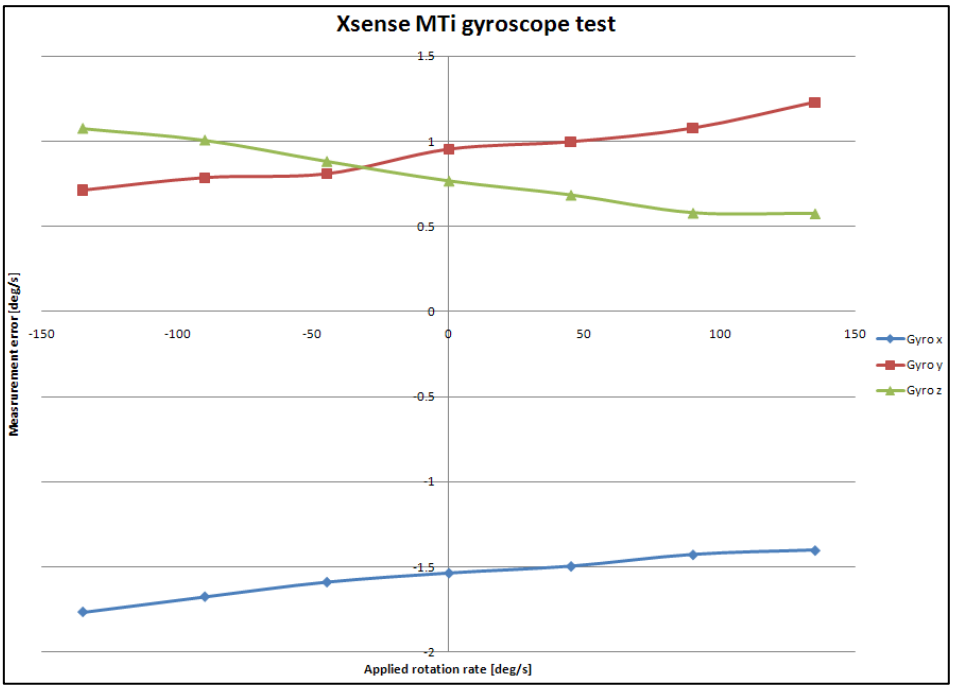

Figure 5-8: Rate table test of the Xsens MTi MEMS IMU gyroscopes, showing the measurement errors versus the applied rotation rate

The results of this test are presented in Figure 5-8. Evidently, the measurements are subject to a certain bias (value at zero applied rotation rate), as well as a scale factor error. The scale factor error causes the measurement graphs to resemble slanted lines. While the scale factor errors stay below 0.18 % for the range of 270°/s, the bias takes values of up to 1.6°/s and is therefore significantly higher than in the previous test.

In summary, the tested MEMS showed good temperature compensation by factory calibration and thus eliminated one of the largest IMU errors. Classical sensor errors like bias and scale factor errors could be demonstrated during the rate table test. These errors also vary from mission to mission and hence cannot be fully calibrated in the factory.

5.2.6 Summary

In this subchapter, inertial sensors , i.e. gyroscopes and accelerometers, have been introduced. The physical principles of the sensors were presented and different types of inertial sensors have been introduced. Finally, MEMS sensors were selected as adequate sensors for pedestrian navigation. Their performance has been demonstrated and discussed using one unit (Xsens MTi) as representative example.

5.3 Pedometer and Pedestrian Navigation System

A pedometer is a system which detects, classifies and counts steps. The pedometer is most often a special application of inertial sensors and exploits the kinematic properties of the walking motion to identify the step pattern in the inertial measurements. In contrast to INS, the accelerations and rotation rates do not necessarily have to be integrated. If the pedometer is combined with heading information, a Pedestrian Navigation System (PNS) can be formed, a dead reckoning system which propagates the user position by step and heading.

While climbing, crawling, jumping and swimming are possible ways of locomotion, pedestrian users most often move by walking, i.e. performing of one or several consecutive steps. The steps are performed in a certain direction and the real user position is propagated by the **step cycles** in the desired direction. If this **motion** shall be **exploited for navigation** purposes, the applicability of inertial sensors is evident: Inertial sensors measure accelerations and rotation rates, which are important aspects of the gait cycle. Two processing schemes are mentioned in literature. One is based on step detection and position propagation in a step, stride and heading approach (e.g. in [48]). The other on is a classical INS processing using phases of the gait cycle for zero velocity updates. In the classical INS approach, the quality of the navigation performance is strongly dependent on the sensor accuracies and the processing algorithms. Often the classical mechanization of a strapdown Inertial Navigation System (INS) does not provide sufficient stability and accuracy for a PNS using low-cost sensors like MEMS type IMUs. This is mainly due to the error behaviour of low-cost MEMS sensors (accelerometers and gyroscopes) and has also been discussed before e.g. in [21], [51] and [56]. The main error sources are the low-cost gyroscopes, which inhibit precise attitude determination and therefore precise gravity cancellation. There are applications of foot-mounted IMUs, which use zero-velocity updates (ZUPT) to stabilize an INS implementation ([5]). However, mounting on the shoe is often impractical or even inhibited by safety at work regulations, and shoe mounted INS can give additional problems, too, e.g. by the strong acceleration peaks.

If mounting of the IMU on the shoe is not considered, PNS systems often do not integrate the measured accelerations, but detect steps, estimate step length and heading and provide dead reckoning by estimating the actual position on the basis of the last known position and the change by the steps counted. Since no integration is performed and position changes are only estimated when steps are determined, no time dependent error is to be expected by this. The actual heading is to be determined by the integration of the gyroscopes' output or is derived by the observation of a magnetic compass. Thus, there can be a heading drift due to the gyro drift or heading errors due to magnetic disturbances. This can lead to a time dependent position error, which is, however, much smaller than in the classical integration.

The PNS system consists of four major elements:

- Step detection
- Step classification
- Stride estimation
- Heading determination

This type of navigation system will be described in detail in chapter 7.

5.4 Magnetometer

The determination of heading is a crucial part of dead reckoning navigation. One important way of determining the heading is the evaluation of the magnetic field of the Earth. Sensors measuring magnetic fields are called magnetometers. If the devices are specifically designed for heading determination, they are referred to as compasses. While early compasses used a magnetized needle pivoted in its center, modern devices use electrical effects to measure the magnetic field.

Classical instruments in aeronautics are the fluxgate and the Hall-effect sensor. In the last few years, a new type of sensor has been developed which has entered the low-cost market quickly. The sensor type is based on the Giant-Magneto-Resistance effect (GMR) and can be seen as a parallel to the MEMS type inertial sensors. GMR sensors use several very thin sheets of magnetized and non-magnetized layers with a thickness of some nanometers. According to the direction of applied magnetic fields, the electrical resistance of the sensor packages changes strongly. This change of resistance is used to determine the magnitude of the magnetic field in the sensitive direction. By using three orthogonal sensors in a bundle, the magnetic field vector can be determined. The discovery of the GMR effect has been awarded with the Nobel Prize in Physics in 1998 [122]. GMR magnetometers are very low-cost, light-weight and small-size sensors and are integrated today in many low-cost MEMS IMUs, e.g. in the IMU used mainly in this thesis, the Xsens MTi ([114]). They seem ideal for pedestrian navigation due to their size, weight, power consumption and pricing. The sensor noise is apparently extremely low.

Several error sources must be considered when using magnetometers for the determination of heading. Heading is defined with respect to the North-axis of the navigation or Earth fixed frame. Since the magnetic North Pole and the geographic North Pole do not coincide, there is an offset between the magnetic and the geographic North. This effect is called “variation” or “declination” depending on the field of application. The declination for a given location can be found in official geodetic tables, its magnitude varies with time and position.

Figure 5-9: Declination as difference between geographic and magnetic North at the campus of the University of the Federal Armed Forces of Munich [123]

In Figure 5-9, the declination at the location of the University of the Federal Armed Forces Munich is shown. The compass rose shows the direction of the magnetic North. The magnitude at the time of calculation was about 1°56’.

While the declination is simple to compensate, other effects on the measured magnetic field are much more severe and hard to correct. The distortion of the measured magnetic field by ferro-magnetic elements or devices next to the compass is referred to as “deviation” in navigation. In recent publications, the terms “hard- and soft iron effects” are frequently mentioned. In modern applications, the influence of the carrier (vehicle) and the installation have to be calibrated in calibration campaigns or in-run calibration routines. While constant disturbances like the deviation can be corrected easily, local disturbances in the proximity of the user are hard to identify and to correct. If the Earth magnetic field is overlapped by local magnetic fields, the compass does not “point” magnetic north anymore, but the vector sum of the Earth magnetic field and the disturbance. The result can be large heading errors.

Most severe error sources are magnetic fields in the navigation environment of the sensor. For indoor navigation these could be electrical wiring, steel reinforcements in concrete walls and ceilings, radiators and many more. These error sources cannot be calibrated since they are principally unknown at the start of navigation, but their influence is severe. To overcome these errors the plausibility of the measurements as well as the compass results must be checked continuously. Especially in the indoor domain these disturbances can be found very often. The use of magnetometers as sole means of heading determination must therefore be avoided.

5.5 WLAN

Wireless local area networks (WLAN) are radio networks developed to connect personal computers and peripheral devices without using cables as physical connection. The most common implementations are based on the IEEE-802.11 standard and its sub-standards (a, b, g, n, ac, ad), using the Ethernet technology ([125]). However, it must be noted that other standards and hardware implementations, e.g. ZigBee, exist, while being not as common in the commercial aspect as the IEEE standard. The precise specification of the standard can be found in the standard IEEE802.11.

WLAN has been used for positioning in several applications and publications, most often for indoor navigation in business or office buildings. Especially modern smartphones use WLAN maps for rough positioning. For that reason, the available WLAN networks and hotspots have been surveyed and their presence gives indication about the rough user position. Since the individual networks and their components do not offer highly precise time synchronization, ranging like in GNSS is not adequate for positioning. Therefore, the received signal strength (RSS) becomes the most important magnitude. More precise algorithms often use a technique called “fingerprinting”.

If the RSS is mapped for several WLAN access points (AP) in a dense net of calibration points, a WLAN RSS map is created. If the actually measured RSS of all APs in sight are compared to this map, the current position can be estimated. This procedure is called fingerprinting. Basically, the measured **set of RSS values** forms a “**fingerprint**”. This fingerprint is compared to a database of previously recorded fingerprints at surveyed locations (calibration points). If the measured fingerprint matches

a database point entry significantly well, the position of this database point is used as user position. Usually, the algorithms allow only the position fixing to the surveyed calibration points, not between the calibration points. Hence, the resolution of the position fixing can be limited to the density of the net of calibration points. Developments by ISTA also focused on positioning between the calibration points. Detailed information can be found in [101] and [100].

Figure 5-10: Typical WLAN equipment as used in the thesis

Two major errors of fingerprinting based positioning are:

- the selection of the false calibration point
- the coarse resolution due to an insufficiently dense net of calibration points

The major drawbacks of fingerprinting are the extremely high calibration and re-calibration efforts and the large influence of the environmental aspects and the room geometry. To achieve a good resolution, many calibration points have to be surveyed, e.g. one per square meter. It is obvious that the costs of calibration would be immense for large buildings. Additionally, if the room geometry or the placement of the WLAN APs would change, e.g. due to new furniture or new WLAN equipment, the calibration would have to be repeated.

Moreover, the RSS map of the building to be navigated in must show a certain degree of "uniqueness", i.e. the RSS fingerprints must be significantly different for the various calibration points. If this is not the case, it becomes very difficult for the algorithm to find the corresponding fingerprint and the risk of false detection is very high. The uniqueness of the RSS map is increasing with the complexity of the room geometry and the number of APs in the rooms. So, for example, a square room with only very few symmetrically oriented APs with identical transmitted power would be very unfavorable for fingerprinting, while a room with complex geometry and many APs in non-symmetrical placement would be very favorable for positioning.

Since it is not guaranteed that the building to navigate in has been calibrated thoroughly, in this thesis a different approach is used. In this thesis, a RSS based proximity positioning system has been developed, which gives position updates if the user approaches an AP. The updates are only available when the user is in close proximity of the AP. Nevertheless, the calibration effort is very low, the algorithm is extremely robust, and the update has a very high accuracy. The algorithms will be described in chapter 9.

5.6 Barometer

The determination of the vertical positions is a classical task of geodesy, survey and aeronautical navigation. When navigating in buildings, the determination of the current storey is a very important factor, in some applications the most important one. Besides, indoor navigation also has a strong need for measuring the user's absolute altitude with respect to the used frame. The determination of the altitude is performed by sensors called altimeters. They can use different principles of determining the vertical position, e.g. laser ranging, radar ranging, ultra-sonic ranging or the evaluation of atmospheric pressure. Basically, it must be distinguished between relative and absolute determination of the vertical position. The altitude reference must be considered carefully.

Barometers are sensors measuring air pressure. If it is assumed that higher atmosphere layers press on lower atmosphere layers with their own weight, the relationship between pressure and altitude can be modeled and calculated. This relationship is the basis of barometric altimetry. A model for a differential element of the atmospheric layers can be seen in Figure 10-1, in which the mathematical model for the air pressure distribution is analyzed. Since the atmospheric air pressure is decreasing with increasing altitude, the air pressure can be used as an important reference for altitude.

One problem of barometric altimetry is the fact that the air pressure is not only dependent on the altitude, but also the current weather situation, i.e. the pressure on sea level and the temperature. The pressure at certain altitudes can be modeled; the most important model is the International Standard Atmosphere (ISA). Since the pressure distribution is also dependent on the temperature profile for different altitudes, one major component of the ISA is the averaged temperature distribution with altitude. In aeronautics, the pressure on sea level is therefore determined and published in the weather report (so called QNH value). If each aircraft in a certain region uses the same sea level pressure on their instruments, they all have the same model based altitude errors. Sensor errors, nevertheless, directly transform to the altitude errors of the sensor.

Classical barometers were manufactured by using evacuated tins of thin metal sheets in combination with mechanical gears. The deformation of the tins with increasing or decreasing pressure was transformed into the motion of the instruments needle. The gear transmission is non-linear and adjustable to the current pressure and weather situation. Today, MEMS technology is used for barometers, too. The basic concept of a low pressure cavity and deformation due to environmental pressure is maintained, while being strongly miniaturized. In contrast to the classical systems, the deformation is measured by a MEMS sensor and directly transformed to voltage, which is then A/D converted. By dedicated model equations, pressure can be derived from these sensors. MEMS barometers are extremely small, lightweight and low-cost. An example of this technology can be seen in Figure 10-4. MEMS barometers are well suited for pedestrian navigation.

A detailed analysis about barometric altimetry, the MEMS pressure sensor and the use for pedestrian navigation will be given in chapter 10.

5.7 Additional indoor positioning sensors

Several other indoor positioning sensors and techniques have been proposed in literature. **Optical sensors** or **IR-beacons** are mentioned in [54][49], [55], [29], [41] and [76]. The use of **WLAN** positioning is discussed in [100], [101] and [85]. **Walking path detection**, the use of **GIS systems** and **path constraints** like walls etc. are mentioned in [55], [14] and [85]. **RFID** systems are mentioned in [48] and [29]. UWB positioning is mentioned in [48]. Several of these techniques have also been studied at the University of the Federal Armed Forces Munich. Since the scope of the presented research is limited, not all kinds of sensors and positioning systems could be included. Some of them shall nevertheless be mentioned for sake of completeness.

Radio frequency identification systems (RFID systems) are used for many commercial applications, e.g. ID cards, entry cards, theft protection systems in shops, logistics, and many more. The technology is mature and has fully entered the market and can be used for positioning. Generally, the user carries a RFID tag, which incorporates active or passive electronic components. When passing RFID readers, the system can identify the tag identity of the user passing by and therefore provide position information to the user. The technology seems very promising, but has certain drawbacks. First of all, the area for navigation has to be equipped with RFID readers in a reasonable dense network to provide a significant number of position updates. It cannot be expected that this infrastructure is present everywhere, and there must be a control center to register, survey and operate all used RFID readers. Additionally, a data link to the user is necessary to provide him with position data. The availability of the position information is therefore reduced and the requirements regarding infrastructure are high.

Optical navigation systems cover optical beacons, camera feature detection, laser ranging and many more. The tracking of optical beacons and optical feature detection are passive systems. The main idea is to detect optical landmarks in the near environment to calculate the azimuth and elevation of the user relative to these landmarks. By intersection of these lines of sight, the user can calculate the position. Other methods cover the correlation of the captured picture with a database. Both systems have the drawback that the environment has to be recorded before the navigation part, and that changes in the optical appearance require new recording and survey. Laser ranging can be effectively used to locate the user within rooms. The accuracy is excellent and the sensor is additionally suited for simultaneous localization and mapping (SLAM) applications. In SLAM, the user is on the one hand side able to georeference detected features in space, which creates and continuously expands a map of the surrounding features. On the other hand side it is possible to analyze the user motion, i.e. position and attitude changes relative to the detected features. This information can then be used as a (relative) position update. Hence, SLAM navigation systems have a feature detection algorithm, a feature matching algorithm and algorithms to calculate the relative user motion with respect to the features. SLAM itself can be implemented e.g. as an extendend Kalman filter. The drawback of the laser sensor is the large size of the sensor, the weight, the power consumption and the price. Hence, laser ranging is not ideal with respect to calibration efforts, ubiquitous positioning and equipment weight and size.

Ultra-Wideband positioning systems (UWB) are radar systems with an active user tag. The user tag sends very short RF pulses, which are registered by several receiver stations using Time Difference Of Arrival (TDOA) or Angle Of Arrival (AOA) methods or combinations of both to calculate the user

position. Ultra-wideband refers to the ultra high bandwidth (BW) of the RF signal, which has by definition a BW larger than 500 MHz or by other definition at least half of the frequency as BW. Often the pulse itself is extremely short. A commercial product is offered e.g. by Ekahau for pedestrian users. The system offers high accuracy and low drift, but requires high investments in infrastructure as well as an intensive calibration of the environment to achieve good performance. Naturally, navigation is only possible inside UWB equipped buildings.

5.8 Application oriented sensor suite

As described in the previous chapters, many sensors can be used for indoor navigation and it is necessary to focus on a limited set of sensors for limitation of cost, energy supply, the complexity of algorithms and the required infrastructure in the individual scenario. Additionally it could be shown, that there is no single sensor that could perform positioning well in all kinds of indoor navigation scenarios. Therefore the choice of sensors is very important for the performance, applicability and cost of an indoor navigation sensor suite.

The following points were considered for the choice of sensors:

- Positioning shall be possible seamlessly in indoor and outdoor environments.
- Costly infrastructure in the building shall be avoided. Only wireless network communication systems should be used since they are present in most buildings today.
- High sensitivity GNSS shall be possible by precise user trajectory replication.
- A tradeoff between system autonomy and taking advantage of additional position fixes and attitude reference must be found.

Hence, the following sensors have been selected:

- **GNSS receiver:** The NavX-SR GNSS receiver, a software receiver produced by IfEN GmbH is used as adjustable and enhanced HS-GNSS receiver. This receiver has been chosen because it is a real time capable software receiver which is especially flexible and can be modified for the individual use case. It allowes the access to the tracking algorithms using APIs which is necessary to integrate the replica generation described in the following chapters. By extension of the coherent integration time superior high sensitivity performance shall be realized.
- **INS:** A MEMS type inertial measurement unit will be used for PNS and trajectory replications with high resolution and high relative accuracy. The IMU has the capability to monitor the antenna motion with high frequency and high short term accuracy. The Xsens MTI IMU will be used as sensor for several reasons. This IMU offers an internal attitude reference (AHRS) and offers several different options for attitude representation. The interface to the unit can be used easily and the provided drivers and code snippets make intergration easier. The temperature calibration is mandatory for the intended use and the unit offers magnetometers, which reduce the number of sensor systems.
- **Magnetometers:** Small GMR type magnetometers will be used as heading reference, while sophisticated calibration and integrity checking is necessary. Magnetic heading can be used to initialize and stabilize the inertial heading. The magnetometers are integrated in the used IMU. A basic problem of using MEMS IMUs for inertial navigation is the heading determination since gyro compassing will in general not work with low-cost sensors. Hence, an additional source for heading determination is very useful.
- **Barometers:** A MEMS type barometer will be used as altitude reference. Initial test were done with an analog sensor, which required an A/D converter. Finally, the Bosch BMP085 has been chosen because of the digital interface and the good temperature calibration.
- **Wireless LAN:** A **WLAN proximity positioning system** for position updates in previously surveyed environments will be used based on commercial IEEE 811.11 standards consisting

of a rover WLAN USB stick and several WLAN access points. The system can provide position updates in WLAN equipped indoor environments. Although systems with external infrastructure demands should be avoided, an exception is made for WLAN, since it can be assumed to be present in most (office) buildings today and the use does not cause additional costs.

- **External systems:** Additional position updates can be received from the **INPOS** positioning system by Telespazio Italy, working with ZigBee motes instead of WLAN access points. Precise timing will be available by a precise OCXO oscillator and network based time transfer.

A general idea was to use sensors and sensor systems with high practical relevance, while the system cost should be limited. The used infrastructure should be common technology, that could be found public or office buildings. The used sensors should be commercial of the shelf technology, while low-cost sensors were preferred.

Radar systems like UWB are too expensive to be found in common buildings, while it must be admitted that the accuracy is excellent. Additionally, each used room would have to be equipped which causes very high cost. RFID can also not be considered to be found in a great number of buildings, while giving precise position updates when crossing. Optical systems will not be used due to the high calibration efforts and eventually high sensor cost, together with the high computer load of optical navigation.

It is the goal of this sensor suite to overcome the individual drawback and weaknesses of the individual subsystems and to exploit the positive properties of each. The GNSS receiver will be used as main overall navigation sensor, while the IMU will be the main sensor for antenna “micro-trajectory” reconstruction, and PNS dead reckoning. With PNS processing, low drift relative positioning can be achieved. The low data rate of the PNS will be enhanced by AHRS/INS processing of the IMU raw data. The magnetometer, as well as the barometer, the WLAN positioning and GNSS updates will be used to correct the errors of the inertial sensors and the AHRS/INS processing. Finally, the GNSS software receiver shall be enabled to integrate coherently GNSS signals with up to two seconds of coherent integration time to achieve supreme HS-GNSS capabilities. The complete sensor suite and the user equipment can be seen in Figure 7-6 and Figure 11-1. The system integrated receiver platform architecture is shown in Figure 11-2.

5.9 Summary

In the previous chapter, a wide range of different techniques and sensors for positioning with special focus on indoor positioning have been described. While each system offers different properties, it could be shown that no single system is capable of seamless indoor/outdoor positioning with the required availability and accuracy. While many sensors and techniques seem appropriate for indoor navigation, many sensors are too expensive, too large or otherwise not suited for pedestrian navigation. Others require expensive infrastructure which cannot be expected in common buildings. Finally, a sensor suite for the given scope has been defined. The algorithms and techniques for these sensors will be described in the next chapters. Generally, it is the scope to combine the positive properties of all sensors to achieve the required system performance.

6. INS

Inertial Navigation Systems (INS) are special cases of dead reckoning navigation, using accelerometers and gyroscopes as ('inertial') navigation sensors. "Inertial navigation involves a blend of inertial instrumentation, mathematics, control system design, and geodesy. The technology is used in many military, civilian, engineering, and scientific activities."[11] Inertial navigation facilitates autonomous navigation, providing instantaneous and autonomous position, velocity and attitude information.

Inertial navigation represents a crucial element of this thesis. It has been used for the precise and continuous reproduction of the user antenna motion, which represents the key technology for the implementation of very long coherent GNSS signal integration. As will be shown in this chapter, inertial navigation is strongly affected by sensor errors. If low cost sensors with usually high sensor errors are used, classical navigation algorithms fail. Thus, for the replication of user motion the classic INS algorithms had to be modified and the actual duration of sensor integration had to be shortened to few seconds.

Due to the importance of INS for this thesis, the basics of inertial navigation will be described in the following chapter. Crucial elements are:

- the physical principle of INS
- the coordinate frames and transformations
- the mathematical attitude representation

Finally the processing of the transformed acceleration and the position, as well as velocity derivation will be discussed. Since the implemented algorithm for position and velocity derivation in the user motion replication differs from classic algorithms, the thesis will outline these parts only shortly. The different sensor types and their properties will be discussed and illustrated by measurements performed with the inertial measurement units (IMUs) present at the Institute of Space Technology and Space Applications. In addition to that, also the error propagation in inertial navigation will be discussed.

6.1 Introduction

Inertial navigation has been developed due to the need of instantaneous, autonomous, high integrity positioning. It is a dead reckoning system. Predecessors are instruments like the gyro compass, and early attitude control systems for aircraft and missile control. The development of inertial sensors is strongly related to the work of several outstanding developers. Some of them are:

- Johann Gottlieb Friedrich von Bohnenberger, the inventor of the "Bohnenberger machine" of 1817, which is the direct predecessor of the gyroscope
- Jean Bernard Léon Foucault and his "gyroscope" from 1852
- Hermann Anschütz-Kaempfe and his "Gyrocompass" from 1907
- Maximilian Schuler, an employee of Anschütz-Kaempfe and inventor of the "Schuler Tuning" ([91])
- Elmar Sperry, a contemporary of Anschütz-Kaempfe, who developed gyrocompasses in the USA as a contemporary of Anschütz-Kaempfe and as a direct competitor.

Early applications of inertial instruments and navigation can already be found at the German A4/V2 missile developed in the late 1930s. The first implementation of a fully operational inertial navigation system for military application was the navigation system for the USS Nautilus, a submarine using nuclear power. The Nautilus was able to operate submerged for significant time. This raised the need for autonomous navigation. The INS deployed on the Nautilus was of a gimbaled type and allowed even polar crossing, a problem of local level frame implementations. One of the most prominent representatives of INS application is the Apollo spacecraft, which used inertial navigation systems to navigate from Earth to the Moon.

The basic problem of autonomous navigation systems is the fact that the position and velocity of the navigation unit or user usually cannot be measured autonomously by common physical phenomenon. Optical navigation systems, which use landmarks or stars as reference, could provide position information, but are not independent since the direct line of sight to the reference objects is needed. They cannot be used in all weather conditions and environments, especially indoors. Speed could be measured by odometers, logs or pitot pipes. However, odometers are not well suited for all kind of users, and logs as well as pitot pipes are dependent on the external information on the stream of the fluid they are used in, which is water or air.

Pedestrian navigation differs significantly from the applications described above. For the pedestrian user, it is unpractical to carry voluminous and heavy navigation instruments. All instruments must be small size and lightweight, since they should not restrict the daily activities. However, the pedestrian user has individual requirements to its navigation system. While 1 nmi accuracy after one hour is a very good accuracy for an aircraft INS, this accuracy is unacceptable for a pedestrian user. On the other hand, the dynamics of the pedestrian user, the velocity and the covered range are strongly limited compared to aircraft and missiles. Hence, INS algorithms and instruments must be adapted to be useful for the pedestrian user.

The development of micro electro-mechanical system (MEMS) technology reduced the size, weight, power consumption and the price of inertial sensors dramatically. This allows INS technology to be applied to the pedestrian user. The drawback of MEMS sensors is the strongly reduced accuracy compared to classical instruments like FOG or RLG systems. To apply INS to the pedestrian user using MEMS technology, a strategy to reduce the INS drift must be found. It is worth consideration to deviate from classical INS processing techniques, and to use motion constraints and systems like the step detection and PNS to reduce the INS drift and the system dynamics, while increasing the accuracy for this special application. This topic will be discussed in detail later in the chapters 7-11.

6.2 Basic properties of inertial navigation

As mentioned before, it is difficult to measure position by autonomous means. The measurement of velocity can also be difficult, e.g. in the vacuum of space. But even if position and velocity are difficult to measure directly, the second derivative of the position, i.e. accelerations, can be measured according to Newton's second law by measuring the force acting on a proof mass:

$$\vec{F} = m\vec{a} \tag{1}$$

$$\vec{a} = \frac{\vec{F}}{m} \tag{2}$$

Symbol	Explanation
$\vec{F}$	Vector of force
m	Mass
$\vec{a}$	Vector of kinematic acceleration

Table 6-1: Symbols used in Newton's second law of motion

Since acceleration is the derivative of velocity, and velocity is the derivative of position, the position can basically be calculated by double integration of the measured accelerations. Instruments measuring accelerations are called accelerometers. By the double integration of the acceleration, firstly the velocity change and secondly the position change could be calculated. An Inertial Navigation System (INS) is therefore formed by the combination of an inertial measurement unit (IMU) and a navigation computer performing the complex kinematical computations.

Nevertheless, several aspects hamper the direct integration of measured accelerations:

- Due to Einstein's rule of equivalence, the accelerometers cannot distinguish between gravitational forces and kinematic accelerations.
- According to Newton's law of gravitation, the gravitational force decreases with increasing distance between the mass centers of the proof mass and the Earth. This is, in other words, the altitude.
- The accelerations must be measured, or at least be transformed and expressed, in the desired frame of navigation to allow direct integration.
- Therefore, the current attitude of the IMU with respect to the navigation frame of the system must be known.
- If not navigating in the inertial frame only, several pseudo-forces are acting on the sensors and must be compensated. These forces are the Coriolis force, the centrifugal force and the Euler force.
- The initial conditions of velocity and position must be known to solve the integrals, as well as the initial attitude.
- Inertial instruments determine acceleration and rotation rates with respect to the inertial frame, but expressed in the sensor or body frame. If the navigation is performed in an individual navigation frame, the rotations and acceleration between the inertial and the navigation frame, as well as the orientation differences must be considered.

6.2.1 Accelerations and specific forces

As a result of his work on the relativity theory, Albert Einstein discussed the principle of equivalence ([15], [16], [17]). In this work, he described the equivalence of gravitation and kinematic acceleration.

Due to Einstein's principle of equivalence, the accelerometers cannot distinguish between gravity and kinematic acceleration. This means that the accelerations, measured by the accelerometers in the body frame, must be corrected for gravity in order to result in the measured kinematic accelerations.

$$\overrightarrow{f^b} = \overrightarrow{a^b} + \overrightarrow{g^b} = \ddot{\overrightarrow{r^b}} + \overrightarrow{g^b} \tag{3}$$

If the calculations are performed in the inertial frame, the system equations using a direction cosine matrix (DCM) implementation:

$$\ddot{\overrightarrow{r^i}} = C_b^i \overrightarrow{f^b} + \overrightarrow{g^i} \tag{4}$$

$$\dot{C}_b^i = C_b^i \Omega_{ib}^b \tag{5}$$

$$\Omega_{ib}^b = \begin{bmatrix} 0 & -\omega_z & \omega_y \\ \omega_z & 0 & -\omega_x \\ -\omega_y & \omega_x & 0 \end{bmatrix} \tag{6}$$

$$C_b^i = C_e^i C_n^e C_b^n \tag{7}$$

$$C_b^n = \begin{bmatrix} \cos\Theta\cos\Psi & -\cos\Phi\sin\Psi + \sin\Phi\sin\Theta\cos\Psi & \sin\Phi\sin\Psi + \cos\Phi\sin\Theta\cos\Psi \\ \cos\Theta\sin\Psi & \cos\Phi\cos\Psi + \sin\Phi\sin\Theta\sin\Psi & -\sin\Phi\cos\Psi + \cos\Phi\sin\Theta\sin\Psi \\ -\sin\Theta & \sin\Phi\cos\Theta & \cos\Phi\cos\Theta \end{bmatrix} \tag{8}$$

$$C_n^e = \begin{bmatrix} -\sin\varphi\cos\lambda & -\sin\lambda & -\cos\varphi\cos\lambda \\ -\sin\varphi\sin\lambda & \cos\lambda & -\cos\varphi\sin\lambda \\ \cos\varphi & 0 & -\sin\varphi \end{bmatrix} \tag{9}$$

$$C_e^i = \begin{bmatrix} \cos\alpha & \sin\alpha & 0 \\ -\sin\alpha & \cos\alpha & 0 \\ 0 & 0 & 1 \end{bmatrix} \tag{10}$$

The Table 6-2 gives a reference to the symbols used in the equations above.

Symbol	Explanation	Unit
f	Specific force	[m/s²]
ω	Rotation rate	[rad/s]
Φ	Roll (Euler attitude angle)	[rad]
Θ	Pitch (Euler attitude angle)	[rad]
Ψ	Yaw (Euler attitude angle)	[rad]
ϕ	Geodetic latitude	[rad]
λ	Geodetic longitude	[rad]
α	Angle between the zero meridian and the vernal equinox (ω*t)	[rad]
F	Absolute force	[N]
G	Gravitational constant	[m³/(kg*s²)]
M	Mass of the Earth	[kg]
m_1	Proof mass	[kg]
R_0	Mean Earth radius	[m]
r	Radius	[m]
ω_s	Schuler frequency	[s^{-1}]

Table 6-2: Symbols used in the INS equations

Gravity can be derived from models and tables and must be propagated for the altitude and local variations. If the proof mass of the accelerometer and the Earth are modeled as point masses, and the geometry is reduced to a scalar case, Newton's law of gravity can be written as:

$$F = -G\frac{m_1 m_2}{r^2} \tag{11}$$

If the equation is vectorized, it can be written as:

$$\vec{F} = -G\frac{m_1 m_2}{|\vec{r}|^3}\vec{r} \tag{12}$$

The force F can be reduced to the specific force f, which yields:

$$\vec{f} = \frac{\vec{F}}{m_1} = -GM\frac{\vec{r}}{|\vec{r}|^3} \tag{13}$$

It is also interesting to examine the change of the specific force with the increasing distance of the centers of gravity. For the scalar case again, the following relation can be derived:

$$\frac{df}{dr}(r = R_0) = 2GM\frac{1}{R_0^3} = \frac{g_0}{R_0} = \omega_s^2 \tag{14}$$

Astonishingly, the derivative has the magnitude of the square of the Schuler frequency.

If local values are used to determine the gravity with eq. (14), the resulting acceleration is slightly higher than the expected normalized Earth acceleration. This effect is caused by the centrifugal forces produced by Earth rotation, which must be considered for calculating gravity.

The centrifugal forces can be calculated by:

$$f_{centr} = \omega_E^2 R \tag{15}$$

If the local latitude and the direction of the centrifugal forces are considered, the centrifugal forces perpendicular to the local level frame can be estimated as:

$$f_{centr} = \omega_E^2 R \cos\varphi \tag{16}$$

It is obvious that there are navigation frames which are advantageous for applying the gravity corrections. One of those frames is the local level navigation frame (index n). In the local level frame, the z-axis points to the mass center of the Earth, it is fixed on the current location of the user on the Earth surface and the x-axis points in the direction of the North Pole. The y-axis forms a right handed coordinate frame. The origin and influence of the pseudo-forces can be demonstrated if the kinematics in the local level frame is analyzed. If the position vector r in the form of equation (4) is differentiated twice to result the acceleration, the following result is obtained:

$$r^i = C_n^i r^n \tag{17}$$

$$\dot{C_n^i} = C_n^i \Omega_{in}^n \tag{18}$$

$$\dot{r^i} = C_n^i \dot{r^n} + \dot{C_n^i} r^n = C_n^i \dot{r^n} + C_n^i \Omega_{in}^n r^n \tag{19}$$

$$\begin{aligned} \ddot{r^i} &= C_n^i \ddot{r^n} + \dot{C_n^i} \dot{r^n} + \dot{C_n^i} \Omega_{in}^n r^n + C_n^i \dot{\Omega_{in}^n} r^n + C_n^i \Omega_{in}^n \dot{r^n} = \\ &= C_n^i \ddot{r^n} + 2C_n^i \Omega_{in}^n \dot{r^n} + C_n^i \Omega_{in}^n \Omega_{in}^n r^n + C_n^i \dot{\Omega_{in}^n} r^n \end{aligned} \tag{20}$$

$$\ddot{r^i} = C_n^i \left(\ddot{r^n} + 2\Omega_{in}^n \dot{r^n} + \Omega_{in}^n \Omega_{in}^n r^n + \dot{\Omega_{in}^n} r^n \right) \tag{21}$$

The first term in the brackets on the right hand side of equation (21) represents the kinematic acceleration of the point mass expressed in the inertial frame. The second term on the right hand side of (21) is called Coriolis acceleration. The third term represents the centrifugal force. The fourth term is called Euler acceleration. These additional acceleration components are caused by the non-static, rotating (navigation) frame. Those components must generally be considered when performing inertial navigation in the local-level frame. It must be noted that especially the Euler acceleration term is extremely small.

As the transformation matrix C_n^i is calculated by integrating its own derivative, further requisites can be stated:

- Gravity in the navigation frame must be known.
- The initial condition of C_n^i must be known.

The initial attitude state, represented in the transformation matrix C, is determined by an algorithm called alignment. The rotation rate matrix Ω must be determined continuously. The gyroscopes of the IMU are used to measure the rotation rates.

The **basic** steps in the standard strapdown algorithm, neglecting several others for the sake of clarity, are:

- Measurement of the specific forces and rotation rates in the body frame
- Update of the attitude angles in the navigation frame due to rotation rate measurements in the body frame and transport rate due to the user's movement
- Transformation of the measured accelerations in the navigation frame
- Correction of the accelerations for the gravity influence
- Correction of the accelerations for pseudo-forces
- Double integration of the accelerations in the navigation frame

It is obvious that errors of the measurement of the specific force will be integrated twice and thus will produce fast growing position errors. But even more impressive are the errors induced by erroneous gyroscope readings. They induce erroneous platform orientations and, as a result, erroneous measurements of specific forces and gravitational acceleration as well as insufficient gravity corrections. If the absolute value of the gravity of nearly 10 m/s² is considered, the induced position error can be estimated. Analysis will be given in chapter 6.8. A mathematical simulation of the INS errors is described in chapter 18.4.

Before starting the strapdown algorithm, the initial attitude angles need to be initialized. In classical instruments this is performed by levelling and gyro-compassing. Levelling means the determination of the horizontal plane by observation of the gravity vector. As a result the attitude Euler angles Φ and θ (roll and pitch) can be estimated. Gyro compassing determines the geographic North direction by the observation of the measured earth rotation rate and is capable of estimating the heading angle Ψ. In several filter steps these estimations are refined and allow a platform orientation with high accuracy. The algorithms will be described in detail in chapter 6.6.

6.3 Reference frames in Inertial Navigation

Coordinate frames have a high importance in all kinds of inertial systems. Some reasons for this are:

- There are frames which can exploit certain natural or mathematical properties, e.g. the direction of gravity or the direction and relative position to fixed points or non-holonomic constraints in vehicle navigation ([14]).
- Measurements are taken in the sensor frame.
- Measurements are related to a second frame, even if they are expressed in the sensor frame, e.g. rotation rate with respect to the inertial frame expressed in the body frame.
- Gravity is by definition parallel to the z-axis in the navigation frame. Hence, deduction of the gravity component from the measured specific forces is very simple in the navigation frame.
- Navigation is often performed in a local level navigation frame, even if the position is finally needed in a global frame.
- Local frames allow simplifications, while the position is often useful only in global frames.

In the following, the most important frames for inertial navigation will be discussed. The choice of frames for the individual application and mechanization will be discussed in the next chapter.

Inertial frame (I-frame)

The inertial frame was defined by the German physicist Ludwig Lange in 1885. Basis for the definition was the analysis performed by Newton, Galilei, Mach and several other physicists ([53]). Therefore, Newton's laws play an important role in the definition of the inertial frame and appear in the inertial frame in their simple form. Lange defined the inertial frame as:

„Inertialsystem heißt ein System von der Beschaffenheit, dass mit Bezug darauf die in einem Punkt zusammenlaufenden, stetig beschriebenen Bahnen dreier gleichzeitig von demselben Raumpunkte projizierter und sofort sich überlassener Punkte (die aber nicht in einer Geraden liegen sollen) sämtlich geradlinig sind. "[53] (quoted in [24]).

The definition includes the first law of Newton, that bodies remain static or move as straight lines with constant velocity if no accelerations act on them. In detail, the inertial frame is assumed to be not accelerating and not rotating. According to Paul Savage, the inertial frame is a "non-rotating inertial coordinate frame used as reference frame for angular rotation measurements". [15]

The enormous relevance of the inertial frame in inertial navigation is the fact that gyroscopes measure the rotation rates in the body frame with respect to the inertial frame. Therefore a gyroscope which is static in an Earth fixed frame would still be measuring the Earth rotation rate with respect to the inertial frame. Since positions are often expressed in the Earth fixed frame, the Earth rotation rate must be compensated, otherwise large errors would occur.

While theoretically simple, it is difficult to find a realized frame that follows the definition of an inertial frame. A realization would be to place the origin of the realized inertial frame in the mass center of the sun while pointing one of the axes in a fixed direction in space. This realization is close to the definition, but is not very convenient for practical use. A more practical approach is the Earth Centered Space Fixed (ECSF) frame. Its origin is the mass center of the Earth. The z-axis points to the North Pole, while the x-axis points towards the vernal equinox, a fixed direction in space. The y-axis forms a right-handed frame. Therefore, the frame is moving, but not rotating with the Earth. Strictly speaking, it is not un-accelerated since the rotation around the sun is an accelerated movement. As the numerical eccentricity of the Earth orbit is only around 0.0167, the orbit can be approximated as circular and the acceleration is compensated by the centrifugal force. Hence the ECSF frame can be approximated as inertial frame.

Earth centered Earth fixed (ECEF) frame (E-frame)

The Earth centered Earth fixed frame is mostly used to express the user's position on a global scale. Its origin is located at the geometrical center of the Earth, its z-axis points to the North Pole. The x-axis lies in the equatorial plane and intersects the Greenwich meridian. The y-axis forms a right-handed frame. The ECEF can be used as Cartesian and as polar coordinate frame. In the polar form, the position is expressed as latitude, longitude and altitude. In the ECEF frame it is possible to relate the actual position with global maps and global landmarks. It is most suitable for global geolocation and global references. The ECEF is strongly related to models of the geometric form of the Earth, as well as to a specific geoid model. The most widely used model and most important realization of the ECEF system is the World Geodetic System of 1984 (WGS 84). It contains an ellipsoid model, a geoid model (EGM 96), and is established and maintained by using many georeference stations around the

world. It has been established by the US Department of Defense and the National Geospatial-Intelligence Agency (formerly National Imagery and Mapping Agency) ([69], [20]). The fact that WGS 84 is the reference frame for GPS is very important for navigation.

User positions are mostly expressed in the ECEF. Since navigation is often performed in local navigation frames, the transformation of coordinates, the orientation and the origin of the local navigation frame in the ECEF must be determined and maintained during the navigation operations. The ECEF rotates around its z-axis with respect to the pseudo-inertial ECSF system. The orientation with respect to the ECSF system is therefore determined by time and rotation rate of the Earth. To maintain the transformation matrix, a precise knowledge of time is crucial. This also reflects one of the oldest problems in ship navigation, known as “longitude problem”.

Body or sensor frame (B-frame)

The body frame is a frame bound to the user or, in many cases, to the vehicle of interest. In strapdown INS, the body frame is often realized as the coordinate system of the inertial measurement unit, and therefore located in the (virtual) center of the inertial sensor installation. The axes are defined by the axes of the sensor triad. Since navigation is usually not performed in the body frame, a simple, standardized transformation to the navigation or ECEF frame is used.

Since the mechanical parts of gimbaled systems can be avoided, the strapdown approach allows very compact, light-weighted IMUs and is therefore especially suited for applications with strict physical limits (weight, size, power consumption, etc.), like in pedestrian navigation.

Local level navigation frame (N-frame)

The local level navigation frame has high relevance for local navigation, i.e. navigation in close proximity to a specified origin. It is often established at the starting point of the trajectory calculation. The N-frame is a frame tangential to the geoid. Therefore, the z-axis is parallel to the local gravity vector that points downwards to the Earth center. The x-axis usually points towards the geodetic North Pole, while the y-axis points east. This right-handed frame has certain advantages:

- As the frame is tangential to the geoid, gravity can be compensated by the simple deduction of the local gravity of the z-axis accelerometer reading. Thus, one of the important problems of INS can easily be implemented by other means.
- If 2D dead reckoning navigation is performed, the results can easily be compared with the INS position. This is particularly useful for PNS and combinations of PNS and INS.
- Navigation in geometrically limited areas, like buildings and factories, can be performed by very simple processing.
- The results can be interpreted easily.

However, if large distances are covered, the N-frame must be re-initialized, i.e. the origin and orientation have to be adjusted to the new position and attitude. Hence, the transformation of the N-frame to the E-frame basically changes constantly.

6.4 Mechanization of sensors

As discussed before, one of the major problems of INS is to separate gravity acceleration from kinematic acceleration. This separation can only be performed if the magnitude and direction of gravity can be predicted precisely. Gravity has been measured by geodesists for centuries and is modeled e.g. in the geoid model EGM 96. Since gravity acts in the z-axis of the local level navigation frame, the separation is very simple in the N-frame. As the accelerations are measured by the accelerometers and therefore in the body frame, two basic approaches exist to construct an INS:

- The sensors are always kept oriented along the navigation frame by a mechanical gimbal system, which makes the B-frame orientation equal to the N-frame orientation with respect to the E-frame: **platform system**
- The sensor readings are mathematically transformed from the B-frame to the N-frame, whereas the orientation of the sensor assembly must be monitored and expressed mathematically: **strapdown system**

Since powerful computers were not available in the early years of INS (around 1950-1970), the first implemented INS were platform systems with three dimensional gimbal systems. After initial alignment, the gyroscope measurements as well as the transport rates from the navigation computer were used to adjust the platform orientation directly to the chosen reference frame. Accordingly, the attitude of the accelerometer and gyroscope assembly is maintained approximately level and can be retrieved by pickups at the gimbals. This approach reduces the computational load dramatically and could also be implemented in analog technology. The accelerations can be integrated directly after gravity, Coriolis and centrifugal force correction. A typical example of this technology can be seen in Figure 6-1. The Litton LN-3 INS uses three full gimbals and one additional limited yaw gimbal to prevent the gimbal lock effect. It was produced for the German air force version of the Starfighter, the F-104G. The unit uses mechanical two-degree-of-freedom gyroscopes of the Dynamically Tuned Gyroscope (DTG) type. Since the mechanical gyroscope can measure two perpendicular rotation rates, only two gyroscopes are needed. The upper gyroscope can easily be identified in Figure 6-1 by the orange heater stripes. The three accelerometers are mounted between the two gyroscopes in the middle of the inner gimbal assembly and are kept aligned with North and the local level plane. The accelerations can be measured directly in the navigation frame. Optional implementations for platform systems include the North-East-Down system, but also the wander-azimuth-system or a space-stable mechanization.

In the strapdown system, the sensors are mounted rigidly to the rover that shall be navigated. The sensors are ‘strapped-down’ to the rover. Strapdown systems development started around 1970, when computers with acceptable computing power appeared on the market and especially in aircrafts. “By year 2000, virtually all inertial navigation systems had become (or were retrofitted to) the strapdown type (an exception being ballistic missile guidance systems which continued to use gimbaled technology).”[87]

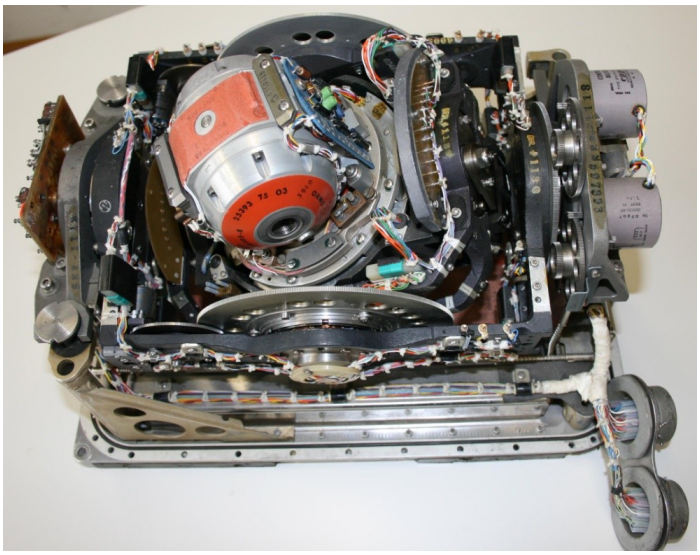

Figure 6-1: LITEF/Litton LN-3 platform INS system used in the F-104 G ”Starfighter”

The mechanical complexity of these systems is much lower than the platform systems, nevertheless the mathematical complexity is higher due to the fact, that the actual attitude between the body (and sensor) and the navigation frame has to be established, maintained and represented by geometric calculations. On the other hand, the sensors could be reduced in dimensions, weight and cost dramatically. An example of a medium accuracy strapdown IMU is shown in Figure 6-2. This unit is a LITTON LN-200 IMU (now Northrop Grumman), using three fiber-optical gyroscopes (FOG) and three MEMS accelerometers ([57]). The unit weights about 700 grams and has a volume of less than one liter. The photograph shows the size in comparison to a standard CD. The LN-200 is widely used in aeronautics, defense and research since 1994 and is still in production (2015). More than 20.000 units have been produced ([118]).

Figure 6-2: LITTON LN-200 strapdown IMU using Fiber-optical Gyroscopes (FOG)

In the following the focus will predominantly be on the strapdown system. The gimbaled platform systems will not be discussed in detail.

6.5 Attitude representation

It has already been mentioned that in strapdown systems, the attitude must be represented mathematically; the measurements must be transformed from the body frame to the navigation frame in order to be useful for navigation. In literature (e.g. [90], [8], [102], [75], [88]), several representations of attitude are discussed and illustrated. The representations mostly used in navigation applications are:

- Euler angles
- Direction Cosine Matrix DCM
- Quaternions

Moreover, the use of a representation using a rotation vector is often discussed, but not often found in navigation related publications.

Euler Angles

Euler angles represent the attitude of the body frame with respect to the local level navigation frame (NED) by using three angles: pitch, roll and yaw. The pitch angle θ defines the angle between the longitudinal axis of the body frame and the horizon. The roll angle Φ defines the angle between the cross axis and the horizontal plane; and the yaw angle Ψ defines the angle between the longitudinal axis and the North direction in the horizontal plane. Since they are so demonstrative, Euler angles are most often the basis for the evaluation of navigation algorithms, and also for the user interface.

The order of rotations and also the axis definitions are critical in this case, as the orientation of the two frames is constructed by using three consecutive rotations. The order of rotations and axis definitions are bound to the definition of the angles and vice versa. Special care must be taken if publications and documents from different origin are used since the order of rotation used might not be identical. Euler angles are the most intuitive form of attitude representation. A drawback is the fact that without any limitation of the angle range definitions, several sets of parameters could describe the same attitude. Thus, the angle range has been defined as in the “Luftfahrtnorm DIN 1300”:

Euler angle	Symbol	Range definition
Pitch	ϕ	]-90°;90°]
Roll	θ	]-180°;180°]
Yaw	ψ	]-180°;180°]

Table 6-3: Definition of Euler angle ranges

The order of rotations to transform from the local level navigation frame to the body frame has been defined to:

- First rotation yaw around local level perpendicular axis with magnitude Ψ
- Second rotation pitch around cross axis with magnitude θ
- Third rotation roll around longitudinal axis with magnitude Φ

DCM

The direction cosine matrix DCM is a rotation matrix that transforms vectors from one frame to the other, e.g. from the body frame to the navigation frame. It is constructed by the multiplication of three individual rotation matrices for each rotation. The rotation angles are the Euler angles and the rotation order is the same as in the definition of the Euler angles. Hence, the change of representation is very simple. The construction of the DCM from Euler angles is described in eq. (22).

$$C_b^n = \begin{bmatrix} \cos\Theta\cos\Psi & -\cos\Phi\sin\Psi + \sin\Phi\sin\Theta\cos\Psi & \sin\Phi\sin\Psi + \cos\Phi\sin\Theta\cos\Psi \\ \cos\Theta\sin\Psi & \cos\Phi\cos\Psi + \sin\Phi\sin\Theta\sin\Psi & -\sin\Phi\cos\Psi + \cos\Phi\sin\Theta\sin\Psi \\ -\sin\Theta & \sin\Phi\cos\Theta & \cos\Phi\cos\Theta \end{bmatrix} \quad (22)$$

The great advantage is that the transformation of a vector, e.g. acceleration or velocity from the body frame to the navigation frame and vice versa, becomes a simple matrix-vector product. While very convenient to use, the DCM representation also has some disadvantages. The first disadvantage is the fact that the backward transformation from DCM to Euler angles has singularities. If the last line of the DCM in (22) is used for re-transformation, the Euler angles can be calculated as:

$$\begin{aligned} \varphi &= \tan^{-1}\left(\frac{C_b^n(3,2)}{C_b^n(3,3)}\right) \\ \theta &= \sin^{-1}\left(-C_b^n(3,1)\right) \\ \psi &= \tan^{-1}\left(\frac{C_b^n(2,1)}{C_b^n(1,1)}\right) \end{aligned} \quad (23)$$

Since the convention for the pitch angle is between ±90°, the third formulation in (23) could produce non-conformant results. Therefore another implementation must be found to avoid this problem. In [88], the implementation is:

$$\theta = \tan^{-1}\left(\frac{-C_b^n(3,1)}{\sqrt{C_b^n(3,2)^2 + C_b^n(3,3)^2}}\right) \quad (24)$$

It is well-known that the denominator of a fraction is not supposed to become zero. Due to definition in (22) this would be the case for steep pitch angles of ±90°. Accordingly, workarounds must be found for such steep attitudes to result in acceptable pitch angle performance.

To show this effect, an AHRS algorithm was developed in Matlab. A test cycle has been recorded with the Xsens MTi MEMS inertial measurements unit. For the test, the unit was rotated along the roll, pitch and yaw axis consecutively for plus and minus 90°. The profile was calculated with the basic quaternion algorithm described below as reference and the unmodified DCM implementation. The test profile can be seen in Figure 6-3. The three separate, consecutive rotations can be identified easily. The unit returns to its original attitude at the end of the run. The rotations have been applied manually. It is not exactly known which internal attitude algorithm is used in the MTi IMU as reference. However, it is assumed that a quaternion based attitude reference is used, in combination with initial heading determination using magnetometers and stabilization of the attitude by observation of the gravity vector and the magnetic field vector. A similar approach has been implemented in the course of this thesis. Phases of very low dynamics have been used to evaluate

the gravity vector in the measured accelerations, and the results are matching the internal attitude very well. For this evaluation, no aiding information has been used. The algorithms developed for this test use the rotation rates as single information for propagating the attitude. The internal attitude is the reference for the evaluation of the individual implementations here.

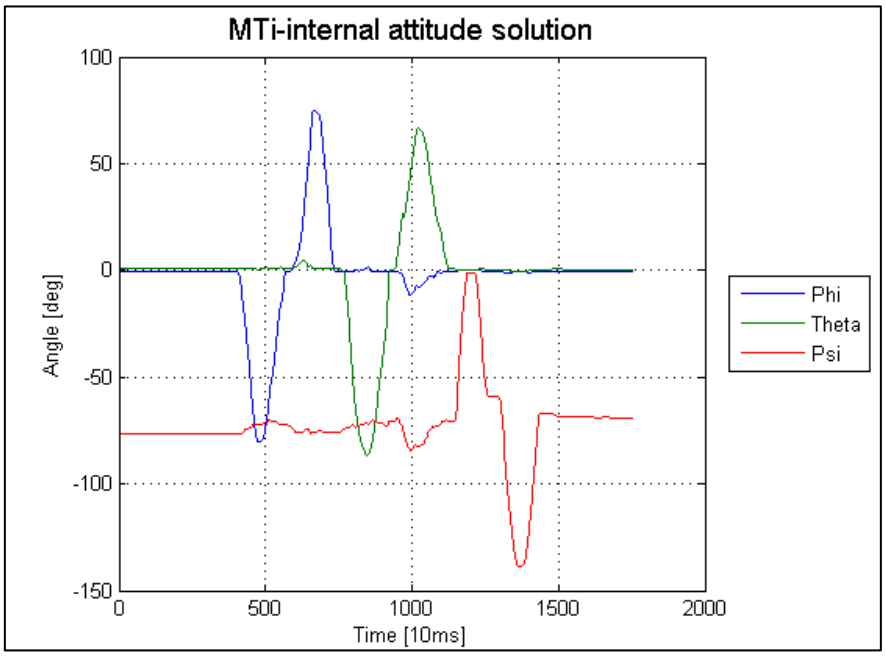

Figure 6-3: Test profile of the implementation test. Reference is the internal IMU attitude reference.

Figure 6-4 shows the attitude calculated with the simple DCM algorithm using the arcsine-relationship described in (23). The results are comparable to the quaternion implementation with the exception of situations when the pitch angle reaches magnitudes close to ±90°. The difference to the quaternion implementation will be presented later in Figure 6-7.

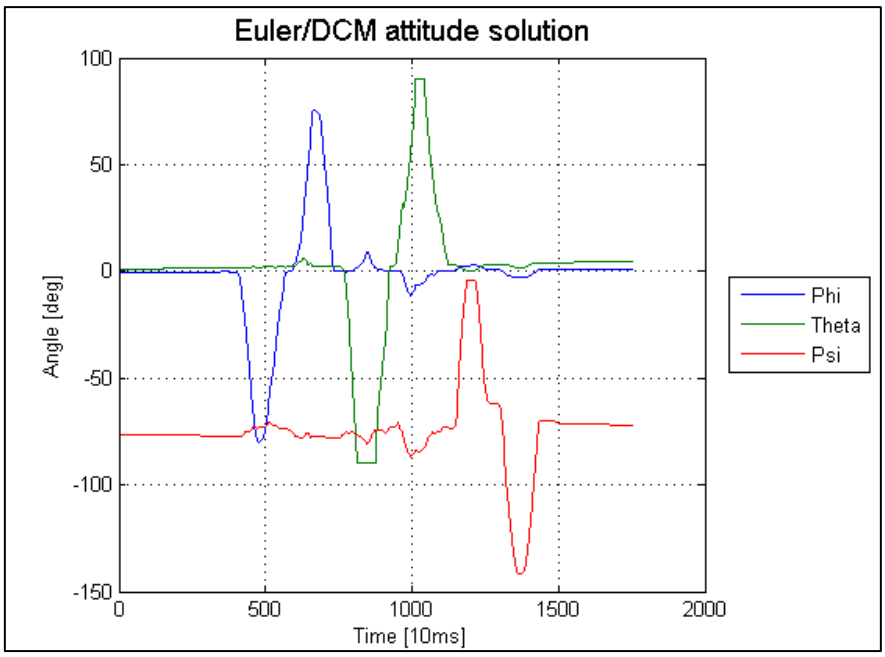

Figure 6-4: Attitude calculated with the DCM implementation

It must be noted that the calculated attitude is precise again shortly after the pitch maneuvers. This fact proves that the propagation of the attitude itself is not affected by this singularity. The problem is the re-transformation of DCM to Euler angles, which leads to the described problems.

The results for using the more complex implementation described in (23) are as presented in Figure 6-5, and later in Figure 6-8 versus the quaternion implementation. In the close vicinity of the singularity, the performance is comparable between both implementations. Only at the singularity itself, the more complex implementation switches the sign of the result, causing a 180° angular offset.

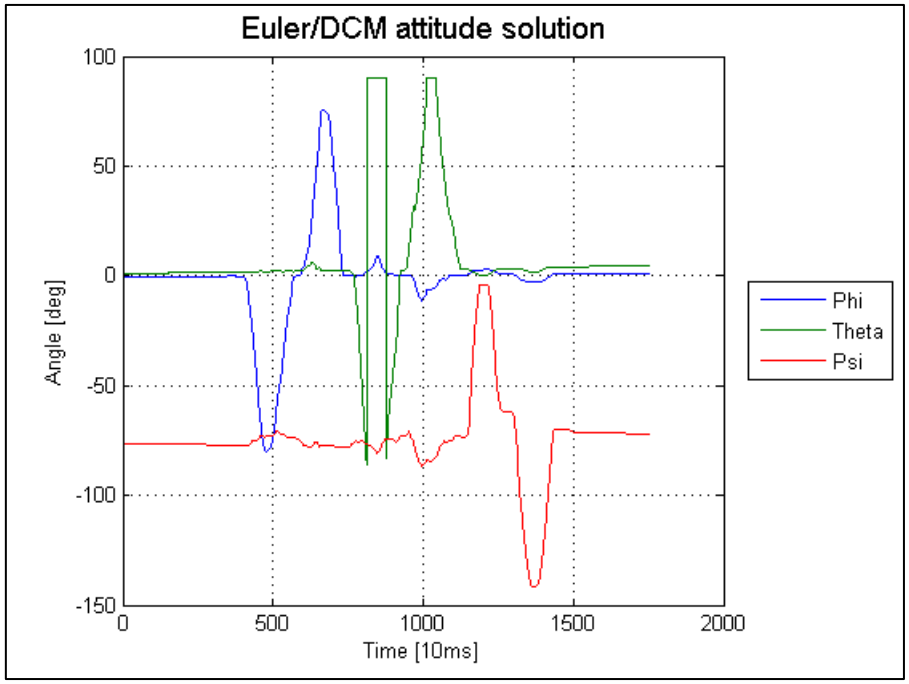

Figure 6-5: Attitude calculated with the improved Theta reconstruction Euler/DCM implementation

It must be noted that Matlab uses advanced error catching algorithms. Therefore imaginary parts of the re-transformation do not cause system crashes and are simply neglected when plotting the results. This must be considered when evaluating the results, especially those of the simple implementation. The results are therefore evaluated for a versatile and powerful math computational tool, not for general purpose programming languages like C++ or ADA, which are used frequently in operational applications. For Matlab, the more complex implementation does not offer advantages. While the results of the simple implementation are not valid at the singularity in a way that the pitch angle result is kept static at 90°, the results of the more complex implementation are not valid at the singularity due to erroneous sign of the results. The accuracy is poor for both implementations.

Quaternions

A different way of attitude representation is the use of so called quaternions. “Quaternions were developed [...] by W.R. Hamilton.”[11] Paul Savage describes the similarity between the quaternions and complex numbers ([88]). Quaternions are 4-element vectors and, as complex numbers, have an imaginary and a real part. In contrast to the two dimensional complex numbers, the quaternions

have one real type component and three imaginary components. In analogy to the "i" in complex numbers, the complex components are often referred to as "i", "j", and "k". While the real part of the quaternion represents the magnitude of rotation, the imaginary part describes the axis of rotation. The basic construction of the attitude quaternions, as specified by [102] and [88], is defined as follows:

$$q = \begin{bmatrix} q_0 \\ q_1 \\ q_2 \\ q_3 \end{bmatrix} = \begin{bmatrix} \cos\left(\frac{\phi}{2}\right) \\ \sin\left(\frac{\phi}{2}\right)\frac{\phi_x}{\phi} \\ \sin\left(\frac{\phi}{2}\right)\frac{\phi_y}{\phi} \\ \sin\left(\frac{\phi}{2}\right)\frac{\phi_z}{\phi} \end{bmatrix} \tag{25}$$

The conjugate complex of a quaternion is formed by inverting the components of the complex part.

It must be noted that the absolute value of the quaternion vector has to equal 1. This fact becomes obvious if the following equation is analyzed:

$$|q| = \sqrt{q_0^2 + q_1^2 + q_2^2 + q_3^2} = \sqrt{\left(\cos\frac{\phi}{2}\right)^2 + \left(\sin\frac{\phi}{2}\right)^2 \left(\frac{\phi_x^2 + \phi_y^2 + \phi_z^2}{\phi^2}\right)} = \sqrt{\left(\cos\frac{\phi}{2}\right)^2 + \left(\sin\frac{\phi}{2}\right)^2} = 1 \tag{26}$$

During the propagation of the quaternions, it is mandatory to maintain the unity length of the quaternions, which can be disturbed by the limited resolution of the numerical representation in computer systems.

The quaternion attitude representation and its back transformation have no singularities and thus offer excellent accuracy and reliability. On the other hand, quaternions cannot be easily interpreted and evaluated due to their complex nature. Although there are even implementations of quaternion based Kalman filters, the attitude will at a certain point finally be transformed back to the Euler angle domain. This back-transformation follows the equations:

$$\begin{aligned} \varphi &= \tan^{-1}\left(\frac{2(q_0 q_1 + q_2 q_3)}{q_0^2 - q_1^2 - q_2^2 + q_3^2}\right) \\ \theta &= \sin^{-1}\left(2(q_0 q_2 - q_1 q_3)\right) \\ \psi &= \tan^{-1}\left(\frac{2(q_0 q_3 + q_1 q_2)}{q_0^2 + q_1^2 - q_2^2 - q_3^2}\right) \end{aligned} \tag{27}$$

In Figure 6-6, the results of the quaternion implementation are shown. Despite a small drift of the attitude for the entire test period of 170 seconds the results match the internal attitude reference

very well. The kinematics could be reconstructed very precisely and no singularities could be identified.

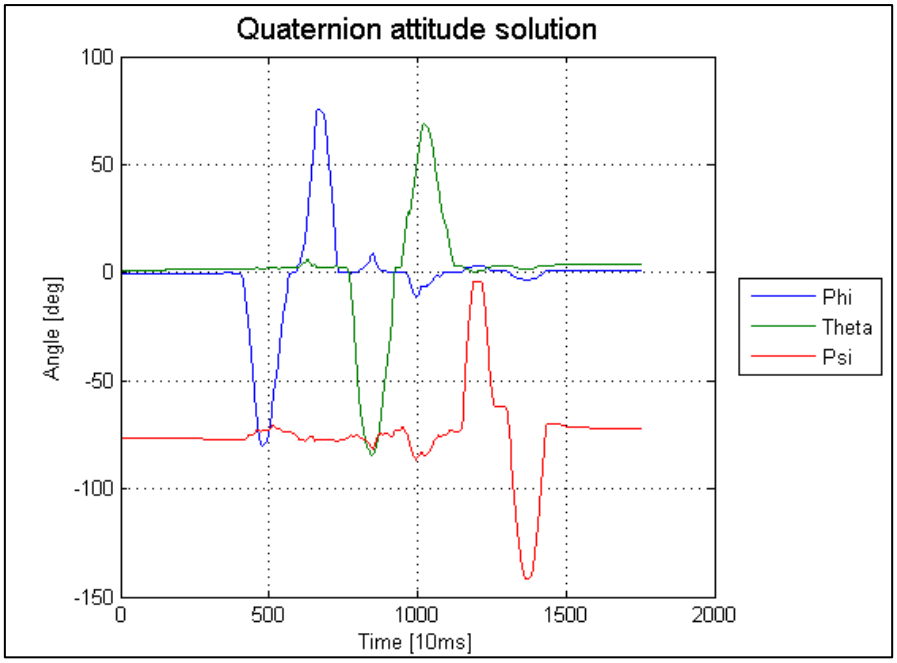

Figure 6-6: Attitude calculated with the Quaternion implementation

To evaluate the performance of the quaternion implementation versus the DCM algortihms, the attitude difference has been calculated. The attitude difference between the implemented simple DCM algorithm and the quaternion implementation is shown in Figure 6-7.

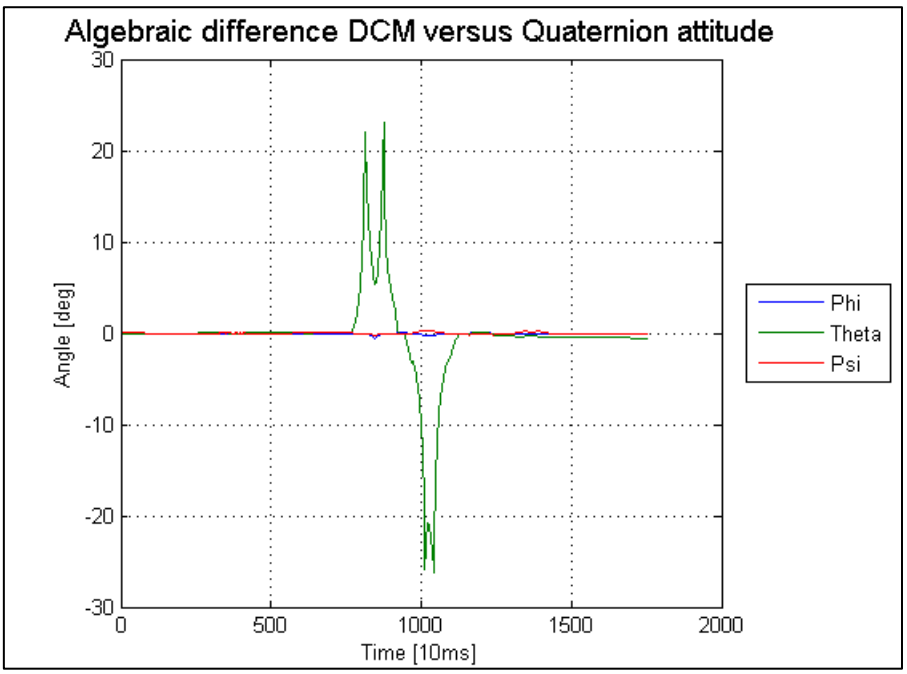

Figure 6-7: Difference between the resultant attitude parameters of the simple DCM and Quaternion implementation

The difference between the quaternion implementation and the DCM implementation with the more complex theta reconstruction is shown in Figure 6-8. Obviously the quaternion implementation performs much better than both DCM implementations and without singularities.

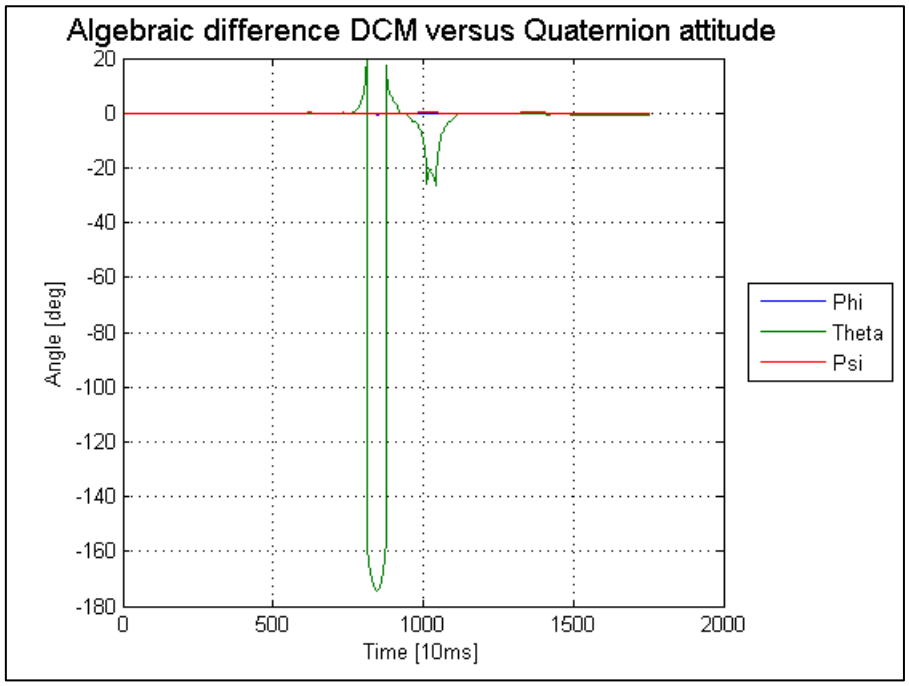

Figure 6-8: Difference between the resultant attitude parameters of DCM and Quaternion implementation for the alternative Theta reconstruction

6.6 Initial Alignment

The goal of the alignment procedure is to determine the attitude of the IMU with respect to the frame of choice at the beginning of the navigation period. Initial sensor error estimation may also take place at this stage. Basically, autonomous alignment and transfer alignment must be distinguished. Autonomous alignment is performed by observation of the Earth rotation rate and the gravity vector with the IMU. During this kind of alignment the IMU is required to stay static with respect to the ECEF frame. Transfer alignment is used if the unit is moving on a mobile platform, which itself has an already aligned IMU of mostly higher quality. The focus in this thesis will be on the autonomous alignment.

The initial alignment is usually performed in several consecutive steps. Pre-filtering may be used to exclude sensor noise or oscillations induced by vehicle vibrations. This filtering can be simple low pass filtering in order to separate the vibration spectrum from the actual carrier/IMU motion. The precise type of filter, as well as filter coefficients, pass band parameters etc. can be determined only, if the spectrum of the vibrations is known. It is, however, the goal of the pre-filtering to separate the rover motion from the induced vibrations. The influence of the vibrations on the attitude calculation shall be reduced while the tracking of attitude changes shall be fully maintained. This pre-filtering, mostly low-pass or band-pass filtering, is often performed e.g. by averaging, sliding window averaging, or Butterworth low-pass filtering. The intention is to exclude certain frequency components of the signal, which are outside the user dynamic envelope and are caused by disturbances like engine vibrations, Eigen-motion of the carrier vehicle or other effects which should not influence the navigation task.

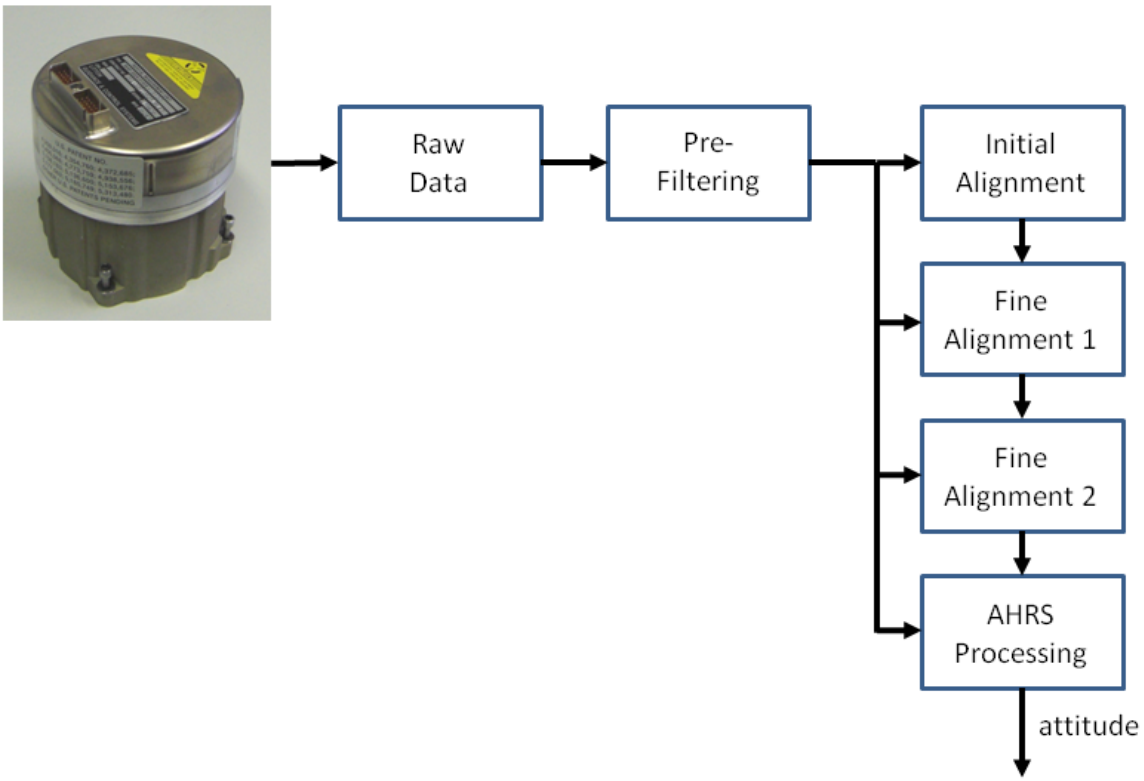

Figure 6-9: Consecutive steps of initial alignment

The first alignment step is called coarse alignment and is used to provide a first estimate of the current attitude. The second and third steps are called fine alignment and are used to estimate the residual errors of the coarse alignment. While coarse alignment as first step can be performed in a simple one-stage procedure, the fine alignment procedures are based on Kalman filtering and provide a refined estimation of the attitude errors.

Coarse Alignment

Algorithms for coarse alignment have been proposed by several authors, including C. Jekeli, D.H. Titterton and J.L. Weston [102] and P. Savage [88]. All approaches consider the same baseline:

- The algorithms use the Earth gravity vector and the Earth rotation vector as observables.
- The East direction is formed by the cross product of gravity and rotation rate.
- The transformation matrix C_n^b is filled with the observations.
- Euler attitude angles are calculated from the direction cosine matrix.

In accordance to the process of aligning platform INS systems the task of coarse alignment is divided into the sub-processes leveling and gyrocompassing. For leveling, it is defined that the local level navigation frame has its z-axis parallel to the gravity vector. If the IMU is static, the true accelerations are the result of the gravity only, since the kinematics are zero by definition. Thus, if the unit is rotated in a way, that the x- and y-axis accelerations become zero, the pitch and roll angle can easily be determined, while the yaw angle is not yet fixed. For gyrocompassing it must be noted that in the NED navigation frame, the Earth rotation rate appears only in the x- and z-axis by the frame definition and simple vector algebra. The rotation rate does not appear in the y-axis. If the unit is rotated until the y-axis rotation rate becomes zero and the x-axis rotation rate is positive, the unit is aligned with the navigation frame and therefore pointing North and the current yaw angle is zero. In Figure 6-10 the relationship between the Earth rotation, the gravity vector and the navigation frame are visualized.

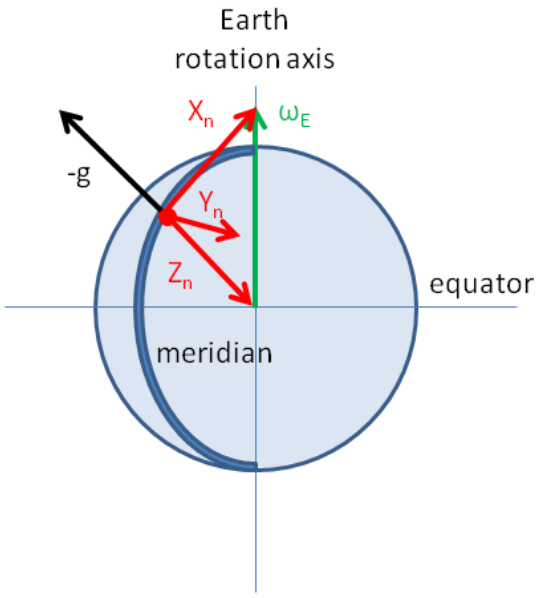

Figure 6-10: Graphical representation of the Earth and navigation frames at coarse alignment

If this practical approach for gimbaled platform systems is transferred to strapdown systems, the assumptions must be defined mathematically. The Earth rotation rate vector ω_{ie} and the gravity vector g are crossing each other in the Earth center. The gravity vector connects the current user position, which is also the (initial) center point of the local level navigation frame with the Earth center. Therefore, the gravity vector and the Earth rotation rate span a plane, which includes the meridian on which the user is located. The East direction is defined as perpendicular vector to the meridian plane with direction to the right. Hence, the East direction can be calculated by the vector cross product between the gravity vector and the Earth rotation vector. This cross product relationship is valid in any given frame and therefore also in the body frame of the IMU. This is illustrated in Figure 6-11.

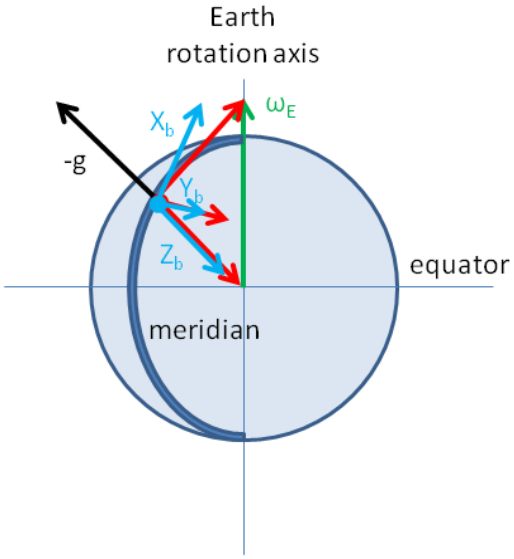

Figure 6-11: Specific forces and rotation rates in the ECEF (green), navigation (blue) and body (red) frame at coarse alignment

For all cross products, respecting the right-hand rule is crucial. The following approach has been described in [88]. The East direction in the body frame is formed as:

$$\overrightarrow{E^b} = \overrightarrow{-g^b} \times \overrightarrow{\omega_{ie}^b} \tag{28}$$

The down direction is defined by the gravity vector, thus it can be written as follows:

$$\overrightarrow{D^b} = \overrightarrow{-g^b} \tag{29}$$

The North direction is again defined as perpendicular to the East and the down direction.

$$\overrightarrow{N^b} = \overrightarrow{E^b} \times \overrightarrow{-g_b} \tag{30}$$

The direction cosine matrix from one frame to the other is defined by expressing the unit vectors of one frame in the axes of the target frame. Accordingly, after normalization, the calculated axes North, East and Down in the body frame can be used to fill a DCM.

$$\overrightarrow{E^b_{norm}} = \frac{\overrightarrow{E^b}}{\left|\overrightarrow{E^b}\right|} \tag{31}$$

$$\overrightarrow{N^b_{norm}} = \frac{\overrightarrow{N^b}}{\left|\overrightarrow{N^b}\right|} \tag{32}$$

$$\overrightarrow{D^b_{norm}} = \frac{\overrightarrow{D^b}}{\left|\overrightarrow{D^b}\right|} \tag{33}$$

The direction cosine matrix becomes then:

$$C^b_n = \left[\overrightarrow{N^b_{norm}} \quad \overrightarrow{E^b_{norm}} \quad \overrightarrow{D^b_{norm}}\right] \tag{34}$$

The transformation matrix C^n_b can be gained by inverting the matrix, which, in case of the DCM, is the transpose of the matrix. The Euler angles can be retrieved from the DCM by using the equations in (23) and (24).

Coarse alignment is not absolutely precise due to sensor errors. Consequently, coarse alignment is only a first step to allow linearization for Kalman filters.

Fine Alignment phase

The coarse alignment shall provide an initial estimation of the IMU's attitude. It is the goal of the initial alignment to achieve an estimation which is close enough to the real value to allow linear estimations for the refinement of the attitude estimation. The fine alignment is based on a two stage strategy:

- observing the Earth rotation over a certain period of time to refine biased attitude estimation
- integrate accelerations and rotation rates over a certain period of time during a zero velocity stage to refine attitude and gyroscope bias estimation

In both stages, a Kalman filter approach is often used. During the fine alignment no external information is used. The only prerequisite is that the IMU is kept static during the entire alignment phase, which includes coarse alignment, fine alignment with acceleration observation ("stage 1") and fine alignment with velocity observation ("stage 2"). The fine alignment terminates after a predefined time and switches over to normal AHRS processing immediately.

In fine alignment stage 1, the state vector has the following elements:

$$\vec{X} = \begin{bmatrix} \Delta\Phi \\ \Delta\Theta \\ \Delta\Psi \end{bmatrix} \tag{35}$$

Symbol	Explanation
$\Delta\phi$	Attitude error of the roll angle
$\Delta\theta$	Attitude error of the pitch angle
$\Delta\psi$	Attitude error of the yaw/heading angle

Table 6-4: Definition of the state vector of fine alignment with observation of accelerations

Since the IMU is required to be static, the only kinematic rotation rate is induced by the Earth rotation rate. If the IMU is not correctly aligned, i.e. the orientation estimation of the body frame with respect to the navigation frame is not accurate, the transformation of the measured quantities from the body frame to the navigation frame will be inaccurate. Hence the attitude in the navigation frame will drift due to incorrect attitude transformation and also due to sensor errors. This relationship is used in the prediction stage of the filter. The calculated accelerations in the navigation frame are used to estimate the residual attitude errors in the update stage.

The error propagation model is:

$$\frac{\delta}{\delta t}\begin{pmatrix}\Delta\Phi\\ \Delta\Theta\\ \Delta\Psi\end{pmatrix} = \begin{pmatrix}0 & -\omega_e \sin\varphi & 0\\ \omega_e \sin\varphi & 0 & \omega_e \cos\varphi\\ 0 & -\omega_e \cos\varphi & 0\end{pmatrix}\begin{bmatrix}\Delta\Phi\\ \Delta\Theta\\ \Delta\Psi\end{bmatrix} \tag{36}$$

Symbol	Explanation
$\Delta\Phi$	Attitude error of the roll angle
$\Delta\theta$	Attitude error of the pitch angle
$\Delta\Psi$	Attitude error of the yaw/heading angle
ω_e	Earth rotation rate
φ	Geographic latitude

Table 6-5: Symbols used in the fine alignment system equation

The filter observations are the horizontal accelerations in the navigation frame. Since the IMU is considered to be static, for the perfectly aligned IMU the accelerations in the horizontal plane should be zero. Measured accelerations are therefore the result of misalignment and sensor errors. The sensor errors are not determined yet at this alignment stage. The observation equation is:

$$\begin{pmatrix}\delta f_N\\ \delta f_E\end{pmatrix} = \begin{pmatrix}0 & g & 0\\ -g & 0 & 0\end{pmatrix}\begin{pmatrix}\Delta\Phi\\ \Delta\Theta\\ \Delta\Psi\end{pmatrix} + w \tag{37}$$

Symbol	Explanation
δf_N	Measured acceleration in North direction in the navigation frame
Δf_E	Measured acceleration in East direction in the navigation frame
$\Delta\Phi$	Attitude error of the roll angle
$\Delta\theta$	Attitude error of the pitch angle
$\Delta\Psi$	Attitude error of the yaw/heading angle
g	Earth gravity acceleration
w	Noise component of measurements

Table 6-6: Symbols used in the fine alignment observation equation

In the second stage of the fine alignment procedure, the measured accelerations are integrated comparable to standard INS processing. In contrast to the INS processing, the interest in position information and vertical velocity is low. The integration is used to calculate the estimated velocity components in the horizontal plane as well as attitude estimations. Using velocities instead of accelerations as observation yields a higher grade of precision. In this stage, the gyroscope bias errors can also be estimated to improve the following AHRS processing. The bias error is "[...] the average over a specified time of gyro output measured at specified operating conditions that has no correlation with input rotation or acceleration. Bias is typically expressed in degrees per hour (°/h)."[32] Physical and mathematical definitions can be found in [39]. It has a high impact on the results of the INS processing. A definition and models for the bias errors can be found in [35], [37] and [39].

The full state vector for the second stage of fine alignment is:

$$\vec{X} = \begin{pmatrix} \Delta\Phi \\ \Delta\Theta \\ \Delta\Psi \\ \Delta d_{GN} \\ \Delta d_{GE} \\ \Delta d_{GD} \\ \Delta V_N \\ \Delta V_E \end{pmatrix} \tag{38}$$

Symbol	Explanation
$\Delta\Phi$	Attitude error of the roll angle
$\Delta\theta$	Attitude error of the pitch angle
$\Delta\Psi$	Attitude error of the yaw/heading angle
Δd_{GN}	Gyroscope bias of the x-axis gyroscope
Δd_{GE}	Gyroscope bias of the y-axis gyroscope
Δd_{GD}	Gyroscope bias of the z-axis gyroscope
ΔV_N	Velocity error in North direction
ΔV_E	Velocity error in East direction

Table 6-7: Symbols used in the fine alignment (2) state vector

The system propagation is defined by the system matrix F:

$$F = \begin{pmatrix} 0 & -\omega_e \sin\varphi & 0 & -1 & 0 & 0 & 0 & \frac{1}{r} \\ \omega_e \sin\varphi & 0 & \omega_e \cos\varphi & 0 & -1 & 0 & -\frac{1}{r} & 0 \\ 0 & -\omega_e \cos\varphi & 0 & 0 & 0 & -1 & 0 & -\frac{1}{r}\tan\varphi \\ 0 & 0 & 0 & 0 & 0 & 0 & 0 & 0 \\ 0 & 0 & 0 & 0 & 0 & 0 & 0 & 0 \\ 0 & 0 & 0 & 0 & 0 & 0 & 0 & 0 \\ 0 & g & 0 & 0 & 0 & 0 & 0 & -2\omega_e \sin\varphi \\ -g & 0 & 0 & 0 & 0 & 0 & 2\omega_e \sin\varphi & 0 \end{pmatrix} \tag{39}$$

Symbol	Explanation
ω_e	Earth rotation rate
φ	Geographic latitude
r	Earth radius

Table 6-8: Symbols used in the fine alignment (2) system matrix

The integrated velocity estimates are considered as velocity errors because the IMU is supposed to be kept static during alignment. The same principle can be applied to the azimuth. Because the IMU is not supposed to rotate, a change in azimuth can be considered as rotation error and therefore be used as additional observation to estimate sensor errors. Consequently, the total observation equation reads as:

$$\vec{z} = \begin{pmatrix} \Delta V_N \\ \Delta V_E \\ \Delta Az \end{pmatrix} = \begin{pmatrix} 0 & 0 & 0 & 0 & 0 & 0 & 1 & 0 \\ 0 & 0 & 0 & 0 & 0 & 0 & 0 & 1 \\ 0 & 0 & 1 & 0 & 0 & 0 & 0 & 0 \end{pmatrix} \begin{pmatrix} \Delta\Phi \\ \Delta\Theta \\ \Delta\Psi \\ \Delta d_{GN} \\ \Delta d_{GE} \\ \Delta d_{GD} \\ \Delta V_N \\ \Delta V_E \end{pmatrix} + w \quad (40)$$

Symbol	Explanation
ΔV_N	Velocity error in North direction
ΔV_E	Velocity error in East direction
ΔAz	Attitude error of the yaw/heading angle
$\Delta\Phi$	Attitude error of the roll angle
$\Delta\theta$	Attitude error of the pitch angle
$\Delta\Psi$	Attitude error of the yaw/heading angle
Δd_{GN}	Gyroscope drift of the x-axis gyroscope
Δd_{GE}	Gyroscope drift of the y-axis gyroscope
Δd_{GD}	Gyroscope drift of the z-axis gyroscope
w	Observation noise

Table 6-9: Symbols used in the fine alignment (stage 2) state vector

After successful convergence of the fine alignment second stage Kalman filter, the system can switch to the standard navigation Kalman filter operation, which uses e.g. position and velocity observations by GNSS or zero velocity observations (ZUPT) as updates for the Kalman filter.

6.7 Attitude propagation for Direction Cosine Matrix and Quaternions

After the initial alignment, the attitude of the body frame with respect to the navigation frame has been determined. The alignment procedure is usually performed under static conditions. One exception is the transfer alignment case, in which the attitude of a reference system is transferred to the "slave" INS. However, this procedure is not the focus of this thesis. After the alignment, the INS will switch to normal operation, in which the IMU is supposed to move freely. To maintain the attitude information between the body frame and the navigation frame, the attitude has to be propagated using the inertial sensor measurements. As stated before, the attitude can be expressed by several representations und there are individual algorithms to propagate those. In this thesis, the DCM and the quaternion representation are presented.

DCM representation:

Attitude is described in the DCM representation as a matrix, which contains the unity vectors of the original frame represented in the actual frame. According to [88], the matrix can be propagated by the following procedure:

$$\dot{C_b^n} = C_b^n \Omega_{nb}^b \quad (41)$$

Since the gyroscopes measure the rotation rates between the body frame and the inertial frame Ω_{ib}^{b}, and not between the body frame and the navigation frame Ω_{nb}^{b}, the measurements cannot be used directly in the update cycle. The measurements have to be corrected for the rotations between the navigation frame and the inertial frame. If the Earth fixed space oriented frame is used as quasi-inertial frame, the rotation rate between navigation and inertial frame is the Earth rotation rate. According to P. Savage [88], the corrections are:

$$\dot{C_b^n} = C_i^n \dot{C_b^i} + \dot{C_i^n} C_b^i \tag{42}$$

$$\dot{C_b^i} = C_b^i \Omega_{ib}^b \tag{43}$$

$$\dot{C_i^n} = C_i^n \Omega_{ni}^n \tag{44}$$

A different approach is to correct the measurements directly for the Earth rotation. In this implementation, the rotation of the Earth with respect to the inertial frame and the rotation of the navigation frame with respect to the Earth fixed frame (transport rate) are transformed to the body frame and deducted from the gyroscope measurements. While mathematically identical, this approach can be implemented more easily especially for systems with low dynamics. When pedestrians or other slow-movers are considered, the transport rate is nearly zero. Additionally the total rotation of the navigation frame during the mission time is negligible in comparison to the sensor errors. Under these circumstances the implementation can be done as:

$$\dot{C_b^n} = C_b^n \Omega_{ib}^b - \Omega_{ei}^n C_b^n \tag{45}$$

$$\Omega_{ib}^b = \begin{bmatrix} 0 & -\omega_z & \omega_y \\ \omega_z & 0 & -\omega_x \\ -\omega_y & \omega_x & 0 \end{bmatrix} \tag{46}$$

$$\Omega_{ei}^n = \begin{bmatrix} 0 & -\omega_{ei}^n(3) & -\omega_{ei}^n(2) \\ \omega_{ei}^n(3) & 0 & -\omega_{ei}^n(1) \\ -\omega_{ei}^n(2) & \omega_{ei}^n(1) & 0 \end{bmatrix} \tag{47}$$

$$\omega_{ei}^n = C_e^n \omega_{ei}^e \tag{48}$$

$$C_e^n = \begin{bmatrix} -\sin\varphi\cos\lambda & -\sin\lambda & -\cos\varphi\cos\lambda \\ -\sin\varphi\sin\lambda & \cos\lambda & -\cos\varphi\sin\lambda \\ \cos\varphi & 0 & -\sin\varphi \end{bmatrix} \tag{49}$$

$$\omega_{ei}^e = \begin{bmatrix} 0 \\ 0 \\ \omega_E \end{bmatrix} \tag{50}$$

Quaternion representation:

According to [88], the quaternion attitude representation can be propagated by the following procedure. The derivative of the quaternion attitude representation is calculated by propagation using the measured rotation rates and corrected for the Earth rotation rate.

$$\dot{q} = \frac{1}{2}\bar{q}\overline{\omega_{ib}^{b}} - \frac{1}{2}\overline{\omega_{ei}^{n}}q \tag{51}$$

$$\bar{q} = \begin{bmatrix} q_0 & -q_1 & -q_2 & -q_3 \\ q_1 & q_0 & -q_3 & q_2 \\ q_2 & q_3 & q_0 & -q_1 \\ q_3 & -q_2 & q_1 & q_0 \end{bmatrix} \tag{52}$$

$$\overline{\omega_{ib}^{b}} = \begin{bmatrix} 0 \\ \omega_x \\ \omega_y \\ \omega_z \end{bmatrix} \tag{53}$$

$$\overline{\omega_{ei}^{n}} = \begin{bmatrix} 0 & -\omega_{ei}^{n}(1) & -\omega_{ei}^{n}(2) & -\omega_{ei}^{n}(3) \\ \omega_{ei}^{n}(1) & 0 & -\omega_{ei}^{n}(3) & -\omega_{ei}^{n}(2) \\ \omega_{ei}^{n}(2) & \omega_{ei}^{n}(3) & 0 & -\omega_{ei}^{n}(1) \\ \omega_{ei}^{n}(3) & -\omega_{ei}^{n}(2) & \omega_{ei}^{n}(1) & 0 \end{bmatrix} \tag{54}$$

The multiplication of the measured rotation rates and the quaternion, as well as the Earth rate and the quaternion must be performed using the quaternion multiplication. Therefore the quaternion in the first case, and the Earth rate in the second case, must be transformed into a 4x4 matrix according to eq. (52) and (54). The quaternions can then be propagated by the derivative calculated in eq. (51) and the time increment. The quaternion must be normalized after calculation to maintain the unity size.

6.8 Position propagation

In the previous chapters, several aspects of attitude representation and attitude propagation have been discussed. The most important elements of the attitude propagation were the measured rotation rates. Although tremendously important, the attitude calculation is only one half of the INS functionality. To derive the current user position and velocity, the measured accelerations have to be transformed to the desired frame and integrated to gain velocity and position information.

Inertial sensors measure accelerations and rotation rates in the body frame in relation to the inertial frame. The navigation itself can be performed in various different frames. In chapter 6.2.1, especially in the equations (17)-(21), it has been shown that additional forces have to be considered, if navigation is not performed in the inertial frame. These forces are the Coriolis, centrifugal and Euler forces.

In this work, the user trajectory shall be calculated in the local level navigation frame to exploit motion constraints of the user, as well as position updates by additional systems like WLAN positioning. Hence, the measured quantities have to be transformed to the local level frame. By integration of the corrected accelerations, the user velocity and position change can be calculated.

The derivation starts at the inertial frame and the position is in the first step transformed to the Earth fixed frame.

$$r^e = C_i^e r^i \tag{55}$$

Hence, by simple differentiating, the velocity and acceleration in the Earth fixed frame can be calculated.

$$\dot{r^e} = C_i^e \dot{r^\iota} + C_i^e \Omega_{ei}^i r^i \tag{56}$$

$$\ddot{r^e} = C_i^e \ddot{r^\iota} + 2C_i^e \Omega_{ei}^i \dot{r^\iota} + C_i^e \dot{\Omega_{ei}^\iota} r^i + C_i^e \Omega_{ei}^i \Omega_{ei}^i r^i \tag{57}$$

A sensor in the Earth fixed frame measures:

$$\ddot{r^e} = C_i^e \ddot{r^\iota} + 2C_i^e \Omega_{ei}^i \dot{r^\iota} + C_i^e \dot{\Omega_{ei}^\iota} r^i + C_i^e \Omega_{ei}^i \Omega_{ei}^i r^i = C_b^e f^b + g^e(r^e) \tag{58}$$

The terms in the middle of equation (58) are the kinematic acceleration, the Coriolis acceleration, the Euler acceleration, and the centrifugal acceleration. Because the Euler acceleration is so small in magnitude, it can be disregarded. On the right hand side of the equation, the measured forces as sum of kinematic forces and gravity can be found. Since gravity and centrifugal forces due to Earth rotation are only depending on the position, they can be combined into one force which is constant at constant position:

$$g^e(r^e) - \Omega_{ei}^e \Omega_{ei}^e r^e = \overline{g^e} \tag{59}$$

To yield the closed form for the navigation frame, the following substitution can be found:

$$\dot{r^e} = v^e = C_n^e v^n \tag{60}$$

By derivation it is found:

$$\ddot{r^e} = \dot{v^e} = C_n^e \dot{v^n} + C_n^e \Omega_{en}^n v^n \tag{61}$$

The substitutions are inserted into equation (95) with the Euler term disregarded:

$$C_n^e \dot{v^n} + C_n^e \Omega_{en}^n v^n + 2\Omega_{ei}^e C_n^e v^n = C_b^e f^b + \overline{g^e} \tag{62}$$

Multiplication with C_e^n yields:

$$\dot{v^n} + \Omega_{en}^n v^n + 2\Omega_{ei}^n v^n = C_b^n f^b + \overline{g^n} \tag{63}$$

With re-arrangement:

$$\dot{v^n} + (\Omega_{en}^n + 2\Omega_{ei}^n) v^n = C_b^n f^b + \overline{g^n} \tag{64}$$

The first rotation rate matrix in the brackets represents the transport rate, which is the result of user motion on the Earth surface. The second rotation rate matrix represents the Earth rotation rate expressed in the navigation frame.

For the position calculation in the navigation frame, the measured accelerations have to be transformed in the navigation frame and corrected for gravity. The measurements are then compensated with the product of the described rotation matrices and the velocity vector of the last instance. The result is integrated to yield the current velocity; by a second integration, the current position in the navigation frame is yielded.

For the pedestrian navigation, several aspects shall be mentioned. The overall velocity of the pedestrian user rarely exceeds 10 km/h. Hence, the rotation correction will take only very small values. Because of this, the transport rate is virtually negligible. The Earth rotation rate is in the order of magnitude of $7.29*10^{-5}$ rad/s. If the user velocity is only 10 km/h, the resulting Coriolis acceleration is around 0.0002 m/s². As will be described in chapter 11, the integration time for the long coherent signal integration was two seconds and the used sensor was of MEMS type. Thus, the rotation corrections did not show any significant change in the positioning result. However, for general applications the correction of transport and Earth rate influences on the measured accelerations must be considered.

6.9 Error propagation

To illustrate the basic influence of the sensor errors on the integrated position and velocity errors, two simulations with a **one dimensional INS** have been performed. The detailed model of the simulation is described in the appendix, chapter 18.3. Several assumptions, as well as detailed derivation and solving of the differential equations are explained there. Only a short description of the system will be given here.

The INS shall consist of one gyroscope and one accelerometer and is only considering the alongside direction. The IMU is oriented to geographic North. In the first simulation, a gyroscope bias was simulated, while the accelerometer bias was set to zero. This setup has been inverted in the second simulation with a simulated accelerometer bias, while the gyroscope bias was simulated as zero. The sensor errors were equivalent to a position error of one nautical mile after one hour, i.e. 0.0167°/h and 0.0023 m/s². By this procedure, the error influences could be separated and demonstrated. The results of the simulation are presented in Figure 6-12.

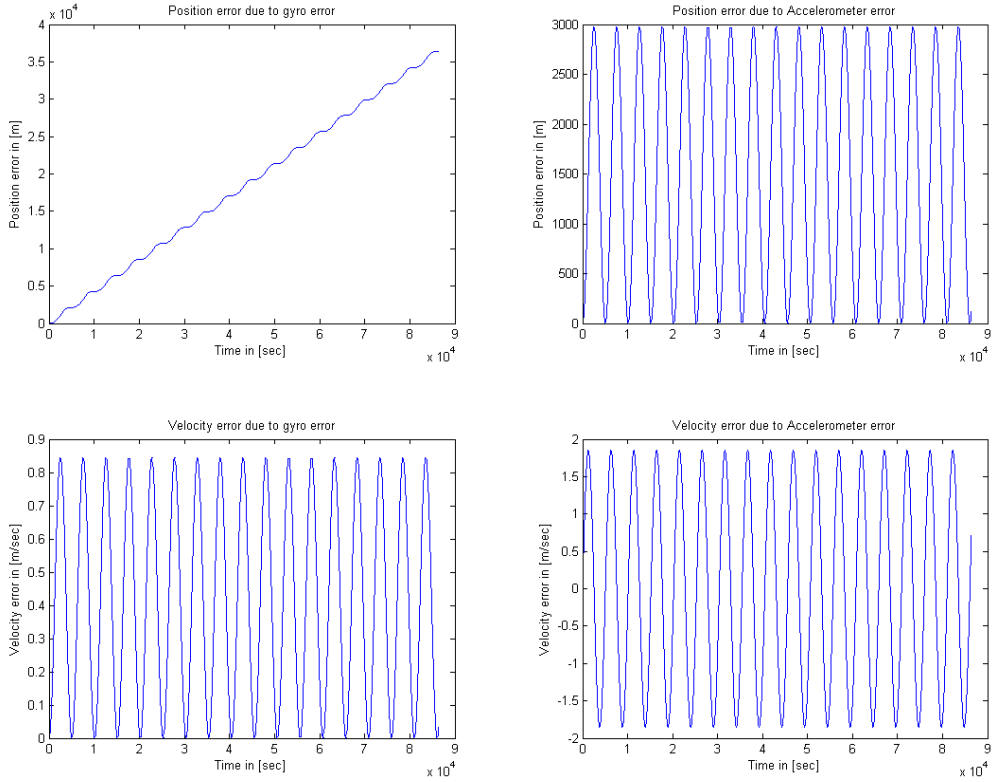

Figure 6-12: Simulated error propagation for a single axis strapdown INS

The simulation shows clearly the connection between the attitude, velocity and position errors and the influence of the Schuler tuning. The gyroscope error induces a platform oscillation, which leads to a pulsating velocity error. The velocity error follows a sine function with a constant offset of a half amplitude. As a result, the position error consists of two major components: a continuously growing linear error and a sine wave oscillation around this linear trend. The frequency of the oscillation is the Schuler frequency. A full period of this oscillation is roughly 84.4 minutes or 5063 seconds. This period can be easily identified in the figure.

The accelerometer bias induces a velocity error. By feedback of the transport rate, a platform oscillation is induced, which corrects and over-compensates the velocity error. The velocity error is a sine function with zero offset, and consequently the position error is a sine function, too. Again, the Schuler period is clearly visible in the figure.

This simple example illustrates the connection between the attitude, velocity and position states of INS. One of the main reasons for this connection is the feedback of the transport rate, which is known as Schuler tuning. Sensor errors of the inertial sensors, but also attitude, velocity and position errors excite the entire system. The periodic components have a period of 84.4 minutes. When short integration intervals of only few seconds are considered, this effect can, therefore, only have marginal impact. This will be important for the long coherent signal integration described in chapter 11.

If a full INS constellation is studied, other effects become obvious that produce a strong instability of the z-component of the INS. To illustrate the influence of the sensor errors on the integrated position and velocity errors of a full INS constellation, a simulation with a three dimensional INS has been performed. A detailed description of the simulation can be found in the appendix, chapter 18.4. As sensor error, an accelerometer bias of 0.1 mg has been applied to the x-axis accelerometer. The results are presented in Figure 6-13.

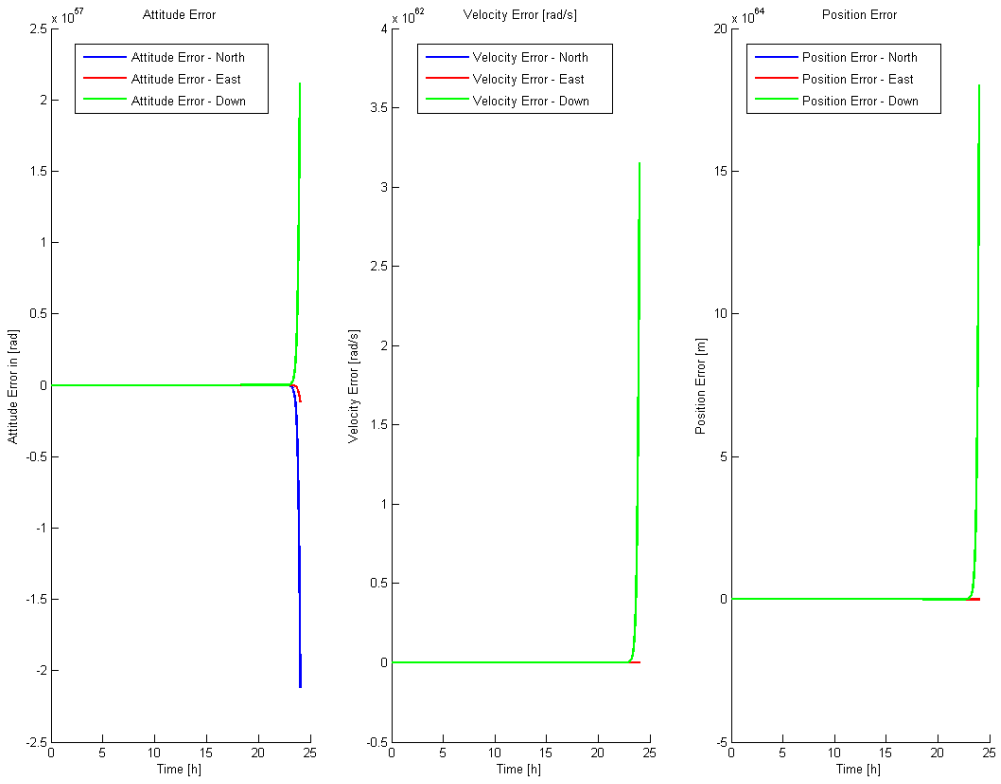

Figure 6-13: Simulated error propagation for a three axes INS

The simulation clearly shows the vertical instability of INS. The instability is caused by the fact that due to the principle of equivalence the INS has to deduct the gravity component of the measured accelerations. The gravity component is estimated in the navigation frame using a map of gravity and the estimated altitude. It is then transformed to the body frame and deducted from the measured

acceleration. Alternatively, the procedure can be performed vice versa in the navigation frame. If the attitude estimation is erroneous, this causes the system to estimate the gravity component in the z-axis as too small. As a result, the system assumes a kinematic acceleration in the z-direction. If the altitude is estimated too high, the estimated actual gravity is too small. The measurements are not corrected strong enough and again a kinematic acceleration in z-direction is calculated. Both effects are stimulating each other. As a result, the calculated INS z-position is highly instable, which is impressively demonstrated in the simulation.

It must be noted that this effect starts slowly and grows continuously over time. It has only marginal influence for very short integration interval like a few seconds, which will be used in the receiver aiding with very long coherent integration.

6.10 Summary

In the previous chapter the fundamentals of inertial navigation for strapdown systems have been discussed. Newton's laws of motion were the basis for the strategy of deriving the user position measuring and integrating its accelerations. Einstein's principle of equivalence gave the need for precise separation of gravity and the kinematic accelerations. In addition to precise determination of the measured accelerations, the precise attitude proved to be extremely important for inertial navigation. For that, the most important navigation related frames have been introduced. Several mathematical representations of attitude have been presented and their properties have been discussed, especially with respect to singularities. The initial alignment, as well as the propagation of the attitude representation has been illustrated. The process chain of integrating the measured accelerations to gain the user position and velocity has been demonstrated and special issues of pedestrian navigation have been mentioned. Finally, the error propagation of INS has been demonstrated on a simplified 1D and a 3D INS simulation.

7. Pedestrian Navigation Systems

In the following chapter, an alternative inertial sensor based navigation system called “Pedestrian Navigation System” (PNS) will be described. PNS are dead reckoning navigation systems that exploit the constraints of human walking. Since the human usually moves by making steps in a certain direction, the position change with time is strongly constraint and, therefore, the navigation solution of a PNS is often less deteriorated by drift than other DR systems. The user position is propagated by detecting steps, determining the incremental distance travelled during this step and adding this position change to the last known position. Since the position is only propagated when steps are detected, unlimited drift is prevented. The PNS will be one of the major elements of the integrated navigation system and is of major importance in this thesis. This chapter will cover the biomechanical step aspects, the influence of the sensor placement on the body, as well as a detailed analysis of the sub-algorithms of the PNS.

7.1 Introduction

Pedestrian navigation has basically the goal of providing the user with information about his current position (so called **positioning**) and providing directions to a desired destination (**guidance**). The term "pedestrian" refers to the human user, who performs steps to move forward. This definition and these limitations are necessary, since apart from walking, also crawling, jumping, swimming, or other ways of movement would theoretically be possible. As explained in [110], the pedestrian user moves in the indoor or light indoor environment for a significant period of time. In contrast to other users, any proposed navigation system must therefore be able to operate in environments with low or fully denied GNSS visibility at least for a reasonable amount of time. Since external infrastructure for ubiquitous position fixing cannot be provided everywhere, this requirement directly leads to dead reckoning systems. The classical DR system today for aircrafts, ships and submarines is inertial navigation. Since the IMUs have been reduced in size, price, weight and power supply during the last few years, IMUs have been considered for pedestrian navigation for some time now. Several samples for the progress in the IMU technologies are depicted in Figure 5-6.

Inertial navigation is typically performed by the strapdown algorithm, which transforms acceleration measurements from the body frame into the local level navigation frame. It corrects for nominal gravity, centrifugal and Coriolis accelerations and double-integrates the resultant acceleration. By feedback of the transport rate by the Schuler loop, the dynamic error behavior could be improved. Sensor and alignment errors, however, produce rapidly growing navigation errors. While accelerometer biases result in an oscillating position and velocity error, which cannot grow over certain limits, the gyroscope biases produce a continuously growing position error by the integration of the gravity vector due to erroneous attitude solutions. Hence, the integration of measured accelerations is a reason for the large position drift of INS over time.

Integration of INS with other sensors, like GNSS or LORAN, has been used for many years now and it has been shown that sensor error estimation, navigation error estimation and correction of both actually work, if sufficient aiding information of reliable quality is available. It is, however, very difficult to obtain this aiding information in indoor scenarios. More information about the strapdown INS aspects can be found in [87], [90], and [102].

The described navigation system is an alternative dead reckoning system. Comparable, but not identical IMU-based PNS are described in several publications like [48], [54], or [63]. The main elements of the PNS are the following subsystems:

- step detection
- step classification
- stride estimation

By adding

- heading determination
- dead reckoning position propagation

a dead reckoning navigation system is formed.

Like odometric systems in vehicles the proposed navigation system offers autonomous navigation with limited error growth. In cooperation with magnetic sensors, gyroscopes and error estimation by position updates, the position drift can be reduced additionally. The functional organization and the data flow of the core elements are presented in Figure 7-1.

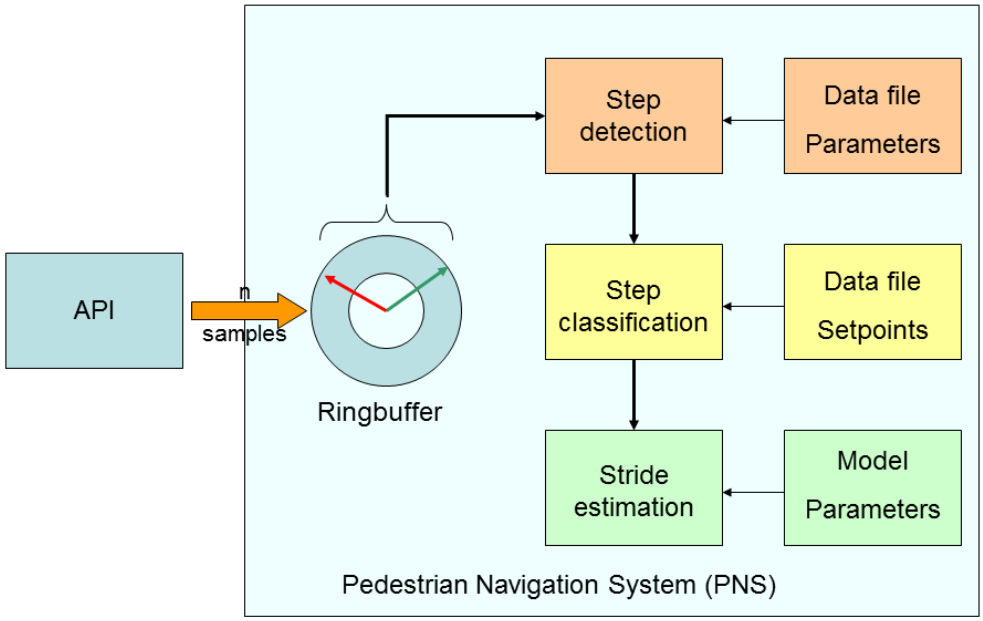

Figure 7-1: Signal flow chart of the pedestrian navigation system

As in the case of other dead reckoning systems, the positioning error grows with distance traveled and elapsed time. Error sources are the erroneous heading estimation, stride estimation errors and errors in the step detection, i.e. lost steps or false detections. The following reasons illustrate the limited error growth of the system:

- The PNS solution is drift-free, if no steps occur. This situation happens frequently and can be used, e.g. for zero velocity updates.
- The average step length can be estimated in general to about 0.7 m. Individual walking behavior, especially the individual stride relation can be determined and modeled, which is an equivalent to a personal calibration. Only step length variations and calibration errors are

present. Hence, the positioning error due to the stride errors is not time dependent but dependent on the distance traveled and is relatively small.

- If no continuous and significant magnetic disturbances are present, the attitude with emphasis on the heading can be stabilized by magnetic sensors. Thus, the heading drift is at least partially compensated and the heading error significantly reduced.

Figure 7-2 gives an impression of the reduced drift and high positioning accuracy of the PNS. The green spot marks the starting point of the walk; blue dots mark the registered steps. The walk stopped at the starting point, which can be monitored in the results. The red silhouette shows the parking lot, which was used as test area. The test was performed using the MTi IMU on an experimental mounting to prove the usability of the unit and the sensor placement on the belt. The test was intended to show the function of the algorithms with this sensor placement. The figure also depicts the discrete nature of PNS: position updates are only available at the instant of a detected step.

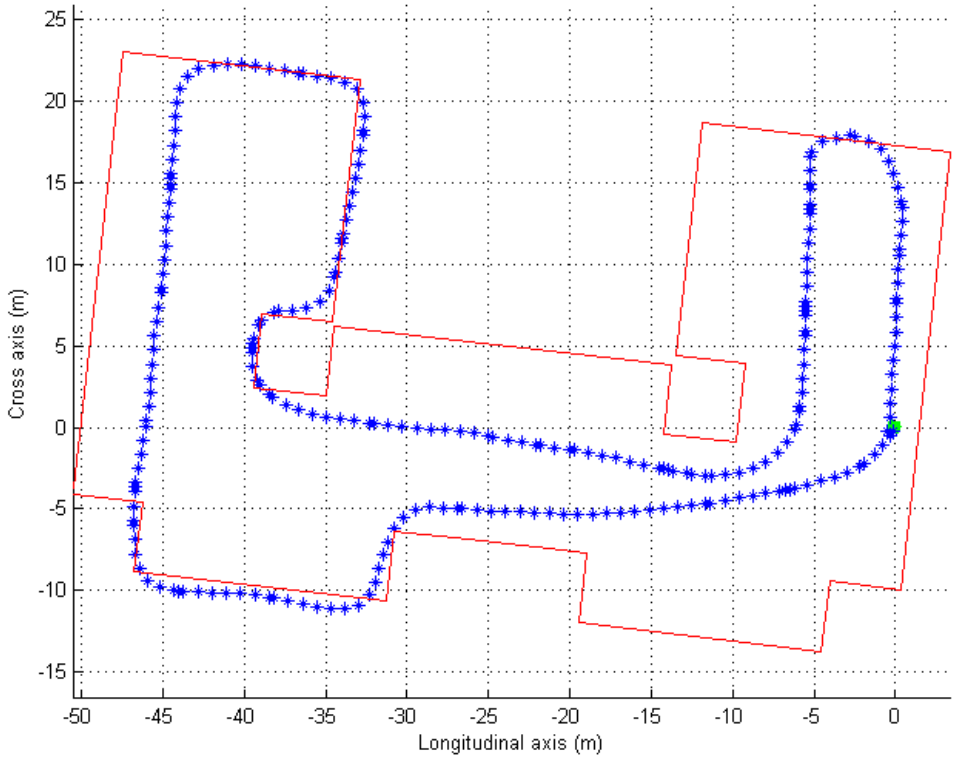

Figure 7-2: Test run on parking lot, using PNS only with Xsens MTi IMU internal attitude

Calibration was not performed for the individual user, but a generic parameter set from an initial calibration campaign has been used. It must further be noted, that only the accurate dimensions of the parking lot were measured, the initial azimuth orientation was fitted to the measured walking path. It is evident that the measured profile follows the ground reference very well. Scale factor errors are low and due to non-individual calibration. Sophisticated calibration as shown in chapter 7.5.2 and 7.5.3 can improve the navigation accuracy.

7.2 Sensor placement on the human body

In the following subchapter, the biomechanical step aspects, i.e. kinematics, accelerations and rotation rates, are analyzed. It will be shown that the placement of the inertial sensor on the user's body has large influence on the measured quantities and on the applicability of various algorithms.

7.2.1 Biomechanical step aspects of walking

Walking is a complex form of movement and consists of several phases. The body's weight is shifted to one leg, while the other leg is lifted, swung forward and set on the ground again with the heel first. Then the foot rolls from heel to toe while the body's weight is shifted to this leg and the circle continues. This movement has been discussed in various medical, physiological and also technical papers; technical descriptions can be found e.g. in [48], [54], and [7]. The publications mostly cover mechanical models of the legs, represented by two levers connected with hinges to the hips and the feet. This model has certain advantages, however, it is neither complete nor does it explain all aspects of walking; especially all the movements of the hips and the rest of the body as well as the interaction between the legs are neglected. Hence for analysis, an experimental approach was chosen and will be discussed here. For this, a BEI Systron Donner MMQ-50 MEMS-type inertial measurement unit was mounted on a belt holder device and attached to the waist of the individual test person. The IMU measured rotation rates and acceleration in the three orthogonal axes north, east and down. The test persons walked a straight test range of 38.5 m length on a rigid, tiled floor. This test range has also been used for the stride evaluation campaign, which is described in chapter 7.5.2. The distance in the case shown in the following figures was crossed in 36 seconds and with 56 counted steps.

Analysis shows that all registered movements of the body during walking have a cyclic form. As can be seen in Figure 7-3, all the acceleration patterns measured at the test walker's belt repeat with every step. They all have a nearly constant mean value caused by the gravity accelerations, the attitude angles with respect to the local horizontal plane and the sensor biases and scale factor errors incorporated in the measurements. The amplitudes vary slightly. While, obviously, not every step has an absolutely identical shape and intensity, the discrete data sampling even with high frequency does not always catch the absolute peak of the signal. The signal slope is relatively high in the context and even the maximum delay of half the sample period, in this case 25 ms, can attenuate the absolute maximal values by a significant amount. Despite these variances, every step causes a noticeable cyclic acceleration pattern in all three body-mounted sensor axes. It is obvious that factors like different leg length, body weight, shoe type or rigidness of the underground will cause different amplitudes of the measured accelerations for different users and test persons. However, the pattern form stays the same if the basic walking cycle does, too.

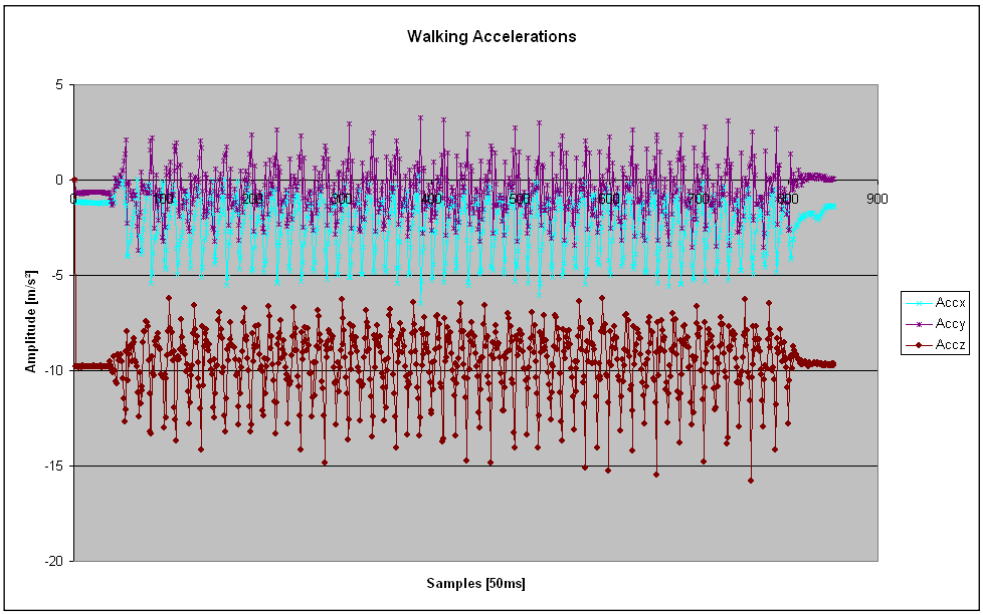

Figure 7-3: Acceleration patterns for walking

As can be seen in Figure 7-3 and Figure 7-4, the accelerometers and also the gyroscopes measure a cyclic signal in all three orthogonal axes. Furthermore, the amplitudes of the measured rotation rates have a similar order of magnitude. Thus, during walking the waist is not rigid but flexible and shows significant rotation in the heading, the roll and even the pitch axis. The stride is elongated by the yaw rotations, i.e. during swing phase not only the leg swings forward but also the waist. And during the shifting of the weight from one leg to the other, a noticeable roll rotation can be noticed. The pitch rotation shows the smallest amplitude which can be explained by the reduced flexibility of the pelvis on the spinal column around this axis as well as balance aspects.

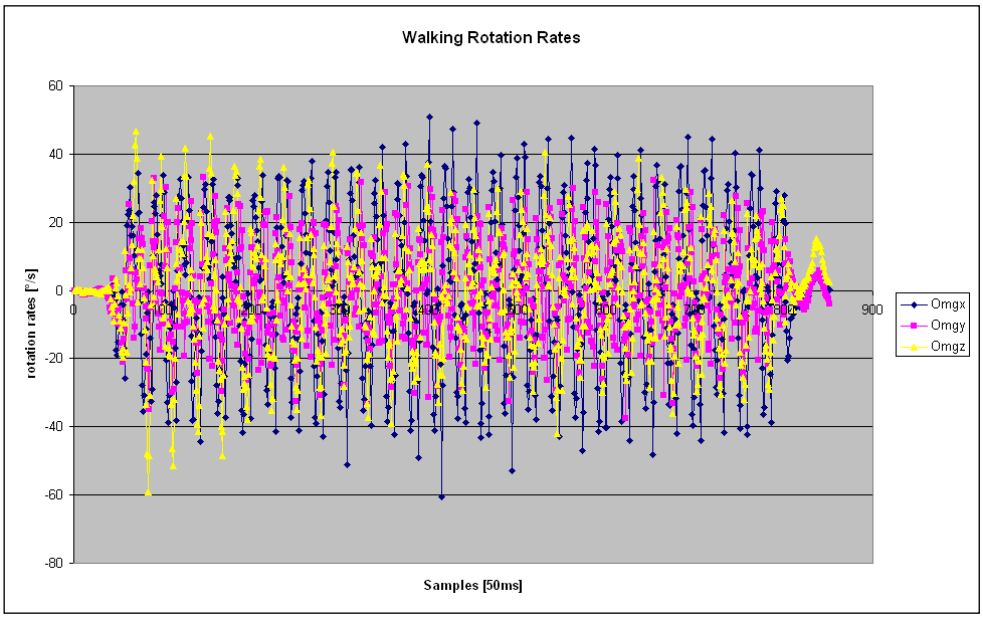

Figure 7-4: Rotation rate pattern for walking

This short analysis shows the limitation of the simple walking models, because it demonstrates that even straight walking is a three-dimensional movement with a lot of body motion involved, which is only weakly represented by the simple mechanical model. On the other hand it shows that, if other moving states can be neglected, nearly all sensor axis measurements are adequate to indicate steps. The phase relationship between the signals of the different IMU axes can be valuable information for the determination of the kind of step, which is necessary to estimate the stride correctly.

7.2.2 Sensor placement on the body

The placement of the sensors on the body is of special interest for the development of algorithms as well as the design of sensors for practical implementation. Obviously, several positions on the body are possible and will show very different results for the same movement. Besides, several operational and ergonomic aspects have to be considered for the decision where to place the sensors. In literature most of the authors use belt mounting of the sensors to the waist of the test persons (e.g. [54], [55], [63]), sometimes also on the lower back (e.g. [21], [41], [51]). Mounting of the sensor on the shoe is also proposed and tested (e.g. in [42], [76], [5], [86]). Multiple sensor suites with sensors e.g. on the thighs, shanks, breast, etc. have been described in [56], [21] and [84]. Overhead placement, like e.g. helmet or head mountings or mounting on the arm of the test person could not be found in the available literature. Generally, the body does not only move while walking, but also while standing, if any kind of activity is performed. If body motion is used to detect steps, the algorithms shall not be negatively influenced by other activities. Sensor placement can play an important role in this respect. When working with the computer, mainly fingers, hands, forearms and the head are moving, while the rest of the body is approximately at rest. When bending the whole upper body, possibly the legs are moving to stabilize the body, shift the center of gravity or bring maximum force behind the torso. Drinking a cup of coffee would only require the movement of the whole arm with the rest of the body staying rigid. These examples show that the measurement of other body movements is dependent on the placement of the sensor. Consequently, positioning the sensor at unfavorable locations can disturb the step detection by measurement of accelerations which are not corresponding to steps.

On the other hand, the body does not only induce accelerations by movement but also attenuates accelerations caused by walking. A hard “heel down” would have much bigger acceleration amplitude but also a shorter impact time when measured at the sole of the shoe than it would have when measured on the head, because the spinal column and the skeleton, the muscles and the liquids in the body damp these peaks significantly. In addition to that, the geometrical amplitudes of the feet are higher than those of the body resulting in bigger accelerations in the longitudinal axis. It has been experienced that the phase relationship between the individual acceleration axes for individual step types, especially the step type ‘down’, is very significant with belt mounting, but lost when using overhead mounting. This is especially interesting for the step classification.

Mounting the sensors on the shoe has both advantages and disadvantages. On the one hand, the bigger amplitudes of acceleration allow a better signal to noise ratio for sensors with strong sensor noise. The kinematic acceleration is significantly higher and allows simple step detection algorithms. On the other hand the strong shocks at the feet strongly influence the inertial sensors. Especially cross-coupling and linear force errors on the MEMS gyroscopes due to the high g-loads seem not optimal for navigation. Furthermore, there is a significant rotation of the feet in multiple axes. These

high amplitudes of motion are generally disadvantageous, since proportional errors like scale factor errors, but also non-linear errors due to shock loads, result in steadily growing attitude errors. On the other hand, the inertial solution can be stabilized using zero velocity updates (ZUPT) during the heel down phase. IMUs with only one gyroscope have to be considered because they offer a significant cost benefit in comparison to full 3D packages. Because they cannot follow the roll and pitch attitude, a mounting as horizontal as possible should be used to avoid misalignment errors. Therefore, mounting the sensor on the shoe is challenging for the inertial sensors and their processing, at least for dead reckoning over longer periods. Practical considerations of the power supply, the data readout, wiring, and not least the protection of the sensors also speak against shoe mounting. For professional use it is critical to modify safety certified shoes e.g. for fire fighters' application. The sensor placement has been studied for belt mounting (Figure 7-5), as well as mounting the sensor overhead (Figure 7-6).

Figure 7-5: Sensor placement on the belt of the test person

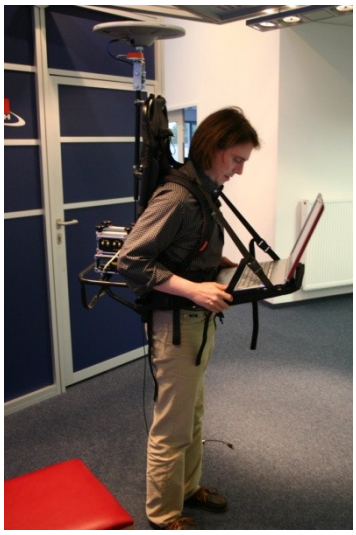

Figure 7-6: Sensor placed overhead of the test person [72]

In both cases the step detection algorithm described in chapter 7.3 does perform well, but with slightly adjusted thresholds. The parameters of the algorithms have to be calibrated according to the sensor mounting to optimize the detection and false alarm rates.

7.3 Step detection

When using PNS, dead reckoning for a pedestrian user is performed by detecting steps, estimating their length (stride) and heading and propagating the next position. By doing so, the step detection has a high priority. Without a correct step detection, the navigation solution will not propagate correctly. If actual steps were not detected, the calculated DR position solution would not propagate at all. False alarms, i.e. step detections without actual steps made, would propagate the DR solution incorrectly. Hence, the step detection algorithms must work with a high detection probability and a low false alarm rate.

Step detection intervals and step classification will have a special application in the stride determination. Since the evaluation of the step type must be applied on the actual data set of the analyzed step, the step detection algorithm gains additional importance for the determination of the step interval time data window.

In the following chapter, several strategies and techniques for step detections will be presented. Some of them were influenced by literature, e.g. in [48], [54], [55], [63] and [56], others were found by principal data analysis and combinations of various techniques. Finally, a combined step detection algorithm will be presented, which will be further used for the operating PNS.

7.3.1 Overview

Many different step detection approaches exist in literature. In most cases the accelerometer outputs, especially that of the z-accelerometer, are used to detect steps. The signal offers several parameters which can be used for step detection. Some of the used signal parameters are:

- the amplitude around the mean value (for the z-axis, the mean acceleration is around standard Earth gravity acceleration)

- signal form
- variance/standard deviation around the mean value
- cross-correlation between the different signal axes
- the frequency spectrum of the sampled data.

Some of these strategies will be discussed in the following chapters of this thesis, before the finally used strategy will be developed. In addition to the detection of actual individual steps, the detection of the principal states of movement, standing still or moving, is sometimes necessary, too. There also exist strategies for this application.

Besides the step detection, the inertial signals of the IMU can also be used for the step classification. Basically the same parameters apply for step classification as well as for step detection beside the fact that the step window between the last step und the actual step is known by the step detection algorithm. Hence, the length of the data sample set to be analyzed can be reduced and the algorithm can work more effectively. There are also solutions described in literature which perform both tasks with only one strategy ([48]). However, the detection as well as the classification need to have a high level of reliability.

The inertial measurements can be evaluated in different domains:

- the time domain
- the frequency domain
- the statistical domain

All of these domains will be evaluated in the following chapters. While the signal time domain deals with the acceleration and rotation rate measurements related to the time of measurement, the frequency domain and the statistical domain use transformed signals. Thus, new information can be gained while on the other hand the original signal is usually lost.

The most important statistical parameters are the mean and the standard deviation (or variance) of the evaluated signals. In inertial measurements, there mostly are problems with biases or misalignments, which deteriorate the time domain signals, especially if no redundant information for error estimation and calibration is available. If the sensor noise is reasonably low, the variances of the inertial signals can deliver good information about movements for detection as well as classification. Thus, e.g. standing still is easy to determine by an evaluation of the acceleration variances. On the other hand, other activities also induce acceleration signals and thus statistical information by itself is not sufficient.

In literature, smoothing of the signal e.g. by band pass filtering to ease step detection and classification is discussed, e.g. in [55], [21], and [51]. Smoothing usually creates significant time lags and attenuates also the original signal, which shall be avoided in this work to keep the system as close to real-time as possible. Consequently, no signal filtering has been used and the developed algorithms must be capable of tolerating the signal noise.

7.3.2 Step detection by Fourier transformation of the acceleration signal

As shown in chapter 7.2.1 the pedestrian movement appears in the IMU measurements as cyclic acceleration and rotation rate patterns. This can be observed in Figure 7-3 and Figure 7-4. Thus, it seems straight forward to analyze these patterns in the frequency domain to determine the step frequency from the inertial data. The integration of the step frequency over time would then yield the actual number of steps traveled, and multiplied with the stride also the traveled distance.

The transformation from the time domain to the frequency domain is usually performed using the Fourier transformation. In the continuous form, the Fourier transformation performs a decomposition of periodic signals (not necessarily pure sine signals) into a set of sine and cosine functions [59]:

$$f(t) = f(t + lT_0) \tag{65}$$

$$l = 0,1,2,\dots$$

$$f(t) = \frac{A_0}{2} + \sum_{k=1}^{\infty} A_k \cos(k\omega_0 t) + \sum_{k=1}^{\infty} B_k \cos(k\omega_0 t) \tag{66}$$

Symbol	Explanation
f(t)	Base function
A	Scalar constant
B	Scalar constant
C	Scalar constant
ω_0	Base frequency of the Fourier transformation
t	Time
k,l	Integer numbers
ϕ	Angle shift

Table 7-1: Symbols used in the Fourier equations

According to [59], the right side of the equation is called Fourier-series, and the coefficients A_k and B_k can be calculated using the following integrals:

$$A_k = \frac{2}{T_0}\int_0^{T_0} f(t)dt = \frac{A_0}{2} + \sum_{k=1}^{\infty} A_k \cos(k\omega_0 t)$$

$$B_k = \frac{2}{T_0}\int_0^{T_0} f(t)dt = \frac{A_0}{2} + \sum_{k=1}^{\infty} A_k \sin(k\omega_0 t) \tag{67}$$

By using addition theorems one yields:

$$f(t) = \frac{A_0}{2} + \sum_{k=1}^{\infty} C_k \sin(k\omega_0 t + \phi_k)$$

$$C_0 = \frac{A_0}{2}$$

$$C_k = \sqrt{A_k^2 + B_k^2} \tag{68}$$

$$\phi_k = \tan^{-1}\frac{A_k}{B_k}$$

$$k = 0,1,2,\ldots$$

If the input signal is not continuous, but discrete, a discrete form of the Fourier transformation exists that combines the row of measurements x(n) with complex roots of unity W [82]. By this, the discrete measurements are connected to continuous periodic function. For a vector of measurements x of the length N this Discrete Fourier Transformation (DFT) is defined in [82] as:

$$X(\mu) = \frac{1}{N}\sum_{n=0}^{N-1} x(n)W^{-\mu n}$$

$$\mu \in Z \tag{69}$$

$$W = e^{2i\frac{\pi}{N}}$$

Symbol	Explanation
X	Fourier transform of the measurements vector
x	Measurement vector
N	Length of measurement vector
W	Complex root of unity

Table 7-2: Symbols used in the discrete Fourier equations

Further analysis on the DSP in the context of GNSS can be found in [64]. The Fast Fourier Transformation (FFT) is an efficient implementation of the DFT. It reduces the number of operations of the DFT strongly, if the length of the sample is a power of 2 [82]. For this analysis, the software Matlab and its implementation of the FFT function have been used to analyze the frequency content of the measured z-axis acceleration. Detailed information about the implementation can be found in the Matlab help documentation. The FFT function yields as result of the transformation complex numbers for each (discrete) frequency step. By analysis of the length of these vectors, the power content in this frequency setpoint can be derived.

The measured acceleration does not only consist of the step movements, but also of other disturbing motions, e.g. the sensor errors, noise, sampling frequency effects and constant gravity acceleration. The Fast Fourier Transformation (FFT) of the z-acceleration measured by the IMU described above yielded the spectrum shown in

Figure 7-7.

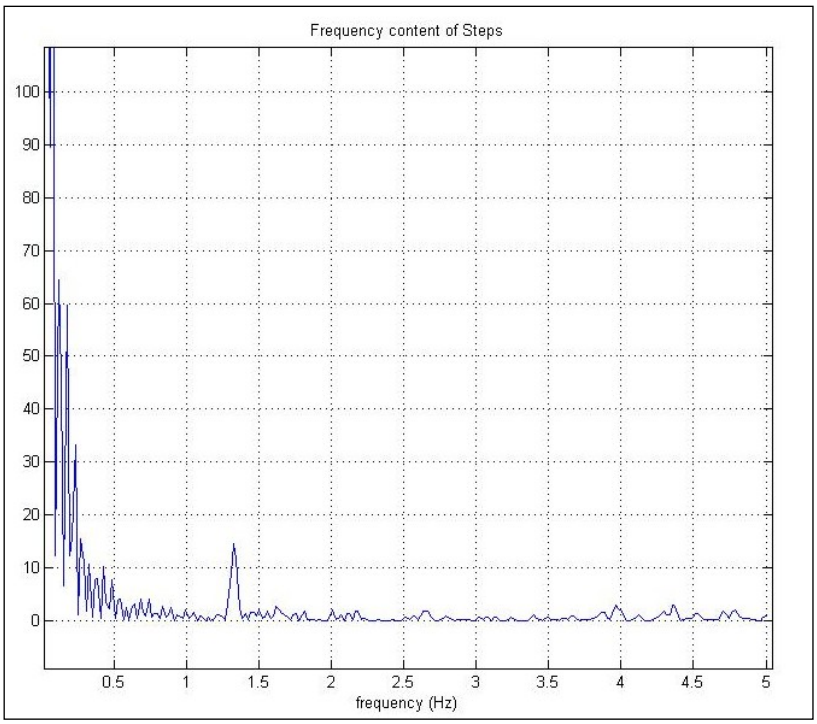

Figure 7-7: Frequency analysis by FFT analysis of the measured z-acceleration

As can be seen clearly the biggest amplitudes of this spectrum are below 0.5 Hz, which is below the expected step frequencies. The main peak results from the large constant gravity acceleration. Step frequencies between 0.5 and 5 Hz have been evaluated as most significant in the walking trials. The result for this frequency window is shown in Figure 7-8.

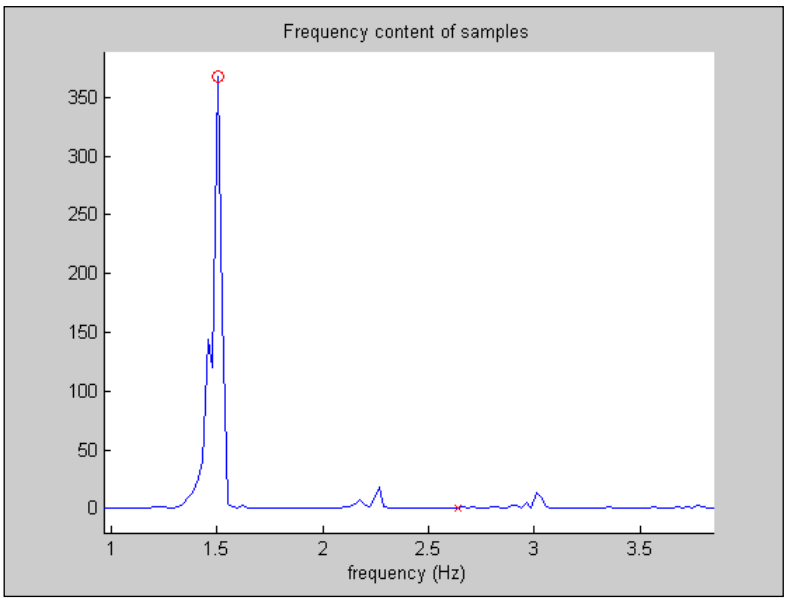

Figure 7-8: Close-up look on the focused frequency spectrum of Figure 7-7

Clearly, a simple peak detection algorithm can find the step frequency in this frequency window (marked with red circle). But also harmonic multiples and other smaller amplitudes remain in the spectrum. The walking trials showed that step frequencies above 5 Hz cannot be achieved by the

common test persons. Even for athletes this high frequency is challenging and hence not the focus of a PNS. On the other hand steps below 0.5 Hz (step period >2 s) are not standard walking behavior either. Thus, the reduction of the frequency window can be made and does not restrict the PNS significantly.

The frequency analysis of the measured accelerations can be performed easily, but has several severe disadvantages.

As it will be shown in the stride estimation chapter, the step frequency must be known with high precision of at least 0.1 Hz. The resolution of the FFT on the other hand is dependent on the length of the used data sample. To achieve the stated resolution of 0.1 Hz, a sample of ten seconds length has to be used. Because no future data is available, this leads to a time delay of the calculated step frequency to the actual step frequency of at least five seconds. This delay is not acceptable for many applications and, as a result, there is a trade off between time delay and frequency resolution when using the FFT for a PNS.

Another issue is the decision about the actual motion state. It is necessary to determine, if the user is actually walking or not. Even if the person is not walking, there will be measured accelerations, like gravity, body motion different from walking, sensor noise, sensor sampling rate effects and many more. Consequently, the FFT would show some peaks in the spectrum. The biggest peak in the proposed frequency window would be detected as walking frequency and the navigation solution would be updated without any steps made. For that reason it is necessary to determine thresholds to identify the walking. Peaks below these thresholds are interpreted as no walking; peaks above enable the navigation processing. However, the threshold magnitude is not easy to determine because of the different walking behaviors of different users, different walking speeds which must be covered by this threshold(s), different undergrounds and so on. This leads to an experimental and not deterministic strategy of threshold determination and is not the most effective one. Additionally, the usage of amplitude thresholds also corrupts the proposed principle of the frequency analysis, which is performed by the transformation of the standard accelerometer outputs in the time domain to their transformed form in the frequency domain.

In addition to that, a lot of information is lost by the transformation of the signals in the frequency domain. One of the main problems is the **loss of the phase relation** between the detected **steps** and the **heading angle** determined at the time of the step. Thus, it becomes difficult to propagate the position in the correct direction. It has been shown in chapter 7.2.1 that significant yaw rotation rates exist during one step cycle. It is important to catch the correct heading angle at the step epoch. For example, a low pass filtered average heading over several epochs will not catch this angle and therefore induce a position error growth.

Parallel to the FFT processing, the usage of the wavelet transformation has also been evaluated. While the wavelets have interesting features e.g. for signal de-noising, the principal problems of the time lag, the resolution problems and the loss of phase relation between the different axes could not be overcome only by this technique.

In summary, the transformation of the IMU signals in the frequency domain showed interesting features, but also the deficiencies of the transformed signal. Although undesired, thresholds need to

be used to distinguish between walking and standing. It has been shown that it is challenging to maintain the relation between the steps and their heading. The frequency resolution, necessary for stride determination, could only be gained by accepting a significant time lag of the data. Consequently, the FFT strategy seems not promising as a step detection strategy.

7.3.3 Step detection by evaluation of stochastical signal parameters

Using stochastical parameters of measured signals can be a powerful strategy because it shows additional properties of the same signal source. Similar to the Fast Fourier Transformation (FFT), the evaluation of a signal's mean and variance transforms the signal to another domain. Additional observations can be produced, but the original signal in the time domain is lost, as well as phase relations to other measurements in the time domain. When using a sliding window, there is obviously a phase relation between the variances, which can be seen in Figure 7-9. For the evaluation of mean and variance, the observed interval or sample time is also of importance. For that reason, a certain time lag, comparable to that of the FFT before, can also be noticed.

Figure 7-9 illustrates the calculated variances of the three orthogonal accelerations measured by an IMU during a test walk and calculated in a sliding window over 10 epochs (0.5 s). Until epoch 160 the test person is standing, then the test walk starts. The variance level at "standing" is extremely low. At the beginning of the walk the variances grow immensely and show a cyclic behavior, while the variance in the y-axis is lower than on the x- and z-axis. It is interesting that, although the original signals are lost, the variances still show the same cyclic form and indicate that the movement in each axis has phases of high and low dynamics. By peak detection, individual steps can be found in the variance pattern. This algorithm is strongly influenced by other sources of signal variance.

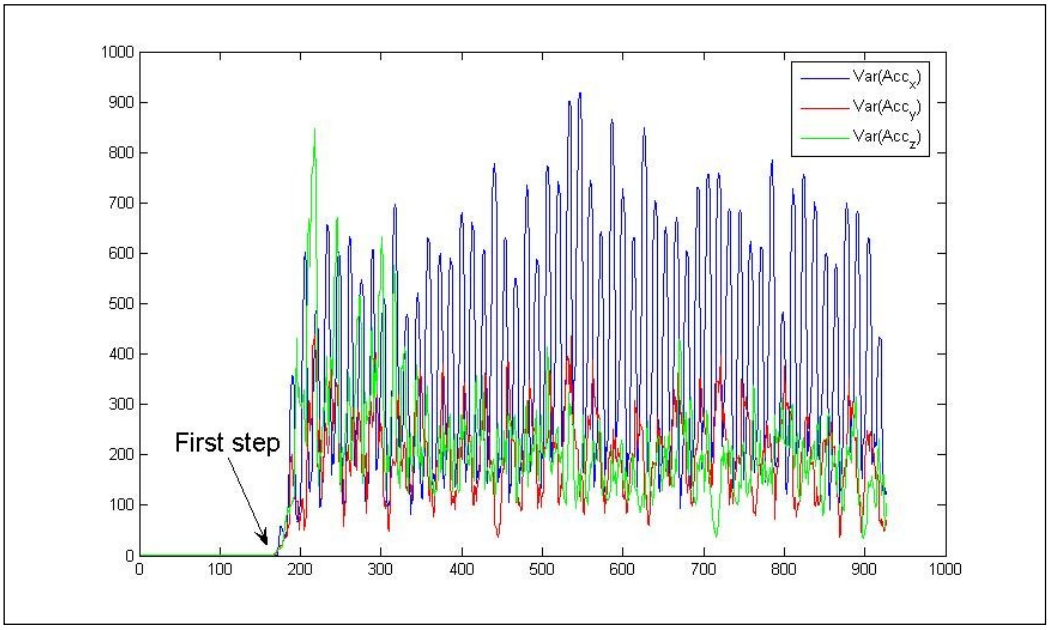

Figure 7-9: Variances of the 3D-acceleration during a test walk (sliding window, 10 samples)

It is obvious that the variances can be used to detect walking, but with certain restrictions. As stated in [54] and [56], the phase correlation between the signal variances can also be used to determine the kind of steps (up, down, level).

The cross-correlation function can be used to determine the degree of similarity between two signals. This similarity is calculated as function of the time shift between the two signals. According to [82], the continuous form of the cross-correlation function is given as:

$$R_{X,Y}(t) = \lim_{T\to\infty} \frac{1}{2T} \int_{-T}^{T} X(u)\, Y(u+t)\, du \tag{70}$$

Symbol	Explanation
$R_{X,Y}(t)$	Cross-correlation of functions X and Y for the time shift t
X	First correlated function
Y	Second correlated function
t	Time shift of both functions
T	Limit of integration interval
u	Integration variable

Table 7-3: Symbols used in the cross-correlation function

According to [64], the discrete form of the cross-correlation function for samples of limited length can be written as:

$$R_{X,Y}(n) = \frac{1}{N} \sum_{i=0}^{N} X(i) Y(i+n) \tag{71}$$

Symbol	Explanation
$R_{X,Y}(n)$	Cross-correlation of the discrete functions X and Y for the time shift n
X	First correlated function
Y	Second correlated function
n	Time shift of n samples of the functions
i	Number of individual sample
N	Length of samples

Table 7-4: Symbols used in the discrete cross-correlation function

Figure 7-10 shows the cross-correlation of the variances of the x- and the z-axis, calculated for 56 consecutive steps, using Matlab and the function *xcov*. The interval ranges from one step detection to the next and the steps have been detected by the algorithm described in chapter 7.3.4. Hence, it is possible to determine the correct intervals of observation for the actual measurements and calculate the correct variances. In addition to that, unusual motions and non-walking motion can also result in acceleration signal variations. This is the main reason for not using the variations for step detection. If the step has been detected by other means, it is helpful to also evaluate the variances of the signal from step to step.

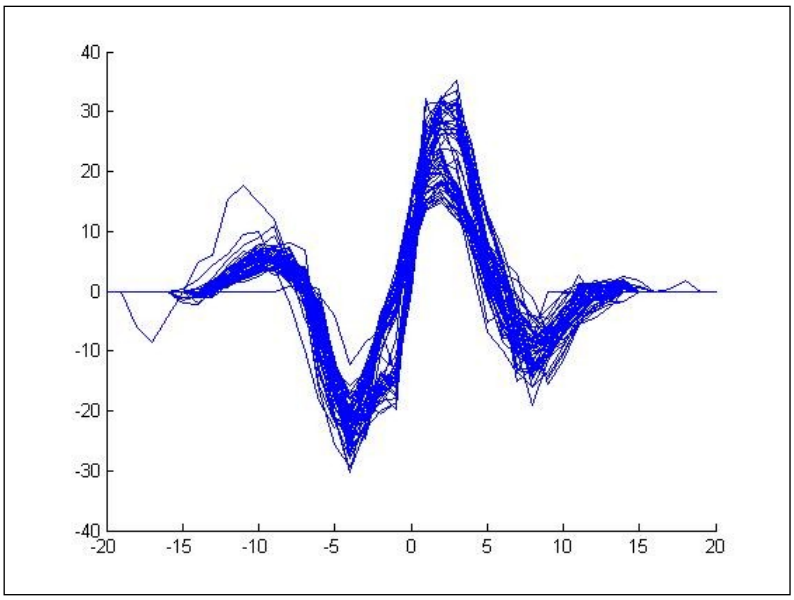

Figure 7-10: Cross-correlation of the variances between x- and z-axis (level walking)

As can be seen in Figure 7-11 the rotation rates also show the same significant signal variances as the acceleration. In Figure 7-12 the first step has been magnified.

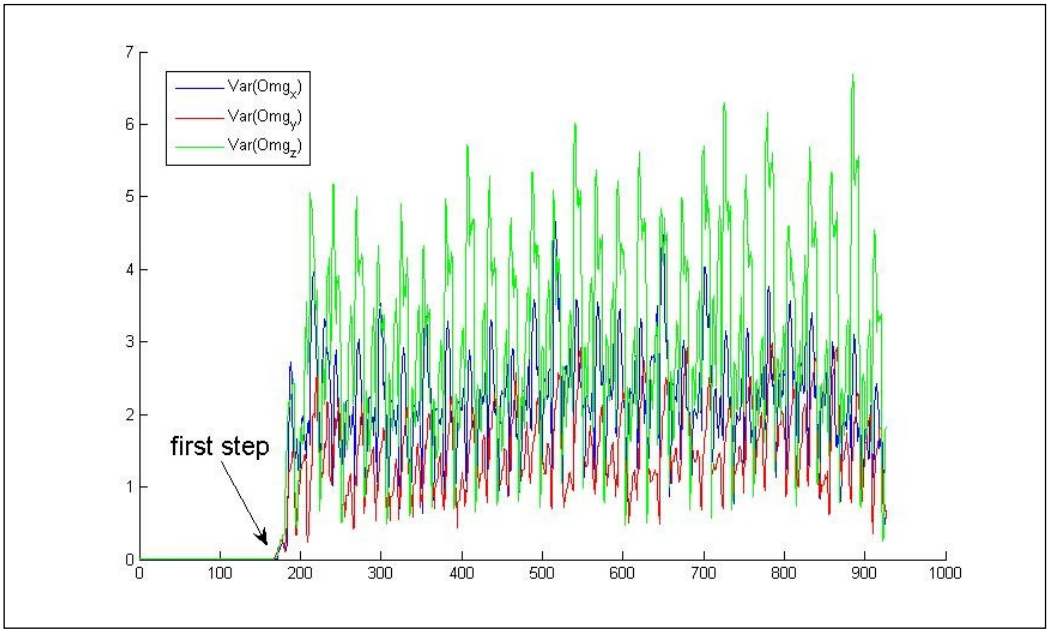

Figure 7-11: Variances of the 3D rotation rates during a test walk (sliding window, 10 samples)

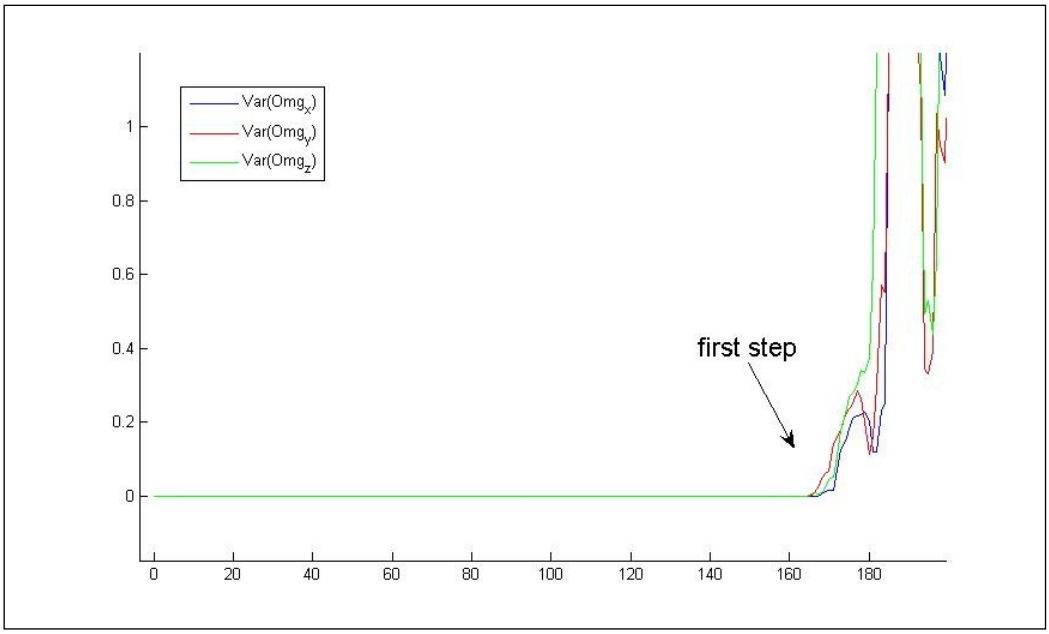

Figure 7-12: Variances of the 3D rotation rates (zoomed)

The evaluation shows that the variances in the inertial measurements can be used for step detection, but with certain restrictions in the reliability and the processing. First of all, high variances show high activity, but not necessarily steps. It is possible to induce high variances in the acceleration axes without walking and, therefore, misinterpretations are possible. Since the variances are not crossing zero, it is difficult to reject false peaks and keep the peaks correlated to the steps. Hence, thresholds had to be used which are again very specific for each individual pedestrian. There is no information about the direction of the activity available from the variance observations, only the magnitude. Finally the phase relation between the individual axes is changing for different step types, which makes it harder to determine the correct heading at the step detection event. Consequently, although it could be used with limitations, the stochastic evaluation of the inertial measurements will not be used for step detection in this thesis. It is more advantageous to detect the steps by observing the continuous signals and then determining the kind of steps using their variances.

7.3.4 Step detection with amplitude and constraints evaluation

Influenced by the results of the first walking test campaign an optimized step detection algorithm was developed. This algorithm takes advantage of the basic walking motion and determines the steps on the accelerations level (time domain signal) instead of using a signal transformed to the frequency domain. The step frequency is then determined by the inverse of the smoothed step period between several following step detections. The absolute values of the extremes in the acceleration profile can sometimes be misleading for interpretation. Due to the shock effects during the feet down phases and its very sharp slopes. This is increased by the discrete sampling interval which does not secure the catch of the absolute maximum. For that reason the interpretation of absolute extremes must be handled with care.

Several requests on the algorithm have been formulated before the development:

- Reliable step detection, i.e. high detection and low false alarm probability
- Minimum time lag between step and step detection
- High resolution step frequency determination
- Minimum customizing for different users

The demand of minimum time lag does not only exclude the frequency domain transformation, as it has been demonstrated in chapter 7.3.2, but also the extensive smoothing of the measured signal. The step detection would otherwise show a certain time lag to the actual position. But even more disadvantageous is the loss of phase relation especially to the yaw gyro and the heading state. Therefore, heading errors and heading error induced position errors could occur, which should be limited by the algorithm design. The step detection algorithm has been designed to work with the raw acceleration signal, not with a smoothed or low-pass filtered signal. To avoid problems with misalignment, the **total acceleration** has been used as main source for step detection.

The step detection works in four steps continuously with every new acceleration measurement. The four steps are:

- Detection of local extremes
- Application of the amplitude criterion of extremes
- Application of the motion constraint of extremes
- Application of the frequency criterion of step motion

While the first algorithm will give many indications of possible steps, the following three stages will filter out the actual steps for detection.

Since the step starts and ends with a foot touching the ground, in the first step the acceleration signal is searched for a **local extreme**. The local extreme is defined by a change of the slope (negative-positive or positive-negative) at the point of the extreme. In order to determine the slope immediately after the point of interest, the next data point must be known. As a result, a time lag of at least one epoch (in this case 50 ms/10 ms, depending on the used IMU data rate) cannot be avoided.

Figure 7-13 shows an idealized walking acceleration profile. It has been modeled for the z-axis, assuming a lifting and lowering motion during each step. The vertical velocity and acceleration are produced by derivation of the z-axis position. For the acceleration, gravity is also added to simulate the sensor output.

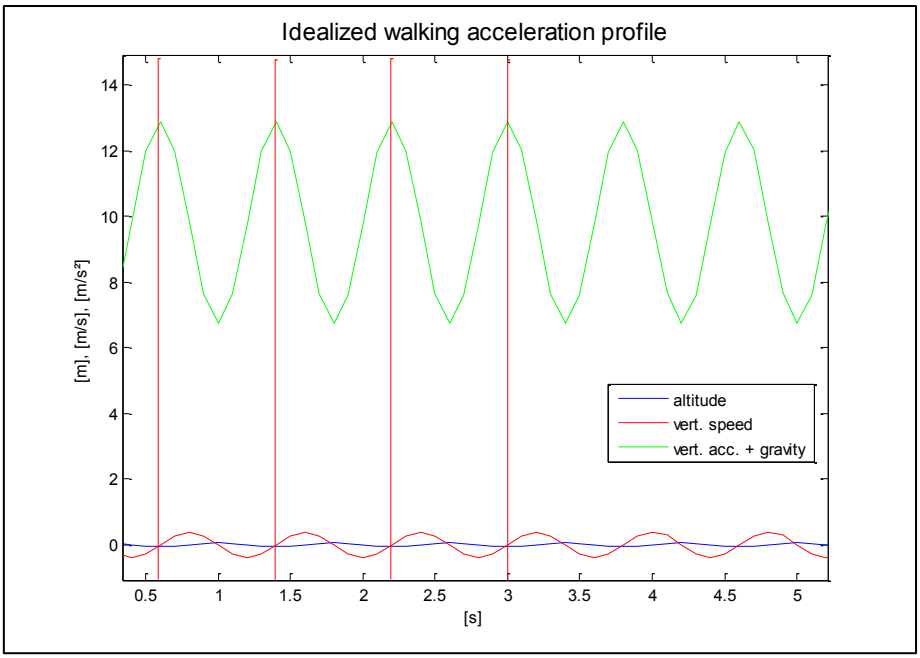

Figure 7-13: Idealized model of walking kinematics in the vertical domain

In contrast to the simple theoretical model, the measured acceleration during normal and level walking has been analyzed. As can be seen in Figure 7-14, many local extremes exist in the measured acceleration. The total acceleration, the absolute value of the total acceleration, has been used here. The algorithm, however, would work for the z-acceleration as well. Local maxima are marked with purple circles, local minima with green circles. It is obvious, that any kind of noise like signal distortion can cause additional extremes other than steps and therefore step detection only on a basis of local extremes cannot work sufficiently. Hence, an additional screening of the found extremes must be performed, which is the main purpose of the following three steps.

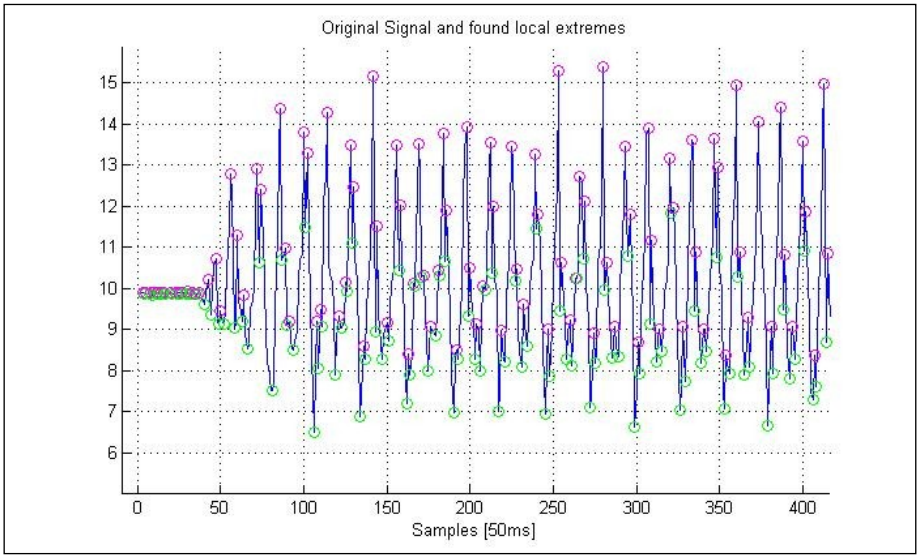

Figure 7-14: Result of the local extremes search in the total acceleration signal

As can be seen on the left hand side of Figure 7-14, there are many extremes detected in the range before sample number 50. They are caused by sensor noise as well as by small body movements

different from steps. And also after start of walking, after around 40-50 samples there can be extremes detected near the mean gravity value. These disturbing local extremes shall be removed by the **amplitude criterion for local extremes**. For this criterion, a region around the normal mean gravity value is established in which no steps are expected ("dead zone"). The test walking trials showed significant amplitudes for the lift as well as for the touch phase of the steps. These amplitudes are supposed to lie far out of the dead zone around the mean measured gravity. The dead zone was defined in the test campaigns between ±1.1 and ±1.5 m/s² around the standard gravity value. The basic idea behind this region is to filter out small peaks, which arise from sensor noise, body motions other than steps and other error sources. The step acceleration extremes are supposed to lie far outside this region, even for slow walking, and are for that reason not affected by this "rake" screening.

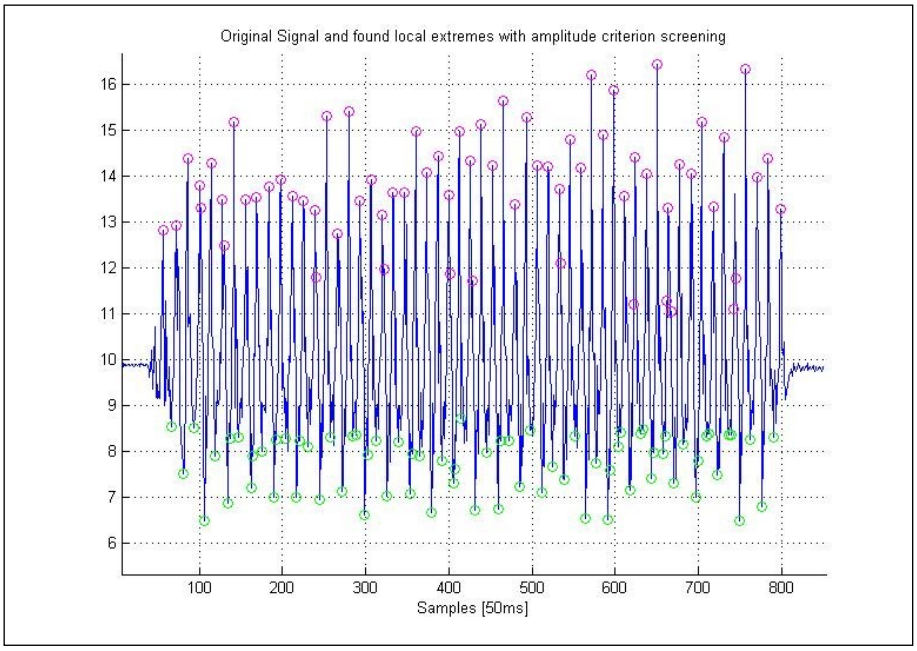

Figure 7-15: Local extremes after "amplitude criterion" screening step

Figure 7-15 shows the effect of the dead region screening. As a result all the local extremes at the beginning of the sampling have disappeared; besides, many local extremes around the mean gravity acceleration have been removed. These local extremes can result from the weight shifting process, but are reliably filtered out here. However, there are still several local extremes which do not indicate steps. They have to be removed by the remaining filter steps.

As a **constraint of the walking motion** a minimum of acceleration has to follow a maximum and vice versa. Due to the cyclic motion of walking, a step cannot consist of a maximum without a minimum. Consequently, multiple minima or maxima following each other cannot be part of several steps. Additionally, maxima have to lie above the dead zone around the local gravity acceleration and minima have to lie below the local gravity acceleration. Therefore, extremes not following these rules can be neglected and are not considered for the step detection. In summary, the motion constraint filters out consecutive maxima and minima, as well as extremes on the wrong side of the dead zone.

The final constraint is the **step frequency constraint**. The step frequency cannot take on unlimited values. As described in several publications (e.g. [63], [81]), step frequencies above 5 Hz are unlikely.

The test campaigns performed at ISTA gave the same indications. If the elapsed time since the last detected step is less than 0.2 seconds, the new step detection is neglected. Hence, detections impossible due to frequency limits are rejected reliably.

The result of the algorithm using all four constraint categories is shown in Figure 7-16. The detected steps are marked with a red “x” in the green circle of the local minimum. Obviously, peaks inside the dead zone are not registered. All steps consist of one maximum and one corresponding minimum. Several peaks are disabled by the last three constraints. It is possible that, e.g. by noise effects, the step is declared on a secondary peak which appears slightly before the primary one, but by smoothing of the step periods over three epochs this error is minimized. The step frequency as inverse of the step period will have a strong influence on the stride estimation models.

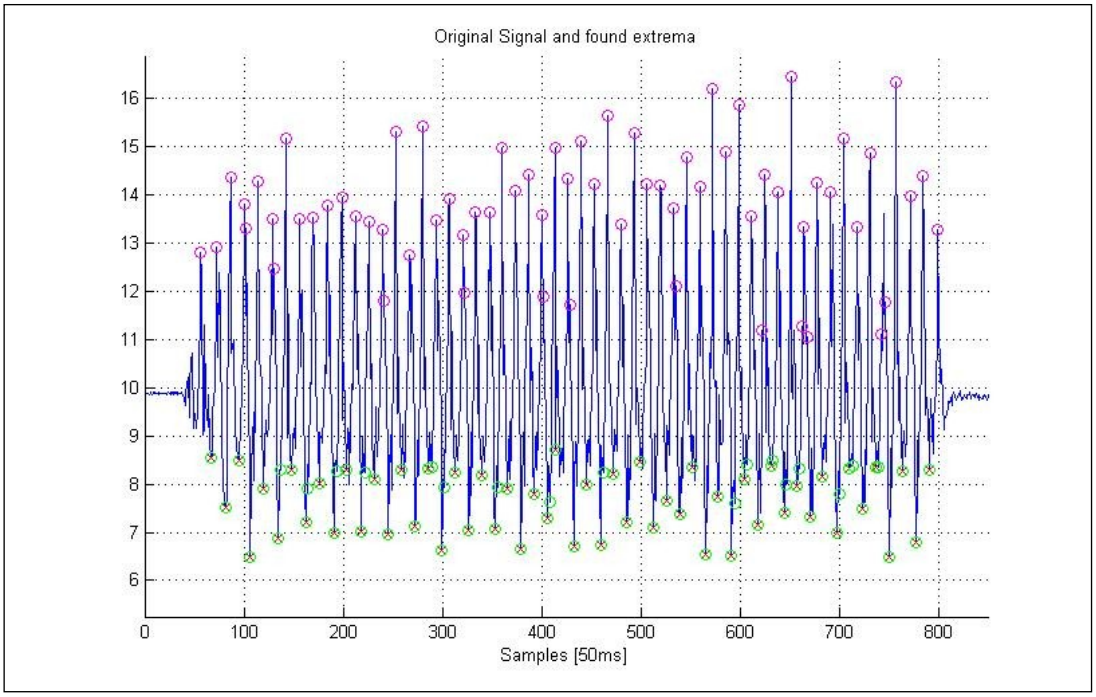

Figure 7-16: Step detection by amplitude and constraint evaluation

The algorithm proved to be reliable and tolerant on raw data. No smoothing or low-pass filtering has been applied to the sensor data. This results in a very low time lag of the step detection with respect to the actual step.

7.3.5 Practical implementation of step detection

The practical application of the algorithms described above includes changes in data handling, buffer operations and triggering of the algorithms, since the sensor is streaming the measurements continuously, while the search algorithm is bound to the available data windows. For practical application, the algorithms described in the previous chapter were implemented in C++ and compiled as a DLL. The DLL was triggered by the software receiver. IMU data is passed to the DLL from the SwRx by a sensor API.

Figure 7-17 shows a functional flow chart for the step detection algorithm, as it was implemented in the described DLL. In contrast to the experimental implementation, the data has not been read from a file and evaluated a posteriori, but passed to a ring buffer as soon as the measurements were

available. The step parameters, like the thresholds for the dead zone, as well as the maximum and minimum step frequencies, have been stored in a filter parameters' file and are read by the program at start-up. The ring buffer is continuously filled and overwritten by the sensor data. Two pointers are established, pointing to the beginning and the end of the detected step. The search for the new step starts at the detected end of the last step and ends with the step detection. The pointers are reset after the step detection; special procedures apply if no step is detected for the entire ring buffer length.

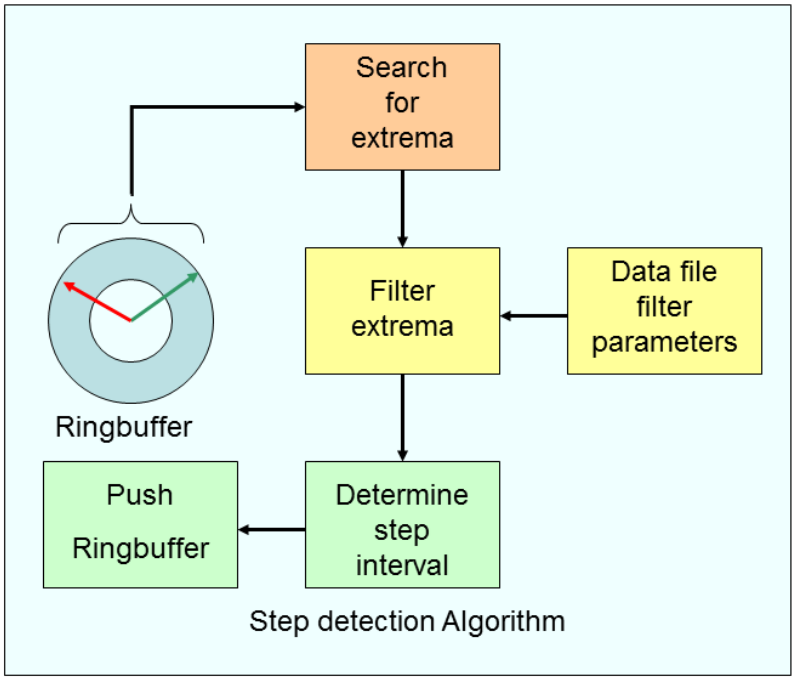

Figure 7-17: Step detect algorithm flowchart

After data update of the ring buffer by the API, the algorithm searches in the current part of the ring buffer for extremes. This is performed by calculating the total acceleration of the IMU and a search for points, in which the derivative of the total acceleration changes is sign (peak detection).

The extremes are categorized as maxima and minima, while an area around zero ("dead zone") is assumed to be forbidden for extremes (amplitude criterion). Maxima are only allowed in the region above the dead region, minima only below the dead region. Experiments proved that a dead zone of +-1.1 m/s² filters the body motion noise effectively for most users. A step is finally detected if the motion constraint and the frequency constraint are fulfilled. The step interval is than passed to the step classification algorithm to free the ring buffer data.

7.3.6 Summary

In this chapter one of the major parts of the pedestrian navigation system, the step detection algorithms have been addressed. At first the biomechanical aspects of walking have been evaluated. Then the placement of the sensor suite on the test person's body has been discussed. Several step detection algorithms have been found in literature and have been tested and discussed. Finally a step detection algorithm based on several criteria has been developed and described. The algorithm has been implemented finally into a software receiver as part of an operational PNS system.

7.4 Step classification

Step classification is the second core element of a PNS. As mentioned before, not only the detection of steps but also the classification of the step type is important to propagate the user position correctly. Step classification is important because different kinds of steps exist which demand different processing. Running, normal walking and slow walking are among those step types. But even more important are steps with vertical components like climbing stairs. It is obvious that climbing stairs does not only change the horizontal position, but also the vertical position. Since the position solution has to cover the floor number, too, the vertical position must also be tracked. For that reason the step types “up” and “down” must be covered. Without step classification, PNS is usually only a two dimensional system. Therefore user motion with significant height components, e.g. on stairs, could not be followed correctly by the navigation system. In the following chapter, several types of steps are discussed and parameters for the identification of the step type are discussed. Then several techniques of step classification are introduced and evaluated. Finally, a fuzzy logic based step classification system is introduced, which has been implemented in the prototype system.

7.4.1 Types of steps and parameters for classification

Several types of steps can be distinguished, demanding special treatment during navigation processing. These types could be for example:

- Inclination types:
  - Level step
  - Step down (e.g. on stairs)
  - Step up (e.g. on stairs)
- Velocity types
  - Running
  - Normal walking
  - Slow walking

The inclination types are especially important, because inclined steps do not only change the current height of the pedestrian and for that reason are an important indicator for floor transitions, but also shorten the horizontal length of the stride and so the estimated stride must be adjusted. An average change of height of approximately 0.17 m could be measured in several test campaigns in different stairways, while the average horizontal distance has been around 0.25-0.3 m on the stairs.

The velocity kinds are interesting for improvement of the stride estimation. As can be seen in Figure 7-28 for step frequencies above 2.7 Hz the curvature of the stride-step frequency relation changes its properties. This is due to the change of the motion type from “walking” to “running”. Consequently, another adjustment of the estimation function could result in a better convergence and therefore improve the distance estimation; the step estimation only based on the step frequency had to be overridden or assisted by the step classification. On the other hand a transition from a closed algebraic relationship to look up tables or other customization could also replace the velocity states by customizing to individual pedestrians.

Several observations exist to support the decision between the different walking states. These are basically the same as for the step detection, but possibly with different data processing:

- Acceleration amplitudes (x, y, z)
- Rotation rate amplitudes (x, y, z)
- Means and variances of the data in the individual sensors
- Phase relationship between the inertial measurements (cross-correlation)
- Step frequency determined by the step detection algorithm

Since walking states are to be determined and multidimensional observations are to be used for the detection of the state, fuzzy logic systems seem especially suited for this task. For definition of the individual membership functions of such a fuzzy logic system often calibration data has to be collected and evaluated to gain individual set points. It must be pointed out that the measured quantities and the statistical, as well as phase relation properties change with placement of the sensor on the body. The fuzzy setpoints, as well as other criteria are specific for the individual placement of the sensor, may it be overhead, on the belt, or on the shoe.

7.4.2 Step classification by signal cross-correlation

As shown in chapter 7.2.1, walking consists of several cyclic movements. The phase relationship between these signals seems relevant for decisions about the walking behavior. Thus, in literature, algorithms have been developed to determine the cross-correlation between the inertial measurements ([48], [54], [55]). To analyze the reliability of these cross-correlations, the cross-correlation was determined for several signal combinations between each of the consecutive steps. In an evaluation campaign most of these relations did not prove to be significant enough for step classification. However, one combination showed significant results, i.e. the cross-correlation between the **x-acceleration** and the **z-acceleration** signals. It is important to mention that this is true especially for belt mounting of the sensor. It is not reliable for overhead mounting.

For the evaluation the acceleration data was sampled and separated in the individual step intervals. The sensor has been placed on the belt of the user. Then for each step (period approximately 13 epochs = 0.65 s) the cross-correlation for ±20 epochs time shift has been calculated and plotted. Since the sample length is shorter than the maximum time shift, the cross-correlation at the edges reaches exactly zero and the integral over the whole range results in zero.

In the first test the test user performed only level steps. Figure 7-18 shows the signal cross-correlation for level walking. Is it obvious that the shape of the curvatures is approximately symmetrical, with the symmetric axis slightly in the positive; the curves consist of a sharp maximum in the center, two minor maxima on the outside and two minima of approximately the same size.

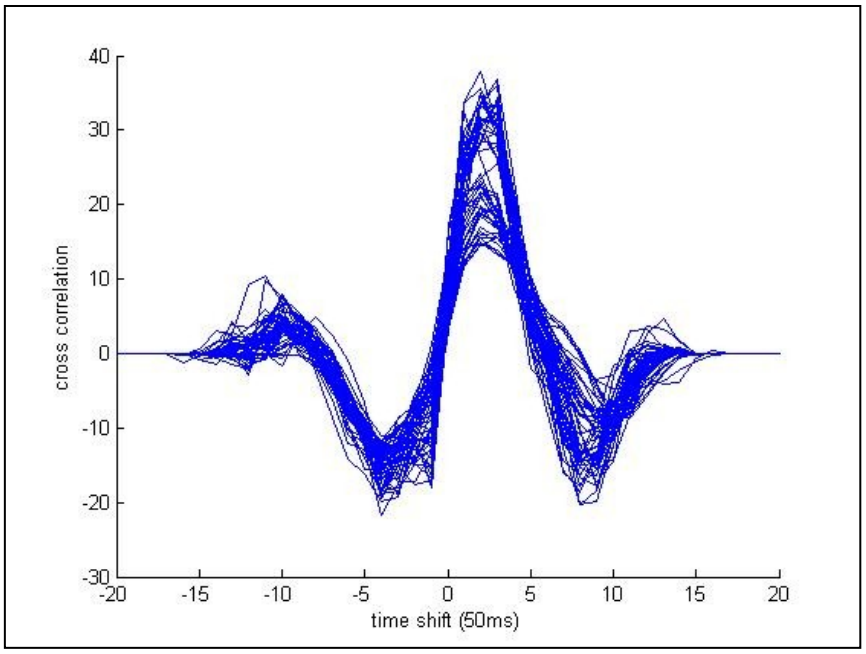

Figure 7-18: Cross-correlation of x- and z-axis acceleration signals for level walking

Then a test campaign on a staircase has been performed. The test path is shown in Figure 7-19. The path consisted of 3 steps run-up, followed by 11 stairs up, 1 level step, followed by 10 stairs up. The run was finished by 3 level steps.

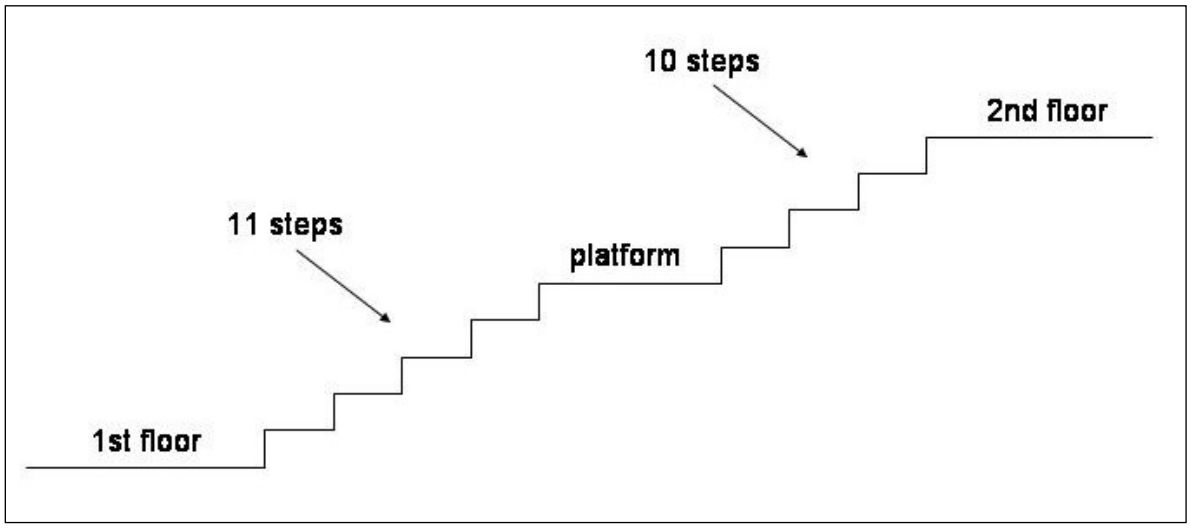

Figure 7-19: Schematic plot of the staircase used for development and testing

Figure 7-20 shows the same data for the described stairs with a small platform in the middle. While the plots seem slightly distorted, the basic form is constant. There is a difference in the amplitude for level and up walking in this case, as well as a slight time lag of the maximum for the level steps in comparison to the up-steps. Nevertheless, this is extremely user dependent and is not specific enough for a general rule.

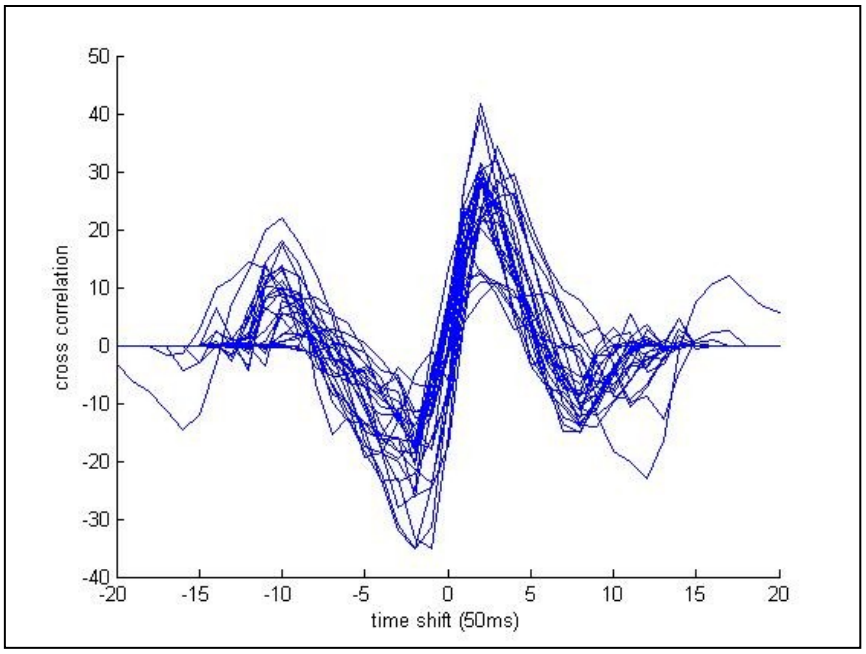

Figure 7-20: Cross-correlation of x- and z-axis acceleration signals for up and level walking (21 up / 7 level)

Figure 7-21 on the other hand shows an exemplary cross-correlation of a **downward step** and was measured in one of the walking trials. There is significant difference in the shape of the cross-correlation function in comparison to the level and upward steps. The attributes of the shape are very significant and can be found very reliably at downward steps.

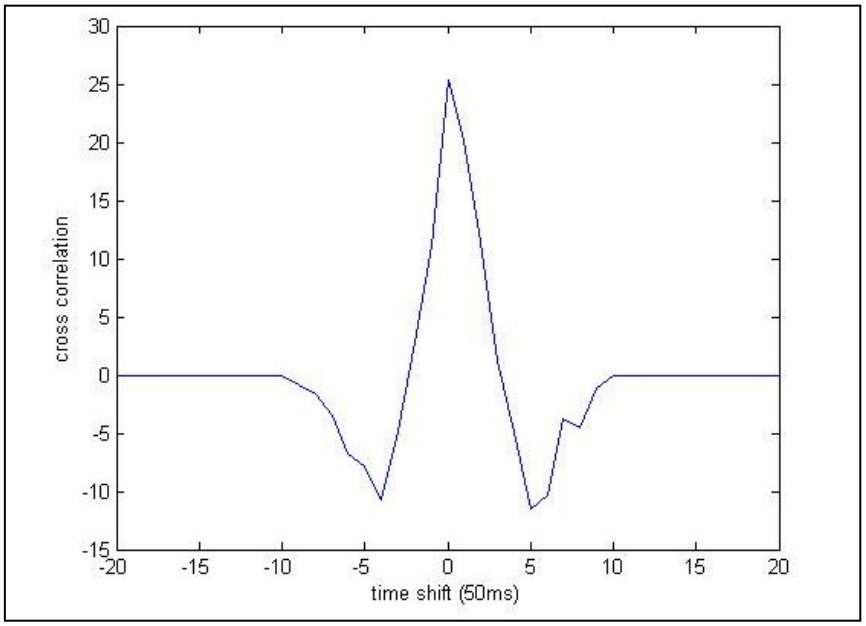

Figure 7-21: Cross-correlation of x- and z-axis acceleration signals for down walking

The test campaigns showed that while the level and upward steps have a cross-correlation function in the form of a double-S-curve, the downward steps have a cross-correlation function in the form of a “W”. To use this difference in the shape of the cross-correlation function between x- and z-axis acceleration a mathematical or numerical representation for the function was developed. The basic idea behind this algorithm is to divide the data in two half intervals, which are separately integrated.

As was stated earlier, the integral over the complete time lag range results in zero for time shifts larger than the step interval. This is true for the whole integral, therefore it is also true for the sum of two splitted integrals, dividing the integration time in the middle or in other words, integrating the negative time lag and the positive time lag separately. It is not true for the difference between these separate integrals, which is the major criterion in this algorithm. The cross-correlation is integrated for the positive and negative time lags separately. The result of the sum and difference of the two sub-intervals is used to determine downward steps from level and upward steps. This relationship is formulated as:

$$R_{X,Z}(n) = \frac{1}{2N}\sum_{i=-N}^{N} X(i)Z(i+n)$$

$$R_{X,Z,1} = \frac{1}{N}\sum_{i=-N/2}^{0} R_{X,Z}(n)$$

$$R_{X,Z,2} = \frac{1}{N}\sum_{i=0}^{N/2} R_{X,Z}(n) \qquad (72)$$

$$\Delta R_{X,Z,1,2}(n) = R_{X,Z,1}(n) - R_{X,Z,2}(n)$$

Symbol	Explanation
$R_{X,Z}(n)$	Cross-correlation of the measured accelerations X and Y for the time shift n
$R_{X,Z,1}(n)$	Sum of the cross-correlation values of the measured accelerations X and Y for negative time shifts
$R_{X,Z,2}(n)$	Sum of the cross-correlation values of the measured accelerations X and Y for positive time shifts
N	Number of samples during the step interval
X	Measurement vector of the x acceleration
Z	Measurement vector of the z acceleration
i	Number of individual sample
$\Delta R_{X,Z,1,2}(n)$	Metric of the step classification by cross-correlation

Table 7-5: Symbols used in the step classification cross-correlation function

To prove the concept, a test walk and experimental implementation of the algorithm has been performed. In Figure 7-22, a test walk on the same stairs as in Figure 7-19 is evaluated. The walk consisted of the following sections:

- 3 level steps run-up
- 11 stairs upward steps
- 1 level step on a stairs plateau
- 10 stairs upward steps
- 3 level steps run-out
- turn around/standing still
- 3 level steps run-up
- 10 stairs downward steps
- 2 level step on a stairs plateau
- 11 stairs downward steps
- 3 level steps run-out

The figure shows the measures explained above. The cross-correlation function is calculated for every step period after the step detection. It is parted for positive and negative time lags and the two intervals are integrated separately.

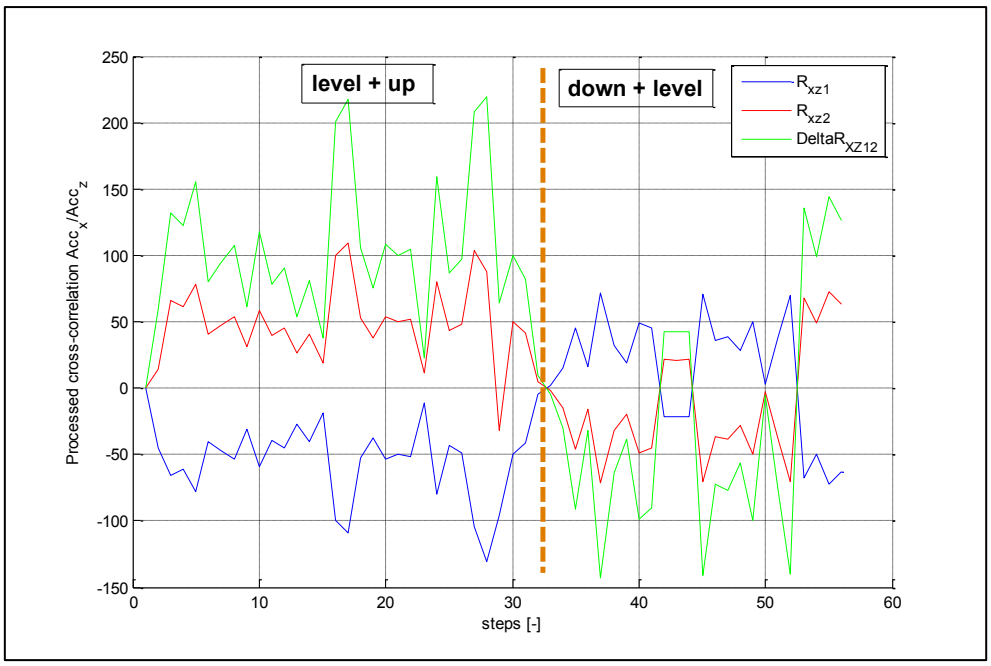

Figure 7-22: Evaluation of integrated cross-correlation of x- and z-axis acceleration signals

The separate integrals are represented by the blue and the red solid lines. The metric, the difference is plotted green. The metric shows the distinction of downward steps to the other step types: for **level and upward steps** it shows **positive values**, for **downward steps negative values**. As can be seen in the right part of the figure even the level steps on the plateau on the walk downwards are clearly detected. Hence the difference of the partly integrated cross-correlation function of the x- and z-axis acceleration is an **excellent indicator for downward steps**.

The distinction between the level walking and the upward stairs walking is more difficult, since the cross-correlation is not specific enough to distinguish between upward and level steps. As it has been

shown in Figure 7-18 and Figure 7-20, the signal pattern does not change significantly between level and upward walking. The integral difference does not offer a significant and reliable criterion to distinguish between these walking states. As it was stated earlier signal amplitudes in the time domain are also not applicable, because the mounting of the platform on the body as well as the body pitch during walking is neither constant nor generally predictable.

7.4.3 Step classification by Fuzzy Logic

Since the measured accelerations and rotation rates for the individual walking states are highly user dependent, a step classification algorithm based on fuzzy logic will be presented in this chapter. Detailed information on the principles and capabilities of the fuzzy logic approach can be found in [117] and [116].

Several information sources have been evaluated for the step classification besides the already mentioned measures. These included:

- Signal amplitudes
- Signal variances
- Signal means
- Other cross-correlations than x/z-acceleration
- Time dependencies of amplitudes

Single observations cannot offer a clear, unambiguous measure to determine the type of step (up, level). In addition to that, the measures vary between individual test persons. No common method or dataset could be found to perform general walking classification for all possible users with high probability of correct step classification. For step classification, an approach including several independent measurements and the option of calibration to individual users has been chosen. A combination of several criteria offers the chance of reliable and customizable step classification.

An example for this is the mean x-axis acceleration in the body frame. It can be an indicator for upward steps, but is not absolutely reliable and can therefore only be one element of several criteria. It is mentioned in several publications, and has also been experienced during the test walks, that the body leans forward during climbing of stairs, inducing the gravity vector to appear as negative acceleration in the x-axis accelerometer outputs. This fact can generally be observed, but the extent is user and use case specific. Negative x-acceleration does not automatically indicate forward movement, but the measurements would show significant lower values compared to level walking. Figure 7-23 shows the mean x-axis acceleration during the walk already described for Figure 7-22. It can be noted that the mean x-axis acceleration is significantly lower for level and downward walking, than it is for upward walking, which is the result of the body pitch.

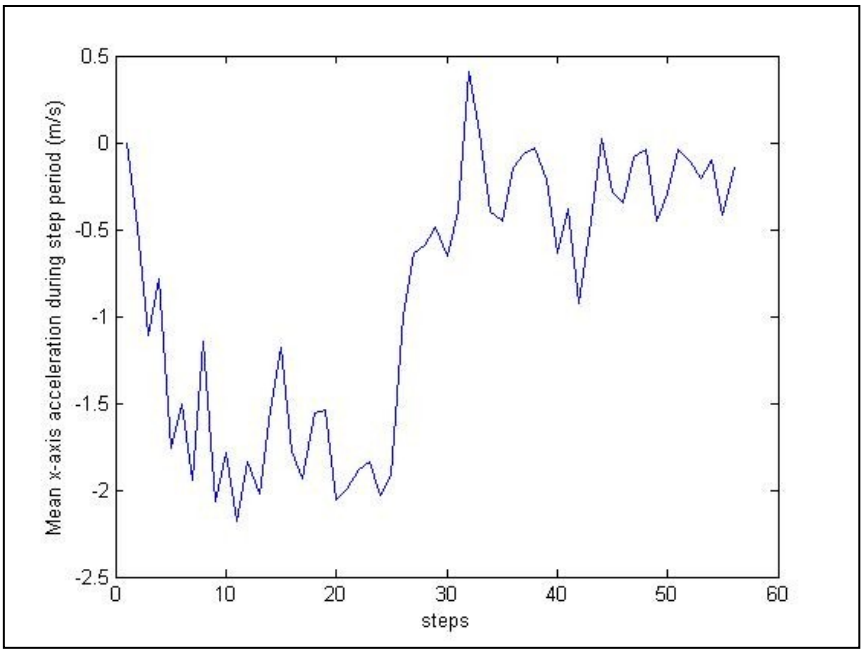

Figure 7-23: Mean x-axis acceleration during up and down walking of a staircase

Fuzzy logic is a strategy to estimate the current system status by using various "fuzzy" input variables. Fuzzy logic systems determine states by evaluating multiple observations to form a decision value. Based on this decision value the current state is estimated. The basis of fuzzy logic is the principle of fuzzy **"memberships"**. In contrast to common set theory, fuzzy logic allows degrees of membership of elements to sets. The membership is expressed by the magnitude μ, which can vary between 0 and 100%. So called **"fuzzy rules"** are used to map these memberships to decisions about the actual state.

In practice, a walking state shows certain attributes in measured data, e.g. the variance of the x-axis acceleration or the amplitude of the z-acceleration during one step. **Set points** can be modeled for each **attribute** which represent e.g. the average value of this measurement for a specific walking situation and a specific pedestrian. A measurement matching this set point exactly would mean 100% membership to the set defined for this attribute, walking state and person. On the other hand, with increasing difference of the measurement to the set point the degree of membership must decrease as well. The relation between difference from the set point and degree of membership is called **"membership function"**.

Several possibilities exist to model the membership functions. Some possibilities are linear functions (triangle, square, straight lines, etc.), continuous functions, exponential functions and many more. The integral over the full input range does not have to equal any specific value, but the membership function's result must fall between 0 and 1. Although the modeling of the membership function can be accomplished freely, the modeling must optimize the result in any way; therefore deterministic development is to be preferred.

To visualize the statements above some examples for exponential membership functions of Gaussian type are shown in the following. They have been used in the developed fuzzy logic approach, too, because the measurements performed for individual test persons can easily be taken into this model by evaluation of means and standard deviations of the calibration measurements.

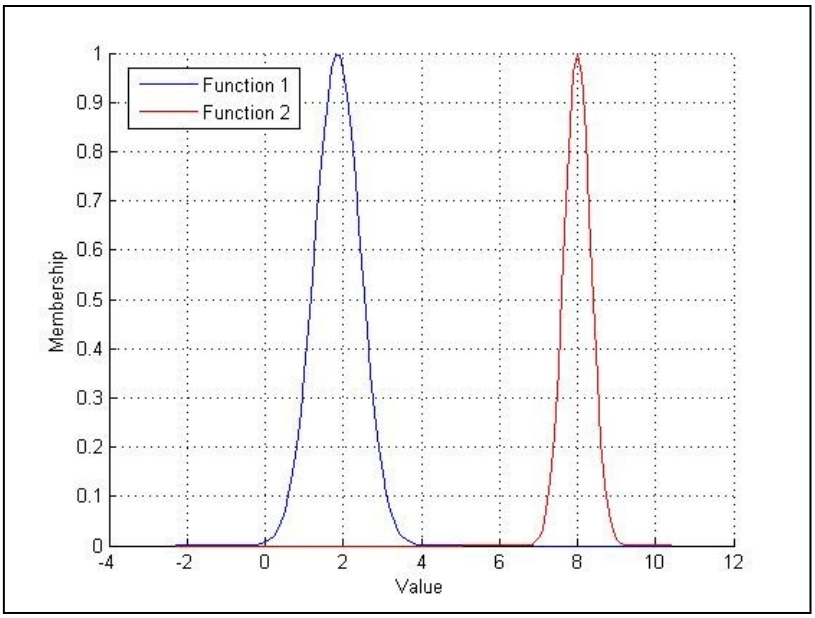

Figure 7-24: Fuzzy membership functions nearly without ambiguities

Figure 7-24 presents two membership functions for an observed variable ("Value"). The membership functions show quite significant separation of their means (blue function approximately '2', red function approximately '8') and different, but both small standard deviations. If the blue function represented the membership function of "level walking", and the red function represented the membership function of "upward walking", a measurement of e.g. 3 would result in a higher membership to "level" than to "up". On the other hand measurements between 4 and 6 would not result in significant degrees of membership to any of the functions. Consequently, regions exist, where the placement into one set is rather unambiguous, while regions exist where no significant membership can be determined.

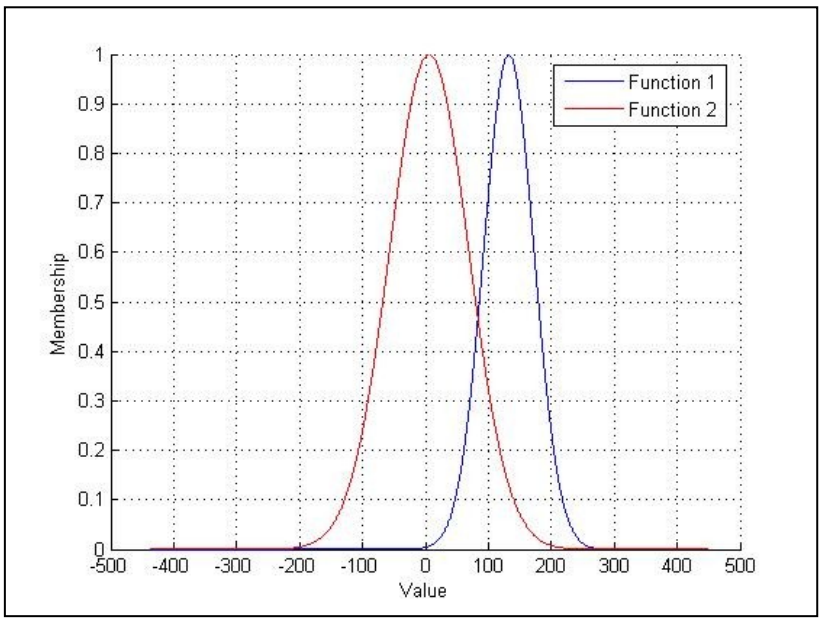

Figure 7-25: Fuzzy membership functions with moderate ambiguities

Figure 7-25 shows moderate ambiguities by crossing of the curvatures at a degree of membership of around 46%. This results in a larger area of ambiguity and a higher risk of false detections around the crossing point. Additionally, even for high degrees of membership to one function, the other function will also result in a degree of membership noticeable larger than zero. On the other hand there is no area between the two functions without significantly high memberships. Memberships near zero are obtained only far outside of both function center points.

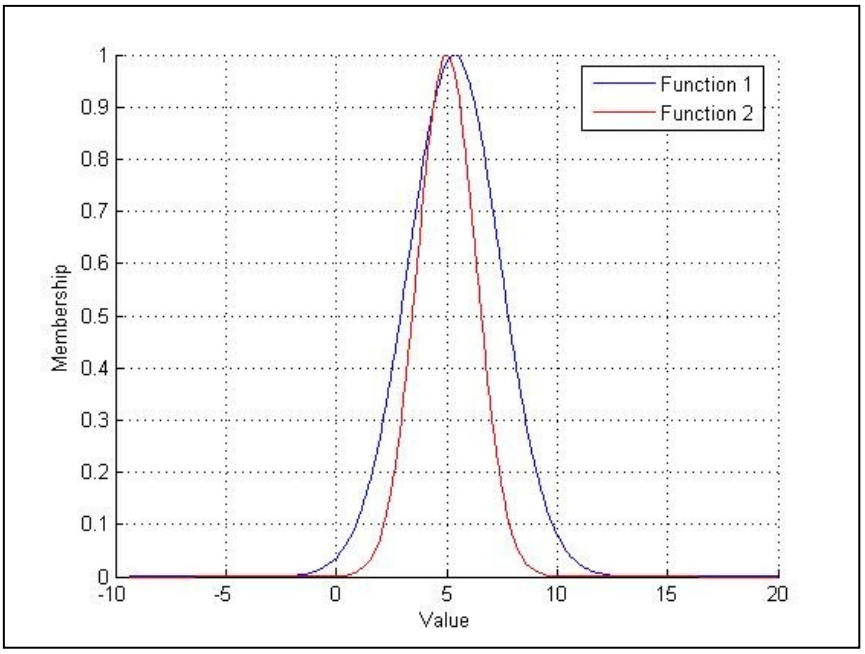

Figure 7-26: Useless fuzzy membership functions because of extremely high ambiguities

Figure 7-26 shows a set of memberships which is particularly misleading in practice. Both functions show basically the same set point with only different width of the membership function (standard deviation). Therefore, the standard deviation estimated in the calibration phase is the only information used for the determination of the membership. Because the calibration has only a limited extent, big errors can be induced here. Extremely high ambiguities are induced in a modeling like this. On the other hand, measurements near the set point would not reveal any information. Since the standard deviation in this case is extremely small, resulting in extremely steep membership functions, even small deviations from the set point can result in big differences of the calculated memberships.

It is obvious that measurements and quantities to be used as membership functions have to be evaluated carefully before usage to avoid misleading modeling and wrong interpretations. Additionally, if using multiple arguments for several membership functions a weighting of these memberships need to be applied for optimization. The influence of function sets with little significance can be reduced by appropriate weighting of the fuzzy membership results, while the influence of highly significant sets can be increased. On the other hand, the input measurement can vary significantly and the walking is not consistent mandatorily. Thus also the case, in which even usually highly significant function sets do not reveal a great deal of information must be covered. Automatized evaluation and weighting reduces manual efforts for practical application.

7.4.4 Implementation of step classification

In the previous sub-chapters, two techniques for step classification have been described. The complete algorithm is a combination of both strategies. In the first step it is evaluated, if a downward step is present. This is done in the way described in chapter 7.4.2. As described, the cross covariance criterion is critical here. If this is not the case, level and upward steps are evaluated. The individual weighted memberships are therefore summed up and compared. The walking type with the highest sum of membership values is selected.

For this use case a modeling of a fuzzy set consisting of the following variables has been constructed:

- Rotation rate amplitude around x-axis (during one step period)
- Acceleration amplitude along the z-axis (during one step period)
- Variance of measured accelerations along the x-axis (during one step period)
- Variance of measured accelerations along the z-axis (during one step period)
- Variance of measured rotation rates around the z-axis (during one step period)
- Mean acceleration along the x-axis (during one step period)
- Integrated height change by barometer
- Sub-integrals analogue to cross-correlation method

Several parameters are included for measurements in the body and in the navigation frame.

The differences of the calculated memberships for up, level and down have been used as main weighting parameter. The weighting is followed by summation and a decision based on majority can be seen as special form of fuzzy rules. As described before the step classification is important for the PNS. While the step detection gives information about the walking state, the kind of motion, the direction and the covered distance cannot be determined by the step detection algorithm. Therefore, the kind of step has to be categorized in an additional algorithm. The main categories for the steps are:

- Up
- down
- level

The membership functions are of Gaussian design.

$$\mu = e^{-\left(\frac{u-m}{s}\right)^2} \tag{73}$$

Parameter	Explanation
μ	Degree of membership
u	Measurement
m	Mean, set point of membership function
s	Standard deviation, “width” of membership function

Table 7-6: Parameters of the Gaussian membership functions for step classification

The set points for the membership function are read from a data file and are the result of a calibration campaign. For each of the mentioned parameters the memberships are calculated. The individual results of the fuzzy system are combined by a set of gains. These gains are determined by significance of the measurement in comparison to the membership function. If the significance is low, also the gains are adjusted to weight this information lower than memberships with higher significance.

$$g = \left|\mu_{p\_s1} - \mu_{p\_s2}\right| \tag{74}$$

Parameter	Explanation
g	Gain for membership function
μ	Degree of membership
p	individual parameter
s	state of motion: level, up, down

Table 7-7: Parameters of membership weighting algorithm

The memberships for up level and down walking are summed up, using the weights defined in (74).

$$\mu_{total,type} = \sum_{i=1}^{N} \mu_{i,type} \cdot g_{i,type} \tag{75}$$

Parameter	Explanation
$\mu_{total,type}$	Total degree of membership of step to a type
$\mu_{i,type}$	Individual degree of membership of step to a step type
$g_{i,type}$	Gain for individual membership function
type	Type of motion: level, up, down
N	Total number of membership functions per type of step

Table 7-8: Parameters of membership weighting algorithm

The step type with the highest total membership value is selected. The total degree of membership is not normalized; hence values above 100% are possible.

Since the walking behavior of each human being is specific, there is the need for individual calibration. The calibration can be performed by a short test campaign, during which parameters for the individual step types are evaluated. For example a level walk on the floor, a down-walk on stairs, etc. can be used and evaluated statistically. By evaluation over several steps the individual walking behavior can be estimated and new set points for the fuzzy system can be determined.

7.5 Stride estimation

Besides detecting the actual step, like demonstrated in the previous chapter, also accurate estimation of the step length ("stride") is important for precise pedestrian dead reckoning. Unfortunately, the stride is usually not observable by MEMS type IMUs mounted on the belt or overhead of the user. Thus the stride must be estimated by observable measures, which requires a mathematical model to relate the stride with observable parameters, e.g. the step frequency. For this reason, a calibration campaign has been performed with several test participants to identify parameters for the stride model. The test campaign was also used to evaluate the need of a flexible stride model in comparison to a fixed stride model. For applications with limited calibration time the model was additionally generalized to be used as default model without the necessity to calibrate for each person. Finally, the model has been integrated with the step detection algorithm to be executed together with collected data.

7.5.1 General aspects of stride estimation

The stride is defined as the range which is covered during one step in longitudinal direction. This definition is sufficient in two dimensional movement, e.g. without changing the floor. The stride is sometimes assumed as constantly around 0.7 m in literature (e.g.[63]), several sources describe the stride as within a certain interval around 0.7 m (e.g. [48]), and several attempts to measure the stride directly could be found. Often special sensors were used which are not part of the scope of this thesis. Publications describe the mounting of the IMU directly on the shoe to take advantage of the zero velocity phases during the heel down phase. For the given scope in this thesis, direct measurement of the stride was impractical.

During the test campaign, which was held during the progress of this thesis, the amplitude of the stride varied from 0.5 to 2.0 m depending on several parameters (Figure 7-28). While for standard walking with an average walking speed the fixed estimation of 0.7 m fits roughly, significant deviations can be detected if the walking speed changes, or if other factors influence the result. The difference to the fixed estimation of 0.7 m nevertheless is too big as to keep the fixed stride model for navigational purposes. A deviation over 1 m per step is not acceptable for indoor applications. Hence, the need for a user specific stride model is evident and could be shown in the test campaign. Using a constant stride for DR is not precise enough for the given task.

Stride changes also for vertical and horizontal walking. If vertical movement e.g. on stairs has to be considered, too, standard stride estimation is not sufficient. On stairs the motion is constraint to the stair height and stair depth, and possibly multiples of them if more than one step is climbed at once. The motion pattern changes significantly in comparison to level walking. Hence, a strong relation between the step classification and the stride estimation exists in non level walking. For vertical movement the position propagation must be modified to keep track of the actual altitude, not only the horizontal position.

It should be noted that even for the same person step length can vary significantly, e.g. if heavy loads are carried. For a test person equipped with a backpack and approximately 6 kg load on the back, the step size on the described test range shortened by 15%.

7.5.2 Data basis and test campaign

Like mentioned in the previous chapter, a test campaign has been performed to acquire field test data for stride estimation. A test range consisting of a straight, 38.5 m long and tiled floor has been used for the first walking test campaigns and also for the stride evaluation trials. Several test persons tried to walk this range several times with different walking speeds. The individual number of steps as well as the individual walking time as a measure of the walking speed have been recorded and evaluated. The test persons included female and male test persons of different size and weight as well as different age. The test runs were repeated several times to gain information about the repeatability of the results.

Intentionally, during the individual test runs the walking speed should remain approximately constant. To assure that, the test track was shortened for the “high speed” runs for the sake of acceleration and safe deceleration run-outs. The test track was shortened to 35 and 30 m depending on the speed to be reached and the data has been corrected for the different track lengths. The test walk trajectory should stay close to a straight line and the walking motion should stay as normal as possible. The number of steps as well as the time needed to cover the distance of the test track has been registered. The runs showed a good repeatability for the individual test persons.

Figure 7-27 shows some result of the test walking campaign. It has not been possible to direct a certain walking speed to the test participants. Instead of this, the participants were asked to walk at a constant speed and then directed by “faster”, “slower” or “same speed again”. As a result the step frequencies of the participants can only be compared by evaluating the whole dataset. It is obvious that a direct relation between the number of steps and the time of travel exists and follows the same rules for all participants.

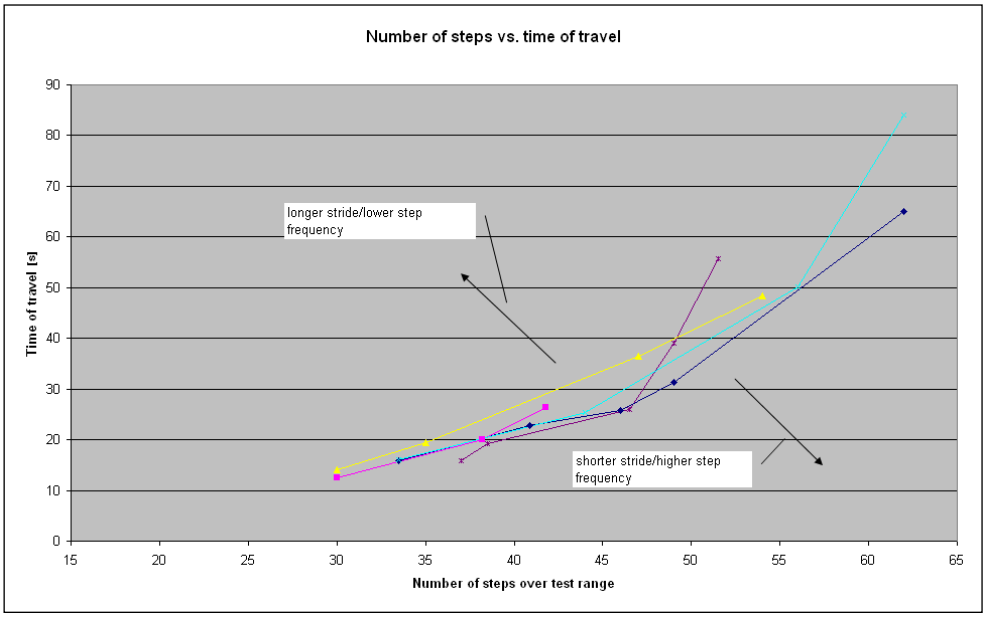

Figure 7-27: Number of steps versus time of travel on the test track for several test persons

This becomes even clearer when the data is modified to show the stride versus the step frequency. This is visualized in Figure 7-28. The data shows an exponential curve which is flattened when reaching extreme high step frequencies. The test campaign showed that stride as well as step

frequency is individually limited. This means that at reaching a certain stride the velocity can only be increased by increased step frequency.

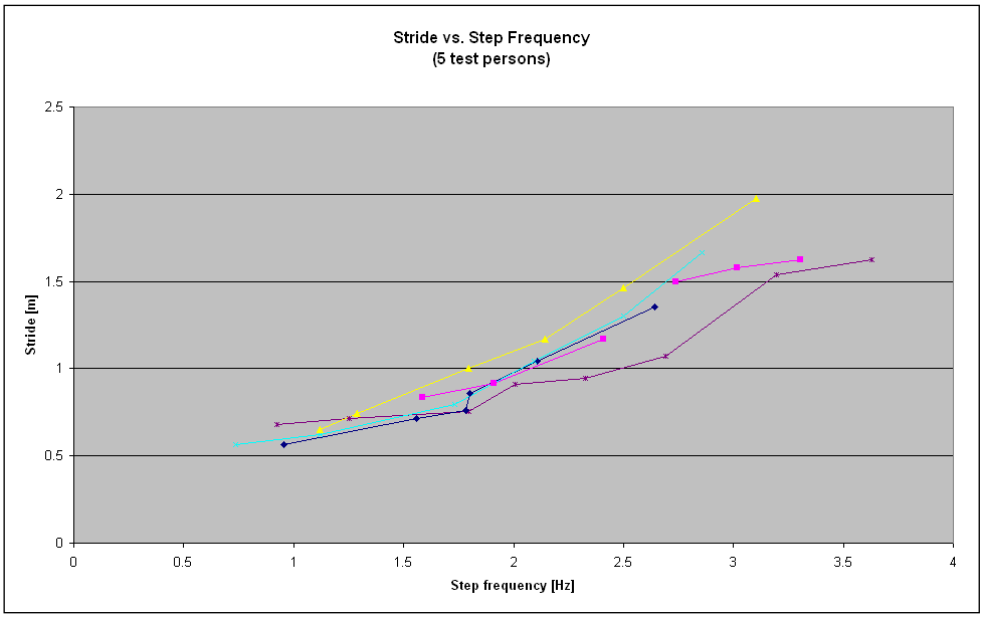

Figure 7-28: Stride versus step frequency for several test persons

7.5.3 Parameter identification for the stride model

Several approaches for stride estimation with several strategies and parameters exist in literature. While some authors use complex fuzzy logic systems and multiple parameters (e.g. [55]), others use geometric properties of the user's legs and measured thighs and shanks angles ([84]), direct measurement of stride ([5][2]), or look up tables and look up functions for estimation of the stride (e.g. in [48], [54]). Some authors model the stride as constant value and model and estimate the stride variation as noise process (e.g. [63]). In principle it must be distinguished between adaptively trained systems and systems which use a common database for all users.

Adaptive systems can be adjusted for each user individually. They use a set of parameters as well as a mathematical system to estimate stride by observation of the parameters and individual reference data gained in a training or calibration phase.

Several systems use a common database which is gained by observing many test participants (e.g. in [51]). In parameter identification phase this data is analyzed to gain a model which defines a relation between the analyzed parameters and the stride measured for the test persons. In practical use the PNS stimulates the general model derived from the test campaign with the measured parameters and estimates the stride.

For this thesis, a least squares adjustment of several recorded test cases has been performed to gain a closed steady formulation instead of look up tables. Several parameters have been evaluated, e.g. signal amplitudes, step frequency, body height, etc. For the most robust solution, the step frequency was identified as most crucial parameter for stride estimation. It was recognized that for different walking behaviors like "walking", "running" or possibly "jumping" the solution can even be improved, while the individual strides vary more significantly with increasing step frequency. Signal amplitude is

a critical parameter, because the measurement of the acceleration peaks has a high uncertainty due to the discrete sample time of the IMU and the short time effects of shocks.

The solution can also be improved by choosing an appropriate subgroup of the database, e.g. based on gender, body height or weight. However, the developed general estimation approximation shows good results for a general modeling as well, as can be seen in Figure 7-29. Individual fine tuning or customizing can be applied to increase the accuracy.

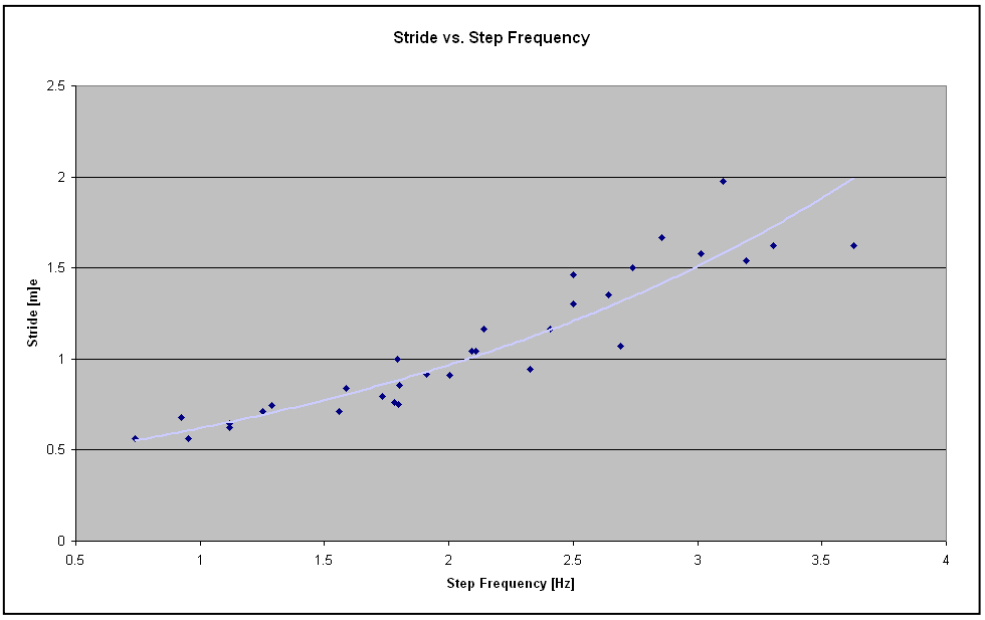

Figure 7-29: Generalized stride/step frequency model

The stride can be approximated by an individual stride function and reflects the walking behavior of a person. Main identified parameter is the step frequency. While a standard function has been derived that is usable with reduced accuracy for most adults, individual calibration results in additional accuracy. The stride model equation is:

$$s = ae^{bf} \tag{76}$$

Parameter	Explanation
s	Stride estimation
a	Linear individual parameter of stride function
b	Exponential individual parameter of stride function
f	Step frequency [Hz]

Table 7-9: Parameters of stride estimation function

For the calibration, the measured parameters, average stride and step frequency are used as observations in a linear adjustment of the parameters a and b. During the setpoint calibration campaign for the step classification system, also the parameters a and b are calibrated for each individual user.

7.6 Dead Reckoning

Dead reckoning is performed by propagating the user position triggered by the step detection algorithm. Assuming that the step is in the level plane, the distance traveled in the two coordinate directions can be assumed as:

$$dx = s \cos \Psi \tag{77}$$

Parameter	Explanation
dx	x-axis position increment in local level Cartesian coordinate frame
s	Stride estimate
Ψ	Heading estimate

Table 7-10: Parameters of dead reckoning x-axis increments

and respectively:

$$dy = s \sin \Psi \tag{78}$$

Parameter	Explanation
dy	y-axis position increment in local level Cartesian coordinate frame
s	Stride estimate
Ψ	Heading estimate

Table 7-11: Parameters of dead reckoning y-axis increments

For non-level steps the stride model must be adjusted. On stairs a normative length of around 0.3 m is adequate in most cases. Additionally, a lift or drop of the step of 0.17 m can be assumed for single stairs. For this case the third dimension has to be considered as:

$$dz = n * dAlt \tag{79}$$

Parameter	Explanation
dz	z-axis position increment in local level Cartesian coordinate frame
n	type of step: (0: level, 1: up, -1: down)
dAlt	Step lift or drop

Table 7-12: Parameters of dead reckoning z-axis increments

The heading information can be derived from the AHRS algorithm described in chapter 6, or from an internal attitude reference, if the IMU system, like the Xsens MTi, offers this feature. The MTi provides the current attitude with 100 Hz rate and configurable as quaternions, Euler angles or direction cosine matrix (DCM). For the real-time implementations, quaternions have been chosen

and are configured by the used SwRx. The heading has to be determined between the consecutive steps, as the hip follows the leg in the swing phase. The actual heading of walking can therefore be determined best in the neutral phase between two steps.

The conversion from the local level coordinate frame to the WGS 84 Earth-Centered-Earth-Fixed frame is performed by a standard coordinate transformation:

$$Pos_{WGS84} = Pos_{WGS84,0} + C_n^e Pos_{n,locallevel}$$

$$r^e = r_0^e + C_n^e r^n \tag{80}$$

$$C_n^e = \begin{bmatrix} -\sin\varphi\cos\lambda & -\sin\lambda & -\cos\varphi\cos\lambda \\ -\sin\varphi\sin\lambda & \cos\lambda & -\cos\varphi\sin\lambda \\ \cos\varphi & 0 & -\sin\varphi \end{bmatrix}; C_e^n = C_n^{e^T}$$

Parameter	Explanation
λ	Longitude
ϕ	Latitude
C_n^e	Transformation matrix from n-frame to e-frame
$Pos_{n,locallevel}$	Linearization point of local level navigation frame

Table 7-13: Parameters of the transformation of n-frame dead reckoning results to Earth frame coordinates

7.7 Summary

In the previous chapter, an alternative dead reckoning system for pedestrian users, the PNS, has been introduced and described. The PNS performs the basic tasks of step detection, step classification, stride estimation, heading determination and position propagation. Heading determination has been described in chapter 6. A MEMS type IMU has been used as main sensor. The trials and implementations have been performed with a BEI Systron Donner MMQ50 as well as an Xsens MTi IMU, both of MEMS type. It was shown that the placement of the sensor on the body has large influence on the measured quantities and influences the application of several algorithms. The placement therefore is a compromise between mechanical properties and user requirements. The individual algorithms have been explained in detail, with focus on step detection and step classification techniques. Several alternatives were discussed and the final algorithms were adapted to the use case in this thesis.

8. PNS Kalman filtering

Kalman filters are common tools for sensor fusion. If receiver aiding is performed, in this case ultra-tightly coupling, often centralized Kalman filter approaches are used to avoid cascaded filter architectures with their cross-coupling problems. In this application, the deep indoor GNSS position has often a low accuracy due to the low signal to noise ratios, even if the receiver is aided by a DR position. To maintain basic navigation capabilities under all circumstances, and to provide stable inputs to the receiver aiding, a separated filter approach has been studied and implemented.

Since the basic functions of the Kalman filter are widely known, the Kalman filter itself will only be described shortly in this chapter. Detailed information can be found in [23], [44] and [61], practical aspects are discussed in [27]. Following the introduction, a dead reckoning navigation Kalman filter is described, which is used to limit and correct the PNS position drift. The filter is designed as tightly coupled error state Kalman filter and uses mainly GNSS pseudorange and magnetometer heading updates (chapter 5.4), but can use all available position updates when available, e.g. WLAN based position updates as described in chapter 9. The filter will be evaluated in a simulation. The field test evaluating the entire navigation system will be described in chapter 11 and will include the performance of the implemented PNS filter.

8.1 Introduction

According to M. Grewal and A. Andrews, "[…] the Kalman Filter is an estimator for what is called the *linear-quadratic problem*, which is the problem of estimating the instantaneous "state" […] of a linear dynamic system perturbed by white noise – by using measurements linearly related to the state but corrupted by white noise. The resulting estimator is statistically optimal with respect to any quadratic function of estimation error." [27]

In this short quotation, many of the properties of the Kalman filter are summarized. The Kalman filter is an estimator, not a time series filter. It combines magnitudes, which are perturbed by (white) noise in a statistically optimal way. Good explanation for the functions of the Kalman filter can be found in [61]. In the Kalman filter, the magnitudes, which are to be estimated, are called "states". The filter has a two stage design: **prediction** and **update**. The states are predicted using a system model, and corrected by combination with (external) measurements in a way that the combined result has the lowest possible uncertainty, expressed by its covariance matrix. In the quotation, this fact is referred to as "the linear-quadratic problem". This design, using a **prediction** and an **update** stage, enables the filter to give estimations of its state magnitudes at any required epoch, even if no actual observation by measurements is available.

The filter process or system is mathematically modeled by a state vector (X) and a system matrix F. Since it is assumed that the process is linear, the dynamics of the process can be modeled by a Jacobian matrix, which relates the derivative of the state with the state itself. Perturbations from outside are included. If the system equations are non-linear, they have to be linearized around the current magnitudes of the state (extended or linearized Kalman filter). The linearization is only valid in close proximity of the linearization points, which is one of the major drawbacks of the linearized Kalman filter.

The Jacobian matrix is called system matrix (F). If the propagation of the state is performed in a discrete instead of a continuous form, the system matrix transforms into a transition matrix (Φ). The transition matrix can be constructed with:

$$\Phi_k = I + F\Delta t \tag{81}$$

Parameter	Explanation
Φ_k	Transition matrix at epoch k
I	Identity matrix
F	System matrix
Δt	Prediction time increment

Table 8-1: Parameters of the transition matrix calculation

The propagation of the state vector and the state covariance matrix (P) form the prediction stage of the Kalman filter. Therefore, the basic equation for the prediction stage of the Kalman filter is for the state vector:

$$\tilde{x}_{k+1} = \Phi_k \tilde{x}_k + w \tag{82}$$

Parameter	Explanation
x	State vector
ϕ	Transition matrix
w	White noise
k	Current epoch of the estimation
k+1	Next epoch of the estimation

Table 8-2: Parameters of the state prediction stage of the Kalman filter

For the system covariance matrix, the prediction equation is:

$$\tilde{P}_{k+1} = \Phi \tilde{P}_k \Phi^T + Q \tag{83}$$

Parameter	Explanation
P	State vector covariance matrix
Φ	Transition matrix
Q	System noise matrix
k	Epoch of the estimation

Table 8-3: Parameters of the state covariance prediction stage of the Kalman filter

The tilde "~" symbol is used to indicate the predicted values, the roof symbol "^" will be used to indicate updated magnitudes. In literature, other nomenclature like "+" and "-" and other similar indicators can be found.

The system noise matrix Q can be constructed by mapping the sensor or process noise vector (q) to the state vector covariance matrix using a noise inference matrix (G).

$$Q = \mathrm{G}\vec{\mathrm{q}} \tag{84}$$

Parameter	Explanation
Q	System noise matrix
G	Noise inference matric
$\vec{\mathrm{q}}$	Sensor or process noise vector

Table 8-4: Components of the system noise estimation

The estimated states can be corrected by using external measurements (z). If a process noise covariance matrix is used, eq. (84) becomes:

$$Q = \mathrm{G}\bar{q}G^T \tag{85}$$

Parameter	Explanation
Q	System noise matrix
G	Noise inference matric
$\vec{\mathrm{q}}$	Sensor or process noise covariance matrix

Table 8-5: Components of the system noise estimation

Measurements are usually produced by additional sensors or other external information. Hence, information about the state vector from at least two sources can be compared and combined. It must be noted that only measurements, which are linearly related to the state, or can be expressed using a linearization, can be used as updates. If they are linearly related to the state vector, i.e. the measurements are linear combinations of the state variables, they can be predicted by multiplying the estimated state vector with an observation matrix (H).

$$z_k = \mathrm{H}\tilde{\mathrm{x}}_\mathrm{k} + \mathrm{v} \tag{86}$$

Parameter	Explanation
z_k	Predicted observation at epoch k
H	Observation matrix
$\tilde{x}_k$	Predicted state vector at epoch k
v	Sensor noise

Table 8-6: Parameters of the measurement prediction

The sensor noise can be described in the measurement noise covariance matrix (R). If the individual sensors are independent of each other, only the main diagonal of the matrix is filled with elements other than zero. It is important to model the sensor noise properties correctly in R, since it is used as direct input to the calculation of the combination weight (Kalman gain).

The difference between predicted and actual measures is directly related to the state vector. If this difference is combined with the state vector using optimal weights, the variance of the state estimation becomes minimal and thus optimal in statistical respect. This weight is called Kalman gain matrix. It is the optimal combination of the variance of the state vector and the variance of the innovation. A helpful description for this process is given in [106]. The Kalman gain is combining the predicted state vector and the observations in a way that the combined covariance is minimal in statistical respect.

$$K_{k+1} = \widetilde{\mathrm{P}}_{\mathrm{k+1}} H_{k+1}^{T} \left(H_k \widetilde{\mathrm{P}}_{\mathrm{k+1}} H_{k+1}^{T} + R \right)^{-1} \tag{87}$$

Parameter	Explanation
K_{k+1}	Kalman gain matrix at epoch k+1
H_{k+1}	Observation matrix for the epoch k+1
$\widetilde{\mathrm{P}}_{\mathrm{k+1}}$	Predicted state covariance matrix at epoch k+1
R	Sensor noise covariance matrix

Table 8-7: Parameters of the Kalman gain calculation

For that, the state covariance matrix is mapped to the observation space and added to the sensor covariance matrix. The term within the brackets is called “covariance of the innovation” and describes the covariance of the difference between predicted measurements and real measurements.

The updated state vector is calculated by:

$$\hat{x}_{k+1} = \tilde{x}_{k+1} + K_{k+1}(l - H_{k+1}\tilde{x}_{k+1}) \tag{88}$$

Parameter	Explanation
$\hat{x}_{k+1}$	Updated state vector at epoch k+1
$\tilde{x}_{k+1}$	Predicted state vector at epoch k+1
K_{k+1}	Kalman gain matrix at epoch k+1
H_{k+1}	Observation matrix for the epoch k+1
l	Measurements vector

Table 8-8: Parameters of the state update equation

The updated state covariance matrix is calculated by:

$$\hat{P}_{k+1} = H_{k+1}^{T}(I - K_{k+1}H_{k+1})\tilde{P}_{k+1} \tag{89}$$

Parameter	Explanation
$\hat{P}_{k+1}$	Updated state covariance matrix at epoch k+1
H_{k+1}	Observation matrix for the epoch k+1
I	Identity matrix
K_{k+1}	Kalman gain matrix at epoch k+1
$\tilde{P}_{k+1}$	Predicted state covariance matrix at epoch k+1

Table 8-9: Parameters of the state covariance update equation

At least one prediction is needed before every update, but also several predictions can occur between individual updates. The ratios are not necessarily fixed by the algorithm. Due to the simple standardized structure the Kalman filter is especially suited for use in computer systems. Besides, even if the basic structure is simple, the design and the tuning of a Kalman filter are not. The major challenges in Kalman filter design are:

- Advantageous and robust design of state vector and system model
- Precise modeling of the covariance matrices R and Q, as well as the initial values for matrix P
- Design that ensures the observability of the system
- Exclusion of measurement outliers

The design of the state vector and the system model has to take account for numerical stability. If e.g. a GPS/INS close integration is performed, a modeling of the clock errors in seconds would result in badly conditioned matrices and thus numerical instabilities. A modeling of the clock errors as distance errors reduces this numerical problem significantly. Additionally, it is possible, that the number and kind of observables, in combination with a weak transition matrix, are not sufficient to observe all state variables. In this case the filter is not able to correctly estimate the state vector and the results are not fully reliable. Hence, observability analysis is necessary and the design must reflect this criterion. The filter tuning is especially conducted by modeling the process and sensor noise. Modifications especially change the dynamic properties of the filter, as well as the convergence of the filter. Outlier exclusion is a critical point in the design of a Kalman filter. On the one hand, the outliers of measurements occur naturally and are part of the statistical distribution. Excluding the outliers from updates violates the mathematical formulation of the filter and the filter is not optimal with respect to statistics in this epoch. On the other hand, the absolute results of the filter are often improved significantly, if presumably erroneous measurements are excluded from the update process. In [106], the covariance of the innovation is used to exclude outliers. If the residual is bigger than three times the covariance, the measurement is excluded.

8.2 Kalman filter application for PNS dead reckoning

Dead reckoning is an integrating navigation method, which propagates the last user position by using the distance travelled and the direction of travel. In this thesis, a pedestrian navigation system is used for DR. Hence, the distance travelled is calculated by counting steps, classify the step as up, level or down, estimate the stride and apply the travelled distance using the calculated heading. Errors can occur due to heading errors, misdetection of steps, and erroneous estimation of the stride.

The main reasons for heading errors are erroneous initial alignment, as well as gyroscope errors, especially of the yaw axis gyroscope. The pitch and roll axes are stabilized using the measured accelerations during static phases in the AHRS algorithm described in chapter 6. Therefore pitch and roll errors are limited strongly and they contribute only marginally to the heading error of the PNS.

The longitudinal errors by missed or misdetected steps, errors in step classification and stride estimation, are very hard to separate from each other and therefore the correction of the stride model is not as easy as described in some publications. This is the major limiting factor for online user calibration and stride model improvements. Estimated errors for the stride must not be applied directly to the stride model, if misdetections and misclassifications cannot be excluded. Hence, the main focus of this filter is the improvement of the user position, using all possible navigation information. It will be shown in chapter 11 that this approach proved very effective and valuable, even if it is not totally straight forward scientifically.

For correction of the residual errors of dead reckoning additional observations can be used. This information can be the output of the magnetometers (electronic compass), the measured pseudoranges from a GNSS receiver, position information by the WLAN positioning engine and various other inputs. An error state Kalman filter will be used, its error states are:

$$\vec{x} = \begin{bmatrix} \Delta x \\ \Delta y \\ \Delta z \\ \Delta \Psi \\ \Delta \dot{\Psi} \\ \Delta S \\ \Delta T_c \\ \Delta \dot{T}_c \end{bmatrix} \tag{90}$$

Parameter	Explanation
Δx	Position error x-coordinate [m] (WGS 84)
Δy	Position error y-coordinate [m] (WGS 84)
Δz	Position error z-coordinate [m] (WGS 84)
$\Delta\psi$	Heading error [rad]
$\Delta\dot{\psi}$	Heading error rate [rad/s]
ΔS	Stride error [m]
ΔT_c	Receiver clock error [m]
$\Delta\dot{T}_c$	Receiver clock error drift [m/s]

Table 8-10: Elements of the Kalman filter state vector

The error states are propagated during prediction state of the filter by the system matrix Φ. The matrix for level walking is defined by the following equations. For non-level walking the propagation is enhanced by the step lift and also the expected variations of the step lift, as well as reduced stride for non-level steps.

$$\Phi = \begin{bmatrix} 1 & 0 & 0 & \Phi(1,4) & 0 & \Phi(1,6) & 0 & 0 \\ 0 & 1 & 0 & \Phi(2,4) & 0 & \Phi(2,6) & 0 & 0 \\ 0 & 0 & 1 & \Phi(3,4) & 0 & \Phi(3,6) & 0 & 0 \\ 0 & 0 & 0 & 1 & \Delta t & 0 & 0 & 0 \\ 0 & 0 & 0 & 0 & 1 & 0 & 0 & 0 \\ 0 & 0 & 0 & 0 & 0 & 1 & 0 & 0 \\ 0 & 0 & 0 & 0 & 0 & 0 & 1 & \Delta t \\ 0 & 0 & 0 & 0 & 0 & 0 & 0 & 1 \end{bmatrix} \tag{91}$$

Parameter	Explanation
S	Estimated stride [m]
φ	Latitude [rad]
λ	Longitude [rad]
ψ	Estimated heading [rad]
Δt	Prediction interval [s]

Table 8-11: Parameters of the transition matrix

Since dead reckoning is performed in the local level navigation frame, but the observations are made in the WGS84 frame, a frame transformation is necessary. Hence, more complex elements of the transition matrix are:

Parameter	Explanation
$\Phi(1,4)$	$S\big(sin(\varphi)cos(\lambda)sin(\psi) - sin(\lambda)cos(\psi)\big)$
$\Phi(2,4)$	$S\big(sin(\varphi)sin(\lambda)sin(\psi) + cos(\lambda)cos(\psi)\big)$
$\Phi(3,4)$	$Scos(\lambda)sin(\psi)$
$\Phi(1,6)$	$-sin(\varphi)cos(\lambda)cos(\psi) - sin(\lambda)sin(\psi)$
$\Phi(2,6)$	$-sin(\varphi)sin(\lambda)cos(\psi) + cos(\lambda)sin(\psi)$
$\Phi(3,6)$	$S\big(sin(\varphi)cos(\lambda)sin(\psi) - sin(\lambda)cos(\psi)\big)$

Table 8-12: Elements of the transition matrix

The coefficients described above result from the basic DR equations for level walking in the local level frame. The DR equations are driven by the stride and the heading only. The partial derivatives for each axis must be transformed to the Earth fixed frame. For this, the transition matrix C_n^e is used. The results are given above in the elements $\Phi(1,4)$ to $\Phi(3,6)$.

The design or observation matrix, relating the observations to the state vector, is:

$$\mathrm{H} = \begin{bmatrix} -(X_{est} - X_{Sat,1})/R_1 & -(Y_{est} - Y_{Sat,1})/R_1 & -(Z_{est} - Z_{Sat,1})/R_1 & 0 & 0 & 0 & 1 & \frac{1}{2}\Delta t^2 \\ -(X_{est} - X_{Sat,2})/R_2 & -(Y_{est} - Y_{Sat,2})/R_2 & -(Z_{est} - Z_{Sat,2})/R_2 & 0 & 0 & 0 & 1 & \frac{1}{2}\Delta t^2 \\ & & \vdots & & & & & \\ 0 & 0 & 0 & 1 & 0 & 0 & 0 & 0 \\ 0 & 0 & 0 & 0 & 1 & 0 & 0 & 0 \end{bmatrix} \quad (92)$$

Parameter	Explanation
$(X,Y,Z)_{est}$	Estimated user position, WGS 84 [m]
$(X,Y,Z)_{Sat,n}$	Estimated position of satellite n, WGS 84 [m]
R_n	Estimated distance between user and satellite n [m]
Δt	Prediction interval [s]

Table 8-13: Elements of the observation matrix

The first lines of the matrix describe the reconstruction of the differences in the measured pseudoranges, the final two lines the reconstruction of the heading and heading drift, which are observed by the difference between the magnetic and inertial heading, as well as their derivative. If position updates from WLAN or ZigBee positioning become available, the H matrix can be complemented by additional lines. Since the position updates are in WGS 84 coordinates, the matrix is complemented by lines with single ones at the Δ(x,y,z) positions.

8.3 Simulation of the filter

The PNS Kalman filter is an integral part of the full navigation system. Therefore a simulation for the full system is possible, but the results are then difficult to evaluate individually. Hence, an individual simulation for the PNS Kalman filter has been developed to demonstrate basic properties and capabilities of the filter. Several simulations of the filter have been executed in the Matlab environment to evaluate the filter properties and capabilities. The basic parameters for the simulations are presented in Table 8-14.

Parameter	Value
Simulation time	2000 steps
Step frequency	1.3 Hz
Start position	48.0778°N, 11.6287 E, 594 m (University location) 4182047 m, 860632 m, 4723101 m (WGS 84)
Update interval	2..20 steps
Average stride	0.73 m
Heading	35°
Initial heading error	2°
Gyroscope bias	0.1°/s (360°/h)
UERE	1.1 .. 7.1 m
Nb. of satellites	8
$\sigma_{compass}$	10°
σ_{stride}	0.05 m

Table 8-14: Simulation parameters for evaluation of the PNS Kalman filter

As observations, pseudoranges from 8 satellites, as well as magnetometer heading and the heading drift since the last observation were used. The satellite positions were a snapshot of a real satellite constellation at the starting point of the simulation. Thus the satellite configuration is realistic. In the evaluation, various setups using pseudoranges only, pseudoranges with magnetometer heading, pseudoranges with magnetometer heading and heading change observations, etc. were tested. Various pseudorange qualities (UERE) and update rates were tested.

The results of a simulation using an update rate of 20 steps and a UERE of 3 m is shown in Figure 8-1 and Figure 8-2. The figures show three individual aspects of the simulation:

- Simulated reference user trajectory (red line)
- Biased DR trajectory using erroneous gyroscope heading, initial position offset and stride errors (blue line)
- Kalman filter corrected DR trajectory (green line, markers show individual steps)

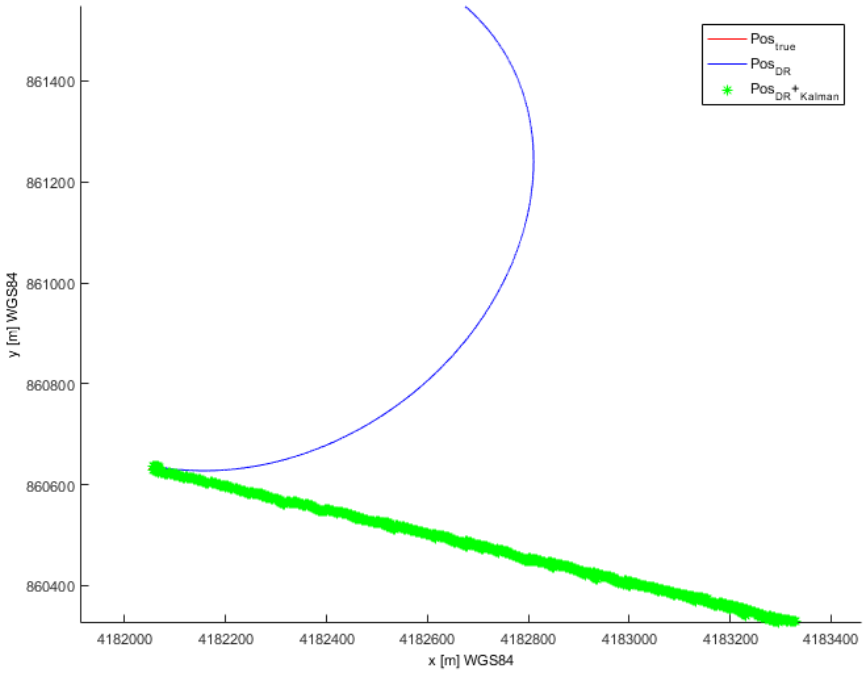

Figure 8-1: Simulation of the PNS Kalman filter simulating 200 steps with pseudorange updates

As can be seen in the figures the filter is able to adjust the DR position to the position calculated by GNSS observations. While the PNS solution would drift to a circular shape due to the gyroscope bias, the adjusted trajectory matches the real trajectory very well.

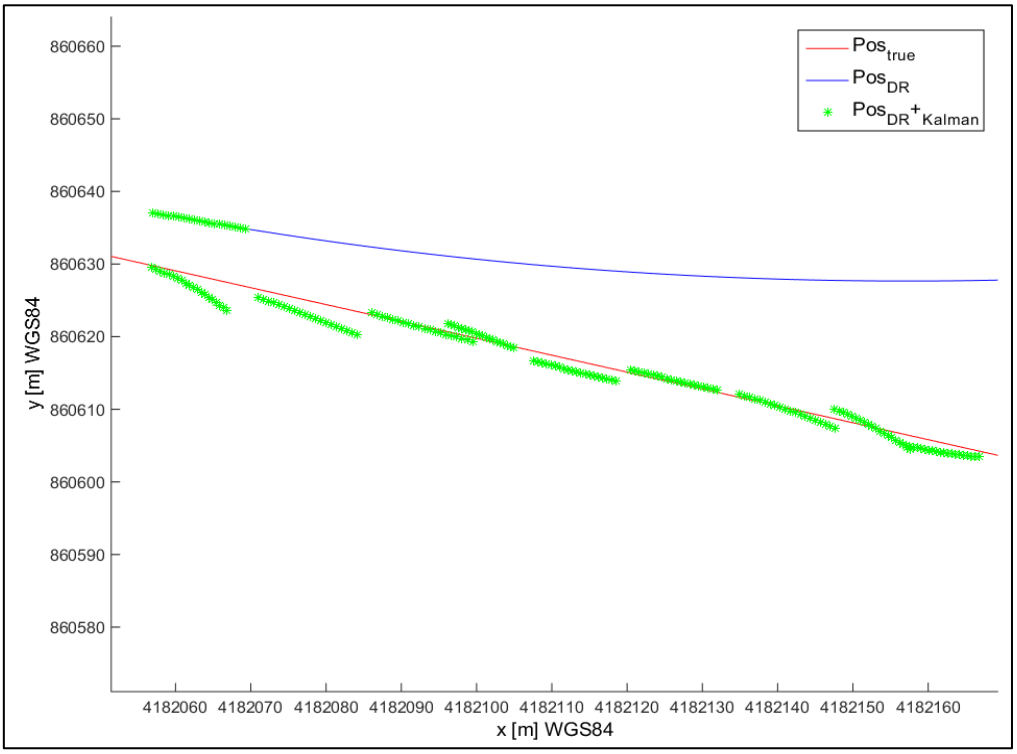

Figure 8-2: Close-up of the PNS Kalman filter simulation result

In the close-up (Figure 8-2), the filter convergence can be observed, too. Prior to the first observation, the combined user position follows the DR stand-alone trajectory. After the first observation, the initial position errors are corrected and the user position is reset almost to the true user position. Heading and heading rate error are correctly estimated after some update steps. The simulation shows the influence of the noisy pseudorange measurements, too. Even if the DR positions during the prediction phase are close to the true trajectory, the pseudorange updates can set the user position estimation slightly off track. The same effect applies to the user heading. Variation of the update intervals and the simulated UERE shows that the short-term stability of the PNS can be much higher than the measurement updates by noise pseudoranges. In the evaluation of the complete system in chapter 11.5, this fact will be demonstrated. The distance traveled between the updates can be very short, i.e. only a few meters or even less. The step frequency has been simulated with 1.3 Hz. If high update rates are used, the GNSS positions have a higher uncertainty as the distance traveled. This fact makes stride estimation very difficult when the UERE is large and the update rate is high. Neglecting stride as state variable on the other hand is not a practical approach and results are not acceptable.

The same observations apply to the user heading error and heading error rate for simulations when the magnetometer heading and heading rate is not used as observation. It is not practical to use realistic, noisy pseudorange observations to correct the user heading errors and heading error rate. For useful heading corrections, a heading reference like the magnetometer is necessary. This is especially true for slow user dynamics and short traveled distances between updates.

Even if the filter is optimal with respect to statistics, the individual corrections might give larger errors for the individual epoch. Direct application of stride estimations is not very stable and accurate in the short term evaluation. To use the stride estimation, longer smoothing is necessary. This limits the stability of online-calibration, too. Heading stabilization by external heading updates is necessary. Position updates are not sufficient for heading correction of pedestrian users, if the pseudoranges do not have uncommonly high accuracies.

8.4 Implementation of the PNS Kalman Filter

As described in chapter 8.1, the Kalman filter is a two stage process of prediction and update. Since the update stage is a comparison between predicted observations on basis of the system states and measured observations, it is mandatory that the prediction and the update process refer to the same epoch, i.e. both processes need to be synchronized. Sensor fusion in practical implementations is often limited by sensor synchronization. Several sensor outputs can only be combined to a consolidated navigation solution, if they refer to the same epoch.

On the hardware side, synchronization could be realized by triggering all sensors in a centralized way using a common timing machine. This approach is often not practical, especially if the individual sensors have different sampling frequencies, different trigger delays, or transmission delays. The filter has to delay its operation for an optimized period to be sure that all available measurements have been received.

Another approach is to determine the precise time of sampling (time-tagging) of each measurement and each sensor in a common time frame. Since the measurements are not expected to occur at the same instant, one of both data streams has to be interpolated or extrapolated. The filter states have

to be predicted to the instant of the measurement observation, or the magnitudes derived from the measurements have to be extrapolated to the prediction epoch. It is advantageous to use the data stream with lower data rate for updates since it reduces to number of interpolation operations and increases the interpolation accuracy. It is useful to operate the filter some seconds in the past to wait for delayed measurements. If the state vector is not changing rapidly, the application of slightly delayed error estimations to the observed process is still possible.

This approach has been realized in the integrated system studied in this thesis. All sensor measurements are time-tagged on hardware basis and time stamps are applied using the system time of a precise OCXO oscillator. PNS is used for the prediction stage. Since the GNSS observations are essential for positioning, but are delayed strongly due to the long replica length, the classical procedure of performing an update of the states cannot be used. Hence, the following processing chain is proposed. The filter will always wait for a GNSS update to perform operations. PNS data, WLAN observations and DR observations are stored for later use as long as no GNSS updates are available. When a new set of pseudoranges is delivered to the Kalman filter, it will first perform predictions to the point of time of the next pending observation, e.g. WLAN, using the stored PNS data at that point of time and then doing an observation update. The procedure is repeated until the prediction and the GNSS observation update is performed. Then the filter is pausing until the next available GNSS update. The resulting states like position, heading errors and sensor errors are provided to the respective subsequent DR procedures. The principle of the timeline of events and measurements is shown in Figure 8-3. DR, WLAN and GNSS measurements are registered and stored. The measurements have a timestamp (t_1, t_2, …), but are delayed by different delay periods. Here, the GNSS observation is delayed for three seconds, while the other measurements are less delayed. The WLAN measurement of t_6 has already been received, as well as DR measurements of t_4 and t_5 have been registered and stored, when the GNSS measurement of t_3 is registered.

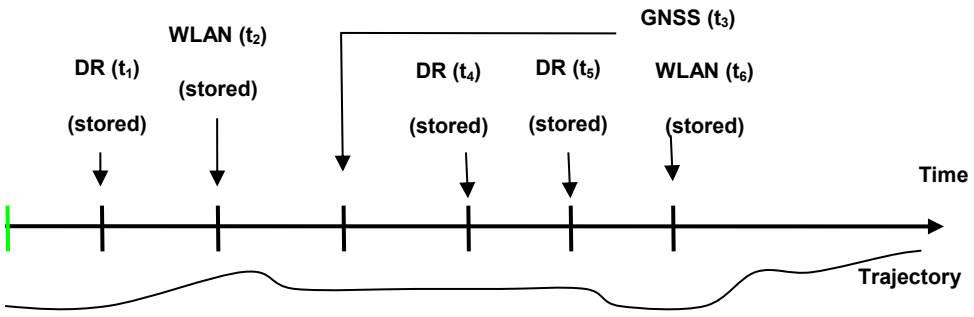

Figure 8-3: IKF situation at t=6 [92]

In Figure 8-4, the processing of the stored measurements is presented. After receiving the GNSS update, the measurements and events are brought in the correct order and the filter performs the prediction operations first to the WLAN positioning update event at t_2 and then to the GNSS update event at t_3. The later events (t4, t5, t6) are stored until the next GNSS update becomes available. Hence, the filter has a latency of three seconds in this case. Since the PNS error dynamics are very low, i.e. the position error accumulated in three seconds is nearly negligible, this delay is not critical and the corrections calculated by the filter can be used to correct the DR position solution. To avoid

very long delay times, a maximum delay time has been defined, after which the filter will definitely propagate its estimation. GNSS updates received after this maximum delay will be disregarded.

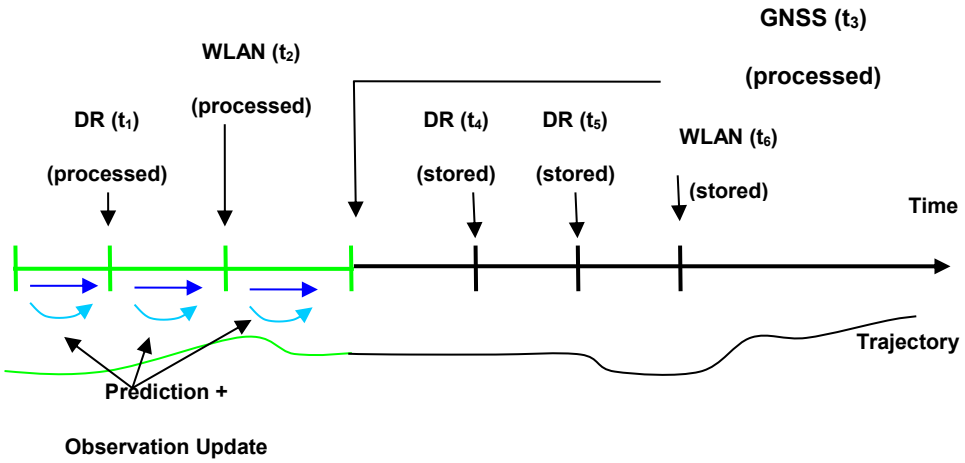

Figure 8-4: IKF situation at t=6 after update to t=3 [92]

8.5 Summary

In the previous chapter the design, simulation and implementation of a PNS Kalman filter has been described. The need for this filter is based on the fact that DR systems like the PNS accumulate position errors during progress and the DR position has to be corrected after some time to increase the long term stability and accuracy of the PNS. A linearized Kalman filter has been proposed that propagates the navigation errors based on the walking model of the PNS. The major influences are the stride error and the heading error, as well as the heading error drift. Since GNSS pseudoranges shall be used as input, the error states of the receiver clock error and the receiver clock drift had to be added. This eight state filter has been implemented in Matlab and tested in a simulation which showed basic capabilities of the filter, but also showed the influences of low pseudorange accuracy and low user velocity. Finally aspects of the implementation on the final platform have been discussed and especially the aspect of different data delays for predictions and updates has been presented. A timing scheme for data handling has been demonstrated which tries to maximize the use of GNSS updates while limiting the overall filter delay.

9. Wireless LAN Positioning

WLAN is a communication system widely used today for mobile and stationary wireless network communication. It is present in nearly all public locations today. Several navigation applications have been proposed, using networks and access point mapping, fingerprinting and several other principles (e.g. in [59], [100] and [101]), since due to lack of precise synchronization a ranging application like in GNSS has not been possible so far. In the integrated navigation system described in chapter 11 of this thesis, wireless network navigation has been provided by "INPOS", a system of Telespazio Italy, using ZigBee motes instead of WLAN access points ([66], [110], [78]). This system uses fingerprinting techniques, too.

Since ZigBee infrastructure is not as widely available as WLAN, it has been desirable to have basic WLAN positioning capabilities, while the calibration and technological burden of WLAN fingerprinting techniques should have been avoided. Hence, an alternative, basic WLAN positioning system has been developed. This system provides a positing alert system, which gives position updates when registered WLAN access points are passed by in close proximity. With this technique, relatively precise position updates become available without the heavy burden of a full and precise calibration campaign, as e.g. in WLAN fingerprinting. In the following chapter, the principles and implementation of this alternative positioning system are described.

9.1 RSS based proximity positioning

Wireless local area networks (WLAN) are infrastructures which can be found in most urban places. They are used in most office environments and have been standardized by the IEEE 802.11 standard. The system consists of several so called access points (AP), which represent the bridge from a stationary cable-based network to the WLAN. Several mobile or stationary computers can be connected to the network via WLAN cards or WLAN-USB-sticks.

WLAN can be used for positioning inside buildings basically by measurement of the received signal strength (RSS). Often the RSS is expressed by a quality indicator called Received Signal Strength Indicator (RSSI). The unit of the RSSI is not Watt or dBW/dBm, but an internally defined reference value (maximum 100). Ranging of several APs like in the GNSS systems is not feasible today, since the precise time synchronization of the APs, like it is standard for the satellites in the GNSS systems, is not implemented so far. This may change in the future. If several WLAN access points are visible for the rover, "fingerprinting" is a technique often used for wireless network based positioning inside buildings. If patterns of several RSS values of different APs are compared to a database, a position of maximum likelihood can be determined. This requires a database of calibration points at which the RSS values are measured in a calibration campaign and referenced to their geometric position. The calibration point with the best match to the actually measured signal pattern is selected as position update. Since WLAN is used in the integrated navigation system to provide the assisted GNSS information, it shall also be used for deriving positioning information, too. For redundancy reasons, the INPOS system present on the navigation platform shall not simply be doubled on another standard, but a different solution had to be found. For that reason a WLAN proximity positioning system had to be developed. In contrast to the INPOS fingerprinting system, the WLAN proximity positioning system is supposed to provide a position information if the user gets close to a registered access point. The registered position of the AP is then used as position update to the IKF. This

algorithm acts in the manner of a proximity warning or local marker system, since it provides the update information only in proximity to the AP. The APs act as local markers.

9.2 Algorithm outline

For the development of the algorithm a simple test scenario was generated, which is presented in Figure 9-1. On a straight office floor two access points called AP_1 and AP_2 have been placed at the beginning and at the end of the floor. A laptop has been equipped with a USB-WLAN-stick to act as rover, and moved from the eastern end of the floor to the western end and back again. The floor has a length of approximately 30m. The closest distance between rover and the respective access point is about 1.5m. The RSSI values were extracted and recorded.

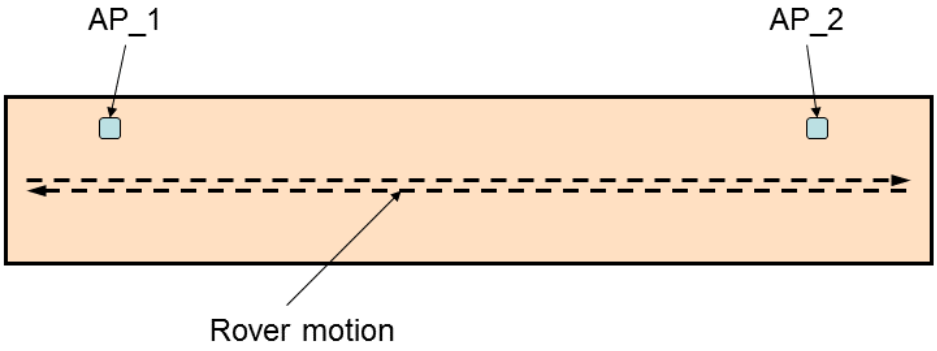

Figure 9-1: Test scenario for WLAN proximity positioning

The results of the test run are demonstrated in Figure 9-2.

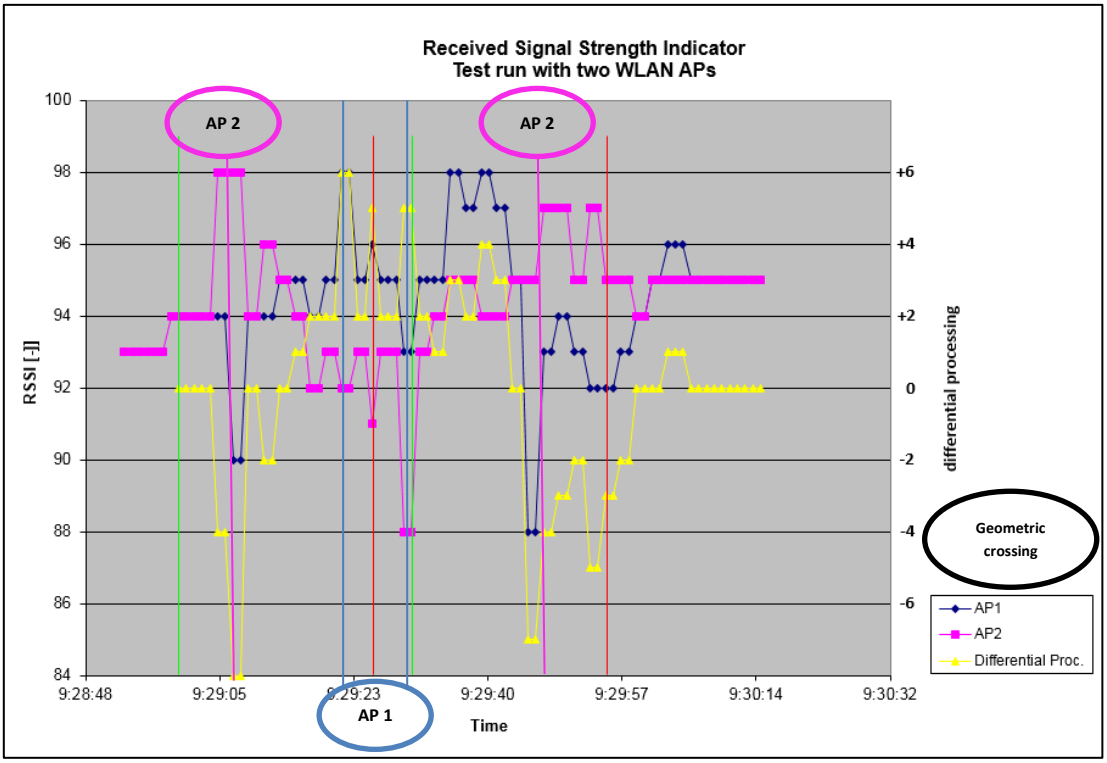

Figure 9-2: RSSI of two WLAN access points during test run

The modeling of the signal propagation in an office environment is specific for each environment. This fact limits the usability of the RSS of one AP for stand alone range estimation and for continuous distance to AP evaluation, too. The individual signal power of a WLAN access point is usually between 20-40 mW, corresponding to 13-16 dBm. However, the true signal strength is again dependent on several factors including the antenna, the placement of the AP, the environmental conditions and many more. Hence, an algorithm using the evaluation of specific patterns in the received signal quality instead of pure power levels has been chosen.

An evaluation of the RSSI has been conducted for each received access point. As already mentioned, the RSSI is an internal quality indicator for the received signal strength. It cannot be directly interpreted as absolute signal power like e.g. “dBm”. RSSI is used in relation to an arbitrary, receiver manufacturer dependent reference value. However, the maximum RSSI for each AP is a magnitude which can be easily evaluated in very simple measurement campaign and can be stored in a database together with the AP location.

In this case, the maximum registered RSSI in proximity of the APs is 98, mostly values between 95 and 98 are expected. On close approach to or at the passing of the respective access point the signal strength is increasing strongly, usually by 3-4 units, while due to interference the RSSI of the other AP decreases significantly.

The difference in the RSSI is depicted as yellow graph in Figure 9-2. The green lines give the start of run, the red lines the end of run. The geometric crossings of the access points are indicated by the ellipses for AP1 and AP2. As can easily be seen, the extrema of the differential processing of both RSSI values give good indication for the direct passing of the waypoints in short distance. This phenomenon can be exploited for the WLAN proximity positioning system. The absolute value of the distance to the access point at detection can be adjusted. A value of 2 m has been achieved in the test campaigns.

For the final algorithm, several features and aspects can be listed:

- The position is not constantly calculated and estimated, but provided in a proximity warning manner at discrete events.
- The proximity position has a high accuracy due to the sensitive algorithm.
- WLAN Access points act as local markers, giving their own position as position updates for the rover.
- To derive a position by the system, the positions of the access points must be registered in a data file.
- Unregistered APs cannot contribute to the position evaluation, since their position is not known.
- If proximity to an access point is determined, the position of the access point is evaluated and passed to the IKF together with the accuracy estimate. This estimate is equal to the detection distance of the algorithm.
- Basis of the proximity detection algorithm is an evaluation of the received signal strength (RSSI) of various access points. At least two access points are needed.
- At crossing of the AP the difference of the signals reaches characteristic peaks at the crossing of the AP, which is between 4 and 8 units. These peaks are used as detection event.

9.3 Implementation

The RSSI measurements for each visible access point are provided to the algorithm with an update rate of 1 Hz by the sensor API. In principle, the data is derived from the WLAN controller of the used laptop platform. The dataset shall contain the access point's name or MAC address as well as the RSSI value and the time stamp. Figure 9-3 gives a schematic overview over the data flow and functional flow inside the WLAN proximity positioning module.

The WLAN proximity positioning module is embedded in a DLL. Via the sensor API, the respective datasets of measurements are passed to the DLL and to the WLAN positioning module. For the algorithm it is necessary to have the latest measurements of all access points available, so that derivatives and differences can be built. Therefore a stack buffer is filled with the latest (actual) RSSI measurements for each access point, while the oldest measurement is skipped. Then the algorithm tries to detect a close proximity to each AP, based on the algorithm and rules described in chapter 9.2. If positive detection is declared, the routine return a positive flag and hands over the registered position to the positioning Kalman filter (IKF), together with a position accuracy estimate, which is set to the trigger sensitivity of the algorithm.

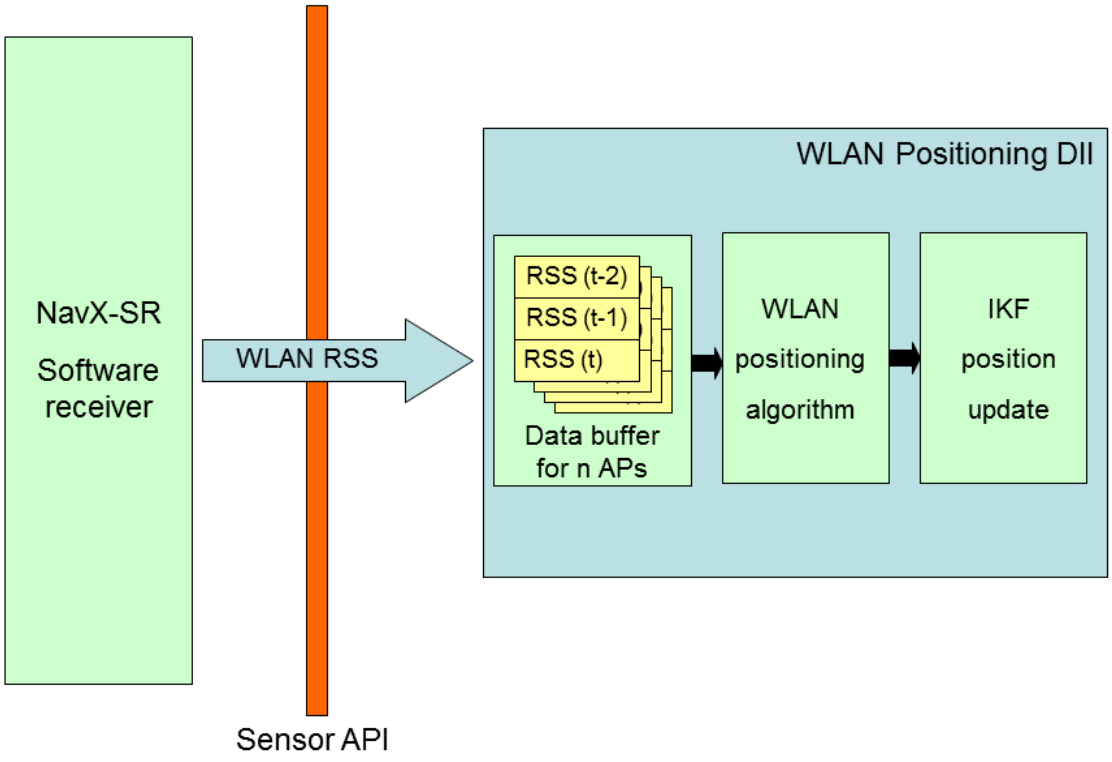

Figure 9-3: Flowchart of WLAN positioning processing

It is possible to run APs in an automatic power adjustment mode. In this mode, the transmission power is adjusted automatically to the estimated distance of the user. This feature must be disabled to allow the algorithm to work correctly. The received power level should only be influenced by the distance and geometry of the user antenna to the AP antennas. In other words, the transmitted EIRP of the AP must be constant. The maximum RSSI is measured in a simple calibration campaign and is stored in the database together with the AP position and MAC address.

Figure 9-2 shows the received signal strength of two APs on an office floor, as well as the differenced signals. The passing of the access points is clearly visible in the differential processing. Additional test in two additional full test campaigns in other premises showed similar results and the algorithm proved its functionality with high reliability.

9.4 Summary

In the previous chapter, the development, implementation and testing of an alternative WLAN based positioning system has been described. In contrast to fingerprinting algorithms and database operated positioning systems, the developed approach offers proximity warnings when WLAN access points are passed by. The only needed calibration is the registration of the used APs, the position determination of the AP in the building coordinate frame and the measurement of the maximum RSSI of the AP, which can be performed by the same hardware, which is used for user positioning. Therefore, the calibration effort for operating this positioning system is very low in comparison to other systems. The system offers not continuous positioning, but singular position updates when passing registered APs. The chapter gave insights in the implementation of the algorithm and some test results from an office building.

10. Barometric altitude determination

In pedestrian navigation, often the horizontal coordinates are of major importance and several navigation systems focus only on these parameters. For aiding the GNSS receiver, the vertical component is of major importance due to geometric reasons. The influence of altitude changes on the LOS vector is often significantly larger than the horizontal components. On the other hand it is difficult to provide a stable absolute altitude reference. The air pressure can be used as physical altitude reference by using sensors called barometers.

The atmosphere consists of compressible gases, which can be modeled as layers around the Earth. Since the weight of the higher layers presses on the lower layers, the pressure of the atmosphere increases with decreasing altitude und decreases with increasing altitudes. This phenomenon has been used for vertical navigation in the aeronautical domain for decades. Due to new MEMS based sensors, also miniaturized pedestrian application is possible today. For this thesis, the MEMS type barometer Bosch BMP085 has been used.

In this chapter, the physical relationship between pressure and altitude will be presented. The pressure sensor used in this thesis will be introduced and measurement data as well as calibration of the sensor will be presented.

10.1 Physical model of the atmosphere

The properties of atmospheric pressure can be evaluated by dividing the atmosphere in differential volume elements and analyzing the forces on the vertical axis. The forces acting on a theoretical differential volume element are shown in Figure 10-1. If only forces in vertical direction are evaluated, the element is compressed by the pressure on the upper boundary (p+dp) and the pressure on the lower boundary (p). The pressure is always defined as perpendicular to the surface it is acting on. Additionally, its own weight acts on the element, which is mass multiplied by gravity.

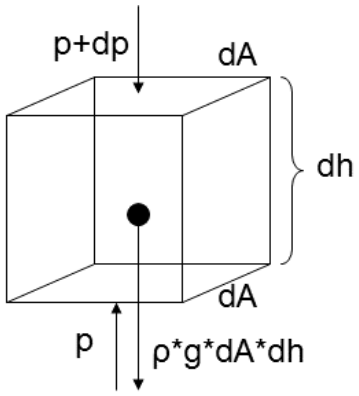

Figure 10-1: Forces acting on a differential volume element

If a stable vertical layering is assumed, the following equations can be derived:

$$p\,dA - (p + dp)dA - \rho dhdAg = 0$$

$$dp = -\rho dhg$$

$$\rho = \frac{p}{RT} \tag{93}$$

$$\frac{dp}{p} = -\frac{g}{R}\frac{dh}{T}$$

Parameter	Explanation
p	pressure [Pa]
dA	differential area [m²]
dp	differential increase of static pressure [Pa]
dh	differential increase of altitude [m]
ρ	density [kg/m³]
T	absolute temperature [k]
R	specific gas constant of air, 287.058 [J/(kg*K)]
g	Gravity [m/s²]

Table 10-1: Parameters of the atmospheric pressure model

Obviously, the temperature of the atmosphere, or its temperature profile with height, has enormous influence on the atmospheric layers. In the International Standard Atmosphere (ISA), the temperature progression with altitude has been modeled considering averaged statistical meteorological data. Up to an altitude of 11 km, the temperature progression is modeled linear with a decrease of -6.5 K/km.

$$T_h = T_0 + kh$$

$$k = -6.5 \cdot 10^{-3}\frac{K}{m} \tag{94}$$

$$\frac{dp}{p} = -\frac{g}{R}\frac{dh}{T_0 + kh} = -\frac{g}{R}\frac{dh}{kh+T_0}$$

Parameter	Explanation
T_h	temperature in altitude h [K]
T_0	temperature in altitude 0 m [K]
k	height coefficient with altitude [K/m]

Table 10-2: Parameters of the atmospheric temperature model

Integrating both sides yields:

$$[\ln(p)]_0^h = -\frac{g}{Rk}[\ln(|kh + T_0|)]_0^h$$

$$\ln\left(\frac{p(h)}{p(0)}\right) = -\frac{g}{Rk}\ln\left(\frac{kh + T_0}{T_0}\right)$$

$$\frac{p(h)}{p(0)} = \left(1 + \frac{kh}{T_0}\right)^{-\frac{g}{Rk}} \tag{95}$$

$$p(h) = p(0)\left(1 + \frac{kh}{T_0}\right)^{-\frac{g}{Rk}}$$

Parameter	Explanation
p(h)	pressure in altitude h [Pa]
p(0)	pressure at sea level [Pa]

Table 10-3: Parameters of the pressure integration

The ISA gives the following standard values for the meteorological magnitudes on sea level:

$$T_0 = 288.15\ K$$

$$p(0) = P_0 = 101300\ Pa \tag{96}$$

$$\rho_0 = 1.225\frac{Kg}{m^3}$$

Parameter	Explanation
T_0	Average temperature on sea level [K]
P_0	Average pressure on sea level [Pa]
ρ_0	Average air density on sea level [Kg/m³]

Table 10-4: Standard sea level conditions of ISA

Figure 10-2 gives a graphical representation of the equations given above. As can be seen the pressure decreases non-linearly with increasing height, while the slope is highest at zero height. This effect is plausible, since the air column with all its weight above the reference point is highest there, hence the pressure, and also the density, is highest there. Due to the second equation of (93), the differential pressure is proportional to the density of the fluid.

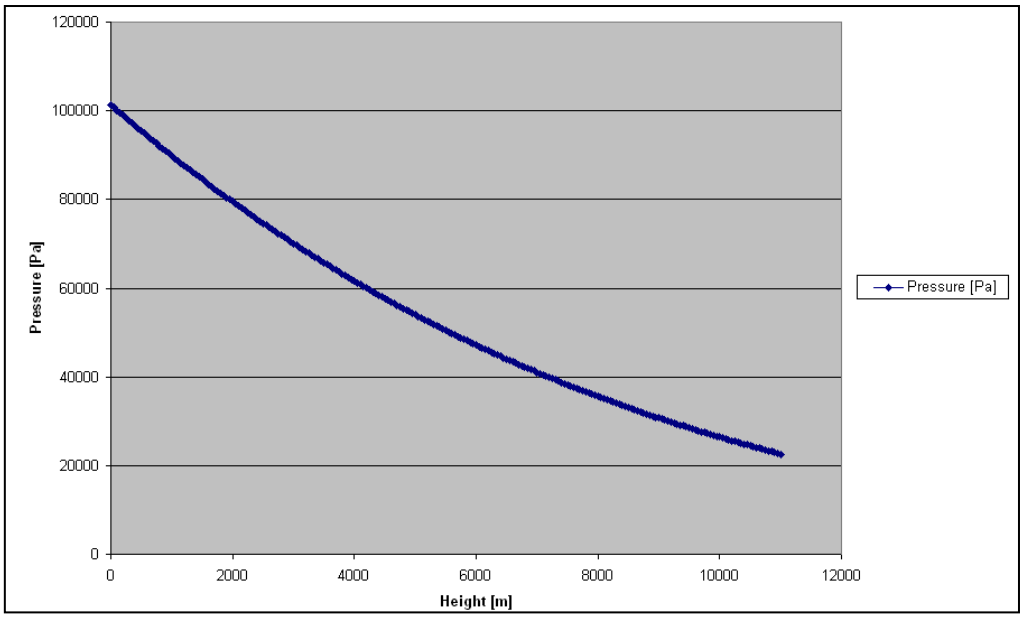

Figure 10-2: Air pressure as function of height in accordance to ISA

If the height range is limited, the pressure progression becomes nearly linear. This is shown in Figure 10-3. In this graph, the range of height is limited to 0-2000 m. The graph is only slightly curved and can be approximated as linear in the vicinity of the linearization point. This vicinity can be more than hundred meters with good approximation.

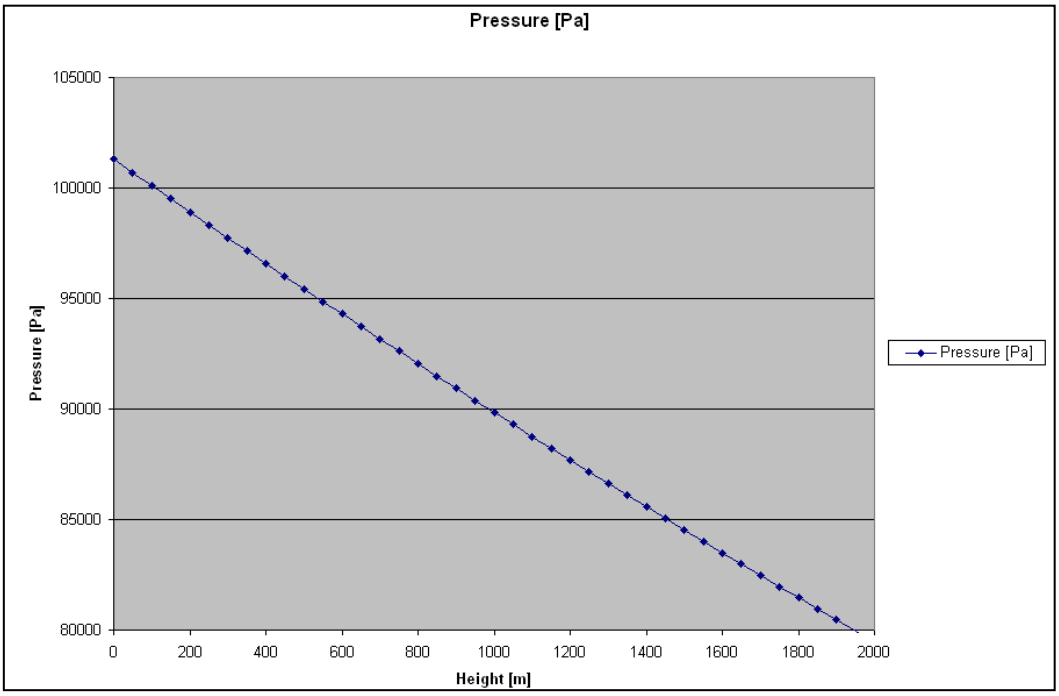

Figure 10-3: Close-up of the ISA air pressure in low heights

In this simplified model, an increment of height is linearly equivalent to a certain increment of pressure. If the conditions at Neubiberg, Germany, are considered, the following approximations can be used:

$$H_0 = 547m$$

$$T = 293.15K$$

$$P_{0,typ} = 95000Pa$$

$$\rho_{0,typ} = 1.12915\frac{Kg}{m^3} \tag{97}$$

$$\left(\frac{\Delta p}{\Delta h}\right)_{H_0} \cong -11.077\frac{Pa}{m}$$

$$\left(\frac{\Delta p}{\Delta h}\right)_{ISA} \cong -11.065\frac{Pa}{m}$$

Parameter	Explanation
H_0	Reference altitude at university campus (above sea level, geoid) [m]
T	Typical temperature in office building [K]
$P_{0,typical}$	Typical pressure at reference position [Pa]
$\rho_{typical}$	Typical air density at reference position [Kg/m³]
$\left(\frac{\Delta p}{\Delta h}\right)_{H_0}$	Typical pressure increment per meter height at reference location [Pa/m]
$\left(\frac{\Delta p}{\Delta h}\right)_{ISA}$	ISA model pressure increment per meter height at reference location [Pa/m]

Table 10-5: Parameters for the estimation of pressure change per meter altitude change

As can be seen, the difference in the pressure increment per meter height at the reference location between model and typical values from measurements is nearly identical, the difference is neglectable for pedestrian navigation and MEMS type sensors.

The calculations and statements above are valid only for static and low dynamical application. If the user is moving with reasonable speed, the properties of pressure can change significantly. In subsonic conditions this behavior is described by the laws of Bernoulli and the Navier-Stokes-equation:

$$\frac{\rho}{2}v^2 + p = const$$

$$p = p_0 - \frac{\rho}{2}v^2 \tag{98}$$

Parameter	Explanation
ρ	Air density [Kg/m³]
v	Velocity of air flow [m/s²]
p	Static air pressure [Pa]
p_0	Total pressure (static and dynamic) [Pa]
$\frac{\rho}{2}v^2$	Dynamic pressure [Pa]

Table 10-6: Parameters of the Bernoulli and Navier-Stokes equations

Equation (98) shows, that moving the sensor with high velocity can cause the measured pressure to decrease in comparison to static measurements. Therefore highly dynamic velocities can cause misinterpretation of altitude information, if not considered properly.

10.2 Sensor description

The sensor used in this thesis is the MEMS-type Bosch Sensortec BMP085 digital pressure sensor. Its footprint is 5 mmx5 mm, with a height of only 1.2 mm. The sensor offers internal A/D conversion and a digital communication I²C-interface. This is favorable in many respects. First of all there is no loss of analog data (e.g. in the cables, the amplifiers or attenuation circuits), since the data is transmitted in digital format. Secondly the I²C interface allows sending commands to the unit, e.g. to retrieve the factory calibration values, or to manually retrieve the basic measurements sensor temperature and measured pressure. Thirdly the integration of the sensor is much easier, since no analog components have to be integrated and many required elements are already integrated on the chip.

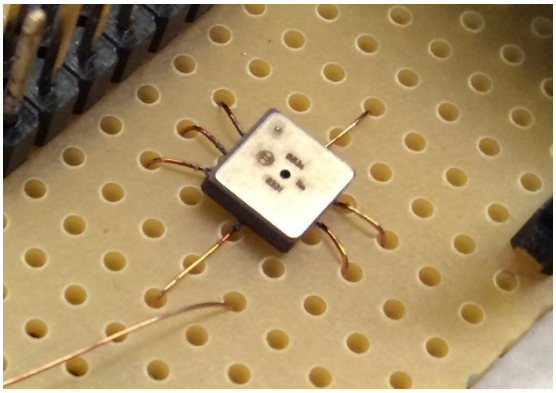

Figure 10-4: Bosch BMP085 sensor package on a dot matrix board (hole spacing 0.1 inch)

Most positive is the fact that temperature control is enabled by the manufacturer and the product, since the sensor temperature can be read out of the sensor by its API. The calibration model is supplied by the manufacturer and does not have to be developed by the customer.

To exemplify this feature, Figure 10-5 shows the measurements taken from the sensor. After warming up by idle operation of the sensor indoor for around 10 minutes the barometer was placed outside on a day with temperatures below 20°C. Therefore the sensor cooled down to around 19°C during operation. After it has been taken indoors the sensor temperature reached relatively stable 24°C. This is illustrated by the blue curve in the figure and quantized by the right hand side bar. The

saw tooth pattern on the right half of the graph can be explained by the limited resolution of the temperature output of 0.1°C. This is nevertheless more than adequate for the calculations.

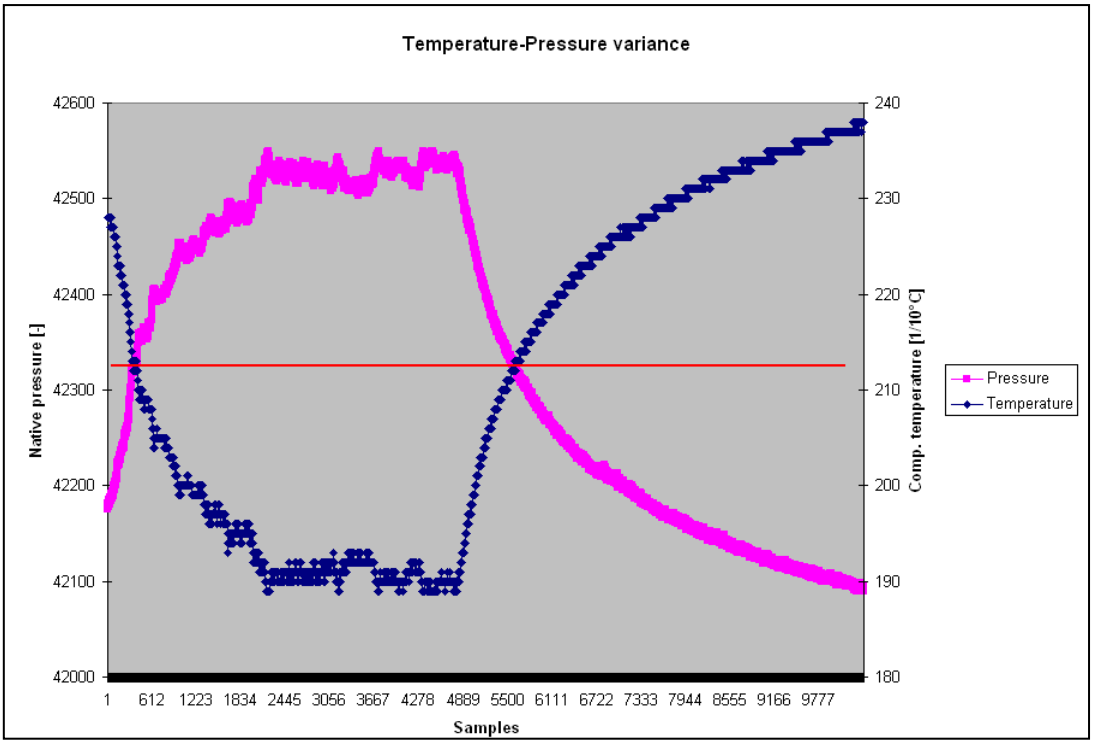

Figure 10-5: Relationship between calibrated sensor temperature and raw pressure readings

The magenta curve shows the response of the temperature raw data, which was recorded during the test run. As already mentioned for the MEMS IMU, MEMS sensors react very sensitive on temperature stress. At constant pressure and only influenced by a temperature shift of less than 5°C, the measurements drifted of more than 400 units, which corresponds to some 900 Pa in measured pressure. It is obvious that temperature compensation is crucial for the operation.

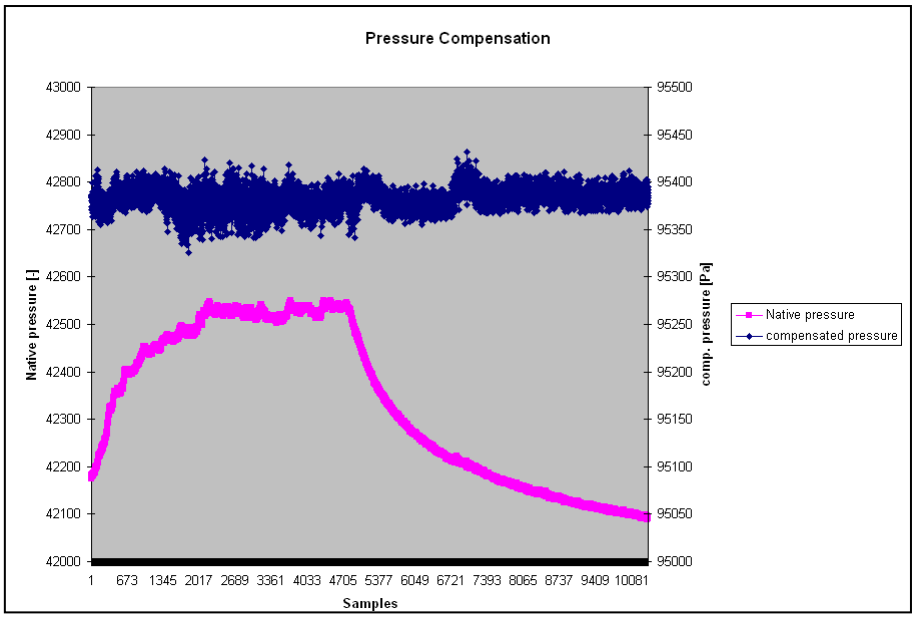

Figure 10-6: Results of temperature compensation of BMP085 pressure sensor

Figure 10-6 shows the results of the temperature compensation with the algorithm proposed by the manufacturer and the provided factory calibration parameters. It is obvious that the strong thermal drifts are cancelled by the temperature compensation. The measurement noise of the MEMS sensor can be clearly observed, too. It can be clearly identified that the sensor noise has a range of nearly 50 Pa, corresponding to several meters of altitude. Hence, centimeter accuracy cannot be expected by short term observations. This fact influences the usability of the pressure sensor for direct altitude aiding as well as direct step classification.

10.3 Barometer for 3D pedestrian navigation

Since the PNS based navigation system described in the previous chapters provides a 3D navigation solution, the barometric height determination shall be integrated in the navigation processing. Barometric sensors have dissimilar error propagation as inertial navigation systems, GNSS or WLAN/INPOS positioning systems, therefore it seems very promising to use barometric height as update in a Kalman filter. However, the barometric height determination has several flaws, which inhibit the direct use of the barometric height. First the weather conditions are not always in accordance with the standard atmosphere. Due to meteorological high and low pressure zones the calculated absolute height might be misleading or have a high bias. Secondly the remaining sensor bias cannot be determined easily during operation, which can also cause a bias in the absolute height calculation. The sensor noise must be considered. Finally, dynamic air flow due to rapid movement can cause pressure measurement deviations as described above. Hence, the direct usage of barometric altitude is not favorable. The results of a test run in the staircase of a six storey office building are visualized in Figure 10-7. The sensor has been carried by a pedestrian climbing the stairs from ground level up to the sixth storey.

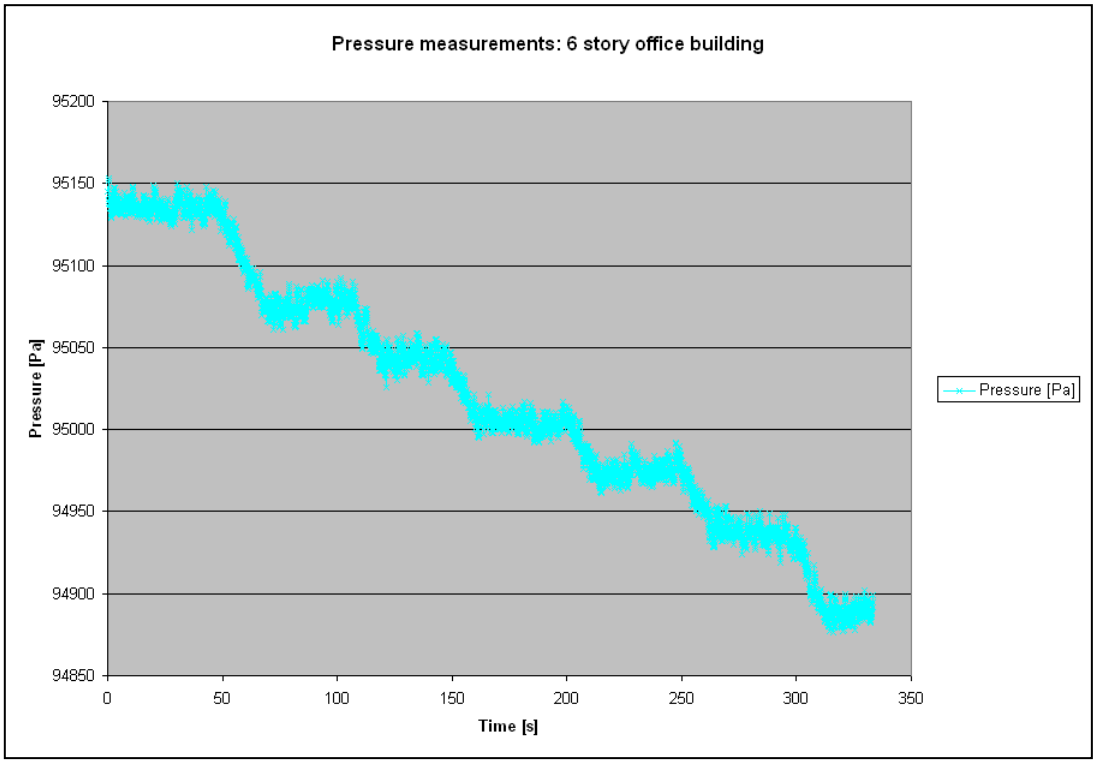

Figure 10-7: Measured pressure during a walk over 6 floors

The figure shows the temperature compensated pressure measured during the test run. The stairs, as well as level platforms between the stairs can be identified easily. Nevertheless, the present sensor noise is easily recognizable, too. Therefore, direct use of the pressure and the derived altitude is not advantageous for altitude updates. The noise reduction by low-pass filtering is shown in Figure 10-8. Averaging or low-pass filtering can reduce the sensor noise strongly, but could erase the original altitude dynamics, too, or at least add a time lag of the measurements to the system. In the step detection chapter, the reduced time lag has been a major development prerequisite. Therefore,

neither direct processing of the altitude updates of the barometer, nor low-pass filtered data shall be used in this thesis. An alternative implementation has to be considered.

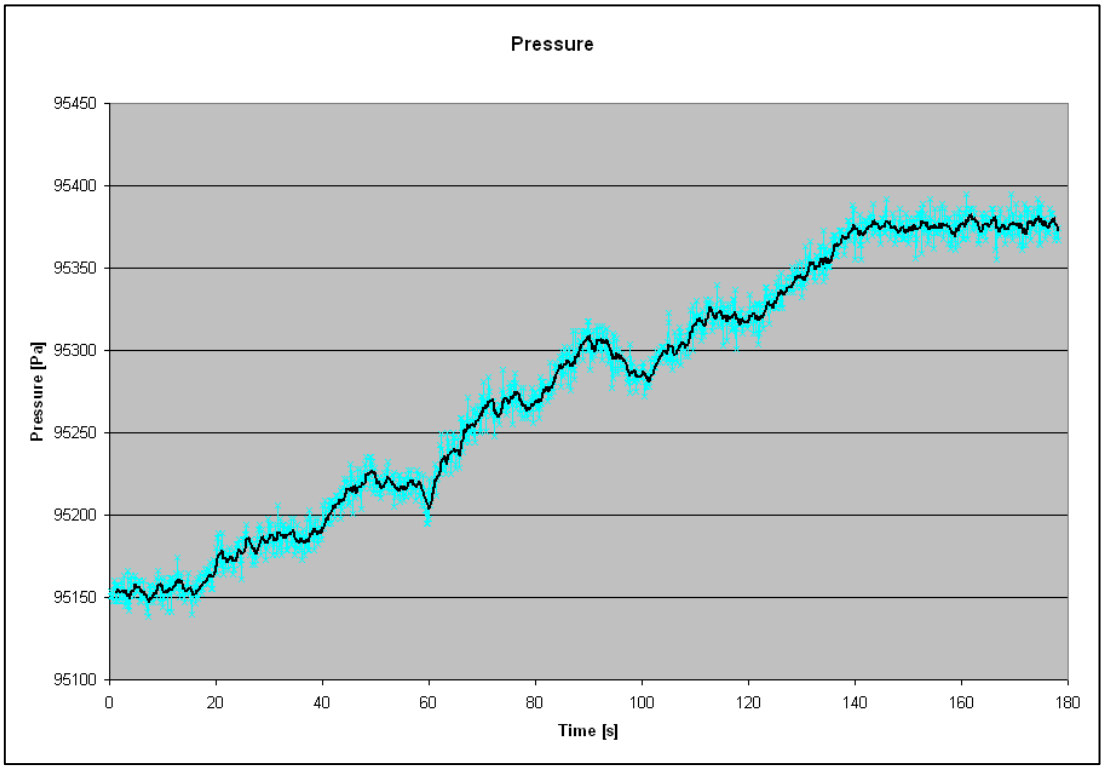

Figure 10-8: Low pass filtered barometer measurements

The basic idea of this alternative algorithm is to use the barometric information as input source for the fuzzy logic system, which determines the step type in the PNS navigation algorithm. The PNS is an extremely low noise and low drift system. Therefore the measured pressure is integrated over each step period and compared to the last integrated value. The integration reduces the noise of the pressure measurement additionally by:

$$\sigma_{baro,step} = \sigma_{baro}\frac{1}{\sqrt{n}}$$
$$n = f_{baro}\Delta t_{step} \tag{99}$$

Parameter	Explanation
$\sigma_{baro,step}$	standard deviation of integrated pressure [Pa]
σ_{baro}	standard deviation of single pressure measurement [Pa]
n	number of averaged samples
f_{baro}	sample frequency of barometer [Hz]
Δt_{step}	step interval from PNS [s]

Table 10-7: Parameters of the barometer inputs to the fuzzy logic system

If a sample frequency of 20 Hz, a sensor noise of 4 Pa and a step interval of 0.66 s (1.5 Hz) is considered, the standard deviation of integrated pressure shall reduce to 1.095 Pa. This related to a height standard deviation of 9.8 cm at the Neubiberg university premises, which is around a half step height.

The biases are compensated by the differencing between two consecutive steps. Additionally consecutive steps with high velocity changes (accelerations) shall be dismissed from the calculation to avoid problems with the dynamic pressure influence.

In the fuzzy logic system a new set of Fuzzy membership functions is implemented for the states Up-Level-Down. As mean setpoints, the model step height is assumed which relates to:

Fuzzy parameter	Values
μ_{level}	0m => 0Pa
μ_{up}	0.17m => -1.8819 Pa (at base level)
μ_{down}	-0.17m => 1.8819 Pa (at base level)
$\sigma_{up,level,down}$	values for single measurements: ~0.25 m integrated measurements: ~6.85 cm

Table 10-8: Barometer model set points for the fuzzy logic step detection system

10.4 Summary

In the previous chapter, the use of a low-cost, MEMS based barometric sensor for indoor positioning has been discussed. The physical principles of barometric altitude determination have been discussed and the relations for the International Standard Atmosphere (ISA) have been demonstrated. The used sensor has been introduced and characterized. Especially the temperature compensation has been demonstrated. Finally real test data for a staircase walk of a six storey building has been analyzed and an alternative integration in the PNS implementation has been introduced.

The sensor noise and the small pressure changes for single steps on a staircase showed that direct use of the measured pressure and its derivative was not possible. An alternative strategy for the use of barometric altitude determination had to be found. The core strategy was to integrate the noisy pressure readings over the step interval to reduce the measurement noise, and to differentiate the altitude change with respect to the last step. The determined height difference was used as input parameter of the fuzzy logic step classification system. By this procedure, no additional time lag for the dead reckoning system is introduced and the sensor is integrated in the existing step classification system.

11. Receiver Integration

In this chapter, the integration of the techniques described in the previous chapters in a software GNSS-receiver and an innovative receiver aiding technique is described and evaluated. The technique is called “ultra-tightly coupling” and uses, besides other important elements, all navigation techniques described in this thesis. The main element of the algorithm is very long coherent correlation of the received satellite signals with a respectively long internal replica signal. The integration time for dynamic use cases is up to 2 seconds and therefore one hundred times the GPS navigation data bit length, while common high sensitivity GPS receivers usually only use up to 20 ms. As will be demonstrated, the additional correlation gain together with other receiver techniques, especially vector tracking loops, allows the receiver to track very weak indoor GNSS signals.

Several inputs are needed to form replicas of a length of several seconds. The focus in this thesis is on the user motion. Although the highest Doppler components of the received signals are caused by the satellites’ motion, the Doppler variations are caused mostly by the user or antenna motion. The antenna motion is estimated for the integration interval by using all navigation techniques described in this thesis. The so called “micro-trajectory” will be used as major input for the replica construction. The author’s contribution to the described system is formed by the dead reckoning PNS including barometer and magnetometer processing, the WLAN proximity positioning, the design of the PNS Kalman filter, and the micro-trajectory generation based on all these subsystems. The used GNSS software receiver has been developed by other contributors ([110], [6]). Since the authors contribution can only be evaluated in the context and integration with all other contributions, the entire system will be described and evaluated. The key enabling technology is a fully adjustable and software GNSS receiver that can be modified to the user’s needs. The receiver used for this thesis is the NavX-NSR by IfEN GmbH.

In this chapter, the basic technique of receiver aiding will be presented. The system components will be described and several implementation aspects will be shown. Finally, the performance of the system will be evaluated by analysis of data produced in several test campaigns.

11.1 Introduction

GNSS receivers acquire and track satellite signals transmitted by GNSS satellites. These GNSS signals are transmitted with a very low EIRP. Because of the long distance between the satellites and the receivers on the Earth surface, the received signal strength is very low. Even under open sky conditions, the signals are below the average noise level. A description and exemplary calculation of the GNSS link budget can be found in chapter 18.1. The signals can only be evaluated by correlation of the signals with an internal signal replica. This process yields the pseudoranges to the satellites, but also the relative velocity derived from the signal Doppler frequency.

In the acquisition process, the signal processing unit has to check for the presence of the desired satellite signal by trying replicas with various time/range and Doppler shifts. These search points are referenced as “range bins” and “Doppler bins”. The more bins there are to be searched, the more effort and time is needed to acquire the signal. If the receiver is moved very dynamically, it is possible that the receiver tracking loops are not able to follow the signal dynamics. Additionally, if the signals are attenuated strongly, the receiver might not by sensitive enough to find the signal in

the noise floor. In all of these cases, receiver aiding, in which additional sensors are used to provide trajectory information, is a promising option. Most often INS is used to provide this dynamical information, since INS and GNSS are complementary in the position and velocity domain. While several different types of receiver aiding algorithms exist, in this thesis the receiver aiding method "Ultra-Tightly Coupling" will be described. A mathematical analysis on the tracking loop stability, dynamical tracking error and receiver aiding is given in chapter 18.2.

If the signal is attenuated strongly inside a building, many commercial receivers cannot acquire and track the signals anymore. The main technique of the developed algorithm is to increase the correlation gain of the receiver by forming a longer signal replica. The internal replicas used for correlation are constructed based on the knowledge of the signal frequencies and codes, but the time delay and the Doppler shift of the signal are also important inputs for the replica generation. Only if the replica matches the original signal very well, the correlation results in a significant value. In the tracking process, replicas are built with modified time delay (early, punctual, late as expected before correlation), for the Doppler tracking the replica phase is modified (in-phase and quadra-phase). The longer the correlated signals are, the more correlation gain can be achieved. High correlation gain allows the acquisition and tracking of weak signals like the GNSS signals inside buildings. A good description of the fundamentals can be found in [77], [112], [110] and [79].

Main limiting factors for long coherent integration are:

Limiting factor	Explanation	Solution
Oscillator stability	The replica is formed by signal processing using an internal oscillator as frequency reference. Oscillator drift and noise produce errors in the replica forming.	High quality internal crystal oscillator (OCXO or miniature atomic clock)
User antenna motion	The antenna motion causes range and Doppler shifts which cannot be resolved by a static or first order dynamic signal replica.	Precise reproduction of user motion (micro-trajectory)
Navigation data bit transition	The navigation message is modulated on the GNSS signal with a binary phase shift keying (BPSK) modulation. If the navigation bit switch is not anticipated, a correlation loss is induced.	Use of external almanac/ assistance data (assisted GNSS) for the navigation message
Satellite motion	The satellite orbit has to be predicted as precise as possible to predict precise pseudoranges and Doppler variations for the internal signal replica.	Use of external almanac/assistance data (assisted GNSS) and orbit prediction for precise satellite orbits

Table 11-1: Limiting factors and technical solutions

11.2 Overview of various types of GNSS INS integration

Classical GNSS-INS integration has often been categorized into loose, tight, ultra-tight or deep coupling. Customized filters are used to combine GNSS and other sensors and to estimate the individual system errors. Very often, the filter is realized as error state Kalman filter, being propagated by INS and corrected by GNSS observations. Various levels of coupling exist and are sometimes hard to identify or distinguish. Especially in the field of deep or ultra-tight integration, often the wording is not very precise, and various subtle differences between the implementations can be observed. On first sight the level of coupling can be determined by evaluating the kind of data used as observation. If the GNSS receiver position and velocity information is used as update, loose coupling is most certainly used. If pseudorange and Doppler information is used as observations, most certainly tight coupling is used. If the observations are correlator outputs, e.g. early, punctual, late or differences of them, as well as in-phase and quadra-phase values are used, most certainly ultra-tight or deep coupling is used. While the filters have often similar state vectors, the observation or design matrix is different for all kinds of implementations.

Loose and close coupling are not affecting the receiver itself, both GNSS receiver and INS processing chain maintain operation independently of each other. The results are then used to estimate navigation errors of the INS and to correct the INS navigation solution of position, velocity and attitude, most often using an extended Kalman filter (EKF). While in loose coupling the GNSS receiver's position and velocity solution are used, in tight coupling the raw results pseudoranges and Doppler values are used as update measurements. The receiver itself is not affected; therefore, the performance of the GNSS receiver is not improved.

In this thesis the goal is to track and acquire very weak GNSS signals, down to the range of 0 dB-Hz C/N0, thus receiver aiding is necessary. Several kinds of implementations are possible. It is possible to reduce only the receiver search space by using the INS PVA (position, velocity, and attitude) solution to predict PR and Doppler values. This already increases the chance of finding weak signals strongly and reduces the chance of tracking the wrong signal or correlation peaks. It is furthermore possible to directly steer the tracking loops. This technique requires a very precise secondary navigation solution, while especially the Doppler and acceleration are critical. Finally, the replica generation itself can be influenced by the INS solution to adjust the trajectory correction during the coherent integration interval. Especially this technique, beside others, has been used.

11.3 System design of ultra-tightly coupled integration

Several components are needed to realize an ultra-tightly coupled GNSS/INS system. In Figure 11-1, the top-level hardware architecture of the realized system is presented. All elements are mounted on a heavy duty backpack to make the system useable for pedestrians. The backpack carries a GNSS antenna on top to provide best satellite visibility. Next to the antenna, a XSENS MTi inertial measurement unit is placed to monitor the antenna motion. The lever arm between the IMU and the antenna could be reduced to few centimeters. Additionally, the backpack carries a small size MEMS Bosch BMP085 digital barometric sensor. The antenna, IMU signals and barometer data are sampled by the NavX NAVport II RF-front-end. For additional indoor positioning capabilities, a ZigBee based INPOS positioning system is mounted on the backpack and transmits position updates to the laptop. A commercial GPS/Galileo receiver is carried as reference receiver. All data streams are sent to a laptop computer via USB. The laptop communicates to an assisted GNSS server via WLAN. The WLAN transmitter is used for the WLAN proximity positioning system, too.

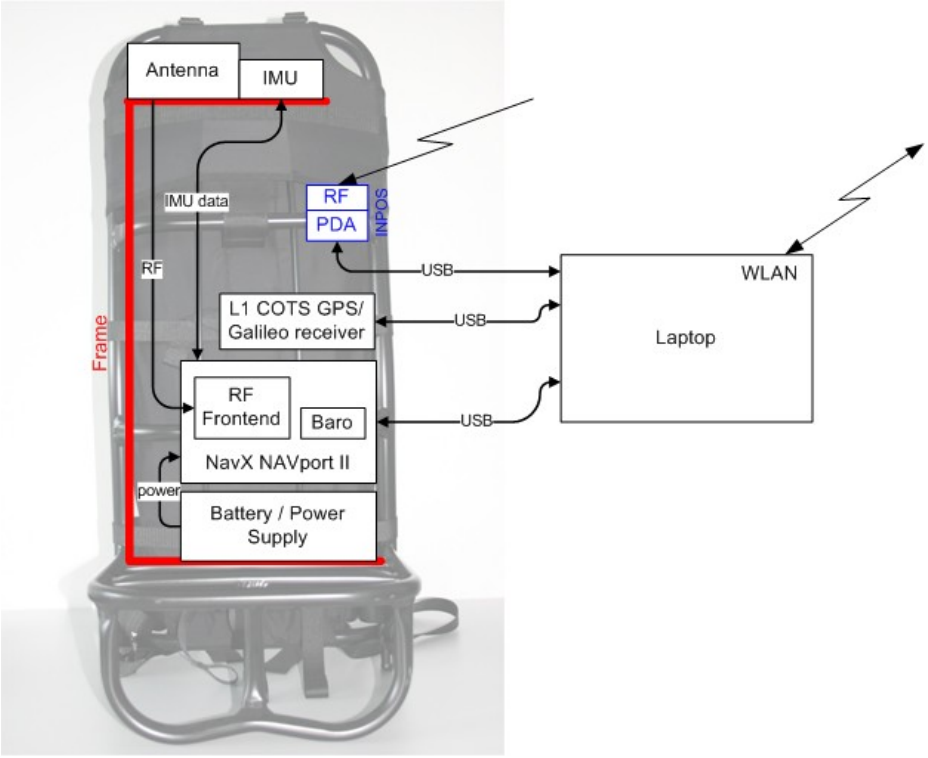

Figure 11-1: Hardware Architecture of the integrated navigation system [72]

From the hardware side, mostly standard interfaces could be used, which reduces the hardware development efforts strongly. The backpack is supplied with power from a battery pack at the bottom of the backpack. The backpack is fixed to the user by a strap system. Additionally, the laptop is held by a strap system like a vendor's tray, giving the user free hands for using the laptop or handling other equipment or activities. The complete unit with the user can be seen in Figure 7-6.

A more detailed view in the hardware architecture of the system can be seen in Figure 11-2. This scheme includes all surrounding infrastructure like GNSS constellation simulators, GNSS test areas like the Galileo test environment GATE and the Italian Galileo Test Range GTR, the ZigBee nodes used for the INPOS positioning system, WLAN nodes for WLAN proximity positioning, and finally an

assisted GNSS server. The RF-frontend is displayed in more detail, revealing an OCXO precise oscillator as time reference, as well as a FPGA as data handling module and two ASICS for the RF signal handling.

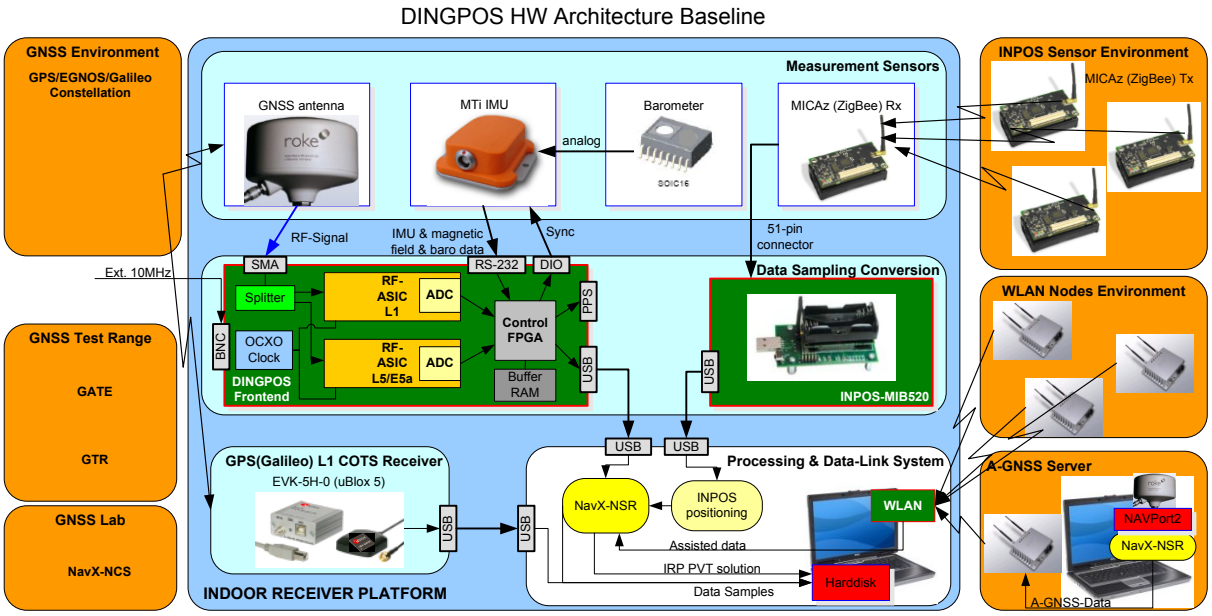

Figure 11-2: Integrated Receiver Platform Architecture, [110]

Even more complex than the hardware side is the organization of the data flow and the cooperation of different contributing algorithms. They are presented in Figure 11-3.

The red blocks in Figure 11-3 show the PNS/Dead reckoning (DR) as well as the strapdown INS part of the system. The data from IMU, magnetometer and barometer is used in the DR system to derive the macroscopic user trajectory. As described in the PNS chapter, the trajectory is called “macroscopic” because it has a low data rate, which is caused by the step detection algorithm. The macro-trajectory is corrected by an integrating Kalman filter, using updates from the WLAN proximity positioning system, as well as GNSS pseudoranges and the external INPOS positioning system. The macro-trajectory has a high relevance for the user. It provides continuous positioning with high availability and relatively low drift even under worst indoor conditions. Additionally, the DR trajectory, corrections from the Kalman filter and, most importantly, the IMU data are used to calculate the micro(µ)-trajectory (green block). The micro-trajectory is produced by a strongly modified strapdown calculation. The micro-trajectory has a data rate of 100 Hz and is stabilized by the PNS dead reckoning solution. It provides the antenna motion with low drift, high data rate and high accuracy, especially in the velocity (relevant for the Doppler) and acceleration (Doppler rate) domain. The algorithms for the trajectory calculation will be described in chapter 11.4.

The yellow blocks indicate all signal acquisition and tracking elements. The micro-trajectory is used in the line-of-sight projection, calculating the line-of-sight (LOS) dynamics of the user antenna with respect to the individual satellites. The results are essential in the tracking and acquisition algorithms, especially in the replica forming algorithms and tracking loop filters. Since the micro-trajectory is especially precise in the velocity and acceleration domain, the signal processing unit is assisted in the coherent integration by precise Doppler and Doppler rate estimations.

As can be seen in the lower part of Figure 11-3, the dead reckoning as well as the strapdown parts can be simulated, too, to test the system without the need for a test range or test walk.

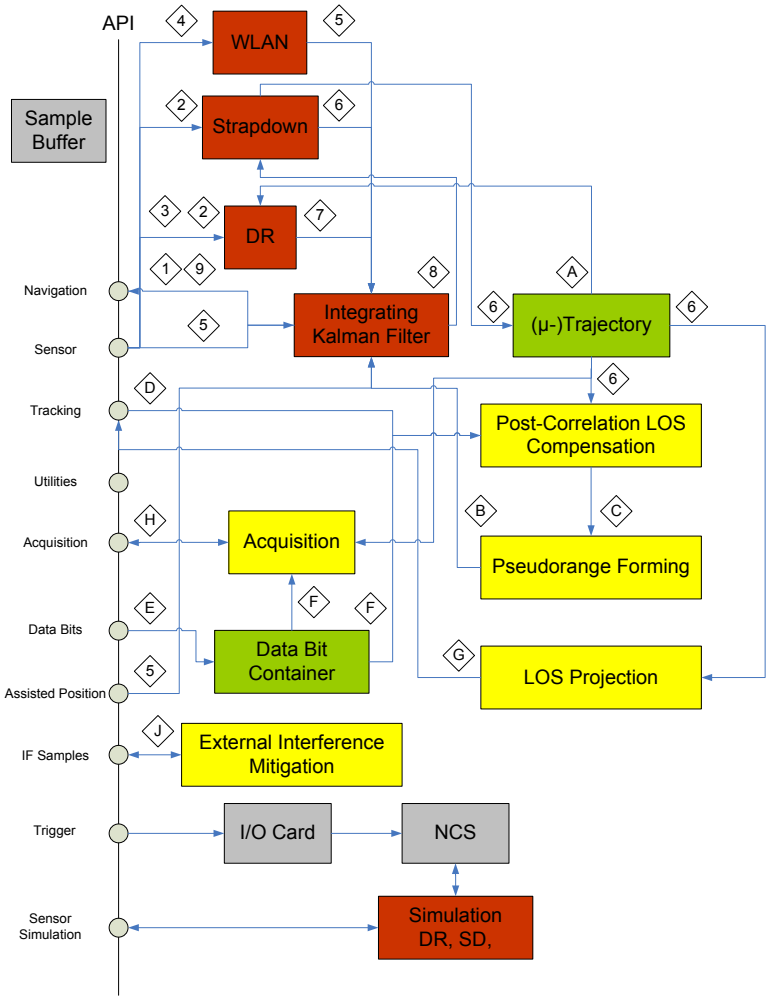

Figure 11-3: Data Flow of the high sensitivity GNSS receiver system [93]

11.4 Reproduction of User Motion

One of the essential elements for realizing very long coherent integration is the precise reproduction of the user antenna motion. The antenna motion, i.e. the antenna velocity, is quite small in comparison to the satellite motion, which can reach more than 3800 m/s. On the other hand, the satellite LOS velocity is changing very slowly, while the antenna velocity is changing very fast. Therefore, while the large part of the GNSS signal Doppler frequency might be the result of the satellite velocity, the Doppler derivative, i.e. the change of the Doppler frequency with time, is caused mainly by the user dynamics, projected on the LOS to the satellites. For very long coherent integration, the GNSS signal replica must match the received signal with an accuracy of only a few centimeters. The maximum tolerance is between 2.5 cm and 5 cm. Hence, the antenna dynamics must be tracked very precisely. The velocity domain becomes important, since a replica length of up to two seconds is required.

INS, as described in chapter 6, is a technology which is able to precisely track the motion of an IMU in 3D with a high update rate. It can provide a PVA solution (Position, Velocity and Attitude). These magnitudes are the required inputs for the user motion reproduction. On the other hand, INS shows significant drift due to sensor errors, misalignment, and position errors. It could be verified in laboratory tests that, especially when using MEMS type IMUs, the accuracy of the user position is not acceptable for replica generation of two seconds or more. Additionally, external updates are not frequent and accurate enough to fully stabilize the IMU sensor errors, as well as the INS PVA errors.

The PNS dead reckoning system presented in chapter 7 provides the pedestrian position with very low drift and good overall accuracy. Nevertheless, the position is only provided with an update rate equally to the user's step rate. Additionally, the provided position does not consider the antenna motion, but propagates the IMU position according to a pedestrian walking model.

To overcome the described problems, both technologies have been integrated to use the high data rate and 3D PVA solution of the INS and the stability and long term accuracy of the PNS. The basic design of this integrated system algorithm is presented in Figure 11-4.

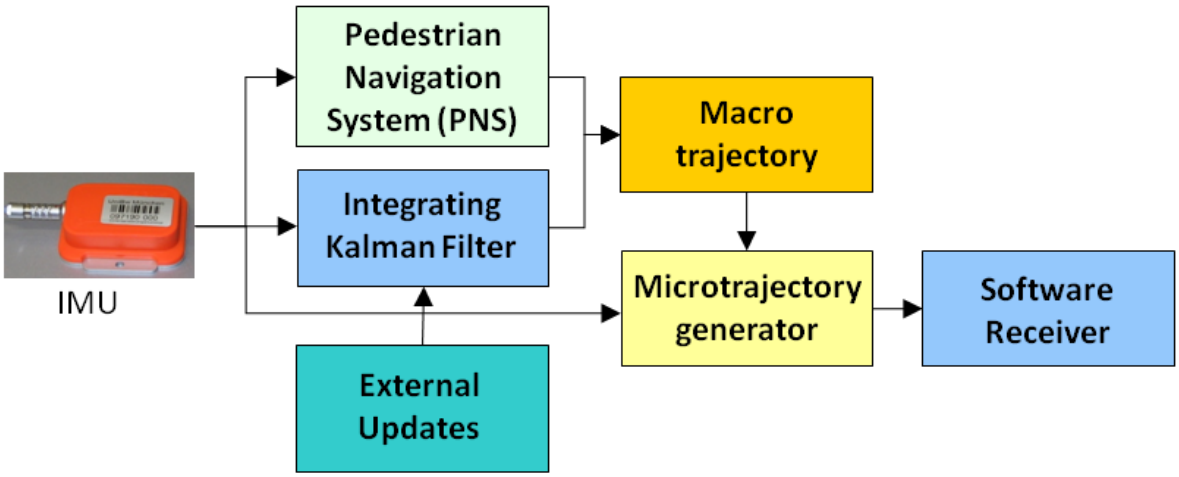

Figure 11-4: Overview of the user motion reproduction in DINGPOS [72]

As a baseline, the IMU raw data is used to calculate a PNS trajectory. The algorithms have already been described in detail in chapter 7. The PNS system is stabilized by a PNS Kalman filter. The filter uses a design analogue to the filter described in chapter 8 and uses external position updates, e.g. WLAN proximity positions (see chapter 9), INPOS position updates, magnetometer measurements, and GNSS updates.

The result is a trajectory of consecutive points which are updated at every step detection event. This trajectory is called “macro trajectory”. Additionally, the user position is interpolated to the epochs that limit the integration intervals of the very long coherent integration. As a result, the user positions at the beginning and at the end of the individual integration interval is known from the dead reckoning system. This is demonstrated in Figure 11-5. The DR positions are presented as circles; the interpolated positions at the ends of the integration interval are presented as crosses.

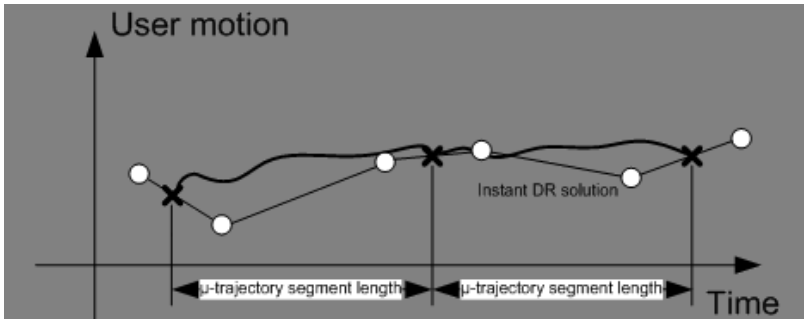

Figure 11-5: Principle of interaction between macro and micro trajectory [72]

INS is used to calculate the “micro-trajectory”, a high frequent 3D position and velocity solution that fits the DR positions and velocity at the ends of the integration interval. The initial conditions are provided by the AHRS of the MTi system, the PNS positions and the Kalman filter corrections. The INS processing as described in chapter 6 is performed for the integration interval. At the end of the interval, the position and velocity difference between the between the PNS and the INS trajectory is determined. Since the reference positions are known a priori, it is possible to calculate bias corrections to the IMU raw data, so that the micro-trajectory is forced to match the macro-trajectory at step detection. In Figure 11-5, the principle is illustrated. While the micro trajectory has a much finer granularity, it is only bound to the macro-trajectory at the end points. Between them, the user dynamics are represented only by the INS algorithms. The matching can be based on position or velocity level, matching the user velocity during the integration interval, or matching the user position at the end of the interval. Only the corrections are adapted while the rest of the algorithms remain unchanged. Extensive testing showed that the velocity matching already gives sufficiently accurate results for the coherent integration.

The INS modifications include simplifications which ensure stable operations. First of all, a total operation period of the length of the integration interval (two seconds) is used, which by itself reduces the drift strongly. The INS is set up at the beginning of each interval with starting values from the PNS and the AHRS. Secondly, the Schuler tuning feedback is disabled. Hence, the attitude solution is much more stable, since the dynamics of the system are broken. The transport rate and attitude correction are extremely low for pedestrians, especially for these short intervals, so the negative influence on the position solution is minimal. The attitude and the position engine are separated by this. When the end of an integration interval is reached, the PNS positions are

interpolated to the epochs of the start and end point of the integration interval. In a first step, a modified INS algorithm calculates a raw micro trajectory, starting at the interpolated PNS start position. The INS based user velocity/position at the end of the interval is compared to the interpolated PNS velocity/position solution at the end of the interval. From this, corrections comparable to a "sensor bias" in the navigation frame are calculated. These corrections are inferred into the modified INS algorithm. As a result, the trajectories match at the beginning and at the end of the integration intervals.

In Figure 11-6, the result of the micro trajectory generator is shown for ten consecutive steps. It can be seen that the actual stride was roughly between 0.7 and 0.8 meters (blue curves). The step interval was between 500 and 600 ms; the red curve shows impressively the lift and drop of the IMU during each step. The green lines show the cross-axis movement caused by the body leaning to the left and to the right. In contrast to the macro trajectory, the micro trajectory has a data rate of 100 Hz and covers all movements within the step interval.

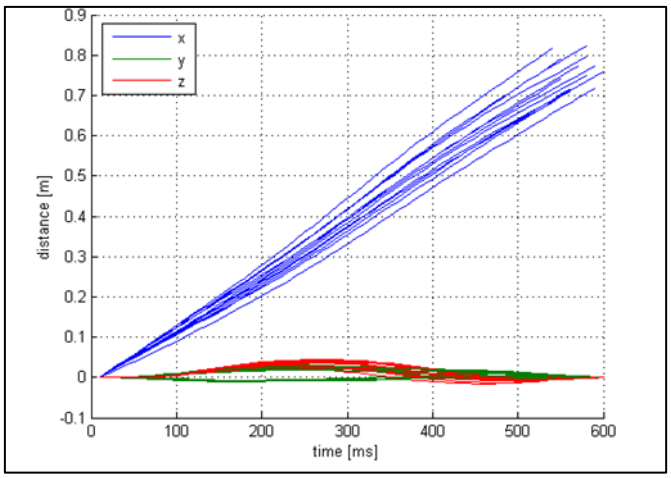

Figure 11-6: Calculated user motion along the walking path for several consecutive steps [72]

To predict the pseudorange and the pseudorange rate correctly, the user dynamics must be projected on the satellites' LOS. The predicted satellite orbit must be added to the user motion. Finally, using the geometry and dynamics, the replica generation can be performed.

11.5 Field test results

In the previous chapter the development of a high sensitivity GNSS receiver using very long coherent integration, with special focus on the user trajectory replication, has been described. The system integrates several different positioning and user tracking subsystems, and tracks GPS as well as Galileo signals. Galileo offers advanced signals in several frequency bands which are advantageous especially for the indoor or urban use case. Additionally it must be assumed that most future (and already many current) receivers will use all available satellite systems. Hence, it was mandatory to test the system with Galileo signals, too. Since the Galileo space segment had not been implemented yet at the time of development, only few ground based Galileo test areas were available to test the system capabilities. Two test sites have been chosen, the Germany based GATE and the Italian based GTR test sites. The tests described in the following have been performed at the Galileo test environment (GATE) at Berchtesgaden, Germany. The GATE environment offers several ground based pseudolite transmitters, transmitting simulated Galileo signals. The transmitters are located at the summits of several surrounding mountains and offer low elevations, which are, nevertheless, larger than zero. In [126], the HDOP is stated as less than 2, while a VDOP of 6-20 is specified.

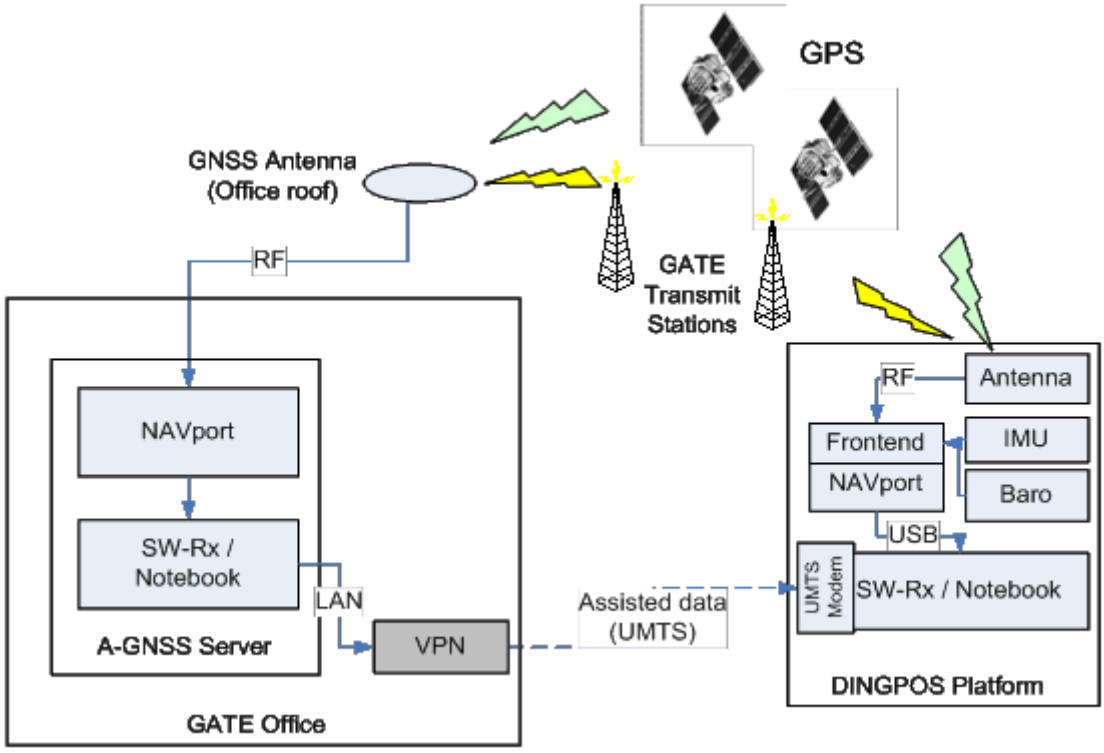

Figure 11-7: Setup for the test campaign in the GATE test area Berchtesgaden [72]

The test setup for the field tests is shown in Figure 11-7. Basically four major components can be identified:

- the GPS space segment
- the GATE ground based pseudolite transmitter stations
- a reference receiver for the assisted GNSS data, placed at the GATE office in Berchtesgaden
- the DINGPOS mobile platform as described above

The test strategy includes outdoor tests in urban-like scenarios as well as indoor tests in a building which is representative for a commercial application. Therefore, a laboratory environment is not suitable, although the available test infrastructure would potentially be more advantageous than in a realistic building. The indoor test building was a hotel complex in the GATE area. For the indoor tests, additionally several WLAN access points were available in the indoor test environment. The WLAN access points were used for the WLAN proximity positioning system. Although a laboratory environment would have had benefits especially regarding the repeatability of tests at any time, weather conditions etc., and especially regarding the ground truth data evaluation, the value of real world data gained during test in a realistic and not artificially modified environment is significantly more valuable.

For the evaluation of the system, outdoor tests with significant multipath and signal blockage have been performed, as well as indoor tests in a hotel building in the GATE test area. Reference data from local survey authorities were available for both tests. A COTS GPS receiver has been used as reference instrument. The goals of the tests have been to prove the seamless indoor/outdoor positioning capabilities of the integrated platform, as well as to prove the supremely high sensitivity of the GNSS receiver using very long coherent integration. The PNS system has been calibrated to the user in a calibration campaign one week before the test campaign. No additional specific calibration has been performed for test.

A basic problem of the test performance evaluation is the lack of precise ground truth data. There has not been any user positioning system available which would have been more accurate in determination of the user's position than the systems already integrated in the platform. Several reasons for this are:

- The test runs are performed in situations with strongly challenged GNSS environment. This causes fast changing satellite constellations as well as blocked line of sights, heavy multipath or even total loss of signals. Using standard GNSS receivers, including RTK, would not be very beneficial in these situations.
- The test runs cover large distance and space. The installation and calibration of reference systems like optical/camera based systems, ultra-wideband, RFID or other techniques would have been by far too expensive and complex.
- Permanent installations in the hotel as well as on the streets were not allowed.

Hence, a different approach has been selected. For the buildings in the test area, official survey data from the local survey authority has been procured. By combining aerial survey photos from the local survey department, the coordinates of the buildings and the trajectories determined by a commercial of the shelf (COTS) GPS receiver, as well as the calculated trajectory by the integrated navigation platform, the accuracy and the plausibility of the positioning solution can be evaluated. The effects of multipath or signal blockage are clearly observable in this projection. For the tracking, the internal C/N0 estimation of the software receiver will be evaluated. The reason for this is the fact that the signal power can only be evaluated after correlation. No commercial reference receiver with comparable sensitivity was available for the test.

11.5.1 Outdoor scenario test and results

The outdoor test runs have been performed in the area around the GATE office in Berchtesgaden, Germany. The area has been selected due to the need for assisted GNSS data. The test site is shown in the aerial photo in Figure 11-8.

Figure 11-8: Outdoor test environment in the GATE test area around the GATE office [127]

The assistance data was generated at a reference station inside of the GATE office and then transmitted to the rover by WLAN. The precise location of the GNSS antenna of the reference station, as well as the calculated trajectories from the COTS reference GNSS receiver (red line) and the DINGPOS integrated platform (blue line) can be seen in Figure 11-9. In this figure, the precise survey data of the buildings, provided by the local survey authorities, are integrated as overlays. For the test, the user started the run at the front of the GATE office and walked the same closed path around the neighboring four houses five times.

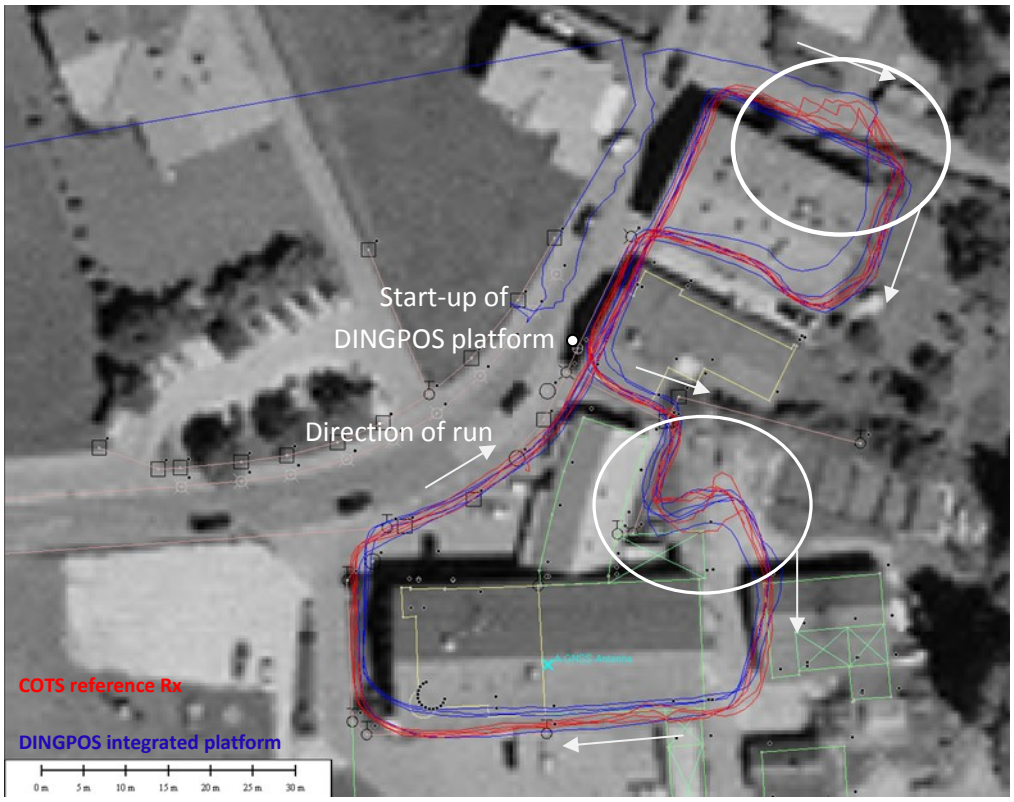

Figure 11-9: Results of the GATE outdoor test: red line shows reference receiver trajectory, blue line shows DINGPOS platform positioning results [72]

In this scenario, the GATE transmitter constellation emulates so called “urban canyons”. In this constellation, the LOS between receiver antenna and the satellites is blocked by high buildings. Additionally, the signal is often reflected by the front surfaces of the buildings, causing strong multipath effects. Since the GATE transmitters have a very low elevation, even the lower buildings at the test area show similar effects as skyscrapers in metropoles. The integrated system is physically affected by this effect more strongly, since the reference receiver uses only GPS satellites, while the DINGPOS platform uses GPS and GATE Galileo signals. Since the GPS satellites have most of the time a much higher elevation than the pseudolites, the multipath and signal blocking effect is much less on the reference receiver. As can be seen in Figure 11-9, the DINGPOS platform shows significant position errors at the startup of the system and the beginning of the test run. At the beginning, the filters of the system need time to correctly estimate the error states and to fully synchronize to all signals. But already after circulating the first house, the platform is able to precisely track the user’s position. The system filters have converged. The effects of multipath and signal blockage are not visible from that point on. As can be seen in Figure 11-10, the platform is able to track between eleven and twenty satellite signals. Hence, the system looses and acquires satellites regularly without noticeable loss of accuracy.

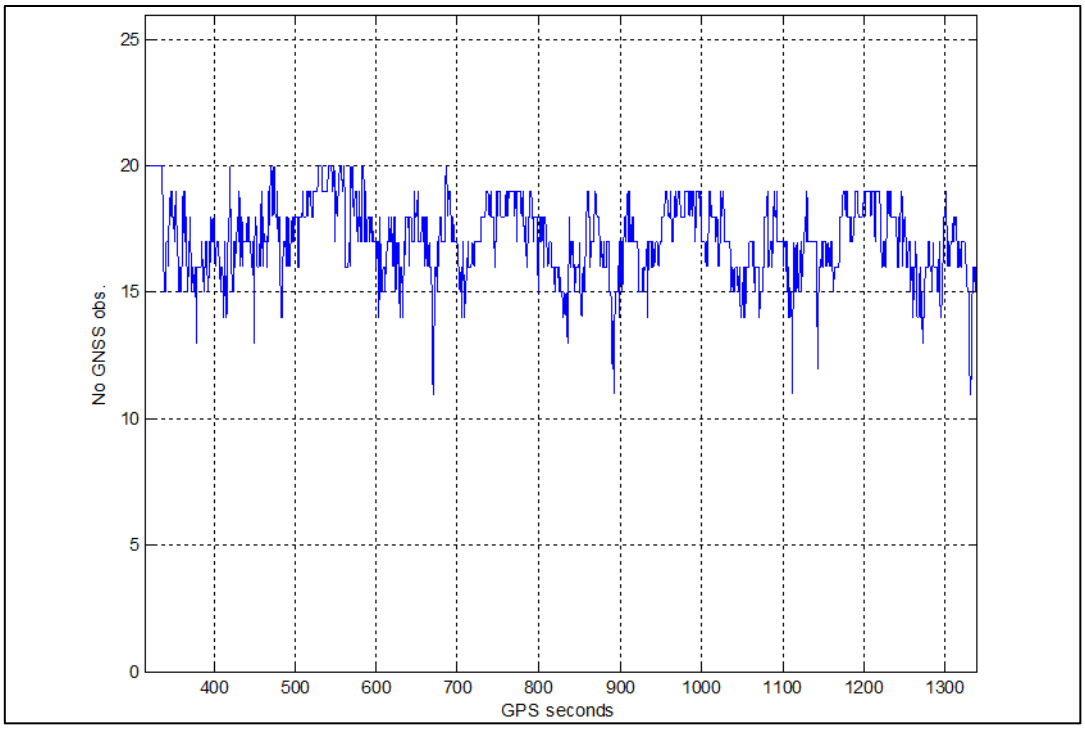

Figure 11-10: Dynamic outdoor test run: Number of tracked signals [72]

In areas, where signal blockage and reflections are present from buildings in the South-West of the trajectory, the performance appears to be even more consistent than the trajectory of the COTS reference receiver. These areas have been marked with white ellipses in Figure 11-9. Obviously, the vector DLL and the long coherent integration also improve the multipath resistance of the software receiver.

11.5.2 Indoor scenario test and results

The dynamic indoor test run has been performed at a hotel premises in the GATE area. The hotel has been chosen as test building for several reasons:

- the building is quite large, consisting of several individual, but linked sections
- the building has several floors connected by staircases (3D navigation)
- the building offers many different room layouts, e.g. corridors, guest rooms, restaurant, spa area, front and backyard, etc.
- the building is located in the GATE test area where Galileo signals are available
- the base layout of the building, as well as the coordinates could be provided by national survey authorities
- a WLAN infrastructure is present and can be used for WLAN positioning
- the building is a natural, not an artificial test environment, thus increasing the authenticity of the test

The test site can be seen in Figure 11-11. The large size of the building, as well as the different sections, which have been constructed after each other, can be noticed.

Figure 11-11: Test location for the indoor test scenario: hotel premises in Berchtesgaden, Germany [127]

Five WLAN access points were available for WLAN positioning. Four of the access points were located in corridors, placed in the walls under small lids. As an unusual feature, the access point AP2 was mounted outside of the main building on the outer wall of a garage. This AP is considered to provide WLAN access at the outside spa area. The APs have been surveyed before the test campaign for

precise position updates. In Figure 11-12, the survey coordinates of the buildings, the positions of the WLAN APs and the navigation results of the COTS reference (red) and the DINGPOS platform (blue) can be seen.

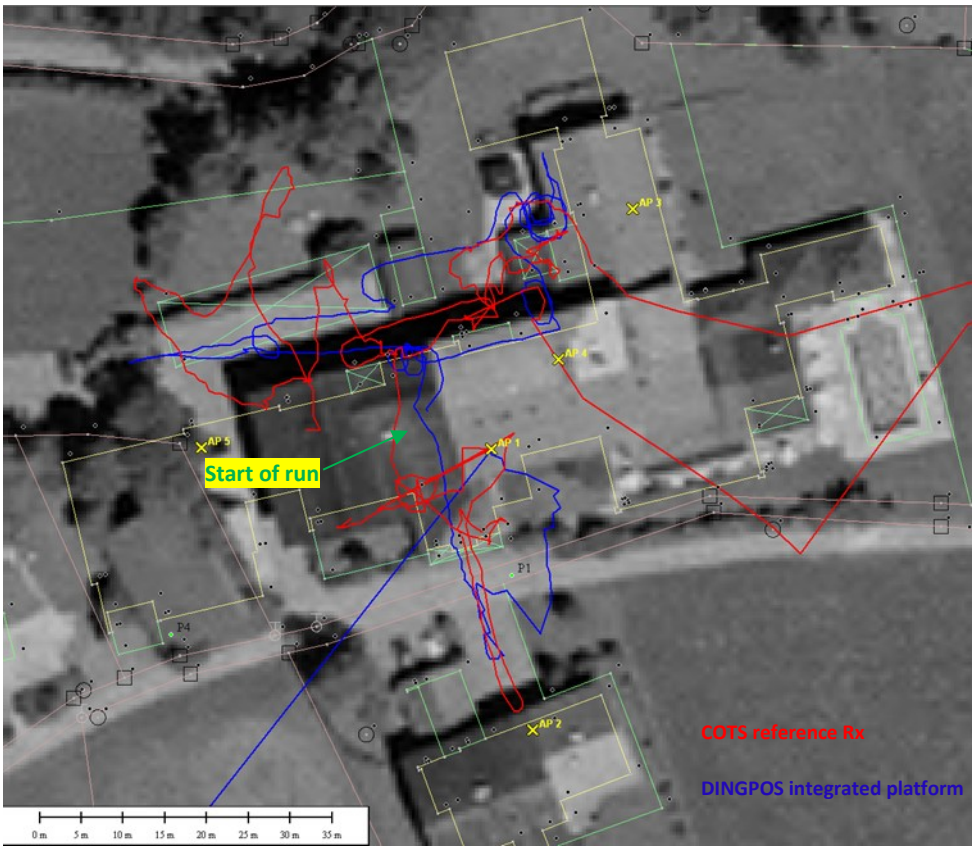

Figure 11-12: Navigation results for the dynamic indoor test run in hotel premises (GATE area): COTS reference receiver (red line) versus DINGPOS integrated platform (blue line)

The test run started in the lobby of the main building. The user performed the initialization, then left the building in southern direction walking to the garage, where AP2 is mounted. The user turned and entered the building again. The test run covered four sections and three floors of the building. The third section was reached by crossing the backyard. The run stopped at the start position in the lobby again. Hence, the test run covers a combined indoor/outdoor scenario, a 3D trajectory over several stories and GNSS conditions from outdoor to extremely deep indoor scenarios. All available positioning techniques and sensors were used in the integrated navigation platform excluding the INPOS positioning system due to the lack of ZigBee nodes infrastructure. These are the HS-GNSS receiver, the IMU, the PNS, WLAN proximity positioning system, magnetometer, barometer, micro-trajectory generation and PNS Kalman filter.

As it turned out during the test run, this hotel provides a very tough indoor environment. The GNSS signal strength inside the building varies strongly due to strong signal attenuation and limited LOS. Additionally, the building showed very strong magnetic interference, disturbing the magnetometer operation.

The reference receiver provides its position estimation after initial acquisition of the satellite signals. The outdoor performance is precise and continuous. In contrast to the integrated platform there is

no noticeable filter convergence time. Extreme position outliers are often present when the reference receiver is used in the indoor environment. Also loss of track and large jumps in determined position can be observed. These interruptions can be identified in Figure 11-12 and even more clearly in Figure 11-16, when the trajectory is distorted by position results far outside of the test area. The deep indoor user trajectory is often not usable, although the reference receiver is a HS receiver. The deep indoor environment inside the hotel has a large impact on the performance of a conventional standalone hardware GNSS receiver.

The integrated navigation platform provides continuous and seamless indoor/outdoor positions. The system needs time and several observations for initialization and Kalman filter convergence. In Figure 11-12, the platform shows a small, nearly constant position offset, from the initialization until end of run. The trajectory is very smooth in comparison to the reference receiver. All building features, like e.g. staircases and corridors, are clearly visible. The PNS and the receiver aiding are stabilizing the signal tracking as well as the overall position solution. It must be noted that pseudoranges with such very low C/N0 have limited range accuracy. This fact limits the accuracy of the Kalman filter updates and increases the influence of the PNS. The number of the signals in track is shown in Figure 11-13. The number of tracked satellites varies from 2 to 15 satellites. Two examples for the achieved tracking performance can be seen in Figure 11-14, where the tracking of two individual signal channels is shown. While the coloured line shows the instant C/N_0 estimation, the black line shows a smoothed estimation.

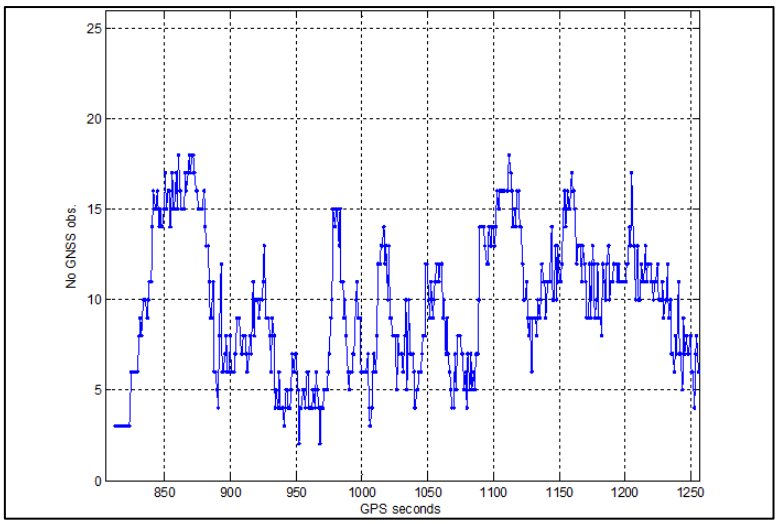

Figure 11-13: Number of tracked signals for the dynamic indoor test run

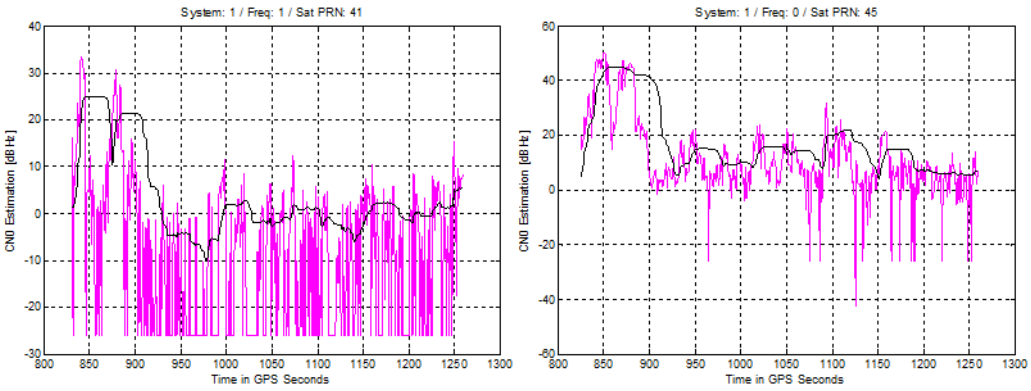

Figure 11-14: Examples of tracked signal C/N0 for the dynamic indoor test run (GATE test signals)

The evaluation of the overall tracking and acquisition performance showed that a signal tracking down to -1.5 dBHz could be achieved. Even with this high sensitivity, no continuous tracking of all satellites could be secured. The environment proved to have extremely hard indoor conditions.

11.5.3 PNS and dead reckoning performance evaluation

The integrated system trajectory is a product of all available sensors and especially the received GNSS signals. The subsystems like HS-GNSS receiver, IMU, PNS etc. contribute to the overall system performance. If the integrated system performance is evaluated, the individual contribution of a subsystem can usually not be identified anymore. However, one essential part of this thesis is the PNS dead reckoning system. To evaluate the individual contribution of the PNS, which is an important part of this thesis, it is worth comparing the “standalone” performance of the PNS with the overall system performance.

The PNS is a dead reckoning system; therefore the initial position of the PNS must be set by external information. Additionally, the initial heading must be determined for dead reckoning. Since the low-cost MEMS sensors are usually not accurate enough for gyro-compassing, the initial heading must be generated by an external source. In this evaluation, the initial PNS position was determined at the first WLAN position fix. The initial heading was derived from the magnetometer after executing the magnetometer calibration routine. After this initialization, the PNS was running freely using dead reckoning. As a reference, the integrated navigation system was used. If this comparison is extended by using the building coordiates as overlay, the performance of the integrated system and the PNS dead reckoning system can be compared.

This comparison can be seen in Figure 11-15. The PNS trajectory is initialized by WLAN proximity positioning for the position and the calibrated magnetometer measurements for heading determination. Initial errors arise from the real distance of the user from the WLAN AP at proximity declaration, as well as heading errors by magnetic disturbance. From this moment on, the IMU is the main sensor for the PNS. It is obvious that the position errors will therefore be induced by erroneous step detection, step classification and stride estimation, as well as heading drift due to inertial sensor errors.

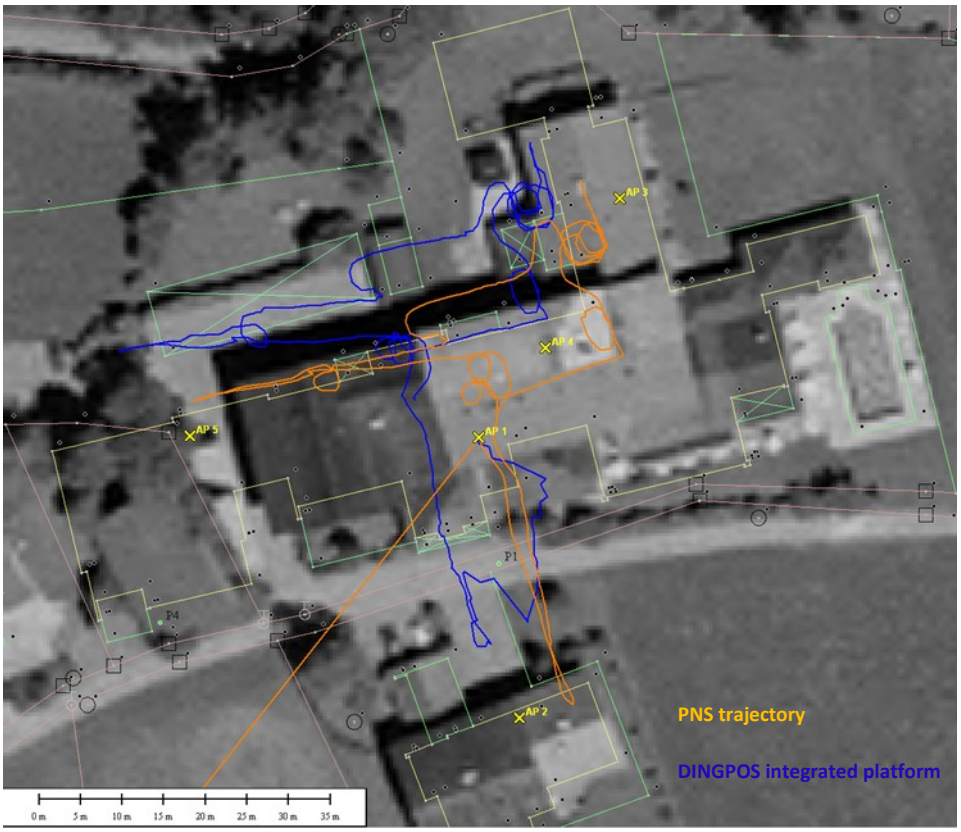

Figure 11-15: Comparison between integrated navigation results and PNS navigation results

Several aspects of the PNS system are important for evaluation:

- Absolute and relative position accuracy, including stride estimation
- Reliability of the step classification and height determination
- Accuracy of the heading determination

Accuracy

In the birds' view of Figure 11-15 it becomes obvious that the PNS is one of the most precise and stable positioning system on the integrated platform, at least if runs of several minutes duration are considered. The trajectory is smooth and plausible, and compared to the building plan very consistent. For the given test case, 618 steps have been detected in 442 seconds, giving an average step rate of 1.4 Hz. The barometer data has been used in the step classification system of the DINGPOS platform. The magnetometer data has been used in the heading and heading error estimation algorithm.

Absolute accuracy is difficult to evaluate since precise ground truth data is not available. Due to algorithmic points of view and the results analysis with projection into aerial pictures, the overall position accuracy is supposed to stay below the size of the building, which is 30 m. In the Figure 11-16, several different data sources give their estimation of the user trajectory. It can be seen that a commercial GNSS receiver (blue) is overstressed in this deep indoor scenario. Many outliers and loss of track events can be recognized. The trajectory looks torn and unsteady. Often the accuracy of the trajectory is obviously low.

The difference between the PNS only solution, the platform integrated solution and the WLAN fixes (red stars) is very small, maximum deviation is around 5m. This is due to the fact that the access points are not always accessible and therefore the AP coordinates may not match the walking path of the user precisely. In those harsh indoor scenarios, it is often more advantageous to lower the detection threshold of WLAN positioning to increase the number of position fixes. As mentioned in chapter 9, the absolute positioning error can be larger in this case. However, even lower quality updates for the Kalman filter contribute to the stabilization of the calculated user position.

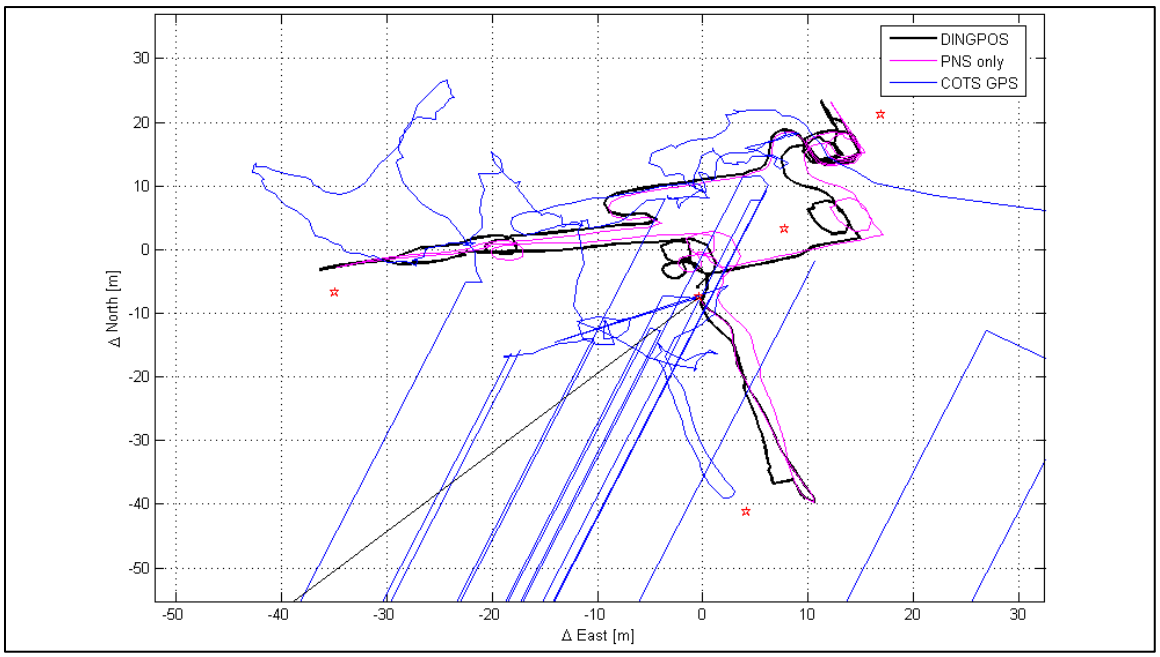

Figure 11-16: Comparison between Dead Reckoning (PNS), commercial GPS receiver and DINGPOS platform integrated result; red stars mark WLAN proximity positioning fixes

The PNS is a dead reckoning system and therefore dependent on the initial position information. If this initial position is erroneous, this error will stay present until the end of the trajectory. Nevertheless, the DR system can be very accurate while still showing this constant offset. Since no precise position reference is available, the absolute accuracy cannot be evaluated precisely and would not be of additional value. The relative accuracy, i.e. the position errors within the walked trajectory are much easier to evaluate, and the evaluation will show effectively the performance of the system.

For assessing the relative accuracy, it is of great advantage that the trajectory starts and ends at the same location in the lobby of the hotel. The ends of the trajectory meet by a distance of 6.64 m for a distance travelled of 308 m, determined from the PNS. This relates to an error of 2.16%. In this total error budget, all DR errors like step detection, classification, stride determination and also the heading errors are represented. The trajectory and the position offset between start and end can be seen in Figure 11-17.

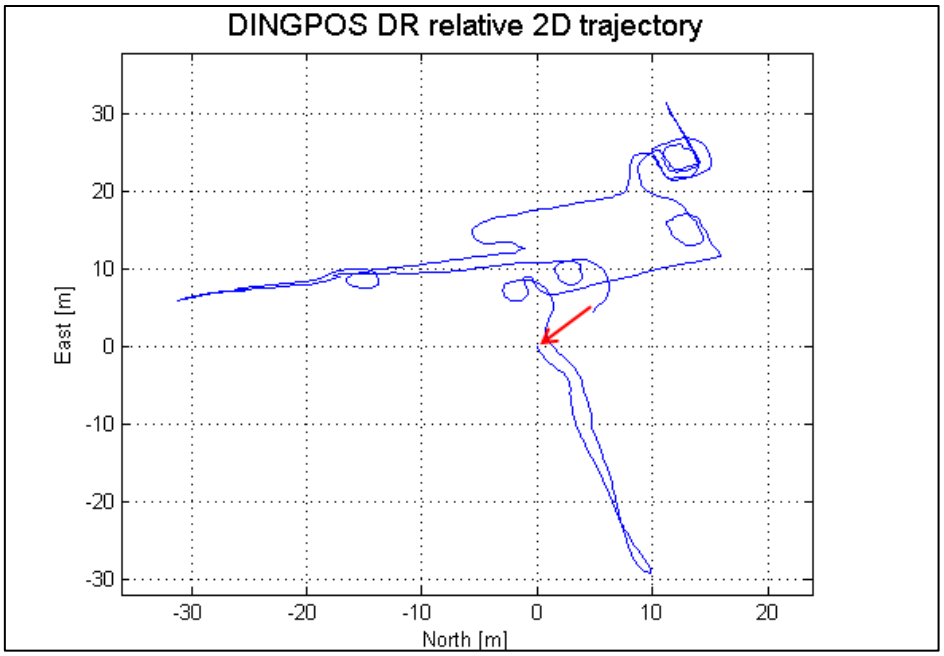

Figure 11-17: Dead reckoning trajectory of indoor scenario in GATE; The 308m trajectory matches beginning and end point to 6.65m, which is an error distance to distance travelled of 2.16%

Step classification and height determination

Figure 11-18 shows a section of the DR derived trajectory inside the hotel. It is clearly indicated by the graph that the PNS is able to classify steps mostly correctly under standard conditions, since on constant level the height is not jumping significantly and same levels are repeated correctly, which is expressed by the dashed lines. It can be seen that the difference in determined heights on the (logically) same level is much lower than 1 m in general.

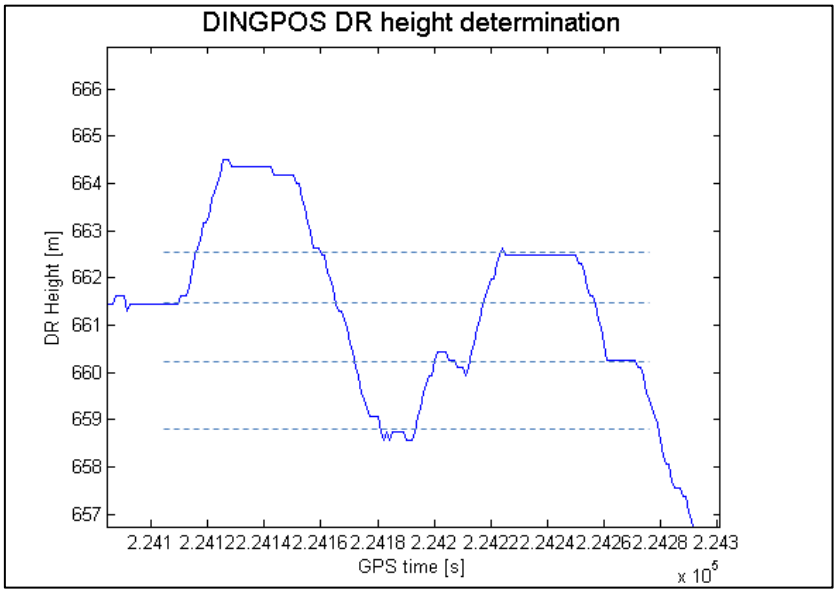

Figure 11-18: Dead reckoning height determination in the indoor scenario (hotel complex)

However, it must be noted that conditions exist under which the step classification can be disturbed by the environment or the user. These conditions are e.g. inclined surfaces without stairs or very

rough ground material like cobble stone pavement. Those conditions are found in the backyard of the hotel. The results during these conditions are highlighted in Figure 11-19.

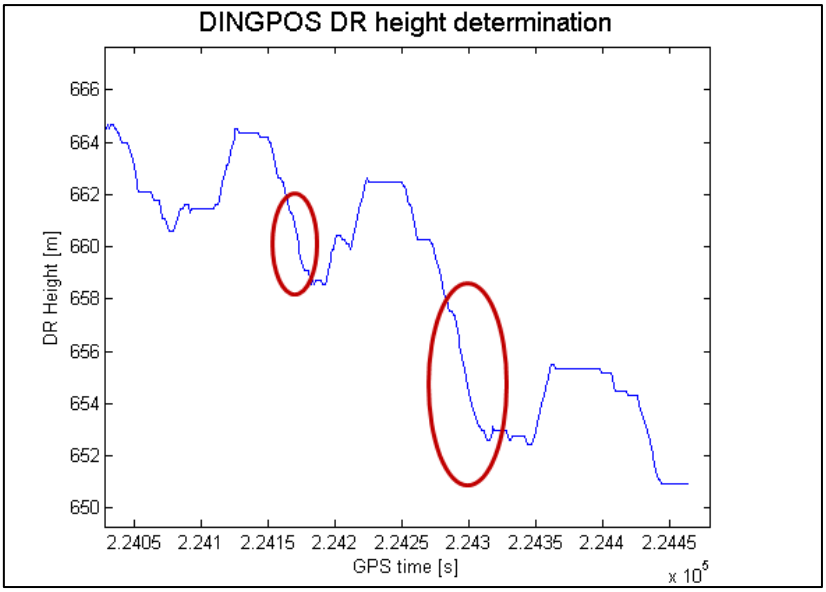

Figure 11-19: Critical use cases of step classification system for non-standard environments (here inclined surfaces and cobble stone pavement outdoors)

As a result of these conditions, a drift of some meters has occurred especially during the outdoor part of the trajectory. This is the main reason why the end part of the trajectory does not match the beginning exactly. These errors are not typical for the indoor domain, and in outdoor scenarios the availability of GNSS is high and would correct the height errors in the PNS Kalman filter.

Heading determination

Heading is one of the most important magnitudes in navigation, and most often incorrect heading produces the largest position errors. Thus, the evaluation of the heading determination errors is a crucial part of the performance evaluation. The evaluation is very difficult due to lack of reliable ground truth data. Since the floors have a width of several meters, it cannot be assumed that the user would only walk a strictly straight trajectory. Therefore, the repeatability is very hard to evaluate. For this reason two straight line segments were chosen. The first one is the most western part of the trajectory with a U-turn at its end. Its mean heading is -105.08°. The second sub-trajectory is located exactly opposite, at the south-eastern edge of the trajectory. The mean heading is -108.35°. From map data, the orientation of the building was calculated to -103.7°. Therefore both trajectories give a difference below 5°. The trajectories are presented in Figure 11-20.

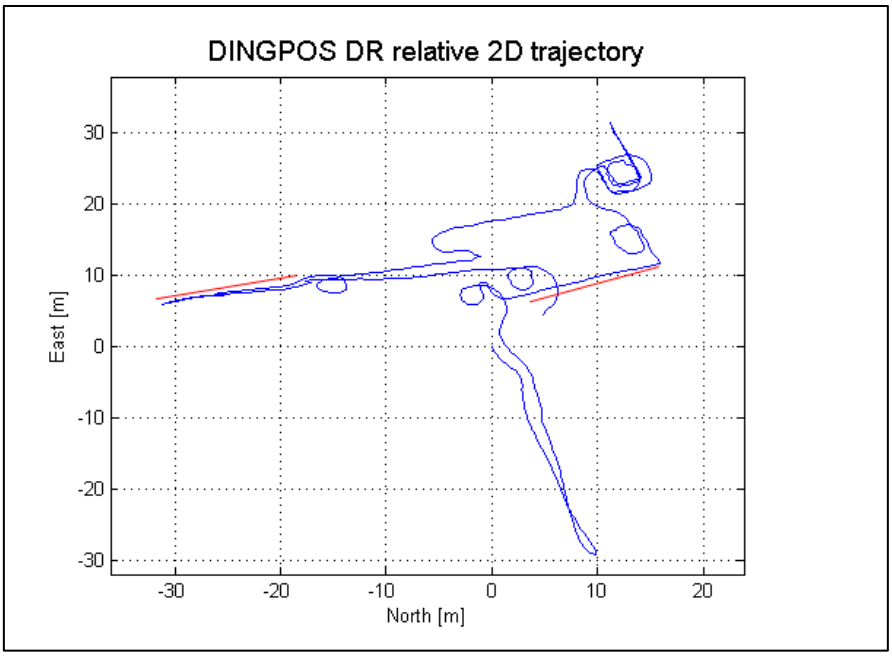

Figure 11-20: Red markings show the test trajectories for the heading accuracy evaluation

WLAN positioning updates

WLAN position updates are important sources of information in GNSS denied environments. Since the GNSS positions are either not available, or have a poor accuracy at very low signal strength, the dead reckoning navigation system can be stabilized, if additional positioning information can be acquired by WLAN position updates.

The WLAN access points AP1-AP5, as well as the walking path of the user during the test run have been presented in Figure 11-15 and Figure 11-16. The user walking path crosses all five access points in close distance. The user starts inside the building near AP1, and then leaves the house heading for the garage in front of the building. At leaving, the AP1 is passed by in close distance at the garage the user comes into close distance of AP2. When re-entering the house, the APs 1 and 4 are passed by. AP3 and AP5 are passed two times after each other, since the floors in which they are located are dead ends. The user has to turn around and leave the floor the same way as it has been entered. At the end of the run the user approaches again the starting point in close proximity of AP1. Hence, the logical order of detections, defined by the walking path, should be:

- AP 1 – 2 – 1 - 4 – 3 – 3 – 5 – 5 – 1

The position fixes of the WLAN proximity positioning system are summarized in Table 11-2. In the first column the timestamps of the proximity position detection is given in the GPS time frame. The coordinates of the detected access point in the WGS 84 frame are given in the next three columns. The different APs are identified by their MAC address, which is unique for each AP. In the last column, the name of the AP is given in clear text.

GPS Timestamp [s]	x coordinate [m]	y coordinate [m]	z coordinate [m]	MAC address	AP nr.
224004.46937	4197843.347	967325.085	4688642.377	00-0F-34-ED-EE-27	AP1
224013.56031	4197843.347	967325.085	4688642.377	00-0F-34-ED-EE-27	AP1
224065.01680	4197868.708	967335.576	4688622.061	00-15-62-CD-A1-9D	AP2
224098.31782	4197843.347	967325.085	4688642.377	00-0F-34-ED-EE-27	AP1
224140.71233	4197835.082	967331.578	4688651.098	00-0F-34-89-27-2E	AP4
224227.37877	4197821.296	967337.771	4688664.458	00-0F-34-ED-EE-25	AP3
224239.50441	4197821.296	967337.771	4688664.458	00-0F-34-ED-EE-25	AP3
224372.77347	4197853.470	967291.913	4688646.060	00-0D-ED-4D-00-98	AP5
224390.96016	4197853.470	967291.913	4688646.060	00-0D-ED-4D-00-98	AP5
224454.55105	4197843.347	967325.085	4688642.377	00-0F-34-ED-EE-27	AP1

Table 11-2: Detection results of the WLAN proximity positioning system during the indoor test runs in the GATE area

The detections follow the detection order as it has been predicted theoretically above. All access points have been identified correctly by their MAC address. The individual AP location could be successfully read from the AP database. The AP1 is detected twice at the beginning of the test run. The first detection has been indicated during a more or less static phase before the start of the walk; the second detection happened and at the beginning of the test run when crossing the AP with the user trajectory. The system does generally not show any double detection. Double detection describes the case that the same access point is detected several times after each other without user movement. This could influence the user navigation, since the Kalman filter would place the user gradually to the AP location, even if the user is passing by in a certain distance. The data shows that the algorithms effectively suppress double detections. Between consequent fixes, several seconds, in case of AP1 more than nine seconds, pass between individual position fixes. The detection logic works robust and as expected.

11.6 Summary

The previous chapter described the technique of receiver aiding by using all techniques described in the previous chapters, and by forming so called “micro-trajectories”, which resemble the antenna motion during the long coherent integration interval. The principles of this receiver aiding have been demonstrated. The data flow, hardware and algorithms for very long coherent integration have been presented. Finally two test scenarios have been presented, which have been performed in the Galileo Test Environment (GATE) in Berchtesgaden, Germany. For this test, GPS satellites as well as Galileo pseudolites have been used. The two scenarios included an outdoor scenario with high multipath effects and signal blocking, and a combined indoor/outdoor scenario with a very tough indoor environment.

The outdoor scenario did not show strong signal attenuation, therefore the integrated platform was not tested in a high sensitivity operation. Nevertheless, the scenario showed very strong multipath and signal blockage for the GATE Galileo signals, which have a low elevation. Hence, the navigation platform, using GATE and GPS signals, was challenged more strongly in this respect to the reference GPS receiver. The test run covered five rounds of a closed trajectory between several houses around the GATE office building. It took some seconds for the platform to fully synchronize and allow the internal filters to converge. After some second the platform showed fully comparable results to the COTS GPS reference receiver. At two locations with strong reflections and multipath, the platform even showed better performance than the commercial receiver.

In the indoor scenario, the integrated system experienced outdoor, mixed indoor/outdoor and deep indoor environments. The test building had a very complex footprint, offering several floors, corridors, guest rooms, lobby and backyards. The test trajectory had a length of more than 300m. The test run took 450s and covered three stories. The full sensor suite, excluding the INPOS positioning subsystem, was available. WLAN proximity positioning was enabled by the presence of five WLAN access points.

The platform showed superior tracking sensitivity down to -1.5 dB-Hz. The system was able to provide continuous positioning to the user with relatively low positioning errors. Indoor and combined indoor/ outdoor navigation could be performed seamlessly.

Special focus of the evaluation was placed on the PNS system. The PNS was the most precise positioning system in the indoor environment. Unusual surfaces like cobble stone pavement or inclined surfaces showed some influence on the step classification algorithm. The availability and the overall accuracy of the system were high.

12. Thesis summary

GNSS has developed into the most versatile and widely used commercial navigation system. The thesis presented the benefits of GNSS and pedestrian navigation, but also raised the problems of indoor navigation using GNSS. The need for a precise and reliable indoor/outdoor pedestrian navigation system with GNSS as main sensor was stated and a fully customizable software-based GNSS receiver was selected as main sensor. The main innovative idea for indoor navigation was the increase of the coherent signal integration time of the receiver to two seconds. For that, the precise replication of the user antenna motion with high accuracy and update frequency became the key problem. Major parts of this thesis are dealing with this problem. A combination of Pedestrian Navigation System (PNS), customized strapdown INS and Kalman filter has been proposed as a micro-trajectory generator. The micro-trajectory was used to form the signal replica, which was used for long coherent signal integration. The increased sensitivity was demonstrated successfully in several test campaigns.

The thesis presented the problems resulting from the harsh GNSS environment and the need for additional autonomous positioning techniques. Various sensors and their properties have been analyzed and a set of sensors and positioning systems have been chosen for the task of monitoring the GNSS antenna motion. The main cornerstones have been INS/AHRS, IMU-based pedestrian navigation system (PNS), WLAN proximity positioning system, integrating PNS Kalman filter and the generation of a so-called micro-trajectory as heart piece for the GNSS receiver signal replica generation.

The development, implementation and test of contributions to an integrated pedestrian navigation system for seamless indoor and outdoor navigation have been described. The main goal has been to increase the coherent integration time of a software based GPS/Galileo receiver to up to two seconds. As result, highly attenuated signals with signal strength down to -1.5 dB-Hz could be successfully tracked inside and outside buildings. For this goal, the dynamic motion of the GNSS antenna had to be determined very precisely by means other than GNSS.

The individual challenges and aspects will be described in the following passages.

INS/AHRS

In the original work, time and budget concerns limited the implementation of a custom AHRS system based on the used Xsens MTi IMU. Therefore the internal attitude reference of the IMU was used. Since the thesis would be incomplete in this respect, the theory of INS and AHRS have been analyzed and presented. Then the quaternion attitude representation has been selected, implemented and tested with real measurements from the MTi. It could be shown that the custom implementation yields comparable accuracy and functionality as the commercial internal attitude reference. Hence, the subject of INS based attitude determination could be demonstrated completely.

The INS based attitude determination using the strapdown and quaternion algorithms has been augmented using magnetometer measurements in the heading domain and accelerometer measurements in the pitch and roll domain. By this, the drift of the attitude could be limited and the navigation accuracy could be stabilized. For the use of the magnetometer a calibration algorithm had

to be developed and tested to account for internal and external disturbance. For the pitch and roll stabilization an algorithm for re-alignment has been demonstrated.

PNS

The second major element of the integrated navigation system has been the pedestrian navigation system (PNS). Although the PNS is using the IMU measurements like the INS/AHRS system, the navigation system shows extremely limited position drift due to the fact that no accelerations are integrated. Therefore, small misalignments and sensor errors could not destroy the navigation performance. For the PNS, the position has been propagated only at step detections in the determined direction of walking. The position error has been introduced therefore by misdetections of steps, misclassification of step types, erroneous stride estimation and erroneous heading determination. Several algorithms for step detection have been studied; finally a custom approach has been developed, tested and demonstrated. It could be demonstrated that the step detection algorithm works with a very high reliability and robustness by evaluating the total acceleration and a set of logical rules. The step classification showed good reliability, but required a high effort of calibration and the performance could be deteriorated by extraordinary surfaces, e.g. like cobble stones. Also inclined surfaces caused some erroneous classifications.

Stride estimation has been performed by a model using the step frequency as main parameter. The model parameters have been derived by a calibration campaign and it could be demonstrated that generic stride models can also be used with reduced accuracy.

WLAN proximity positioning system

An approach to use WLAN access points for positioning applications has been developed, implemented and tested. The goal has been to avoid the huge calibration efforts needed to perform WLAN fingerprinting, but to take advantage of the presence of the WLAN infrastructure at low implementation and sensor cost. For this reason a proximity alert system has been developed which gives indication when WLAN access points are passed by. While no continuous position update has been produced, the system showed very high ruggedness, reliability and very low calibration efforts. The position updates were extremely helpful for long term navigation in harsh GNSS environments, as it has been found in a hotel in the Bavarian Alps.

PNS integrating Kalman filter

The PNS integrating Kalman filter has been designed to improve the PNS positioning accuracy, using all available observations, e.g. magnetometer, WLAN, or GNSS pseudoranges. Since the PNS is the main sensor of the filter, the state vector has a different, simpler shape as in classical GNSS/INS applications. The filter estimates the receiver clock error and clock error drift, position errors, heading and heading drift errors and the average stride error. It provides corrections to the PNS as well as to the software receiver itself. It uses all available position updates, including WLAN proximity position messages, ZigBee based INPOS fingerprint positioning and GNSS pseudoranges. The filter performance could be demonstrated in the test campaigns and simulations.

Micro-trajectory generator

The micro-trajectory generator has been a major step to fuse all efforts of the dead reckoning systems to provide the antenna dynamics to the software receiver. The micro-trajectory generator used all inputs of the dead reckoning systems and the PNS Kalman filter, as well as the unprocessed IMU measurements to reproduce a high-frequent, limited drift sub-trajectory. It represented the major connection between the dead reckoning systems and the receiver tracking loops. The main strategy behind the micro-trajectory generator is to combine the properties of the MEMS-based INS, with its high frequency but also high drift, with the solution of the PNS, with its low drift but also low update rate. The result is a high precision, high frequency motion replication of the user GNSS antenna. It could be shown that the generator works well and enables antenna tracking during the integration intervals with high precision, resulting in high quality replicas and high integration gain.

GNSS receiver aiding

Although the development of the software receiver algorithms have not been the task of this thesis, the effects of the contribution have been demonstrated. The dead reckoning algorithms have been implemented in the software receiver using API interfaces and were executed by the receiver. In simulations as well as real life test campaigns the system has been tested and demonstrated superior performance in high sensitivity GNSS. In this thesis, especially the results of the test campaigns in the Galileo Test Environment GATE in Berchtesgaden/Germany have been demonstrated and analyzed.

13. Way ahead

This thesis contributed to the task of seamless indoor/outdoor navigation with several algorithms, combinations of sensors and practical implementations, as well as proof of concept of the integration strategies. As a result, a working prototype could be implemented and the system was tested in a realistic environment. The results showed that the concept of very long coherent integration gives excellent performance for seamless indoor and outdoor positioning. However, the development is ongoing, and research and application will be driven mostly by the used hardware in the future.

The hardware used in this thesis was highly specialized equipment and not intended for mass market application. For commercial applications, the hardware is too expensive and the volume and weight of the system is still too high for the mass market. On the other hand, smart phones and tablet pc have rushed on the market and they can be considered as common devices nowadays. Hence, high computing power and outstanding capabilities for visualization are widely available at low procurement cost, and it is very likely that the installed computer power will increase dramatically in the next years. If smart phones and tablet pc shall be used for seamless indoor/outdoor positioning in the future, the algorithms and the strategies will have to be adjusted to the available hardware, as well as accuracy and signal strength concerns.

The PNS proved to be a powerful tool to provide pedestrian dead reckoning with low drift and very high availability. However, the calibrations efforts of the PNS are high and the standalone performance of the step detection, classification and stride estimation are critical to the system performance. A possible strategy to improve this situation is the use of additional sensors. It has been shown in other publications (e.g. [5], [86]) that direct stride calculation with shoe mounted IMUs is possible using zero velocity phases during walking as error limiting techniques. While not particularly helpful in determining the antenna motion, this technique could be very helpful to reduce the calibration efforts for the PNS. The stride length calibration could be replaced by a second IMU mounted on the shoe of the user. This unit could perform INS processing with zero-velocity updates during the stride phases and pass the result to the PNS as stride length information. Secondly, this system could be extended for the step classification algorithm. If the z-axis performance was better than 8 cm per step, the step classification (level, up or down) could be replaced by such a system as major information source for the fuzzy logic step classification system. This could reduce the calibration efforts again.

Heading determination is the most demanding part of the DR navigation, especially with inertial sensors. This fact has also been proved in the present thesis. Gyroscopes are liable to drift and other sensor errors, and this is especially true for MEMS type sensors. To assist the gyroscopes, magnetometers have been used for independent and drift free heading determination. Magnetometers can be disturbed when facing reinforcements, wiring or other magnetic field sources in the building, which disturb the magnetic field significantly. The Kalman filter heading corrections are dependent on the quality of position and velocity outputs, hence erroneous magnetometer readings do influence the estimated heading, too. In comprehension, heading determination inside building over periods longer than several minutes is critical and can only be stabilized with observations of position and velocity with good accuracy, and heading observations with acceptable accuracy. In general, the use of map matching techniques and optical navigation for reducing

gyroscope drift could be helpful in future research. Map matching could be exploited for heading stabilization, while free user movement must be guaranteed. Simple assumptions, e.g. that the user is only allowed to walk in the middle of the floor, or only in straight lines is not sufficient for precise antenna motion replication.

The main navigation system used in thesis was GNSS, especially GPS and the simulated Galileo system in the GATE test area. By replication of user motion, the coherent integration time was raised to two seconds, resulting in superior sensitivity of the receiver. Since GNSS is the main sensor, the evolution of GNSS systems directly influences further research in the receiver development. New GNSS system like Galileo and Compass Beidou are appearing, and several upgrade and evolution programs for all GNSS systems are planned. The new signals will offer advanced indoor capabilities, e.g. the pilot channels of the Galileo signal. Since no navigation data is transmitted on the pilot channels, there is no need for assistance data or data bit change control. Additionally, the number of visible satellites will increase strongly, which increases the chance of receiving more satellites with acceptable signal power.

14. References

[1] Abbott, A. S., Lillo, W. E. (inventors). “Global positioning systems and inertial measuring unit ultratight coupling method”. Patent USA. no. 6516021, 2003

[2] Abdel-Hamid, W.: “Accuracy enhancements of integrated MEMS-IMU/GPS systems for land vehicular navigation applications”. University of Calgary UCGE 20207, 2004

[3] Akasaka, Y., Onisawa, T.: “Construction of Pedestrian Navigation Svstem and Its Evaluation”. IEEE International Conference on Fuzzy Systems, Budapest, 2004

[4] Akasaka, Y., Onisawa, T.: “Individualized Pedestrian Navigation Using Fuzzy Measures and Integrals”. IEEE International Conference on Systems, Man and Cybernetics, 2005

[5] Angermann, M., Robertson, P., Kemptner, T., Khider, M.: "Pedestrian Navigation using Foot-Mounted Inertial Sensors.", 2010 International Conference on Indoor Positioning and Indoor Navigation (IPIN'2010), 15-17 September 2010, Zürich, Switzerland

[6] Anghileri, M., Pany, T., Sanroma-Güixens, D., Won, J.-H. , Sicramaz Ayaz, A. , Stöber, C. , Krämer, I. , Dötterböck, D., Hein, G.W., Eissfeller, B.: “Performance Evaluation of a GPS/Galileo/SBAS Software Receiver”. Proceedings of the ION GNSS 2007 Conference, September 25-28, Fort Worth Convention Center, Fort Worth, TEXAS, USA

[7] Bouten, C.V.C., et al.: ” Effects of placement of body-fixed accelerometers on the assessment of energy expediture during walking”. Medical&Biological Engineering and Computing, Vol. 35; Springer Berlin, Heidelberg, 1997

[8] Britting, K. R.: "Inertial Navigation Systems.”. Wiley-Interscience, Wiley & Sons, New York, London, Sydney, Toronto, 1971

[9] Brogan, D. C., Johnson, N. L.: “Realistic Human Walking Paths”. 16th International Conference on Computer Animation and Social Agents, IEEE CASA 03, 2003

[10] Brown, R.G., Hwang, P.Y.C.: "Introduction to Random Signals and Applied Kalman Filtering.”. John Wiley & Sons, Inc., 2nd edition, 1992

[11] Chatfield, A.: "Fundamentals of High Accuracy Inertial Navigation." American Institute of Aeronautics and Astronautics, Inc., Vol. 174 of Progress in Astronautics and Aeronautics, Cambridge, Massachusetts. Second printing, 1997

[12] Chiang, K.-W.: “INS/GPS integration for using neural networks for land vehicular navigation applications”. University of Calgary UCGE 20209, 2004

[13] Cunha, S., Bastos, L., Tomé, P.: "On the Integration of Inertial and GPS Data with an Odometer for Land Vehicles Navigation”. Proceedings of the ION GPS/GNSS 2003, 9-12 September 2003, Portland, OR

[14] Dissanayake, G., Sukkarieh, S., Nebot, E., Durrant-Whyte, H.: "The Aiding of a Low-Cost Strapdown Inertial Measurement Unit Using Vehicle Model Constraints for Land Vehicle Applications”. IEEE Transactions on robotics and automation, Vol. 17, No. 5, October 2001

[15] Einstein, A.: ”Über das Relativitätsprinzip und die aus demselben gezogenen Folgerungen”. Publication in ”Jahrbuch der Radioaktivität”, volume 4, 1907

[16] Einstein, A.: ”Lichtgeschwindigkeit und Statik des Gravitationsfeldes“, publication in ”Annalen der Physik“, volume 38, Leipzig, 1912

[17] Einstein, A.: ”Einfluß der Schwere auf die Ausbreitung des Lichts“, publication in ”Annalen der Physik“, volume 35, Leipzig, 1911

[18] Eissfeller, B., Teuber, A., Zucker, P.: "Untersuchungen zum GPS-Satellitenempfang in Gebäuden”. Journal "Allgemeine Vermessungs-Nachrichten”. Issue 4/2005, p.137-145, Wichmann Verlag, 2005

[19] Eissfeller, B., Teuber, A., Zucker, P.: "Indoor-GPS: Ist der Satellitenempfang in Gebäuden möglich?”. From "zfv Zeitschrift für Geodäsie, Geoinformation und Landmanagement”. ISSN: 1618-8950, Jg.: 130, Nr.4, 2005

[20] EUROCONTROL: “WGS 84 IMPLEMENTATION MANUAL”. Version 2.4, EUROCONTROL European Organization for the Safety of Air Navigation Brussels, Belgium, IfEN Institute of Geodesy and Navigation (IfEN), University FAF Munich, Germany, 1998

[21] Gabaglio, V., Ladetto, Q., Merminod, B.: ”Kalman Filter Approach for Augmented GPS Pedestrian Navigation”. GNSS 2001, Sevilla, 2001

[22] Gade, K: "Introduction to Inertial Navigation and Kalman filtering”. INS Tutorial, Norwegian Space Centre, 2008

[23] Gelb, A. (Editor): "Applied Optimal Estimation”. The Analytic Science Corporation, The M.I.T. Press, Cambridge, Massachusetts, 1974

[24] Giulini, D.: "Das Problem der Trägheit”. PREPRINT 190, Max Planck Institute for the History of Science, Freiburg, August 2001

[25] Godha, S., Cannon, M. E.: "Integration of DGPS with a Low Cost MEMS - Based Inertial Measurement Unit (IMU) for Land Vehicle Navigation Application”. ION GNSS 18th International Technical Meeting of the Satellite Division, 13-16 September 2005, Long Beach, CA

[26] Godha, S., Petovello, M. G., Lachapelle, G.: "Performance Analysis of MEMS IMU/HSGPS/Magnetic Sensor Integrated System in Urban Canyons”. ION GNSS 18th International Technical Meeting of the Satellite Division, 13-16 September 2005, Long Beach, CA

[27] Grewal, M., Andrews, A.: "Kalman Filtering: Theory and Practise using MATLAB, second edition”. Wiley-Interscience, John Wiley & Sons Inc., New York, USA, 2001.

[28] Hein, G. W., Kreye, C., Zimmermann, B.: ”Entwicklung und Testergebnisse eines Systems zur vektoriellen Fluggravimetrie auf Basis eines kommerziellen, hochpräzisen Strapdown INS”. Final report of the project „Entwicklung der Fluggravimetrie unter Nutzung von GNSS Satellitenbeobachtungen“ (FKZ: 03F0341A). Institute of Geodesy and Navigation, Universität der Bundeswehr München, 2005

[29] Helal, A., Moore, S., Ramachandran, B.: ”Drishti: An Integrated Navigation System for Visually Impaired and Disabled”. IEEE Fifth International Symposium on Wearable Computers, 2001

[30] Hunaiti, Z., Rahman, A., Denideni, M., Balachandran, W.: “The Impact of Galileo on Pedestrians Navigation Systems”. CONIELECOMP 2006, 2006

[31] IEEE STD 337-1972: “IEEE Standard Specification Format Guide and Test Procedure for Linear, Singel-Axis, Pendulous, Analog Torque Balance Accelerometer”

[32] IEEE STD 528-2001: “IEEE Standards for Inertial Sensor Terminology”

[33] IEEE STD 647-1996 : “IEEE Standard Specification Format Guide and Test Procedure for Single-Axis Laser Gyros”

[34] IEEE STD 671-1985: “IEEE Standard Specification Format Guide and Test Procedure for Nongyroscopic Inertial Angular Sensors: Jerk, Acceleration, Velocity, and Displacement”

[35] IEEE STD 813-1988: “IEEE Standard Specification Format Guide and Test Procedure for Two-Degree-of-Freedom Dynamically Tuned Gyros”

[36] IEEE STD 836-2001: “IEEE Recommended Practice for Precision Centrifuge Testing of Linear Accelerometers”

[37] IEEE STD 952-1997: “IEEE Standard Specification Format Guide and Test Procedure for Singel-Axis Interferometric Fiber Optic Gyros”

[38] IEEE STD 1293-1998: “IEEE Standard Specification Format Guide and Test Procedure for Linear, Single-Axis, Nongyroscopic Accelerometer”

[39] IEEE STD 1431-2004: “IEEE Standard Specification Format Guide and Test Procedure for Coriolis Vibratory Gyros”

[40] IEEE STD 1554-2005: “IEEE Recommended Practice for Inertial Sensor Test Equipment, Instrumentaion, Data Acquisition, and Analysis”

[41] Jirawimut, R., Prakoonwit, S., Cecelja, F., Balachandran, W.: ”Visual Odometer for Pedestrian Navigation”. Anchorage, 2002

[42] Jirawimut, R., Ptasjnski, P., Garaj, V., Cecelja, F., Balachandran, W.: “A Method for Dead Reckoning Parameter Correction in Pedestrian Navigation System”. Instrumentation and Measurements Technology Conference IMTC 2001, Budapest, 2001

[43] Jirawimut, R., Ptasjnski, P., Garaj, V., Cecelja, F., Balachandran, W.: “A Method for Dead Reckoning Parameter Correction in Pedestrian Navigation System”. IEEE TIM, 2004

[44] Kalman, R. E.: "A New Approach to Linear Filtering and Prediction Problems." Transactions of the ASME–Journal of Basic Engineering, volume 82 (Series D), 1960

[45] Kaplan, E.D. (ed.): "Understanding GPS Principles and Applications.”. Artech House, 1996

[46] Kawabata, M., Nishide, R., Ueda, M., Ueshima, S.: “The context-adaptable pedestrian navigation system and usability in practical settings”. IEEE Pacific Rim Conference on Communications, Computers and signal Processing, 2005

[47] Kelly, A.: "Modern Inertial and Satellite Navigation Systems”. Lecture Material, Carnegie Mellon University, Ohio, USA (Last visited June 2011)

[48] Kim, J.W., Jang, H.J., Hwang, D.H., Park, C.: ”A Step, Stride and Heading Determination for the Pedestrian Navigation System”. Journal of Global Positioning Systems, Vol. 3 No. 1-2, 2004

[49] Koide, S., Kato, M.: “3-D HUMAN NAVIGATION SYSTEM CONSIDERING VARIOUS TRANSITION PREFERENCES”. IEEE International Conference on Systems, Man and Cybernetics, Tokyo, 2005

[50] Kolbe, T.: “Orientierung und Visualisierung in realen und virtuellen Räumen für persönliche Navigationssysteme”. Institut für Kartographie und Geoinformation, Universität Bonn, 2005

[51] Ladetto, Q., Gabaglio, V., Merminod, B.: ”Two Different Approaches for Augmented GPS Pedestrian Navigation”. Locellus 2001

[52] Landis, D., Thorvaldsen, T., Fink, B., Sherman, P., Holmes, S.: “A Deep Integration Estimator for Urban Ground Navigation”. PLANS 2006, IEEE/ION Position, Location and Navigation Symposium, pp. 927-932, San Diego, California, USA

[53] Lange, L.: "Über das Beharrungsgesetz”. Sitzungsberichte der Kgl. Sächs. Gesellschaft d. Wissenschaft, 1885

[54] Lee, S.-W., Mase, K.: ”Recognition of Walking Behaviors for Pedestrian Navigation”. 2001 IEEE International Conference on Control Applications, Mexico City, 2001

[55] Lee, S.-W., Mase, K.: ”Incremental Motion-Based Location Recognition”. IEEE Fifth International Symposium on Wearable Computers, 2001

[56] Lee, S.-W., Mase, K., Kogure, K.: ”Detection of Spatio-Temporal Gait Parameters by Using Wearable Motion Sensors”. 27th Annual International Conference of the Engineering in Medicine and Biology Society IEEE-EMBS 2005, Shanghai, 2005

[57] Litton Guidance & Control Systems: "LN-200 Fiber Optic Inertial Measurement Unit”. LN-200 IMU Data Sheet, Litton Guidance & Control Systems, Woodland Hills, USA 2011

[58] López-Risueno, G., Jiménez-Baños, D., González-Martínez, F., Waller, P., Colina-Fatjo, M.: “User Clock Impact On High Sensitivity GNSS Receivers”. Proceedings ENC-GNSS 2008, Toulouse, France

[59] Lunze, J.: “Regelungstechnik”. Third edition, Springer Verlag, Berlin – Heidelberg – New York, 2001

[60] Maybeck, P.: "Wander Azimut Implementation Algorithm For A Strapdown Inertial System”. Document AD-784 752, Air Force Flight Dynamics Laboratory, Wright Patterson Airforce Base, Ohio, USA, October 1973

[61] Maybeck, P.: "Stochastic models, estimation, and control”. Vol.1, Academic Press, New York, USA, 1979.

[62] MEMSense: "nIMU Nano Inertial Measurement Unit Series Documentation”. Document: DN00010 Verion 2.5, Dec 2006. MEMSense, Rapid City, SD 57702, USA, 2006

[63] Mezentsev, O.: ”Sensor Aiding of HSGPS Pedestrian Navigation, UCGE Reports Number 20212”. Calgary, 2005

[64] Misra, P., Enge, P.: "Global Positioning System: Signals, Measurements, and Performance”. Ganga-Jamuna Press, USA 2001

[65] Mönikes, R., Teltschik, A., Wendel, J. and Trommer, G.F.: "Post-processing GNSS/INS Measurements Using a Tightly Coupled Fixed-Interval Smoother Performing Carrier Phase Ambiguity Resolution”. Institute of Theory and Systems Optimization in Electrical Engineering, University of Karlsruhe (TH), Karlsruhe, Germany, IEEE 2006

[66] Monti, C., Malvolti, F., Ronchini, R., Saitto, A., Valletta, D.: “Indoor Localization System based on Wireless Sensor Networks”. Proceeding of the European Navigation Conference - Global Navigation Satellite Systems 2009 (ENC-GNSS 2009), Poster Session II, Naples, Italy 2009

[67] Moore T., Hill C., Abdulrahim K.: "Aiding Indoor Pedestrian Navigation with Building Heading." GPS World, Tech Talk Blog, January 12, 2011. URL: http://www.gpsworld.com/tech-talk-blog/aiding-indoor-pedestrian-navigation-with-building-heading-11384-0, downloaded 04/04/2011. GPS World, 201 Sandpointe Ave., Ste. 500, Santa Ana, CA 92707, USA

[68] Motorola: "High Temperature Accuracy Integrated Silicon Pressure Sensor for Measuring Absolute Pressure. On-Chip Signal Conditioned, Temperature Compensated and Calibrated MPXA6115A." Rev. 3, 01-01-07, Motorola, 2007

[69] National Imageray and Mapping Agency: “Department of Defense World Geodetic System 1984, Its Definition and Relationships with Local Geodetic Systems”. NIMA TR8350.2, Third Edition Amandment 1, USA 2000

[70] Niemeier, W.: “Ausgleichsrechnung, Eine Einführung für Studierende und Praktiker des Vermessungs- und Geoinformationswesens”. de Gruyter, Berlin – New York, 2002

[71] Niedermeier, H., Ameres, G., Pany, T., Eisfeller, B., Winkel, J., Lopez-Risueno, G.: “Reproduction of User Motion and GNSS Signal Phase Signatures Using MEMS INS and a Pedestrian Navigation System for HS-GNSS Applications”. Proceedings of the 4th ESA Workshop on Satellite Navigation User Equipment Technologies, NAVITEC, Noordwijk, The Netherlands, 2008

[72] Niedermeier, H., Eissfeller, B., Winkel, J., Pany, T., Riedl, B., Wörz, T., Schweikert, R., Lagrasta, S., López-Risueño, G., Jiménez-Baños, D.: "DINGPOS: High Sensitivity GNSS platform for deep indoor scenarios”. 2010 International Conference on Indoor Positioning and Indoor Navigation (IPIN), 15-17 September 2010, Zürich, Switzerland

[73] Niedermeier, H., Ameres, G., Pany, T., Eissfeller, B.: "First results from supporting long coherent CDMA correlations by a MEMS INS and a Pedestrian Navigation System for HS-GNSS applications”. Workshop on Positioning, Navigation and Communications (WPNC 2009), Leibniz University of Hannover, Germany, March 19, 2009

[74] Niu, X., El-Sheimy, N.:"The Development of a Low-cost MEMS IMU/GPS Navigation System for Land Vehicles Using Auxiliary Velocity Updates in the Body Frame”. ION GNSS 18th International Technical Meeting of the Satellite Division, 13-16 September 2005, Long Beach, CA

[75] NORTH ATLANTIC TREATY ORGANIZATION ADVISORY GROUP FOR AEROSPACE RESEARCH AND DEVELOPMENT AGARD: "STRAPDOWN INERTIAL SYSTEMS (AGARD - LS - 95)”. Lecture series material from Lecture Series No.95, 6-7 June 1978 in London, UK; 9th June 1978 in Copenhagen, Denmark; 12-1 3 June 1978 in Bolkesjo, Norway; 15-1 6 June 1978 in Cologne, Germany, 19-20 June 1978 in Rome, Italy.

[76] Ojeda, L., Borenstein, J.: “Personal Dead-reckoning System for GPS-denied Environments." IEEE International Workshop on Safety, Security, and Rescue Robotics (SSRR2007) in Rome, Italy, September 27-29, 2007

[77] Pany, T., Riedl, B., Winkel, J., Wörz, T., Schweikert R., Niedermeier, H., Lagrasta, S., López-Risueño, G., Jiménez-Baños, D.: "Coherent Integration Time: the Longer, the Better”. Inside GNSS, vol. 4, no. 6 (November/December 2009), extended version available on-line at http://www.insidegnss.com/auto/novdec09-wp.pdf

[78] Pany, T., Winkel, J., Riedl, B., Niedermeier, H., Eissfeller, B., Wörz, T., Schweikert, R., Lagrasta, S., Nicolé, R., López-Risueño, G., Jiménez-Baños, D.: "Experimental Results from an Ultra-Tightly Coupled GPS/Galileo/WiFi/ZigBee/MEMS-IMU Indoor Navigation Test System Featuring Coherent Integration Times of Several Seconds”. Proceedings of the 5th ESA Workshop on Satellite Navigation User Equipment Technologies, NAVITEC'2010, 8-10 December 2010, Noordwijk, The Netherlands, 2010

[79] Pany, T., Winkel, J., Riedl, B., Restle, M., Wörz, T., Schweikert, R., Niedermeier, H., Ameres, G., Eissfeller, B., Lagrasta, S., López-Risueño, G.: "Performance of a Partially Coherent Ultra-Tightly Coupled GNSS/INS Pedestrian Navigation System Enabling Coherent Integration Times of Several Seconds to Track GNSS Signals Down to 1.5 dBHz.”. ION GNSS 2009, September 22-25, Savannah International Convention Center, Savannah, Georgia, 2009

[80] Petovello, M. G., O’Driscoll, C., Lachapelle, G.: “Weak Signal Carrier Tracking Using Extended Coherent Integration With an Ultra-Tight GNSS/IMU Receiver”. Proceedings ENC-GNSS 2008, Toulouse, France

[81] Petovello, M., Pullen, S.: "GNSS Solutions: Quantifying the performance of navigation systems and standards for assisted-GNSS”. Inside GNSS, September/October 2008, pp. 20-23

[82] Rade, L., Westergren, B.: „Springers Mathermatische Formeln. Taschenbuch für Ingenieure, Naturwissenschaftler, Wirtschaftswissenschaftler“. 2nd edition, Springer Verlag Berlin, 1997

[83] Rauch, H.E., Tung, F. Striebel, C.T.: "Maximum Likelihood Estimates of Linear Dynamic Systems" AIAA JOURNAL 1445, VOL. 3, NO.-8, August 1965

[84] Renaudin V., Yalak O.: "Hybridization of MEMS and Assisted GPS for Pedestrian Navigation." Inside GNSS, January/February 2007

[85] Retscher, G.: “Pedestrian navigation systems and location based services”. Proceedings of the Fifth IEEE International Conference on 3G Mobile Communication Technologies, 2004, Wien, 2004

[86] Robertson, P., Angermann, M.: "Simultaneous Localization and Mapping for Pedestrians using only Foot-Mounted Inertial Sensors”. Ubicomp 2009, Sep 30 – Oct 3 2009, Orlando, Florida, USA

[87] Savage, P.G.: “Strapdown System Algorithms”. in Advances in Strapdown Inertial Systems, AGARD Lecture Series No. 133, NATO, Loughton, GB, 1984

[88] Savage, P.G.: “Strapdown analytics”. Strapdown Associates Inc., Maple Plains, Minnesota, USA, 2000

[89] Savage, P.: "Computational Elements for Strapdown Systems”. NATO RTO-EN-SET-116(2008), Paris, France 2008

[90] Schmidt, G.T.: “Strapdown Inertial Systems – Theory and Applications, Introduction and Overview.” in: Strapdown Inertial Systems, AGARD Lecture Series No. 95, NATO, Neuilly-sur-Seine, France.

[91] Schuler, M.: " Einwirkung rhythmischer Momente auf den Kreiselkompaß”. Dissertation at the TH Munich, Germany, 1921

[92] “Signal Processing Techniques and Demonstrator for Indoor GNSS Positioning ‘DINGPOS’: Description of aiding/assisting algorithms (TN-8)”. Internal project report for the European Space Agency/ESA ESTEC, Contract Number 20834/07/NL/GLC

[93] “Signal Processing Techniques and Demonstrator for Indoor GNSS Positioning ‘DINGPOS’: Algorithms Integration and Trade-Off (TN-10)”. Internal project report for the European Space Agency/ESA ESTEC, Contract Number 20834/07/NL/GLC

[94] “Signal Processing Techniques and Demonstrator for Indoor GNSS Positioning ‘DINGPOS’: Recommendations (TN-20)”. Internal project report for the European Space Agency/ESA ESTEC, Contract Number 20834/07/NL/GLC

[95] “Signal Processing Techniques and Demonstrator for Indoor GNSS Positioning ‘DINGPOS’: (TN-22)”. Internal project report for the European Space Agency/ESA ESTEC, Contract Number 20834/07/NL/GLC

[96] “Signal Processing Techniques and Demonstrator for Indoor GNSS Positioning ‘DINGPOS’: Technological Challenges and State-of-the-Art Indoor Positioning Survey (TN-2)”. Internal project report for the European Space Agency/ESA ESTEC, Contract Number 20834/07/NL/GLC

[97] So, H., Lee, T., Jeon, S., Kim, J., Kee, C., Heo, M-B.: “Use of a Vector-based Tracking Loop Receiver for Solving the Near-Far Problem in a Pseudolite Navigation System”. Proceedings ION GNSS-2009, Savannah

[98] Soloviev, A., van Graas, F., Miller, M., Gunawardena, S.: “Synthetic Aperture GPS Signal Processing, Concept and Feasibility Demonstration”. Inside GNSS, vol. 4, no. 3 (May/June 2009), pp. 37-46b (extended version available on-line at http://www.insidegnss.com/node/1453)

[99] Systron Donner Inertial: "MotionPak™, Multi-Axis Inertial Sensing System”. Datasheet 964003 Rev. E, 1998

[100] Teuber, A., Eissfeller, B.: "WLAN Indoor Positioning Based on Euclidean Distances and Fuzzy Logic.”. Workshop on Positioning, Navigation and Communications (WPNC’06), Hannover, Germany, 2006

[101] Teuber, A., Pany T., Eissfeller, B.: " WLAN Indoor Locating Using a Two-Stage Fuzzy Logic Approach.". IEEE/ION Position, Location and Navigation Symposium, PLANS 2006, San Diego, USA

[102] Titterton D.H., Weston J.L.: "Strapdown inertial navigation technology." IEEE RADAR, NAVIGATION AND AVIONICS SERIES 5, Peter Peregrinus LTd. On behalf of the Institution of Electrical Engineers, Stevenage, UK 1997

[103] US Department of Defense, Navstar GPS: "GLOBAL POSITIONING SYSTEM, STANDARD POSITIONING SERVICE PERFORMANCE STANDARD". 4th edition, September 2008

[104] US Department of Defense, Navstar GPS: "GLOBAL POSITIONING SYSTEM PRECISE POSITIONING SERVICE PERFORMANCE STANDARD". February 2007

[105] Watson, J.R.A.: "High-Sensitivity GPS L1 Signal Analysis for Indoor Channel Modelling". PHD Thesis, Department of Geomatics Engineering, University of Calgary, 2005

[106] Wendel, Jan: "Integrierte Navigationssysteme. Sensordatenfusion, GPS und Inertiale Navigation". Second edition, Oldenburg Verlag München, Munich 2011

[107] Wendel, J., Meister, O., Mönikes, R. and Trommer, G.F.: "Time-Differenced Carrier Phase Measurements for Tightly Coupled GPS/INS Integration". Institute of Theory and Systems Optimization in Electrical Engineering, University of Karlsruhe (TH), Karlsruhe, Germany, IEEE 2006

[108] Wimmer, C.: "Position Measurement in Inertial Systems". Moscow-Bavarian Joint Advanced Student School 2006 (JASS 2006), Course 5: Mechatronics - Foundations and Applications, St. Petersburg, Russia, April 2006

[109] Winkel, J.: "Modeling and Simulating GNSS Signal Structures and Receivers". University of Federal Armed Forces Munich, Werner-Heisenberg-Weg 39, D-85577 Neubiberg, <http://www.unibw.de/unibib/digibib/ediss/bauv>, 2003

[110] Winkel J., Wörz T., Dreischer, C., Restle, M., Pany, T., Ameres, G., Niedermeier, H., Eissfeller, B., Schweikert, R., Lagrasta, S., López-Risueño, G.: "DINGPOS - Taking Indoor GNSS Signal Processing to a Quantum Level." Proceedings of the 4th ESA Workshop on Satellite Navigation User Equipment Technologies, NAVITEC, Noordwijk, The Netherlands, 2008

[111] Wolf, R., Löhnert, E.: "Software programming guide for a strapdown INS". Technical Note, Institute of Geodesy and Navigation, Universität der Bundeswehr München, 1995.

[112] Won, J.-H., Dötterböck, D., Eissfeller, B.: "Performance Comparison of Different Forms of Kalman Filter Approach for a Vector-Based GNSS Signal Tracking Loop". Proceedings of ION GNSS 2009, Savannah, Georgia, USA

[113] Xsens Technologies B.V.: "MTi-G 20 Leaflet 2009". www.xsens.com, 2005-2010, Enschede, The Netherlands

[114] Xsens Technologies B.V.: "MTi and MTx User Manual and Technical Documentation MT0100P". Xsens Technologies B.V., Enschede, The Netherlands, 2007

[115] Yang, Y., Farrell, J.A.: "Magnetometer and Differential Carrier Phase GPS-Aided INS for Advanced Vehicle Control". IEEE TRANSACTIONS ON ROBOTICS AND AUTOMATION, VOL. 19, NO. 2, April 2003

[116] Zadeh, L.A.: "Is there a need for fuzzy logic?". Annual Meeting of the North American Fuzzy Information Processing Society (NAFIPS), New York, USA, 2008

[117] Zadeh, L.A.: "Soft computing and fuzzy logic". IEEE Software, Volume 11 , Issue 6, pp. 48-56, IEEE 1994

[118] Online: http://www.es.northropgrumman.com/solutions/ln200/. Last visited 12-4-2012, web site of the LN-200 fiber-optical gyroscope IMU, Northtrop Grumman, USA

[119] Online: http://cddis.nasa.gov/926/egm96/egm96.html. Description of the EGM 96 geoid model. Last visited 27-11-2012

[120] Online: http://compliantmechanisms.byu.edu/content/introduction-microelectromechanical-systems-mems. Last visited 14-1-2012

[121] Online: http://www.wtec.org/loyola/mcc/mems_eu/Pages/Chapter-5.html. Last visited 14-1-2012

[122] Online: http://www.nobelprize.org/nobel_prizes/physics/laureates/2007. Last visited 07-03-2013

[123] Online: http://www.ngdc.noaa.gov/geomag-web/#declination. Last visited 07-03-2013

[124] Online: http://www.ieee802.org/

[125] Online: http://www.elektronik-kompendium.de/sites/net/0610051.htm

[126] Online: http://www.gate-testbed.com/spezifikationen.html. Last visited 28-08-2013

[127] Online: http://geoportal.bayern.de/bayernatlas?base=910. Last visited 28-08-2013

15. Acronyms

A/D	Analog-Digital
AGNSS	Assisted GNSS
AHRS	Attitude and Heading Reference System
AL	Alarm Level
AoA	Angle of Attack
AP	Wireless LAN Access Point
API	Application Programming Interface
ASIC	Application Specific Integrated Circuit
BPSK	Binary Phase Shift Keying
BW	Bandwidth
C/A	Coarse Acquisition
CD	Compact Disc
CDMA	Code Division Multiple Access
C/N0	Carrier to Noise Ratio
CS	Commercial Service
CVG	Coriolis Vibrating Gyroscope
DCM	Direction Cosine Matrix
DFT	Discrete Fourier Transformation
DLL	Delay Lock Loop
DLR	Deutsches Zentrum für Luft- und Raumfahrt
DoF	Degrees of Freedom
DOP	Dilution of precision
DR	Dead Reckoning
DTG	Dynamically Tuned Gyroscope
ECEF	Earth Centered Earth fixed frame
ECSF	Earth Centered Space Fixed frame
EGM96	Earth Gravitational Model 1996
EIRP	Equivalent Isotropically Radiated Power
ESA	European Space Agency

ESG	Electrically Suspended Gyroscope
ETSI	European Telecommunications Standard Institute
FFT	Fast Fourier Transformation
FOC	Full Operational Capability
FOG	Fiber-Optic Gyroscope
FPGA	Field-Programmable Gate Array
GATE	Galileo Test Environment
GMR	Giant Magneto-Resistive (physical effect for a type of magnetometer)
GNSS	Global Navigation Satellite System
GPS	Global Positioning System
GTR	Galileo Test Range
HF	High Frequency
HS-GNSS	High Sensitivity GNSS
HW	Hardware
IEEE	Institute of Electrical and Electronics Engineers
IF	Intermediate Frequency
IMU	Inertial Measurement Unit
IN	Inertial Navigation
INS	Inertial Navigation System
ION	Institute of Navigation (USA)
IOV	In-Orbit-Validation
IR	Infra-Red
ISA	International Standard Atmosphere
ISTA	Institute of Space Technology and Space Applications
ITAR	International Traffic in Arms Regulations
ITU	International Telecommunications Union
LAN	Local Area Network
LF	Low Frequency
LORAN	Long Range Navigation, terrestrial radio navigation system
LOS	Line of sight

MAG	Magnetometer
MEO	Medium Earth Orbit
MEMS	Micro Electro Mechanical System
MTi	Motion Tracker, case type i (Inertial Measurement unit by Xsens)
NED	North-East-Down coordinate frame
NEU	North-East-Up coordinate frame
NTP	Network Time Protocol
NWD	North-West-Down coordinate frame
OCXO	Oven Controlled Crystal Oscillator
OS	Open Service
PC	Personal Computer
PDA	Personal Digital Assistant
PI	Performance Indicator
PLL	Phase Lock Loop
PNS	Pedestrian Navigation System
PR	Pseudorange
PRN	Pseudo-Random Noise
PRS	Public Regulated Service
PVA	Position, Velocity and Attitude
PVT	Position, Velocity and Timing
QNH	Navigation brevity code (Q code), virtual pressure at sea level
RAIM	Receiver Autonomous Integrity Monitoring
RF	Radio Frequency
RFID	Radio Frequency Identification
RLG	Ring Laser Gyroscope
RSS	Received Signal Strength
RSSI	Received Signal Strength Indication
RTCM	Radio Technical Commission for Maritime Services
Rx	Receiver
SD-INS	strapdown INS

SLAM	Simultaneous Localization and Mapping
SNR	Signal to Noise Ratio
SOL	Safety-Of-Life
SW	Software
SwRx	Software Receiver
TDOA	Time Difference Of Arrival
TTFF	Time To First Fix
TX	Transmitter
UERE	User Equivalent Range Error
USB	Universal Serial Bus
UTC	Ultra-Tightly Coupling
UTC	Universal Time Coordinated
UWB	Ultra Wide-Band
WLAN	Wireless Local Area Network
WLS	Weighted Least Squares
ZUPT	Zero velocity Update

16. List of Tables

17. List of figures

18. Appendix

In the previous chapters, on several locations the detailed derivation or analysis of results and assumptions could not be given since it would have required too much space at the individual locations. In this appendix, a more detailed description of mathematical models, simulations and physical relationships will be given.

18.1 GNSS link budget

Global navigation satellite systems (GNSS) are radio navigation systems, which operate in a "one-way-ranging" mode. The user receiver is receiving the weak signals transmitted by the GNSS satellites from a distant medium Earth orbit (MEO) and is able to calculate the ranges to the individual satellites, and by this its own position.

In this chapter of the appendix, the basic GNSS link budget shall be presented and the range of magnitudes of the carrier-to-noise ration C/N0, as well as the signal-to-noise ration SNR, shall be given. In the next chapter, the influence of the C/N0 to the tracking loop performance will be analyzed and the strategy of the replication of user motion, very long coherent integration and ultra-tight coupling will be given. More detailed information on the link budget and tracking loop stability can be found in [64] and [45].

The link budget summarizes all magnitudes contributing to the ratio of the received satellite signal strength and the receiver noise corresponding to a normalized bandwidth of 1 Hz. This link budget is shown in equation (100).

$$\left(\frac{C}{N_0}\right)_{dB-Hz} = P_T + G_T + A_T + A_D + G_R + A_R + A_S + A_{atmos} - T_{sys-dB} - k_{dB} \tag{100}$$

Symbol	Explanation	Expected values outdoor (GPS L1)
C	Received carrier signal strength	-147..-155 dB-W
N_0	System noise figure	-200 dB-Ws
C/N_0	Carrier-to-noise ratio corresponding to a bandwidth of 1 Hz	37..45 dB-Hz
P_T	Satellite signal transmitted power	14..17 dB-W
G_T	Satellite antenna gain	13 dB
A_T	Transmitter antenna attenuation	0 dB
A_D	Free space Loss	157..159 dB
G_R	Receiver antenna gain	5 dB
A_R	Receiver antenna attenuation	-0.2..7 dB
A_S	System losses	7 dB
A_{atmos}	Atmospheric attenuation	2 dB
T_{SYS}	System noise temperature	600 K
k	Boltzmann constant	$1.38065*10^{-23}$ J/K

Table 18-1: Symbols used in the GNSS Link-Budget equation

Indoor signal attenuation additionally reduces the received satellite signal strength and influences the operation and performance of GNSS receivers strongly. If the free line-of-sight to the satellites is obstructed by the components of a building, like the ceiling, walls, windows etc., an additional

attenuation component is added to the link budget and the C/N0 is reduced accordingly. If the attenuations from table 4-1 and 4-2 are analyzed it becomes obvious that the indoor signal can be orders of magnitude smaller than the outdoor signal. The received C/N_0 can drop down below 15 dB-Hz. The relation between the C/N0 and the signal-to-noise ratio (SNR) is given in equation (101).

$$SNR = \frac{C}{N_0} - BW \tag{101}$$

Symbol	Explanation
SNR	Signal to Noise ratio
BW	Noise bandwidth of system
C/N_0	Carrier-to-noise ratio corresponding to a bandwidth of 1 Hz

Table 18-2: Symbols used in the SNR/CN_0 relation

If GPS L1 is analyzed, a signal bandwidth of the receiver front-end between minimum 2 MHz and 4 MHz can be expected. Hence, the SNR at the front-end can be expected to range between -18 dB and -29 dB.

18.2 Influence of the carrier-to-noise ratio on the tracking loop stability

The magnitude C/N_0 has a direct influence on the tracking loop accuracy and stability of a GNSS receiver. Reduced C/N_0 reduces the tracking loop stability and also its accuracy. For indoor scenarios, the signal attenuation can cause severe problems for the GNSS receive. This fact can be analyzed by analysis of the delay-lock-loop (DLL) and phase-lock loop (PLL) stability equations. Thorough derivation of the relationships used in this chapter can be found especially in [45], and also [64]. It will be shown that receiver aiding and very long coherent integration are strategies to acquire and track even very weak signals.

In the following, the equation for the phase-lock loop (PLL) is analyzed. The stability of the PLL is influenced by several different noise components:

$$\sigma_{PLL} = \sqrt{\sigma_T^2 + \sigma_A^2 + \sigma_V^2} + \frac{e(t)}{3} \leq 15° \approx 0.008m \text{ (GPS L1)} \tag{102}$$

Symbol	Explanation
σ_{PLL}	Thermal noise of the PLL tracking loop
σ_T^2	Thermal noise of the system
σ_A^2	Allan variance of the local oscillator
σ_V^2	Vibration induced oscillator jitter variance
e(t)	Dynamical tracking error

Table 18-3: Symbols used in the PLL stability equation

The thermal noise of the tracking loop can be calculated by:

$$\sigma_T^2 = \frac{B_L}{C/N_0}\left(1 + \frac{1}{2T\,C/N_0}\right)\left(\frac{\lambda}{2\pi}\right)^2 \tag{103}$$

Symbol	Explanation
σ_T	Thermal noise component of the tracking loop stability
B_L	Bandwidth of the PLL loop filter
T	Pre-integration time of the GNSS signal
C/N_0	Carrier to noise ratio (1Hz bandwidth)
λ	Wavelength of the carrier frequency (GPS L1: ~0.1905 m)

Table 18-4: Symbols used in the thermal noise component equation

The influence of the Allan variance of the local oscillator can be calculated by:

$$\sigma_A = \frac{c}{2\omega_L}\sqrt{\frac{1}{2}h_{-1}} \tag{104}$$

Symbol	Explanation
σ_A	Square root of Allan variance of the local oscillator
ω_L	Un-attenuated Eigen-frequency of the PLL loop filter
c	Speed of light
h_{-1}	Local oscillator flicker noise

Table 18-5: Symbols used in the thermal noise component equation

For second order loop filters, the tracking loop Eigen-frequency can be approximated as

$$\omega_L = 1.89 B_L \tag{105}$$

The vibration induced oscillator variance can be calculated by:

$$\sigma_V^2 = \frac{c^2 k_g^2 G_g}{4\sqrt{2}\pi\omega_L}\left[\tan^{-1}\left(\frac{\sqrt{2}\omega_L\omega_2}{\omega_L^2 - \omega_2^2}\right) - \frac{1}{2}\ln\left|\frac{\omega_2^2 + \sqrt{2}\omega_L\omega_2 + \omega_L^2}{\omega_2^2 - \sqrt{2}\omega_L\omega_2 + \omega_L^2}\right|\right] \tag{106}$$

Symbol	Explanation
σ_V^2	Vibration induced local oscillator variance
k_g	g-Sensitivity of the oscillator
G_g	Spectral power density of the vibrations [g²/Hz]
ω_2	Upper frequency limit of the vibrations

Table 18-6: Symbols used in the vibration induced component equation

The influence of the vibrations can obviously be manipulated by modification of the loop filter frequency, the choice of an oscillator with different properties and by isolating the oscillator from the vibrations, e.g. by shock mounts. Since the loop filter design is a trade-off between several properties, it seems more appropriate to use a different oscillator or alternatively shock mounts.

The dynamical tracking error can be calculated by:

$$e(t) = \frac{1}{\omega_L^2}\ddot{x_0} \tag{107}$$

Symbol	Explanation
e(t)	Tracking error induced by user antenna motion during signal correlation
ω_L	Frequency of the PLL loop filter
$\ddot{x}$	User antenna acceleration, projected on the signal LOS

Table 18-7: Symbols used in the dynamical tracking error component equation

It becomes obvious that the loop filter frequency is a trade-off between different influences and is a subject of optimization. However, the C/N_0 is directly influencing the thermal noise of the tracking loop. Hence, high indoor attenuation can reduce the tracking loop stability and accuracy. This can make the tracking loop loosing lock, and also reduce the tracking accuracy. Hence, the receiver can become instable and imprecise. If the receiver integration time is increased, the loop filter bandwidth is naturally decreased. By this, the thermal noise component can be reduced. On the other hand, the dynamical tracking error is strongly increased. Increasing the coherent integration time can therefore only be used as a means for the stabilization of the tracking loops, if the dynamical tracking error is reduced by actually tracking the user motion. Then, the dynamical tracking error becomes:

$$e(t) = \frac{1}{\omega_L^2}\Delta\ddot{x}_0 \tag{108}$$

Symbol	Explanation
$\Delta\ddot{x}_0$	Error of the determined user antenna acceleration

Table 18-8: Symbols used in the dynamical tracking error component equation

This result is the basic idea and justification behind the integration method described in chapter 11. Increasing the coherent integration time strongly reduces the thermal noise in the tracking loops. The determination of the user micro-trajectory and ultra-tight coupling replaces the dynamical tracking error with the errors in the determined user acceleration. The user trajectory is replicated by the system described in chapter 11.4. By using the PNS to stabilize the macro-trajectory, the user Doppler estimation can be improved and the user acceleration error can be reduced strongly.

18.3 Error propagation of the single-axis INS

In chapter 6.9, the error propagation of a one-dimensional and of a three-dimensional INS system has been demonstrated. The physical and mathematical background of these simulations shall be presented in this and the next chapter.

To illustrate the basic influence of the sensor errors on the integrated position and velocity errors, two simulations with a one dimensional INS have been performed. The INS consists of one gyroscope and one accelerometer and is only considering the alongside direction. The IMU is oriented to geographic North. In the first simulation, a gyroscope bias was simulated, while the accelerometer bias was set to zero. This setup has been inverted in the second simulation with a simulated accelerometer bias while the gyroscope bias was simulated as zero. The sensor errors were equivalent to position error of one nautical mile after one hour, i.e. 0.0167°/h and 0.0023 m/s². By this procedure the error influences could be separated. The results of the simulation have been presented in Figure 6-12.

In a 1-dimensional INS, the IMU consists of only one accelerometer in the longitudinal or x-axis, as well as one gyroscope in y- or pitch axis. The IMU is considered to move only in a linear direction. For this analysis it is assumed that the IMU is oriented alongside a meridian, i.e. the x-axis is pointing to the North Pole, and is only moving along the meridian. By these assumptions the kinematics and the sensor measurements can be described easily as:

$$f_x = \dot{v}_x \cos\varepsilon - g \sin\varepsilon \tag{109}$$

By re-arrangement this yields:

$$\dot{v}_x = \frac{f_x}{\cos\varepsilon} + g \tan\varepsilon \tag{110}$$

$$\dot{\varepsilon} = \omega - \frac{v_x}{R} \tag{111}$$

$$\dot{x} = \frac{dx}{dt} = v_x \tag{112}$$

Symbol	Explanation
x	Longitudinal coordinate
v_x	Longitudinal velocity
ε	Pitch angle of the IMU, angle between the longitudinal axis of the IMU and the horizon
f_x	Acceleration sensed by the accelerometer
ω	Rotation rate along the pitch axis
R	Earth radius
g	Gravity acceleration
$\frac{v_x}{R}$	"Transport rate" between local level navigation frame and Earth fixed frame

Table 18-9: Symbols used in the kinematical equation

The sensors are assumed to have a measurement bias. Hence, the measured quantities for the accelerometer and the gyroscope are:

$$\omega_m = \dot{\varepsilon} + b_g = \omega - \frac{\dot{v}_x}{R} + b_g \tag{113}$$

$$f_m = \dot{v}_x + b_a = \frac{f_x}{\cos\varepsilon} + g \tan\varepsilon + b_a \tag{114}$$

Symbol	Explanation
ω_m	Measured rotation rate
f_m	Measured acceleration
b_g	Gyroscope bias
b_a	Accelerometer bias

Table 18-10: Symbols used in the measurement equation

By linearization and arranging the equations in a state space notation, the following relationship is yielded:

$$\begin{bmatrix} \dot{\Delta\varepsilon} \\ \dot{\Delta v_x} \\ \dot{\Delta x} \end{bmatrix} = \begin{bmatrix} 0 & -\frac{1}{R} & 0 \\ g & 0 & 0 \\ 0 & 1 & 0 \end{bmatrix} \begin{bmatrix} \Delta\varepsilon \\ \Delta v_x \\ \Delta x \end{bmatrix} + \begin{bmatrix} 1 & 0 \\ 0 & 1 \\ 0 & 0 \end{bmatrix} \begin{bmatrix} b_g \\ b_a \end{bmatrix} \tag{115}$$

This system can be solved using mathematical software like Matlab automatically. In this case, the system can be solved analytically by using the approach:

$$\Delta v_x = a + b\sin(\omega t) + c\cos(\omega t) \tag{116}$$

$$\Delta \dot{v}_x = \omega b\cos(\omega t) - \omega c\sin(\omega t)$$

$$\Delta \ddot{v}_x = -\omega^2 b\sin(\omega t) - \omega^2 c\cos(\omega t)$$

$$\Delta \ddot{v}_x = -\omega^2(\Delta v_x - a)$$

The state space equations can be separated to:

$$\dot{\Delta\varepsilon} = -\frac{1}{R}\Delta v_x + b_g \tag{117}$$

$$\Delta \dot{v}_x = g\Delta\varepsilon + b_a$$

$$\Delta \ddot{v}_x = g\dot{\Delta\varepsilon} = -\frac{g}{R}\Delta v_x + b_g g$$

If both sets of equations are combined, the following relationship is yielded:

$$\Delta \ddot{v}_x = g\dot{\Delta\varepsilon} = -\frac{g}{R}\Delta v_x + b_g g = -\omega^2(\Delta v_x - a) \tag{118}$$

$$-\frac{g}{R}\Delta v_x + b_g g = -\omega^2 \Delta v_x + \omega^2 a$$

This relationship holds for all velocities Δv_x. By variation of Δv_x, linear combinations of this relationship allow solving for all unknowns.

$$b_g g = \omega^2 a \Leftrightarrow \Delta v_x = 0$$

$$-\frac{g}{R} + b_g g = -\omega^2 + \omega^2 a \Leftrightarrow \Delta v_x = 1 \tag{119}$$

$$-\frac{g}{R} = -\omega^2$$

$$\omega = \sqrt{\frac{g}{R}}$$

The resultant frequency ω is called the Schuler-frequency. The polynomial coefficients are:

$$a = \frac{b_g g}{\frac{g}{R}} = b_g R \tag{120}$$

$$0 = a + c \Leftrightarrow t = 0, \Delta v_x = 0$$

$$c = -a = -b_g R$$

If it is assumed that the initial attitude error was zero, the last unsolved coefficient can be calculated as:

$$\Delta \dot{v}_x = \omega b \cos(\omega t) - \omega c \sin(\omega t) = g \Delta \varepsilon + b_a \tag{121}$$

$$\omega b = b_a \Leftrightarrow t = 0, \Delta \varepsilon(t = 0) = 0$$

$$b = \frac{b_a}{\omega}$$

By integration, the following result is produced. To avoid confusion, the symbol of the Schuler frequency has been changed from ω to ω_s.

$$\Delta v_x = b_g R(1 - \cos(\omega_s t)) + b_a \frac{\sin(\omega_s t)}{\omega_s} \tag{122}$$

$$\Delta x = b_g R \left(t - \frac{\sin(\omega_s t)}{\omega_s} \right) - b_a \frac{\cos(\omega_s t)}{\omega_s^2}$$

The results of the simulation of the equations above are presented in Figure 6-12.

18.4 Error propagation of the three-axis INS

In chapter 6.9, the influence of sensor errors on a three-axis INS have been shown. The simulation has been performed using a 9-state error mechanization, including attitude, velocity and position errors. While the system matrix models the inherent instability of the INS mechanization, the disturbance vector contains the sensor bias errors and introduces errors caused by imperfectly calibrated sensors. The simulation has been set up in Matlab and integrated using the Runge-Kutta-method implemented in the function “ode45”.

The system equation for the simulation is:

$$\dot{X} = FX + Gq \tag{123}$$

Symbol	Explanation
X	State Vector
F	System matrix
G	Disturbance matrix
q	Disturbance vector

Table 18-11: Symbols used in the system equation of the INS simulation

The state vector is defined as:

$$X = \begin{bmatrix} \Delta\varphi \\ \Delta\theta \\ \Delta\psi \\ \Delta\dot{\phi} \\ \Delta\dot{\Lambda} \\ \Delta\dot{h} \\ \Delta\Phi \\ \Delta\Lambda \\ \Delta h \end{bmatrix} \tag{124}$$

Symbol	Explanation
X	State Vector
$\Delta\varphi$	Error of the roll angle (attitude error)
$\Delta\theta$	Error of the pitch attitude attitude angle (attitude error)
$\Delta\psi$	Error of the yaw attitude angle (attitude error)
$\Delta\dot{\Phi}$	Error of the latitude rate (velocity error)
$\Delta\dot{\Lambda}$	Error of the longitude rate (velocity error)
$\Delta\dot{h}$	Error of the altitude rate (velocity error)
$\Delta\Phi$	Error of the latitude (position error)
$\Delta\Lambda$	Error of the longitude (position error)
Δh	Altitude error (position error)

Table 18-12: Symbols used in the system equation of the INS simulation

Hence, the state vector contains the attitude, velocity and position errors in the Earth fixed frame. The state is disturbed by the sensor errors of the inertial measurement unit. In this case, only bias errors for the gyroscopes and accelerometers have been considered.

The disturbance matrix G models the influence of the disturbance on the state vector derivative. It is given by:

$$G = \begin{bmatrix} 1 & 0 & 0 & 0 & 0 & 0 \\ 0 & 1 & 0 & 0 & 0 & 0 \\ 0 & 0 & 1 & 0 & 0 & 0 \\ 0 & 0 & 0 & \frac{1}{R_E} & 0 & 0 \\ 0 & 0 & 0 & 0 & \frac{1}{R_E cos\Phi} & 0 \\ 0 & 0 & 0 & 0 & 0 & -1 \\ 0 & 0 & 0 & 0 & 0 & 0 \\ 0 & 0 & 0 & 0 & 0 & 0 \\ 0 & 0 & 0 & 0 & 0 & 0 \end{bmatrix} \tag{125}$$

Symbol	Explanation
G	Disturbance matrix
Φ	Latitude
R_E	Earth radius [m]

Table 18-13: Symbols used in the disturbance matrix

The sensor errors are modeled as:

$$q = \begin{bmatrix} b_{ax} \\ b_{ay} \\ b_{az} \\ d_{gx} \\ d_{gy} \\ d_{gz} \end{bmatrix} \tag{126}$$

Symbol	Explanation
q	Sensor error vector
b_{ax}	Bias error of the x-axis accelerometer
b_{ay}	Bias error of the y-axis accelerometer
b_{az}	Bias error of the z-axis accelerometer
d_{gx}	Bias error of the x-axis gyroscope
d_{gy}	Bias error of the y-axis gyroscope
d_{gz}	Bias error of the z-axis gyroscope

Table 18-14: Symbols used in the sensor error vector

In this case, q is the vector of sensor errors (deterministic). The F-matrix is modeling the system dynamics as can be seen in equation (127).

In the simulation it was assumed that an airplane is located at a latitude of 45° north and is moving with 300 m/s in East direction. Only single sensor bias was modelled to show the individual influence. This basic analysis is not easily possible if combinations of different sensor biases are used.

$$F = \begin{pmatrix} 0 & -(\omega_e + \dot{\lambda})\sin\varphi & \dot{\varphi} & 0 & \cos\varphi & 0 & -(\omega_e + \dot{\lambda})\sin\varphi & 0 & 0 \\ (\omega_e + \dot{\lambda})\sin\varphi & 0 & (\omega_e + \dot{\lambda})\cos\varphi & -1 & 0 & 0 & 0 & 0 & 0 \\ -\dot{\varphi} & -(\omega_e + \dot{\lambda})\cos\varphi & 0 & 0 & -\sin\varphi & 0 & -(\omega_e + \dot{\lambda})\cos\varphi & 0 & 0 \\ 0 & -f_D/R_E & f_E/R_E & -2\dot{h}/R_E & -(\omega_e + \dot{\lambda})\sin(2\varphi) & -2\dot{\varphi}/R_E & -\dot{\lambda}(2\omega_e + \dot{\lambda})\cos(2\varphi) & 0 & 0 \\ f_D/(R_E cos\varphi) & 0 & -f_N/(R_E cos\varphi) & 2(\omega_e + \dot{\lambda})tan\varphi & \frac{-2\dot{h}}{R_E} + 2\dot{\varphi}tan\varphi & -2(\omega_e + \dot{\lambda})/R_E & \left(\ddot{\lambda} + {}^{2\dot{h}}/_{R_E}(\omega_e + \dot{\lambda})\right)tan\varphi + 2(\omega_e + \dot{\lambda})\dot{\varphi} & 0 & -\left(\ddot{\lambda} - 2\dot{\varphi}(\omega_e + \dot{\lambda})\right)\frac{tan\varphi}{R_E} \\ f_E & -f_N & 0 & 2R_E\dot{\varphi} & 2R_E(\omega_e + \dot{\lambda})(\cos\varphi)^2 & 0 & -R_E\dot{\lambda}(\omega_e + \dot{\lambda})\sin(2\varphi) & 0 & \dot{\varphi}^2 + \dot{\lambda}(\omega_e + \dot{\lambda})(\cos\varphi)^2 + 2\omega_S^2 \\ 0 & 0 & 0 & 1 & 0 & 0 & 0 & 0 & 0 \\ 0 & 0 & 0 & 0 & 1 & 0 & 0 & 0 & 0 \\ 0 & 0 & 0 & 0 & 0 & 1 & 0 & 0 & 0 \end{pmatrix} \quad (127)$$

18.5 Error propagation of the magnetometer

Magnetic heading can be derived by analysis of the measured magnetic field in the navigation frame. Since the magnetic field vector is not pointing geographic North, but magnetic North, the heading must be corrected by the horizontal angle between the local magnetic field vector and the geographic North direction. This correction angle is called “declination”. The magnetic field vector is not necessarily pointing in the horizontal plane. The angle between the horizon and the field vector is called “inclination”.

For the analysis, a local level frame is defined which is local level, but the x-axis is pointing magnetic North. This frame is denoted “m” for magnetic. The only difference to the local level navigation frame (“n”) is a rotation around the local vertical (z-axis) with the magnitude of the declination. Then, the magnetic field vector can be written as:

$$m^m = \begin{bmatrix} A\cos(I) \\ 0 \\ A\sin(I) \end{bmatrix} \tag{128}$$

The field vector in the local level frame can be derived by:

$$m^n = C_m^n m^m \tag{129}$$

$$C_m^n = \begin{bmatrix} \cos(D) & -\sin(D) & 0 \\ \sin(D) & \cos(D) & 0 \\ 0 & 0 & 1 \end{bmatrix}$$

An additional local level frame for the magnetometer platform can be defined. This “LL” frame is local level, the x-axis is the projection of the IMU x-axis to the horizontal plane. This frame is denoted “LL”. The magnetic heading in the m-frame can be derived by:

$$\psi^n = \tan^{-1}\left(\frac{-m_y^{LL}}{m_x^{LL}}\right) \tag{130}$$

Symbol	Explanation
m	Magnetic field vector
D	Local declination
Index ‘LL’	Local level frame pointing geodetic North
Index ‘m’	Local level frame pointing magnetic North
Index ‘n’	Navigation frame, local level frame pointing geodetic North
I	Inclination of the field vector with respect to horizon
Ψ	Heading
m_a^k	Magnetic field strength m in direction a of frame k
Δm_a^b	Error of magnetic field strength m in direction a of the body frame b (e.g. sensor bias)
Δm_a^{LL}	Error of magnetic field strength m in direction a of the LL frame b (e.g. hard iron effect)
C_b^a	Transformation matrix from frame b to frame a
ϕ	Roll angle

θ	Pitch angle
Ψ	Yaw angle

Table 18-15: Symbols used in the magnetometer error discussion

The magnetic field measurements in the body frame can be rotated in the LL frame by:

$$m^{LL} = C_b^{LL} m^b \tag{131}$$

$$C_b^{LL} = \begin{bmatrix} \cos(\theta) & \sin(\phi)\sin(\theta) & \cos(\phi)\sin(\theta) \\ 0 & \cos(\phi) & -\sin(\phi) \\ -\sin(\theta) & \sin(\phi)\cos(\theta) & \cos(\phi)\cos(\theta) \end{bmatrix}$$

The magnetic heading in the n-frame can be defined as:

$$\psi^n = \psi^m + D \tag{132}$$

To derive magnetic heading, the following procedure is followed:

- Rotate the IMU magnetic measurements in the LL-frame
- Calculate heading in the m-frame using the relationship in (132)
- Calculate the heading in the n-frame by applying the local declination

For the error propagation, several error sources for the magnetic heading error can be found:

- Magnetometer bias in the three axes
- Levelling errors (determined pitch and roll angles)
- Magnetic disturbance ("hard iron effects")
- Error in the determination of the local declination

Errors in the local declination are directly mapped to the heading error.

$$\frac{d\psi^n}{dD} = 1 \tag{133}$$

The declination is well mapped for nearly all locations in the world. If specific local field disturbance is caused, e.g. by ferromagnetic minerals, this error directly influences the heading determination. If magnetic disturbance is encountered, the mapping of the field disturbance to the heading determination can be calculated using:

$$\frac{d\psi^n}{d\Delta m_x^{LL}} = \frac{1}{1 + \left(\frac{-m_y^{LL}}{m_x^{LL}}\right)} \frac{m_y^{LL}}{{m_x^{LL}}^2}$$

$$\frac{d\psi^n}{d\Delta m_x^{LL}} = \frac{1}{1 + \left(\frac{-m_y^{LL}}{m_x^{LL}}\right)} \frac{-1}{m_x^{LL}} \tag{134}$$

The magnetic measurements in the body frame, but also the sensor bias is mapped to the heading by a transformation to the local level plane. Hence, the current attitude of the magnetometer or the

IMU/magnetometer combination defines the mapping of sensor readings in the body frame to the heading in the navigation frame. For measurements in the local level plane, the error propagation by erroneous levelling can be described as:

$$\frac{d\Delta m_x^{LL}}{d\Delta\varphi} = \cos(\phi)\sin(\theta)\left(m_x^b + \Delta m_x^b\right) - \sin(\phi)\sin(\theta)\left(m_z^b + \Delta m_z^b\right)$$

$$\frac{d\Delta m_x^{LL}}{d\Delta\theta} = -\sin(\theta)\left(m_x^b + \Delta m_x^b\right) + \sin(\phi)\cos(\phi)\left(m_y^b + \Delta m_y^b\right) + \cos(\phi)\cos(\theta)\left(m_z^b + \Delta m_z^b\right) \tag{135}$$

$$\frac{d\Delta m_y^{LL}}{d\Delta\varphi} = -\sin(\theta)\left(m_y^b + \Delta m_y^b\right) - \cos(\phi)\left(m_z^b + \Delta m_z^b\right)$$

$$\frac{d\Delta m_y^{LL}}{d\Delta\theta} = 0$$

The error of the magnetic measurements in the local level frame caused by the sensor errors in the body frame can be described as:

$$\frac{d\Delta m_x^{LL}}{d\Delta m_x^b} = \cos(\theta)$$

$$\frac{d\Delta m_x^{LL}}{d\Delta m_y^b} = \sin(\varphi)\sin(\theta)$$

$$\frac{d\Delta m_x^{LL}}{d\Delta m_z^b} = \cos(\varphi)\sin(\theta)$$

$$\frac{d\Delta m_y^{LL}}{d\Delta m_x^b} = 0 \tag{136}$$

$$\frac{d\Delta m_y^{LL}}{d\Delta m_y^b} = \cos(\theta)$$

$$\frac{d\Delta m_y^{LL}}{d\Delta m_z^b} = -\sin(\varphi)$$

The error propagation of the alignment errors in pitch and roll to the heading error can be derived as:

$$\frac{d\psi}{d\varphi}=\frac{\frac{\cos(\varphi)\,m_z^b+\sin(\varphi)\,m_y^b}{\cos(\varphi)\sin(\theta)\,m_z^b+\sin(\varphi)\sin(\theta)\,m_y^b+\cos(\theta)\,m_x^b}-\frac{\left(\sin(\varphi)\,m_z^b-\cos(\varphi)\,m_y^b\right)\left(\cos(\varphi)\sin(\theta)\,m_y^b-\sin(\varphi)\sin(\theta)\,m_z^b\right)}{\left(\cos(\varphi)\sin(\theta)\,m_z^b+\sin(\varphi)\sin(\theta)\,m_y^b+\cos(\theta)\,m_x^b\right)^2}}{\frac{\left(\sin(\varphi)\,m_z^b-\cos(\varphi)\,m_y^b\right)^2}{\left(\cos(\varphi)\sin(\theta)\,m_z^b+\sin(\varphi)\sin(\theta)\,m_y^b+\cos(\theta)\,m_x^b\right)^2}+1} \tag{137}$$

$$\frac{d\psi}{d\theta}=\frac{\left(\sin(\varphi)\,m_z^b-\cos(\varphi)\,m_y^b\right)\left(\cos(\varphi)\cos(\theta)\,m_z^b+\sin(\varphi)\cos(\theta)\,m_y^b-\sin(\theta)\,m_x^b\right)}{\left(\cos(\varphi)\sin(\theta)\,m_z^b+\sin(\varphi)\sin(\theta)\,m_y^b+\cos(\theta)\,m_x^b\right)^2\left(\frac{\left(\sin(\varphi)\,m_z^b-\cos(\varphi)\,m_y^b\right)^2}{\left(\cos(\varphi)\sin(\theta)\,m_z^b+\sin(\varphi)\sin(\theta)\,m_y^b+\cos(\theta)\,m_x^b\right)^2}+1\right)} \tag{138}$$

The error propagation of the sensor errors to the heading error can be derived as:

$$\frac{d\psi}{d\Delta m_x^b}=\frac{\cos(\varphi)\left(\sin(\varphi)\,m_z^b-\cos(\varphi)\,m_y^b\right)}{\left(\cos(\varphi)\sin(\theta)\,m_z^b+\sin(\varphi)\sin(\theta)\,m_y^b+\cos(\theta)\,m_x^b\right)^2\left(\frac{\left(\sin(\varphi)\,m_z^b-\cos(\varphi)\,m_y^b\right)^2}{\left(\cos(\varphi)\sin(\theta)\,m_z^b+\sin(\varphi)\sin(\theta)\,m_y^b+\cos(\theta)\,m_x^b\right)^2}+1\right)} \tag{139}$$

$$\frac{d\psi}{d\Delta m_y^b}=\frac{-\frac{\cos(\varphi)}{\cos(\varphi)\sin(\theta)\,m_z^b+\sin(\varphi)\sin(\theta)\,m_y^b+\cos(\theta)\,m_x^b}-\frac{\sin(\varphi)\sin(\theta)\left(\sin(\varphi)\,m_z^b-\cos(\varphi)m_y^b\right)}{\left(\cos(\varphi)\sin(\theta)\,m_z^b+\sin(\varphi)\sin(\theta)\,m_y^b+\cos(\theta)\,m_x^b\right)^2}}{\frac{\left(\sin(\varphi)\,m_z^b-\cos(\varphi)\,m_y^b\right)^2}{\left(\cos(\varphi)\sin(\theta)\,m_z^b+\sin(\varphi)\sin(\theta)\,m_y^b+\cos(\theta)\,m_x^b\right)^2}+1} \tag{140}$$

$$\frac{d\psi}{d\Delta m_z^b}=\frac{\frac{\sin(\varphi)}{\cos(\varphi)\sin(\theta)\,m_z^b+\sin(\varphi)\sin(\theta)\,m_y^b+\cos(\theta)\,m_x^b}-\frac{\cos(\varphi)\sin(\theta)\left(\sin(\varphi)\,m_z^b-\cos(\varphi)m_y^b\right)}{\left(\cos(\varphi)\sin(\theta)\,m_z^b+\sin(\varphi)\sin(\theta)\,m_y^b+\cos(\theta)\,m_x^b\right)^2}}{\frac{\left(\sin(\varphi)\,m_z^b-\cos(\varphi)\,m_y^b\right)^2}{\left(\cos(\varphi)\sin(\theta)\,m_z^b+\sin(\varphi)\sin(\theta)\,m_y^b+\cos(\theta)\,m_x^b\right)^2}+1} \tag{141}$$